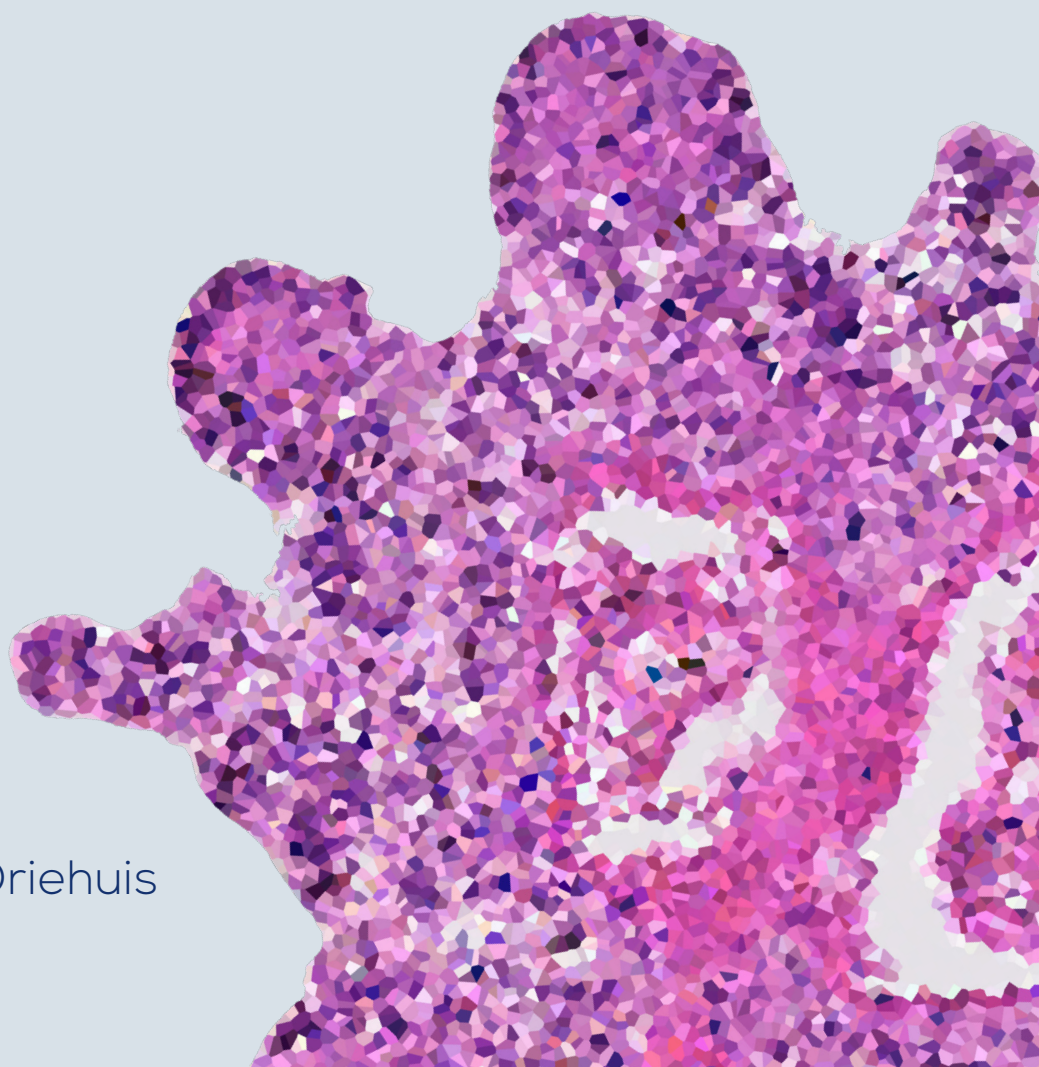


ORGANOIDS
AS A TOOL FOR
FUNDAMENTAL AND
TRANSLATIONAL
ONCOLOGY RESEARCH

Else Driehuis



**ORGANOIDS AS
A TOOL FOR
FUNDAMENTAL AND
TRANSLATIONAL
ONCOLOGY RESEARCH**

Can organoids guide clinical decision making?

Else Driehuis

Author: Else Driehuis
Cover illustration: Else Driehuis
Layout and print: Off Page, Amsterdam

ISBN: 978-94-6182-967-2

© All right reserved. No part of this thesis may be reproduced, stored or transmitted in any form by any means without prior permission of the author

Research described in this thesis was performed at group of Prof. Dr. Hans Clevers at the Hubrecht Institute, Utrecht, The Netherlands

Printing of this thesis was financially supported by Sanbio, Tecan, ChipSoft and Corning.

**ORGANOIDS AS A TOOL FOR FUNDAMENTAL AND
TRANSLATIONAL ONCOLOGY RESEARCH**

Can organoids guide clinical decision making?

**ORGANOÏDEN ALS MODEL VOOR FUNDAMENTEEL EN
TRANSLATIONEEL ONCOLOGISCH ONDERZOEK**

Kunnen organoïden bijdragen aan klinische besluitvorming?

(met een samenvatting in het Nederlands)

Proefschrift

ter verkrijging van de graad van doctor aan de
Universiteit Utrecht
op gezag van de
rector magnificus, prof.dr. H.R.B.M. Kummeling,
ingevolge het besluit van het college voor promoties
in het openbaar te verdedigen op

dinsdag 1 oktober 2019 des middags te 12.45 uur

door

Else Driehuis
geboren op 22 augustus 1991
te Deventer

PROMOTOREN

Prof. dr. J.C. Clevers

Prof. dr. P.J. van Diest

COPROMOTOR

Dr. S. Willems

TABLE OF CONTENTS

General introduction		7
Part I	Organoids as <i>in vitro</i> model for translational oncological research	
Chapter 1	Organoids as an <i>in vitro</i> model: mini-organs in the lab	17
Chapter 2	Oral mucosa organoids as a potential platform for personalized therapy	33
part 2.1	Oral mucosal organoids as a potential platform for personalized cancer therapy	35
part 2.2	How to proceed: <i>in vitro</i> screenings for the Oncode Clinical trial (ONCODE-P2018-0003)	101
Chapter 3	Patient-derived head and neck cancer organoids recapitulate clinically relevant EGFR expression levels and are responsive to EGFR-targeted photodynamic therapy	111
Chapter 4	Patient-derived oral mucosa organoids as an <i>in vitro</i> model for methotrexate-induced toxicity	135
Chapter 5	Pancreatic cancer organoids recapitulate disease and allow personalized drug screening	165
Part II	Organoids as <i>in vitro</i> model to study tumorigenesis	
Chapter 6	CRISPR/Cas 9 genome editing and its applications in organoids	217
Chapter 7	CRISPR-induced <i>TMPRSS2-ERG</i> gene fusions in mouse prostate organoids	237
Chapter 8	Summarizing discussion	253
Addendum	Nederlandse samenvatting	267
	Curriculum Vitae and list of publications	277
	Dankwoord	279

GENERAL INTRODUCTION

The studies presented in this thesis explore the potential of organoid technology to aid clinical practice. Organoids are three-dimensional self-organizing structures that can be grown from stem cells (1–3), that allow researchers to study organ structure and function in the laboratory. These mini-organs retain both functional and structural characteristics of the tissue of origin, and can nowadays be established from many different tissues, diseased or healthy.

The studies presented here investigate to what extent organoids can be used to model disease physiology, including tumor development and therapy sensitivity, thereby focusing on the application of organoids in the field of oncology. The translational potential of this model is explored both at the level of the individual patient, and in a more general way. On the individual patient level, *in vitro* organoid responses are compared to the patient responses, to see if organoids hold potential to guide therapy choices in the clinic. In other studies described in this thesis, organoids are more broadly used as an *in vitro* model to assess the efficacy of anti-cancer therapies in different tumor types, or study the toxic side-effects of methotrexate (a commonly used chemotherapeutic agent). Here, we do not correlate organoid response to the response of individual patients, but rather investigate whether organoids are a good (or better) model compared to already existing ones. Taken together, we believe that the studies presented in this thesis highlight the diverse range of clinical applications of organoid technology. The promise of organoid culture for clinical implementation is underscored by the fact that, based on the model described in this work, an observational study has started to determine the predictive potential of head & neck cancer organoids. The studies focusing on clinical application of organoid technology are described in part one of this thesis (Chapters 1 till 5). Part two (consisting of Chapter 6 and 7) focusses on fundamental biology and the use of CRISPR/Cas9 genome engineering to introduce oncogenic mutations in organoids.

Part I

Chapter 1 of this thesis summarizes the previously performed organoid research in the field of oncology. Relevant studies are reviewed and summarized, and the advantages and limitations of organoid technology are explored. Moreover, the first studies that report on the predictive potential of organoids in the clinic are discussed. This chapter sets the stage for the subsequent chapters two to five, where we use organoid technology to address a diverse range of clinically relevant oncological questions.

In **Chapter 2**, we describe a method to establish organoids from head & neck squamous cell carcinoma (HNSCC) and matched wildtype tissue. HNSCC is a collective term used for tumors of the stratified epithelium that lines the oral cavity, pharynx and larynx (4). HNSCC is one of the most common forms of cancer, and although the molecular characterization of this disease has improved, survival rates have remained poor (5,6). Additional models to study tumor biology at the (individual) patient level and the possibility to test novel

therapeutics on patient-derived material, could potentially improve treatment strategies. Moreover, a means to predict patient response to chemotherapeutics would directly aid current clinical practice, as side-effects of these treatments are severe, no biomarkers to predict patient response are available, and up to 50% of patients relapse after undergoing these harsh treatments (6). Therefore, we set out to establish a model to test therapy sensitivity of patient-derived tumor cells. In Chapter 2, we describe how HNSCC-derived organoids histologically, genetically and functionally recapitulate their tissue of origin. Tumor organoids retain their tumorigenic potential, as transplantation into mice results in tumor formation. When exposed to currently used chemotherapeutics, radiotherapy, and a panel of novel targeted therapies, organoids derived from different patients show different responses to these treatments. Although anecdotal, a correlation between the response of the organoids and the clinical response of the patient is observed. These findings suggest that organoids may have predictive potential and, when validated in a larger cohort of patients, could guide clinical decision making in the future. Additionally, we observe an *in vitro* effect of novel therapeutics that are not yet applied in clinical practice, suggesting that organoids could hold the potential to identify effective therapies to treat HNSCC.

In the remainder of this chapter, we discuss the currently ongoing observational clinical trial (ONCODE-P2018-0003) that was initiated based on the findings described in Chapter 2. Here we advise, based on experience, what we feel is the best approach to perform the *in vitro* screening part of the Oncode Proof of Concept clinical trial that will be executed in the coming years. Moreover, supported by experimental data, we discuss what -in our opinion- are the potential risks of organoid technology for this application and how these should be addressed to minimize their influence on the results.

Chapter 3 describes the application of this novel HNSCC organoid model to test photodynamic therapy (PDT) *in vitro*. PDT is a therapeutic approach where a photosensitizer (PS) is used to target tumor cells. When the PS is activated by light of the correct wavelength, it reacts with oxygen to produce reactive oxygen species that damage DNA, RNA and proteins, thereby ultimately resulting in cell death (7–9). In clinical practice, the PS is administered to the patient, after which the tumor is exposed to a light source (for example during surgery) to initiate tumor cells death. Conjugation of a PS to tumor-targeting agents such as antibodies, has been used to both increase tumor killing and decrease side-effects of PDT. As Epidermal Growth Factor Receptor (EGFR) is commonly found overexpressed in a range of tumor types, including HNSCC (10), EGFR-targeting antibodies and nanobodies (a small antigen binding fragment) have been used to more specifically deliver PS (11,12). The efficacy of killing has been shown both *in vitro* and *in vivo*. EGFR-antibody Cetuximab conjugated to PS is currently explored in clinical trials for the treatment of HNSCC. In Chapter 3, we describe that PDT using EGFR-targeting antibodies and nanobodies shows effective in patient-derived HNSCC organoids. In contrast to the EGFR overexpressing cell lines previously used to test this therapy *in vitro*, organoids express EGFR at levels comparable to primary tumor tissue. Additionally, organoids create the opportunity to

culture both tumor and wildtype cells from the same patient. Therefore, the differential effect of therapy on normal and tumor cells can be studied *in vitro*, something that is not possible using conventional 2D cell lines. We show that EGFR expression is higher in tumor organoids than in matched organoids from normal tissue and that, indeed, tumor cells are more sensitive to PDT than their wildtype counterparts. Response to PDT directly correlates to the level of EGFR expression on tumor cells, highlighting EGFR as a potential biomarker for response to PDT.

In **Chapter 4**, we explore the potential of wildtype oral mucosa organoids to model one of the most common side-effects of methotrexate (MTX), a commonly used chemotherapeutic agent. MTX is used in the treatment of pediatric acute lymphatic leukemia, where its use is associated with severe oral mucositis (inflammation of the oral mucosal layer) (13,14). Mucositis occurs in 20% of patients, where it results in hospitalization and treatment delays (13,14). In pediatric leukemia patients a high dose of MTX is given, followed by a rescue dose of leucovorin between 24 and 48 hours after MTX infusion to reduce side-effects. As no relevant *in vitro* model exists, there is no data to support that leucovorin rescue results in a decrease in the side-effects observed in the oral mucosa. Indeed, until organoid technology, the long-term culture of dividing wildtype cells was impossible. As such, organoids for the first time allow the *in vitro* study of MTX-induced toxicity in wildtype oral mucosa cells. Using this model, we subsequently show that the timing of leucovorin rescue, that differs throughout the world, significantly influences MTX-induced toxicity in oral mucosa cells. These results suggest that a change in clinical protocols could reduce the severity or frequency of mucositis. Moreover, we use this model to explore alterations of the currently applied clinical protocol to further reduce MTX-induced oral mucosa cell death, whilst leaving MTX effects on leukemia cells intact. Taken together, the work described in this chapter illustrates how organoid technology can create a novel clinically relevant *in vitro* model that allows for the validation of-, or testing of alterations from – currently applied clinical protocols.

In **Chapter 5**, we describe the development of an organoid biobank derived from pancreatic tumors. The resulting organoid lines histologically and functionally recapitulate the tumor types of which they are derived. Although pancreatic cancer organoids have been described previously (15,16), we now explore the potential of this system to identify or validate therapeutic approaches that could improve clinical outcome of these tumor types. As such, the established panel of organoid lines was exposed to a wide range of chemotherapeutic agents to see which hold potential in these tumors. We find that a wide range of targeted therapies effectively kills pancreatic tumor cells. Not surprisingly, we find that it differs per patient-derived organoid line which agent is most effective to kill the tumor cells. These results are in line with the general believe that a personalized approach will be required to identify the right drug for the right patient. In total, 76 compounds are screened on 24 patient-derived organoid lines, highlighting the potential of organoid technology to perform high-throughput drug screens.

Lastly, we explore the potential of PRMT5 inhibitors, previously claimed to specifically target tumors with loss of *MTAP*, a gene adjacent to the commonly lost tumor suppressor gene *CDKN2A*. It was previously shown that loss of *MTAP* and PRMT5 is synthetically lethal, and inhibition of PRMT5 therefore exclusively affects *MTAP* negative cells (17–19). Here, we validate these findings in a large set of patient-derived cells and find that *MTAP* negative cells indeed show increased sensitivity to this therapy. Moreover, we observe that a subset of *MTAP* positive organoid lines also shows increased sensitivity to PRMT5 inhibition. We find that these *MTAP* positive tumor cells are characterized by increased levels of the metabolite methylthioadenosine, which is also increased in *MTAP* negative tumors and known to inhibit PRMT5 function. These findings implicate that PRMT5 inhibition might be a sensible therapeutic approach to treat pancreatic cancer, even in a subset of *MTAP* positive tumors.

Part II

In the second part of this thesis, we shift gears to explore the potential of organoids to understand the mechanisms underlying tumorigenesis. To model tumors, genetic alterations commonly found in cancer are introduced in organoids using CRISPR/Cas9. This genome editing tool is based on a bacterial innate defense mechanism that protects bacteria against viral infections. Since the first report of the use of CRISPR to edit the genome, CRISPR technology has quickly evolved. Therefore, **Chapter 6** first gives an overview of previous studies that have applied CRISPR/Cas9 genome editing in organoids. We report the findings of these studies and summarize the advantages and limitations of using this technique. Moreover, we describe how its use in organoids differs from its use in 2D cell lines, and which research questions could be addressed specifically using CRISPR/Cas9 in organoids.

In **Chapter 7**, we describe how CRISPR/Cas9 genome editing was applied in mouse prostate organoids to create an endogenous gene-fusion between the androgen responsive gene *TMPRSS2* and the oncogene *ERG*. This genetic alteration is commonly found in prostate cancer, and is believed to be one of the initiating events in the development of this disease (20–23). *TMPRSS2-ERG* fusion was identified in 50% of the tumors. Although *TMPRSS2-ERG* carrying prostate cancer-derived organoids and cell lines have been described, these contain additional mutations that could influence cell behavior (24). To study how this genetic alteration might initiate tumor formation, CRISPR/Cas9 was used to establish this alteration in an otherwise wildtype background of mouse prostate organoids. Using this approach, we were able to successfully delete a three million base pair long stretch of DNA that separates these two genes. This study showed for the first time that CRISPR/Cas9 could be used to create gene fusions in organoids. As such, in addition to creating a model to study the effects of *TMPRSS2-ERG* gene fusion, this study highlights the potential of CRISPR/Cas9 in organoids.

Chapter 8 discusses the implications of the research that was described in the previous chapters, and explores potential follow-up research that will aid the clinical implementation of organoid technology.

REFERENCES

1. Kretzschmar K, Clevers H. Organoids: Modeling Development and the Stem Cell Niche in a Dish. *Dev Cell*. Elsevier Inc.; 2016;38:590–600.
2. Eiraku M, Sasai Y. Mouse embryonic stem cell culture for generation of three-dimensional retinal and cortical tissues. *Nat Protoc*. 2012;7:69–79.
3. Lancaster M a., Knoblich J a. Organogenesis in a dish: modeling development and disease using organoid technologies. *Science*. 2014;345:1247125.
4. Squier C, Kremer M. Biology of oral mucosa and esophagus. *J Natl Cancer Inst Monogr*. 2001;29:7–15.
5. Fitzmaurice C, Allen C, Barber RM, Barregard L, Bhutta ZA, Brenner H, et al. Global, Regional, and National Cancer Incidence, Mortality, Years of Life Lost, Years Lived With Disability, and Disability-Adjusted Life-years for 32 Cancer Groups, 1990 to 2015: A Systematic Analysis for the Global Burden of Disease Study. *JAMA Oncol*. United States: American Medical Association; 2017;3:524–48.
6. Argiris A, Karamouzis M V., Raben D, Ferris RL. Head and neck cancer. *Lancet (London, England) [Internet]*. 2008;371(9625):1695–709. 2008.
7. Plaetzer K, Krammer B, Berlanda J, Berr F, Kiesslich T. Photophysics and photochemistry of photodynamic therapy: fundamental aspects. *Lasers Med Sci*. Springer; 2009;24:259–68.
8. Trachootham D, Alexandre J, Huang P. Targeting cancer cells by ROS-mediated mechanisms: a radical therapeutic approach? *Nat Rev Drug Discov*. Nature Publishing Group; 2009;8:579.
9. Curtin JF, Donovan M, Cotter TG. Regulation and measurement of oxidative stress in apoptosis. *J Immunol Methods*. Elsevier; 2002;265:49–72.
10. Kalyankrishna S, Grandis JR. Epidermal growth factor receptor biology in head and neck cancer. *J Clin Oncol*. American Society of Clinical Oncology; 2006;24:2666–72.
11. Heukers R, van Bergen en Henegouwen PMP, Oliveira S. Nanobody-photosensitizer conjugates for targeted photodynamic therapy. *Nanomedicine Nanotechnology, Biol Med*. Elsevier; 2014;10:1441–51.
12. Van Driel PBAA, Boonstra MC, Slooter MD, Heukers R, Stammes MA, Snoeks TJA, et al. EGFR targeted nanobody-photosensitizer conjugates for photodynamic therapy in a pre-clinical model of head and neck cancer. *J Control Release*. Elsevier; 2016;229:93–105.
13. Den Hoed MAH, Lopez-Lopez E, Te Winkel ML, Tissing W, De Rooij JDE, Gutierrez-Camino A, et al. Genetic and metabolic determinants of methotrexate-induced mucositis in pediatric acute lymphoblastic leukemia. *Pharmacogenomics J*. 2015;
14. Villa A, Sonis ST. Mucositis: Pathobiology and management. *Curr. Opin. Oncol*. 2015.
15. Seino T, Kawasaki S, Shimokawa M, Tamagawa H, Toshimitsu K, Fujii M, et al. Human Pancreatic Tumor Organoids Reveal Loss of Stem Cell Niche Factor Dependence during Disease Progression. *Cell Stem Cell*. Elsevier; 2018;22:454-467.e6.
16. Tiriack H, Belleau P, Engle DD, Plenker D, Deschênes A, Somerville T, et al. Organoid profiling identifies common responders to chemotherapy in pancreatic cancer. *Cancer Discov*. 2018;
17. Mavrakis KJ, McDonald ER 3rd, Schlabach MR, Billy E, Hoffman GR, deWeck A, et al. Disordered methionine metabolism in MTAP/CDKN2A-deleted cancers leads to dependence on PRMT5. *Science*. United States; 2016;351:1208–13.
18. Kryukov G V, Wilson FH, Ruth JR, Paulk J, Tsherniak A, Marlow SE, et al. MTAP deletion

- confers enhanced dependency on the PRMT5 arginine methyltransferase in cancer cells. *Science*. United States; 2016;351:1214–8.
19. Marjon K, Cameron MJ, Quang P, Clasquin MF, Mandley E, Kunii K, et al. MTAP Deletions in Cancer Create Vulnerability to Targeting of the MAT2A/PRMT5/RIOK1 Axis. *Cell Rep*. 2016;
 20. Demichelis F, Fall K, Perner S, Andren O, Schmidt F, Setlur SR, et al. TMPRSS2:ERG gene fusion associated with lethal prostate cancer in a watchful waiting cohort. *Oncogene*. England; 2007;26:4596–9.
 21. Hermans KG, van Marion R, van Dekken H, Jenster G, van Weerden WM, Trapman J. TMPRSS2:ERG fusion by translocation or interstitial deletion is highly relevant in androgen-dependent prostate cancer, but is bypassed in late-stage androgen receptor-negative prostate cancer. *Cancer Res*. United States; 2006;66:10658–63.
 22. Tomlins S a, Rhodes DR, Perner S, Dhanasekaran SM, Mehra R, Sun X-W, et al. Recurrent fusion of TMPRSS2 and ETS transcription factor genes in prostate cancer. *Science*. 2005;310:644–8.
 23. Klezovitch O, Risk M, Coleman I, Lucas JM, Null M, True LD, et al. A causal role for ERG in neoplastic transformation of prostate epithelium. *Proc Natl Acad Sci U S A*. United States; 2008;105:2105–10.
 24. Tomlins S a, Laxman B, Varambally S, Cao X, Yu J, Helgeson BE, et al. Role of the TMPRSS2-ERG gene fusion in prostate cancer. *Neoplasia*. 2008;10:177–88.

**ORGANOIDS AS *IN VITRO*
MODEL FOR TRANSLATIONAL
ONCOLOGICAL RESEARCH**



CHAPTER

ORGANOIDS AS AN IN VITRO MODEL: MINI-ORGANS IN THE LAB

1



Adapted from publication (in Dutch):

Organoïden als in-vitro model: mini-organen in het laboratorium

E. Driehuis and H. Clevers

Nederlands Tijdschrift voor Oncologie, November 2018, pages 244-251)

ABSTRACT

Organoids are three-dimensional structures cultured from adult, embryonal or induced pluripotent stem cells that have become widely used in scientific research. These structures, that retain both functional and structural characteristics of the tissue of origin, can nowadays be established from many different tissues, diseased or healthy. This type of culture allows for the study of patient-specific tissues and their function in the lab. Organoids, especially adult stem cell-derived organoids, also hold great potential for clinical application. Patient-derived organoids have been shown to predict patient response. This has been proven for organoids derived from cystic fibrosis patients, but also seems to hold true for cancer-derived organoids. Recent publications reveal a correlation between the drug response of tumor-organoids and the tumor response in the clinic. This suggests that organoids hold great potential for personalized medicine. In this article, we provide an overview of what organoids are, how they can be used, and how – in our opinion- they might contribute to oncology research.

E. Driehuis^{1,2} and H. Clevers^{1,2,3}

¹ Oncode Institute, Hubrecht Institute, Royal Netherlands Academy of Arts and Sciences (KNAW),
Utrecht, The Netherlands

² University Medical Center (UMC) Utrecht, Utrecht, The Netherlands

³ Princess Maxima Center, Utrecht, The Netherlands

STEM CELLS

There are two types of stem cells. Pluripotent stem cells (PSCs) only exist shortly after conception and can divide to produce all cell types of the human body. These natural PSCs can be isolated from early embryos and -using the right culture conditions -can be grown indefinitely in the laboratory as 'embryonic stem cells' (ESCs) (1). Additionally, Shinya Yamanaka showed in 2006 that a relatively simple genetic manipulation of adult skin cells can result in the formation of 'synthetic' PSCs. These cells were named induced Pluripotent Stem Cells (iPSCs) (2), and can be used in the laboratory in a fashion similar to ESCs. Adult stem cells (ASCs) remain present in most tissues of the human body throughout adulthood. ASCs are more specialized than PSCs and can divide to produce cells of the organ in which they reside. ASCs are organ-specific and seem to be present in almost all organs. They are responsible for maintaining 'their' organ: they can replace cells that are lost by disease or damage by cell division. There are many types of ASCs, many of which still remain to be discovered.

ORGANOIDS

Organoids, defined here as three-dimensional, self-organizing structures that can be grown from stem cells (3–5), allow researchers to study organ-structure and function in the lab. Sasai and colleagues described the culture of PSCs in "balls of neural cells that self-organize" (6). Around the same time, Sato et al. showed that organoids can be grown from the intestinal epithelium of adult mice. These "mini guts" were grown from ASCs residing in this epithelium, and were shown to contain all cell types that can be found in the intestinal epithelium of the mouse (7).

Organoids can be classified according to the stem cells of which they are derived: PSCs or ASCs. Organoids grown from PSCs can contain cell types from all three germ layers. Amongst others, PSC-derived organoids have been described for brain, retina, thyroid, kidney, intestine, stomach, lung and liver (8–14). Different differentiation protocols can be applied to differentiate PSCs into different types of organoids, depending on the organ aspired to model. Influenced by the type and timing of the growth factors to which the PSCs are exposed, different cell types can be found in these structures. As PSC-derived organoids can be grown from human cells, they provide the unique opportunity to model (part of) embryonal organ development *in vitro*.

ASC-derived organoids only contain cells specific to the organ of which the stem cells were initially derived. In contrast to ESCs or iPSCs, epithelial ASCs can only give rise to daughter cells of epithelial origin. Organoids derived from ASCs have been described for intestine, stomach, salivary gland, esophagus, pancreas, liver, breast, lung, prostate, taste bud, kidney, ovarium, oral mucosa and bladder (Figure 2) (7,8,15–30). ASC-derived organoids are a good model to study tissue-specific stem cell plasticity. Moreover, as ASC-derived organoids can be used to expand patient-specific (tumor) material, they



might serve as a platform to aid the implementation of personalized medicine. Figure 1 shows intestinal organoids viewed through a brightfield light microscope and highlights the presence of multiple intestinal epithelium cell types within one organoid.

When compared to conventional 2D cell lines, organoids more closely resemble the organ of which they are derived in multiple ways. Firstly, as they are grown in 3D, organoids can -to a certain extent- recapitulate the 3D organization of the tissue *in vivo*. Secondly, organoids can consist of multiple cell types. Thirdly, organoids can be grown long-term without genetic or phenotypical changes. This was not possible before; classical 2D cell lines require immortalization. For these reasons, organoids might be regarded as the 'missing link' between 2D cell lines and animal models (31).

Organoids in oncological research

In this review, we discuss the potential of organoid technology for translational oncological research (Figure 3). As ASC-derived organoids are especially suited for this application, the remainder of this review will focus on this type of organoids. This does not mean that PSC-derived organoids cannot be used to study the origin or treatment of cancer. For example, Crespo and colleagues recently showed that iPSC-derived organoids established from patients with familial adenomatous polyposis behaved differently than those established from healthy controls (30). These mini-organs were subsequently used to search for drugs that reverted this altered behavior back to a wildtype phenotype.

Genetic modification of organoids

Organoids can be genetically modified to study the effect of certain (oncogenic) genetic alterations. CRISPR/CAS9 genome editing is a widely applied technique used to introduce genetic alterations. CRISPR/CAS9, originally a bacterial defense mechanism against viruses, was modified to allow genome editing of eukaryotic cells. Using this technique, one can virtually create any desired genetic alteration in any location in the genome (32,33). One year after the introduction of this technique, it was shown that CRISPR/CAS9 can also be applied in organoids (34). Since then, many studies have shown that a combination of these two techniques leads to valuable insights. For example, in 2016, two studies showed that four common oncogenic mutations could be sequentially introduced in healthy human colon organoids (35,36). In this way, tumorigenesis (the process of tumor formation) could be modelled *in vitro*. Following the 'Vogelgram', mutations that are commonly found in colon cancer were introduced one by one. First, an activating *KRAS* mutation was introduced *in vitro*. Subsequently, the tumor suppressor genes *APC*, *TP53* and *SMAD4* were inactivated using the same technique. As expected, the introduction of these mutations resulted in changes in cell behavior that are indicative tumor cells. For example, the authors observed chromosomal instability, sustained growth in the absence of growth factors, and tumor formation upon transplantation into mice. Interestingly, resulting tumors showed different levels of malignancy, depending on which mutations

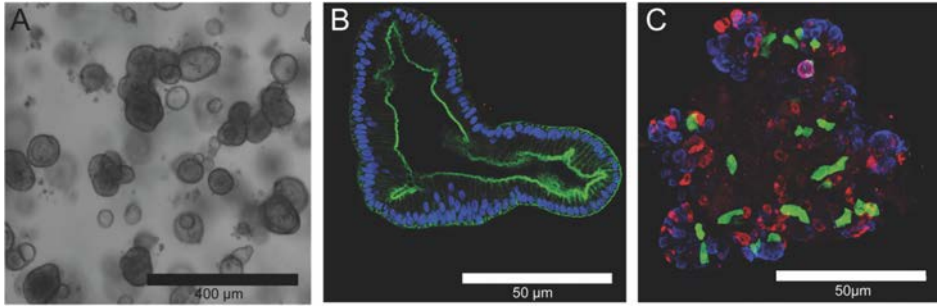


Figure 1. Human intestinal organoids. A. Human intestinal organoids as seen through a light microscope. Using the right culture conditions, the epithelial cells grow out into round structures containing multiple cell types. These structures are called organoids. B. Human intestinal organoids, labelled using immunofluorescence for the nucleus (DAPI, blue) and actin filaments (F-actin, green). C. Mouse intestinal organoids, labelled using immunofluorescence for the following cell type specific markers: chromogranin A (hormone producing cells, red), Cdk1 (Tuft cells, green), Lysozyme (Paneth cells, blue) (μm , micrometer)

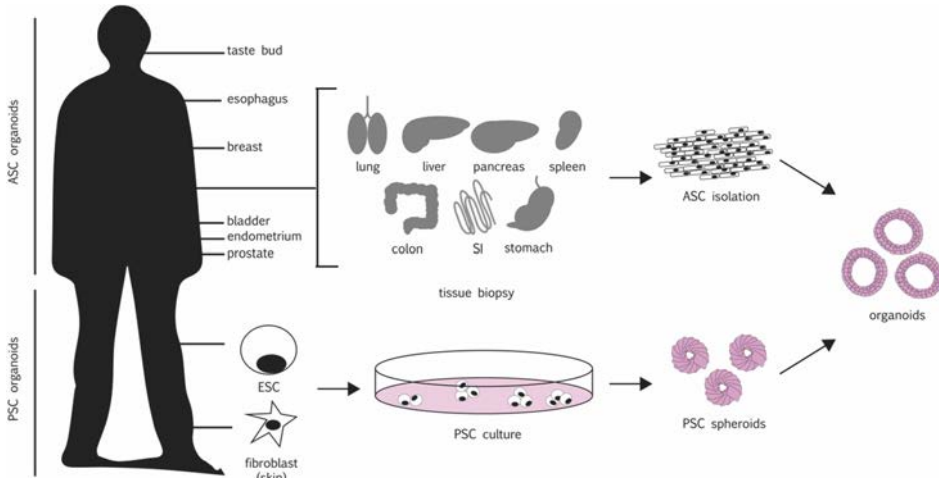


Figure 2. Organoids can be grown from ASCs and PSCs. ASC-derived organoids can be grown directly from tissue, but also from specific cell populations (for example Lgr5+ stem cells of the intestine) that can be obtained using cell sorting. After isolation, the cells are embedded in Matrigel or BME and cultured using media that contains growth factors. The exact composition of this medium depends on the cell type. PSC-derived organoids can be grown from both ESCs and iPSCs. iPSCs can be made from skin fibroblasts, as shown in Figure 2. Depending on the differentiation protocol applied, the stem cells can differentiate into different cell types. (Figure adapted from (55)) (ASC, adult stem cell; PSC, pluripotent stem cell; ESC, embryonal stem cell).

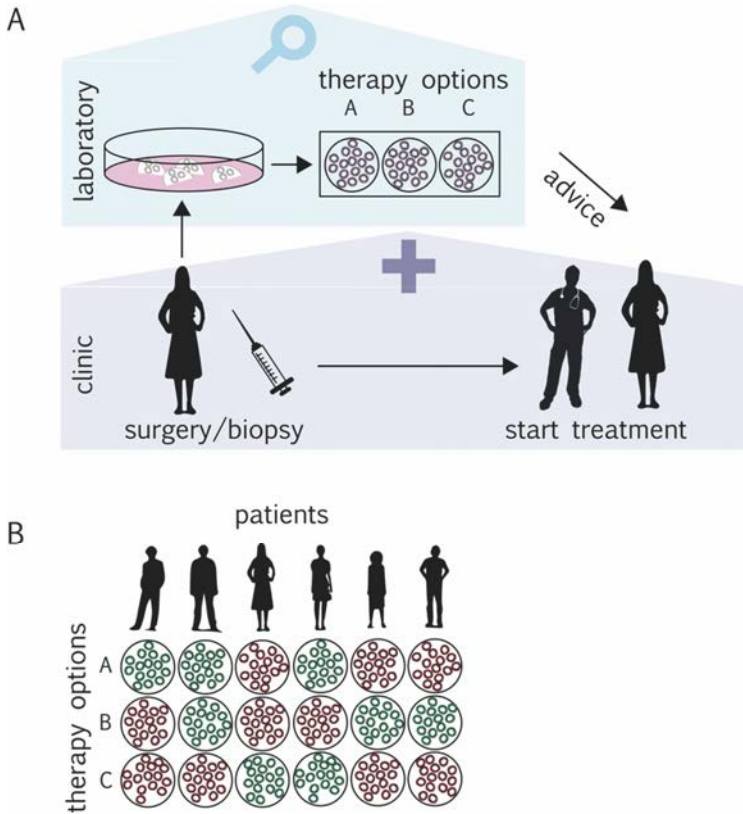


Figure 3. Organoids and their application in oncology. A. Organoids can be derived from tumor tissue (obtained from resection material or biopsies). After expansion, these structures can be used to test a number of drugs. If research shows that organoids indeed have a predictive potential, this organoid response could be used by the clinician to guide therapy decisions for the individual patient. B. In the future, a range of therapies could be tested on tumor-derived organoids for each individual patient. This would then allow to find the right drug for the right patient, by which organoids can contribute to personalized medicine.

were introduced. As these mutations were introduced one by one, the effect of individual mutations on cellular behavior could be studied. An additional advantage of CRISPR/CAS9 (is that it enables researchers to time the introduction of a specific alteration. In this way, also short-term effects of introduced modifications can be studied.

Other applications of CRISPR in organoids have also been reported. CRISPR/CAS9 has been used to study the role of tumor growth factor- β (TGF- β) signaling in tumor progression in both serrated and tubular adenomas (37). The authors of this work wanted to study the role of this growth factor in progression of these two histological and molecular distinct precursor lesions. Tubular adenomas, often carrying an inactivation in

APC, efficiently grew out as organoids when put in culture. As it was found that organoids could not be established from serrated adenomas that often carry an activating *BRAF* mutation, CRISPR/CAS9 was used to introduce an activating *BRAF* mutation (V600E) in wildtype organoids. These CRISPR-modified organoids were subsequently used to study the differential role of TGF- β in both tubular and serrated adenoma progression. The addition of TGF- β activated the growth of the *BRAF*-mutant organoids, whereas the organoids derived from tubular adenomas were actually inhibited by the addition of this growth factor.

Unraveling tumor heterogeneity

Organoid technology allows for the outgrowth of each individual (stem) cell of a tumor. Once established from individual stem cells, resulting organoid lines can be expanded to clonal lines that can be characterized in the laboratory. In this way, organoids can be used to study tumor heterogeneity. A recent study used this approach to study heterogeneity in colon cancer (16). Here, tumor-derived clonal organoid lines were DNA sequenced to determine which mutations were present. Additionally, sensitivity to different chemotherapeutics was determined for each of these clonal organoid lines. The authors of this work conclude that, between different organoid lines, there are large differences in both mutation status and drug sensitivity. As these organoid lines were derived from single cells, this work shows that individual (stem) cells within one tumor can be genetically different, resulting in differential drug responses. Of note, in all three tumors examined, resistant cells already existed for each of the tested drugs before treatment.

This approach enabled the researchers to study the biological changes that cause this heterogeneity. Moreover, this technique allows for the study of resistant cells in the laboratory to look for sensitivity to other compounds. This study would not have been possible with 2D cell lines, as the efficiency of establishment of cell lines is much lower. This work illustrates how organoid technology allows researchers to address research questions that could not be answered before the development of this technique.

Organoids in a living biobank

In recent years, the number of organoid biobanks has increased tremendously. An organoid biobank contains a collection of genetically and/or functionally characterized organoid lines with matched medical and/or genetic information of the donors. Organoid biobanks of esophagus (38), stomach (19,39), liver (40), colon (41–43), oral mucosa (22), breast (29), endometrium (44), pancreas (18,45) and bladder (28) cancer have been described. Moreover, organoids derived from metastasis of colon (43), prostate (46,47) and breast (29) tumors have been reported. Tumor organoids can be established from material obtained during tumor resection, from (needle) biopsies, or even from circulating tumor cells.

Organoid biobanks can be used to address a range of interesting biological questions. As an example, one could use a such a biobank to study the relationship between certain



mutations and response to selected therapies. A recent study showed that the response of breast cancer organoids to certain therapies could be linked to underlying genetic changes. For example, the sensitivity to the PARP-inhibitor Niraparib could be correlated to the presence of BRCA mutations in these cells. Additionally, it was shown that this difference in drug response was retained in the cells upon transplantation in mice. As matched clinical patient data was available for three patient-derived organoid lines, the response of the organoids could be linked to the response of the patients that received this therapy. In all three cases, the organoid response correlated to that of the patient (29).

A pancreas tumor biobank that was published at the beginning of 2018 was used to relate the behavior of cells *in vitro* to their genetic makeup (45). It was found that some of the established tumor organoids could grow in the absence of WNT ligand, a growth factor that is essential for the establishment of organoids from healthy pancreatic tissue. WNT signals are essential to many types of stem cell to prevent differentiation and thereby loss of stemness. The authors discovered that some of the tumor organoids could not grow without the addition of external WNT signals (by adding WNT ligand to the culture medium). Other lines could grow without WNT ligand, and were self-sufficient in providing WNT signals. This mechanism is analogous to that described in colon tumors that often carry APC mutations, making them independent of external WNT signals. Interestingly, mutations in WNT pathway genes are not commonly found in pancreatic cancer. Another important conclusion that could be drawn from this work, was that the behavior of the pancreas cancer organoids in culture was predictive for patient prognosis.

Organoids as predictor of clinical response

Organoid cultures allow researchers to expand and study patient material *in vitro*. Before the start of treatment, the effect of many different therapies can be tested on the patient-derived cells in the laboratory. For cystic fibrosis (CF), it was shown that organoid response *in vitro* is predictive for clinical response (48). For this reason, in the registration of the new CF drug Orkambi in the Netherlands, patients scoring positive on the organoid-test will get access to this drug. In the field of oncology, organoids also seem to have a predictive value. Vlachogiannis and colleagues established organoids from 110 colon cancer biopsies and showed in a number of these that the organoid response *in vitro* was predictive for the patient response to the same therapy (49). This study implies that, also in treating tumors, organoids can have predictive value, that holds the potential to aid the implementation of 'personalized medicine'. Also other studies have shown a correlation between patient and organoid response, although in lower numbers of patients (15,22,29). Additionally, organoids could potentially be used to find additional therapeutic approaches for patients that show resistance to standard therapy.

Organoid trials in Dutch Oncology

In the Netherlands, there are currently two active trials that are comparable to the study of Vlachogiannis et al (49). The TUMOROID trial (NL49002.031.14) includes patients with


metastasized colon cancer, breast cancer, or non-small cell lung cancer. An extra biopsy is taken from participating patients, before the start of treatment (50). Organoids established from this biopsy are subsequently exposed to the therapy that the patient receives in the clinic. In this way, the predictive value of organoids in the setting of metastatic disease can be evaluated (50). Another comparable trial, named the OPTIC trial (NL61668.041.17) was initiated in March 2018. In this study, biopsies from metastatic colorectal cancer are collected to establish organoids. Again, the drug sensitivity of the organoids is determined and compared to the response of the patient, that received the same therapy in the clinic. The main difference between this trial and the previously mentioned TUMOROID trial, is the patient inclusion; the OPTIC trial focuses mainly on first- line patients that were not treated before.

To our knowledge, these are the only currently running clinical trials in the Netherlands that are exploring the predictive value of organoid technology in an oncological setting. However, there are multiple studies that use DNA sequencing to determine mutation status of relevant genes and subsequently correlate this to therapy response. Such trials (including CPCT and DRUP) can potentially be expanded to include organoid establishment. This would allow to compare the potential of both 'mutation status' and 'organoid response' to predict patient response.

Lastly, a trial similar to those described above is initiated in the UMC Utrecht. This trial (ONCODE-P2018-0003) will correlate the response of patients with squamous cell carcinoma of the head and neck to the *in vitro* response of organoids derived from these tumors. Prior to start of treatment, organoids will be established from resection material or biopsies, and will be exposed to the treatment the patient will receive in the clinic. The aim of this study is to see if organoids can predict the response of these patients, and -if so- can contribute to a personalized medicine approach in this patient group. This is especially relevant in this setting, as there is a large group of patients that receive chemotherapy and eventually do not respond. Currently, there are no good biomarkers to predict this response prior to the start of therapy.

The future of organoids: critical remarks

Organoid technology, as any technique, comes with its limitations. Organoids are grown in Basement Membrane Extract (BME) or Matrigel, a gel rich in extracellular matrix proteins. The use of these gels allows the growth of organoids in 3D, as they function as an *in vitro* basal lamina. Organoids are grown in completely defined medium lacking serum, to which specific growth factors are added. Which growth factors are required depends on which tissue the researchers wants to expand. Both BME or Matrigel and used growth factors are expensive, which makes organoids cultures much more expensive than 'classical' 2D cell lines. It is important to realize that the culture conditions of organoids can influence the behavior of the cells *in vitro*. For example, organoids are often grown in medium rich in EGF. When sensitivity to EGF-inhibiting therapies are determined in this system, this EGF concentration directly influences the measured IC50 values. Of note,



serum (a standard component of 2D cell line medium) also contains such growth factors in high concentrations.

Depending on their origin, organoids can grow slower than cell lines, which can lead to longer experiments. This growth speed is -especially for application of this culture technique in personalized medicine- a relevant limitation. If organoids will be used in the future to select the right treatment for the right patient, the time required to expand organoids from patient tissue is essential, since treatment needs to be initiated as soon as possible.

Despite the fact that organoids can be grown from many different tumor- and tissue types, the outgrowth efficiency varies per tumor type, and ranges from 30 to 90%. Although this efficiency is higher than for 2D cell lines, where efficiency ranges from 0.1 to 1%, this is an important side note, especially in light of a personalized approach. This efficiency or 'take-rate', is depending on the amount of tissue, the type of tissue, (pre)treatment of the patient and contamination of tumor tissue with healthy epithelium or necrotic tissue.

Organoids grown from biopsies or resection material are established from the (cancer) stem cells present in this tissue. Seino et al. showed that not every tumor cell will give rise to an organoid when put in culture (45). It is therefore possible that tumor heterogeneity present at initiation of the culture, is lost upon organoid establishment, when certain clones grow faster than others in the used culture conditions. Additionally, it is possible that the piece of tissue that is used to establish an organoid culture is not representative of the entire tumor. Consequentially, this will result in an organoid line that does not represent the entire tumor. Quality checks can be introduced to validate this before continuing analysis. For example, validation of certain genetic alterations could be performed prior to further analysis. Moreover, Voest and colleagues have shown that cultured colorectal cancer organoids do recapitulate tumor heterogeneity in culture (43).

Another important side note that was already mentioned previously, is that ASC-derived organoids only consist of epithelial cells. In the case of carcinoma, tumor cells are therefore enriched *in vitro*, while immune cells, endothelial cells and fibroblast disappear over time from the culture. This is actually an advantage for mutation calling, as 'cancer-driving' genetic alterations can be detected in 100% of the cells whilst contaminating non-epithelial cells disappear under the culture conditions optimized for epithelial cells. However, it is important to keep in mind that, organoids might not be a proper model to address research questions involving the interaction of tumor cells with non-epithelial cells. *In vitro* 'co-cultures', where organoids are grown together with other cell types (such as immune cells or endothelial cells) might help overcome these limitations. Such co-cultures have recently been described (51–54).

CONCLUSION

Organoids are self-organizing structures grown from stem cells that can be used to model organs in the lab. These 'mini-organs' allow researchers to answer biological questions regarding pathophysiology and cancer therapy. First studies indicate that patient response can be predicted from the *in vitro* response of patient-derived organoids. Organoid technology might therefore aid personalized therapy in the future. This potential predictive value of tumor-derived organoids needs to be tested in larger patient cohorts. However, before the introduction of this technique, certain limitations of organoid culture need to be overcome. The first large scale observational studies that investigate the predictive potential of organoid cultures in the treatment of cancer patients have started in recent years.


ACKNOWLEDGEMENTS

We would like to thank Yorick Post, Fjodor Yousef Yengej and Frans Schutgens for critically reading this manuscript. We would like to thank Joep Beumer for contributing the images of Figure 1. We would like to thank Janine Roodhart for her input on clinical trials involving organoids in the Netherlands.

REFERENCES

1. Thomson JA. Embryonic Stem Cell Lines Derived from Human Blastocysts. *Science* (80-). 1998;282(5391):1145–7.
2. Takahashi K, Yamanaka S. Induction of Pluripotent Stem Cells from Mouse Embryonic and Adult Fibroblast Cultures by Defined Factors. *Cell*. 2006;126(4):663–76.
3. Kretzschmar K, Clevers H. Organoids: Modeling Development and the Stem Cell Niche in a Dish. *Dev Cell*. 2016;38(6):590–600.
4. Eiraku M, Sasai Y. Mouse embryonic stem cell culture for generation of three-dimensional retinal and cortical tissues. *Nat Protoc*. 2012;7(1):69–79.
5. Lancaster M a., Knoblich J a. Organogenesis in a dish: modeling development and disease using organoid technologies. *Science*. 2014;345:1247125.
6. Eiraku M, Watanabe K, Matsuo-Takasaki M, Kawada M, Yonemura S, Matsumura M, et al. Self-Organized Formation of Polarized Cortical Tissues from ESCs and Its Active Manipulation by Extrinsic??Signals. *Cell Stem Cell*. 2008;3(5):519–32.
7. Sato T, Vries RG, Snippert HJ, van de Wetering M, Barker N, Stange DE, et al. Single Lgr5 stem cells build crypt-villus structures in vitro without a mesenchymal niche. *Nature*. 2009;459(7244):262–5.
8. Dye BR, Hill DR, Ferguson MA, Tsai Y-H, Nagy MS, Dyal R, et al. In vitro generation of human pluripotent stem cell derived lung organoids. *Elife*. 2015;4:e05098.
9. Lancaster MA, Renner M, Martin C-A, Wenzel D, Bicknell LS, Hurler ME, et al. Cerebral organoids model human brain development and microcephaly. *Nature*. 2013;501(1):373–9.
10. Longmire TA, Ikonomou L, Hawkins F, Christodoulou C, Cao Y, Jean JC, et al. Efficient derivation of purified lung and thyroid progenitors from embryonic stem cells. *Cell Stem Cell*. 2012;10(4):398–411.
11. McCracken KW, Catá EM, Crawford CM, Sinagoga KL, Schumacher M, Rockich BE, et al. Modelling human development and disease in pluripotent stem-cell-derived gastric organoids. *Nature*. 2014;516(7531):400–4.
12. Spence JR, Mayhew CN, Rankin SA, Kuhar MF, Vallance JE, Tolle K, et al. Directed differentiation of human pluripotent stem cells into intestinal tissue in vitro. *Nature*. 2011;470(7332):105–9.
13. Takasato M, Er PX, Becroft M, Vanslambrouck JM, Stanley EG, Elefanty AG, et al. Directing human embryonic stem cell differentiation towards a renal lineage generates a self-organizing kidney. *Nat Cell Biol*. 2014;16(1):118–26.
14. Takebe T, Zhang R-R, Koike H, Kimura M, Yoshizawa E, Enomura M, et al. Generation of a vascularized and functional human liver from an iPSC-derived organ bud transplant. *Nat Protoc*. 2014;9(2):396–409.
15. Tiriác H, Belleau P, Engle DD, Plenker D, Deschênes A, Somerville T, et al. Organoid profiling identifies common responders to chemotherapy in pancreatic cancer. *Cancer Discov*. 2018;
16. Roerink SF, Sasaki N, Lee-Six H, Young MD, Alexandrov LB, Behjati S, et al. Intra-tumour diversification in colorectal cancer at the single-cell level. *Nature*. 2018;556(7702):457–62.
17. Snover DC. Update on the serrated pathway to colorectal carcinoma. *Hum Pathol*. 2011;42(1):1–10.
18. Boj SF, Hwang C-I II, Baker LA, Chio IIC, Engle DD, Corbo V, et al. Organoid models of human and mouse ductal pancreatic cancer. *Cell*. 2015;160(1):324–38.
19. Bartfeld S, Bayram T, Van De Wetering M, Huch M, Begthel H, Kujala P, et al. In vitro expansion of human gastric epithelial stem cells and their responses to bacterial infection. *Gastroenterology*. 2015;148(1):126-136.e6.

20. Ren W, Lewandowski BC, Watson J, Aihara E, Iwatsuki K, Bachmanov AA, et al. Single Lgr5- or Lgr6-expressing taste stem/progenitor cells generate taste bud cells ex vivo. *Proc Natl Acad Sci U S A*. 2014;111(46):16401–6.
21. Hill SJ, Decker B, Roberts EA, Horowitz NS, Muto MG, Worley MJ, et al. Prediction of DNA Repair Inhibitor Response in Short Term Patient-Derived Ovarian Cancer Organoids. *Cancer Discov*. 2018 Sep;
22. Driehuis E, Kolders S, Spelier S, Lohmussaer K, Willems SM, Devriese LA, et al. Oral mucosal organoids as a potential platform for personalized cancer therapy. *Cancer Discov*. 2019 Jan 1;CD-18-1522.
23. Huch M, Dorrell C, Boj SF, Van Es JH, Li VSWW, Van De Wetering M, et al. In vitro expansion of single Lgr5+ liver stem cells induced by Wnt-driven regeneration. *Nature*. 2013;494(7436):247–50.
24. Schutgens F, Rookmaaker MB, Margaritis T, Rios A, Ammerlaan C, Jansen J, et al. Tubuloids derived from human adult kidney and urine for personalized disease modeling. *Nat Biotechnol*. 2019;37(3):303–13.
25. Mullenders J, de Jongh E, Brousalı A, Roosen M, Blom JPA, Begthel H, et al. Mouse and human urothelial cancer organoids: A tool for bladder cancer research. *Proc Natl Acad Sci*. 2019 Mar 5;116(10):4567 LP – 4574.
26. Karthaus WR, laquinta PJ, Drost J, Gracanin A, Van Boxtel R, Wongvipat J, et al. Identification of multipotent luminal progenitor cells in human prostate organoid cultures. *Cell*. 2014;159(1):163–75.
27. Huch M, Bonfanti P, Boj SF, Sato T, Loomans CJM, van de Wetering M, et al. Unlimited in vitro expansion of adult bi-potent pancreas progenitors through the Lgr5/R-spondin axis. *EMBO J*. 2013;32(20):2708–21.
28. Lee SH, Hu W, Matulay JT, Silva M V., Owczarek TB, Kim K, et al. Tumor Evolution and Drug Response in Patient-Derived Organoid Models of Bladder Cancer. *Cell*. 2018;173(2):515-528.e17.
29. Sachs N, de Ligt J, Kopper O, Gogola E, Bounova G, Weeber F, et al. A Living Biobank of Breast Cancer Organoids Captures Disease Heterogeneity. *Cell*. 2018 Jan;172(1–2):373-386.e10.
30. Crespo M, Vilar E, Tsai S-Y, Chang K, Amin S, Srinivasan T, et al. Colonic organoids derived from human induced pluripotent stem cells for modeling colorectal cancer and drug testing. *Nat Med*. 2017;23(7):878–84.
31. Fatehullah A, Tan SH, Barker N. Organoids as an in vitro model of human development and disease. *Nat Cell Biol*. 2016;18(3):246–54.
32. Gasiunas G, Barrangou R, Horvath P, Siksnyš V. Cas9–crRNA ribonucleoprotein complex mediates specific DNA cleavage for adaptive immunity in bacteria. 2012;109(39):2579–86.
33. Jinek M, Chylinski K, Fonfara I, Hauer M, Doudna JA, Charpentier E. A Programmable Dual-RNA – Guided DNA Endonuclease in Adaptive Bacterial Immunity. 2012;337(August):816–22.
34. Schwank G, Koo BK, Sasselı V, Dekkers JF, Heo I, Demircan T, et al. Functional repair of CFTR by CRISPR/Cas9 in intestinal stem cell organoids of cystic fibrosis patients. *Cell Stem Cell*. 2013;13(6):653–8.
35. Drost J, van Jaarsveld RH, Ponsioen B, Zimmerlin C, van Boxtel R, Buijs A, et al. Sequential cancer mutations in cultured human intestinal stem cells. *Nature*. 2015;521(7550):43–7.
36. Matano M, Date S, Shimokawa M, Takano A, Fujii M, Ohta Y, et al. Modeling colorectal cancer using CRISPR-Cas9-mediated engineering of human intestinal organoids. *Nat Med*. 2015;21(3):256–62.
37. Fessler E, Drost J, van Hooff SR, Linnekamp JF, Wang X, Jansen M, et al. TGFβ signaling directs serrated adenomas to the mesenchymal

- 
- colorectal cancer subtype. *EMBO Mol Med.* 2016;8(7):e201606184.
38. Sato T, Stange DE, Ferrante M, Vries RGJ, Van Es JH, Van Den Brink S, et al. Long-term expansion of epithelial organoids from human colon, adenoma, adenocarcinoma, and Barrett's epithelium. *Gastroenterology.* 2011;141(5):1762–72.
 39. Seidlitz T, Merker SR, Rothe A, Zakrzewski F, von Neubeck C, Grutzmann K, et al. Human gastric cancer modelling using organoids. *Gut.* 2018 Apr;
 40. Broutier L, Mastrogiovanni G, Verstegen MM, Francies HE, Gavarró LM, Bradshaw CR, et al. Human primary liver cancer-derived organoid cultures for disease modeling and drug screening. *Nat Med.* 2017;23(12):1424–35.
 41. Van De Wetering M, Francies HE, Francis JM, Bounova G, Iorio F, Pronk A, et al. Prospective derivation of a living organoid biobank of colorectal cancer patients. *Cell.* 2015;161(4):933–45.
 42. Fujii M, Shimokawa M, Date S, Takano A, Matano M, Nanki K, et al. A Colorectal Tumor Organoid Library Demonstrates Progressive Loss of Niche Factor Requirements during Tumorigenesis. *Cell Stem Cell.* 2016;18(6):827–38.
 43. Weeber F, van de Wetering M, Hoogstraat M, Dijkstra KK, Krijgsman O, Kuilman T, et al. Preserved genetic diversity in organoids cultured from biopsies of human colorectal cancer metastases. *Proc Natl Acad Sci U S A.* 2015 Oct 27;112(43):13308–11.
 44. Turco MY, Gardner L, Hughes J, Cindrova-Davies T, Gomez MJ, Farrell L, et al. Long-term, hormone-responsive organoid cultures of human endometrium in a chemically defined medium. *Nat Cell Biol.* 2017;19(5):568–77.
 45. Seino T, Kawasaki S, Shimokawa M, Tamagawa H, Toshimitsu K, Fujii M, et al. Human Pancreatic Tumor Organoids Reveal Loss of Stem Cell Niche Factor Dependence during Disease Progression. *Cell Stem Cell.* 2018 Mar 1;22(3):454–467.e6.
 46. Gao D, Vela I, Sboner A, Iaquinta PJ, Karthaus WR, Gopalan A, et al. Organoid cultures derived from patients with advanced prostate cancer. *Cell.* 2014;159(1):176–87.
 47. Drost J, Karthaus WR, Gao D, Driehuis E, Sawyers CL, Chen Y, et al. Organoid culture systems for prostate epithelial and cancer tissue. *Nat Protoc.* 2016;11(2):347–58.
 48. Dekkers JF, Wiegerinck CL, de Jonge HR, de Jong NWM, Bijvelds MJC, Nieuwenhuis EES, et al. A functional CFTR assay using primary cystic fibrosis intestinal organoids. *J Cyst Fibros.* 2012;11(7):S32.
 49. Vlachogiannis G, Hedayat S, Vatsiou A, Jamin Y, Fernández-mateos J, Khan K, et al. Patient-derived organoids model treatment response of metastatic gastrointestinal cancers. *Science (80-).* 2018;926(February):920–6.
 50. Weeber F, Ooft SN, Dijkstra KK, Voest EE. Tumor Organoids as a Pre-clinical Cancer Model for Drug Discovery. Vol. 24, *Cell Chemical Biology.* 2017. p. 1092–100.
 51. Nozaki K, Mochizuki W, Matsumoto Y, Matsumoto T, Fukuda M, Mizutani T, et al. Co-culture with intestinal epithelial organoids allows efficient expansion and motility analysis of intraepithelial lymphocytes. *J Gastroenterol.* 2016;51(3):206–13.
 52. Lindemans CA, Calafiore M, Mertelsmann AM, O'Connor MH, Dudakov JA, Jenq RR, et al. Interleukin-22 promotes intestinal-stem-cell-mediated epithelial regeneration. *Nature.* 2015;528(7583):560–4.
 53. Ibiza S, García-Cassani B, Ribeiro H, Carvalho T, Almeida L, Marques R, et al. Glial-cell-derived neuroregulators control type 3 innate lymphoid cells and gut defence. *Nature.* 2016;535(7612):440–3.
 54. Neal JT, Li X, Zhu J, Giangarra V, Grzeskowiak CL, Ju J, et al. Organoid Modeling of the Tumor Immune

Microenvironment. *Cell*. 2018
Dec;175(7):1972-1988.e16.

55. Driehuis E, Clevers H. CRISPR/Cas 9 genome editing and its applications in organoids. *Am J Physiol - Gastrointest Liver Physiol*. 2017;312(3):G257-65.

CHAPTER

ORAL MUCOSA ORGANOIDS AS A POTENTIAL PLATFORM FOR PERSONALIZED THERAPY



**ORAL MUCOSAL ORGANOID
AS A POTENTIAL PLATFORM
FOR PERSONALIZED
CANCER THERAPY**

2.1

ABSTRACT

Previous studies have described that tumor organoids can capture the diversity of defined human carcinoma types. Here, we describe conditions for long-term culture of human mucosal organoids. Using this protocol, a panel of 31 head and neck squamous cell carcinoma (HNSCC)-derived organoid lines was established. This panel recapitulates genetic and molecular characteristics previously described for HNSCC. Organoids retain their tumorigenic potential upon xenotransplantation. We observe differential responses to a panel of drugs including cisplatin, carboplatin, cetuximab and radiotherapy *in vitro*. Additionally, drug screens reveals selective sensitivity to targeted drugs that are not normally used in the treatment of HNSCC patients. These observations may inspire a personalized approach to the management of HNSCC and expand the repertoire of HNSCC drugs.

Else Driehuis¹, Sigrid Kolders¹, Sacha Spelier¹, Kadi Löhmußaar¹, Stefan M. Willems², Lot A. Devriese³, Remco de Bree⁴, Emma J. de Ruiter², Jeroen Korving¹, Harry Begthel¹, Johan H. van Es¹, Veerle Geurts¹, Gui-Wei He¹, Richard H. van Jaarsveld¹, Rurika Oka⁵, Mauro J. Muraro^{1,6}, Judith Vivié^{1,6}, Maurice M.J.M. Zandvliet⁷, Antoni P.A. Hendrickx⁸, Nino Iakobachvili⁹, Priya Sridevi¹⁰, Onno Kranenburg¹¹, Ruben van Boxtel⁵, Geert Kops¹, David A. Tuveson¹⁰, Peter J. Peters⁹, Alexander van Oudenaarden¹, Hans Clevers^{*1,5}

¹ Oncode Institute, Hubrecht Institute, Royal Netherlands Academy of Arts and Sciences (KNAW) and University Medical Center Utrecht, The Netherlands

² Department of Pathology, University Medical Center Utrecht, The Netherlands

³ Department of Medical Oncology, University Medical Center Utrecht, The Netherlands

⁴ Department of Head and Neck Surgical Oncology, University Medical Center Utrecht, The Netherlands

⁵ Princess Maxima Center, Utrecht, The Netherlands

⁶ Single Cell Discoveries, Uppsalalaan 8, 3584CT, Utrecht, The Netherlands

⁷ Department of Clinical Sciences of Companion Animals, Faculty of Veterinary Medicine, Utrecht University, Netherlands

⁸ Department of Medical Microbiology, University Medical Center Utrecht, the Netherlands

⁹ M4I Division of Nanoscopy, Maastricht University, 6229 ER, Maastricht, The Netherlands

¹⁰ Cold Spring Harbor Laboratory, Cold Spring Harbor, New York, United States

¹¹ Utrecht Platform for Organoid Technology (U-PORT), Utrecht Medical Center Utrecht, The Netherlands

* Corresponding author

INTRODUCTION

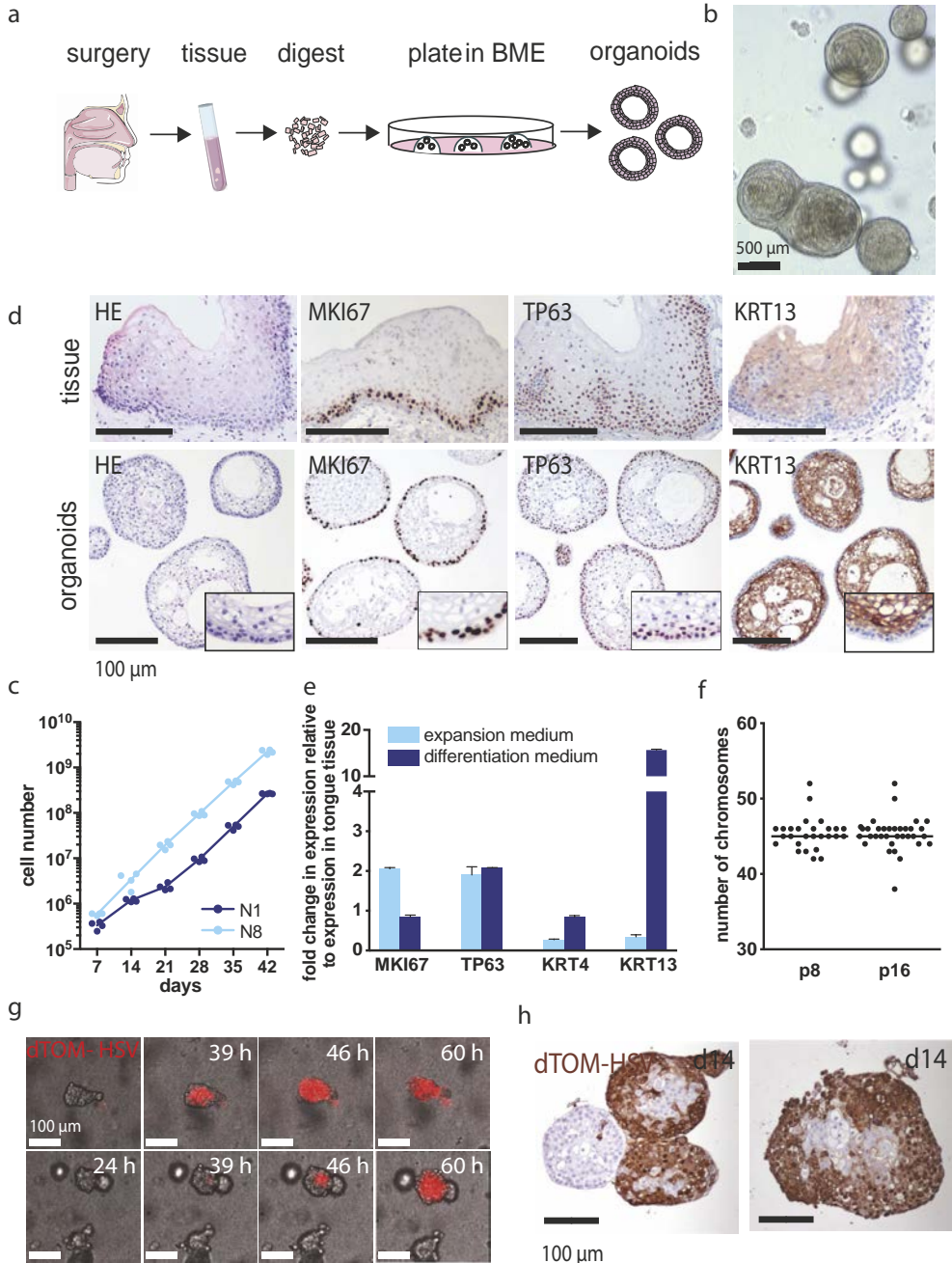
The oral cavity, pharynx and larynx are lined by a stratified mucosa that protects the underlying structures. These epithelia are keratinizing or non-keratinizing, depending on the anatomical location (1). Neoplasias commonly arise in this epithelium, with a worldwide incidence of over half a million patients a year (2). Well-known risk factors are alcohol and tobacco (3). Treatment of head and neck squamous cell carcinoma (HNSCC) is difficult, partly because of their anatomical location that complicates surgery, and partly due to the highly variable treatment response. Advanced cases require combinations of surgery, radiotherapy and chemotherapy. Taken together, this results in relapse rates of over 50% (4). Currently there are no reliable models to predict therapy outcome and guide treatment decisions.

In vitro studies of this epithelium have relied on tumor-derived 2D cell lines (5) and on primary keratinocyte cultures (6). Success rates to establish HNSCC-derived cell lines range from 11-33% (7). For primary keratinocyte cultures, keratinocytes are grown on feeder cells (mouse fibroblasts) in 2D and have a limited lifespan. *In vitro* drug screens of 2D lines have been used to characterize variability in drug response among tumors and as a tool to understand resistance mechanisms of tumor cells (8,9). In an attempt to overcome limitations of these 2D systems (10,11), HNSCC lines have been replated in a 3D format. Compared to 2D cell lines, these 3D models better recapitulate characteristics of *in vivo* HNSCC (12,13). In addition to *in vitro* models, HNSCC xenograft mouse models were introduced over thirty years ago (14). Moreover, transgenic mouse models have been developed to understand molecular drivers of HNSCC tumorigenesis (15). Although these models provided important insights in HNSCC, they are lacking the potential for a personalized approach. Recently, two studies have reported on the generation of 3D HNSCC cultures, giving an initial description of this technology (16,17).

The oral mucosa can be subject to viral infection (18). Herpes Simplex Virus (HSV) is amongst the most commonly encountered viral infections of the oral cavity (18). HSV is known to infect keratinocytes and give rise to herpes labialis (cold sores) (19). Infection with Human Papilloma Virus (HPV) is associated with oropharyngeal HNSCC and characterizes a genetically distinct subgroup of tumors with better prognosis than HPV HNSCC (20). *In vitro* culture systems to study the interaction of keratinocytes with HPV are limited to the use of immortalized cell lines, or to primary cells that can only be cultured short-term (21).

Protocols to grow organoids from adult human tissues have been described for single-layered (simple) or (pseudo)stratified epithelia, such as those that line the colon, intestine, liver, pancreas, stomach, esophagus, prostate, lung, breast, and fallopian tube and cancers derived thereof (22). Tumor organoids have previously been shown to phenocopy the tumor from which they are derived, allowing *in vitro* drug responses to be linked to genetic alterations present in the original tumor (22). A recent study on gastrointestinal cancers documented a strong correlation between patient clinical outcome and the response of the corresponding tumor organoids (23).

Here, we set out to establish organoids from the epithelial lining of the oral cavity, larynx and pharynx. Next, we apply these conditions to derive tumor organoids from HNSCC patients and to explore their potential to aid personalized therapy.




RESULTS

Organoids derived from healthy oral mucosa recapitulate morphological and functional characteristics and can be used to model oral mucosa pathology

2.1

To propagate organoid formation, we tested a range of media compositions described in previously published protocols for growth support of oral mucosa. Conditions that were successful to grow mouse tongue epithelium (see Figure S1A and S1B) were refined on human material obtained from surgical resections. In brief, the epithelial layer was micro-dissected from the surgical specimen to remove fat and muscle, digested in 0.125% trypsin, filtered and the resulting cell suspension was then plated in Basement Membrane Extract (BME), a Matrigel^R equivalent (Figure 1A). Within the first few days after plating, organoids grew out from single cells or small cell clumps (Figure S2A and Movie S1). Over time, these organoids developed into dense structures, often with keratinized centers (Figure 1B). On average, organoids could be passaged within 10-14 days. After the first passages, organoids typically expanded exponentially, being passaged every ten days with a split ratio of 1:5 (Movie S2). We received surgical material from 40 patients, of which 26 (65%) grew out into organoids. Established organoid lines could be expanded long-term (> 15 passages) and could be cryopreserved and recovered successfully. We assessed

-
- ◀ **Figure 1. Organoids can be derived from healthy oral mucosa, recapitulate morphological and functional characteristics and can be used to study oral mucosa pathology.** A. Schematic outline of the digestion and initial culture condition of oral mucosa organoids. If the patient signs informed consent, tissue that is obtained via biopsy or resection is collected, digested using trypsin and subsequently plated. Over time, organoids grow out from the primary tissue. B. Brightfield microscopy image of an organoid lines derived from oral mucosa epithelium, *scalebar 500 μm*. C. Total cell numbers obtained from organoid cultures over the course of 6 weeks. Cell numbers were determined in two independently established normal oral mucosa organoid lines (N1 and N8). Counting was performed in quadruplicate. Quantification shows stable growth of the organoid lines. D. Hematoxylin and eosin (H&E) staining and immunostaining for MKI67, TP63 and oral mucosa specific KRT13 of paraffin-embedded N8 organoids and control tissue. As can be seen, proliferating basal cells (MKI67 and TP63 positive) reside in the periphery of the organoids, while more differentiated keratinocytes (KRT13 positive) reside in the center of the organoid. *Scalebar 100 μm*. E. Quantitative PCR of a normal oral mucosa organoid line (N5) for proliferation marker MKI67, basal cell marker TP63 and KRT13, Prior to RNA collection, growth factors were withdrawn from the medium to induce differentiation. Expression levels are calculated using $\Delta\Delta C_t$ method. For each marker, fold change in expression is shown relative to expression of this markers in human primary tongue tissue, which is set to 1. *n=3, individual data points are shown, bars represent average*. F. Number of chromosomes was determined for N8 organoids in early passage (p8) and later passage (p16) by metaphase spread analysis. G. Live cell imaging of dTOM-HSV infected organoids. Two organoids were followed over time and pictures of the following timepoints are depicted in this figure: t=0, 24, 39, 46 and 60 hours, *scalebar 100 μm*. H. Immunohistochemical staining for dTomato performed on paraffin-embedded organoids that were infected with HSV-dTomato and maintained in culture for two weeks, *scalebar 100 μm*.
-



proliferative potential over 5 passages in expansion medium (Figure 1C) and observed unabated exponential growth. Scanning electron microscopy revealed that organoids are composed of tightly connected cells (Figure S2B). Immunohistochemical staining for basal cell marker TP63 and proliferation marker MKI67 of paraffin-embedded organoids showed that the organoids recapitulate the tissue of origin. Proliferative MKI67⁺/TP63⁺ basal cells were located in the external organoid layer touching the basal membrane substitute BME, recapitulating the tissue of origin (Figure 1D). Differentiation marker KRT13 was detected in cells in the interior of the organoid. Characteristics of keratinocytes such as abundant tonofilaments and desmosomes were observed using transmission electron microscopy (Figure S2C). Upon withdrawal of growth factors from the medium, differentiation increased, as shown by >45 fold increase in KRT13 expression, and halted proliferation (decreased expression of MKI67) (Figure 1E, Figure S2D). Lastly, we assessed genetic stability of normal tongue epithelium- derived organoid by metaphase spread analysis and observed normal numbers of chromosomes at passage 6 (median 46±0.42, n=26) and at passage 16 (median 45±0.34, n=33) (Figure 1F).

Oral mucosa organoids can be productively infected with Herpes Simplex Virus and Human Papilloma Virus

We explored the use of this model to study viral infection with Herpes Simplex Virus type 1 (HSV1), a virus known to infect keratinocytes (19) and to give rise to herpes labialis (cold sores). Using fluorescence microscopy, we followed infection of organoids with tdTomato labelled HSV (24) (Figure S3A). Using live imaging, spreading of the infection in organoids was observed two days after initial infection (Figure 1G and movie S3). After two weeks in culture, infection had spread throughout entire organoids (Figure 1H). Infection of organoids resulted in an increase in viral DNA, which could be inhibited by the addition of acyclovir (viral TK inhibitor) in all three organoid lines tested (Figure S3B).

As HPV is known to contribute to oncogenesis of a subset of HNSCC tumors (3,25), HPV16 particles were used to infect oral mucosa organoids (26). Viral replication was quantified by increase in HPV DNA levels (Figure S3C). After splitting of the organoids, an increase in HPV DNA could be observed, implying lasting infection (Figure S3D). Lastly, transfer of filtered supernatant taken 12 days post infection from infected organoids, resulted in re-infection, proving virion production in organoids (Figure S3E). Taken together, we conclude that oral mucosa-derived organoids allow infection with HSV1 and HPV16, validating the organoid model as an *in vitro* model for mucosal pathology.

HNSCC tumoroids recapitulate molecular and morphological characteristics of the original tumor

We next set out to grow organoids from patient-derived HNSCC samples, either obtained from surgical resections or biopsies. We successfully established tumoroids from 31 patients, ranging in age from 48 to 91 (average age at diagnosis: 69). Tumoroids were

established from tumors originating in the oral cavity (floor of mouth, tongue and gingiva/alveolar process), pharynx, larynx, salivary gland, nasal cavity and neck (Figure 2A). Patient clinical data corresponding to established organoid lines can be found in Table S1. Of the 31 established tumoroid lines, 16 were fully characterized molecularly at the date of first submission (data on all others will be added when these become available). These lines were named T1, T2, T3 etc., while the corresponding normal epithelium-derived line of T1 was termed N1 etc. The success rate to establish organoids from tumor tissue was ~60%. Tumoroids grew either as dense structures (similar to the normal wildtype epithelial organoids) or as cystic structures (Figure S4 and S5). Tumoroids derived from different patients showed different morphologies, as based on brightfield microscopy (Figure S4) and H&E staining (Figure S5). Comparison of organoids with the original tumor tissue and adjacent normal epithelium of the same patient revealed tumor-specific histopathological changes that were retained in culture (Figure S6).

Comparing immunohistochemical stainings of the primary tumor specimens with the corresponding tumoroids revealed that these retained histological characteristics of the epithelial tumor cells (Figure 2B). However, as described for other adult tissue-derived organoids, tumoroids only contain the transformed epithelial tumor cells, but not the immune-, connective tissue- or vessel-elements. This was evident by the keratin staining that marks all cells of the organoids, but only the epithelial component of the tumor section (Figure 2B).

A complication of growing tumoroids from other carcinoma types has been the gradual overgrowth by normal wildtype organoids (27,28). Yet, to confirm the tumor identity of our tumoroids, several approaches were taken. Nutlin-3, an Mdm2 agonist, prevents the growth of TP53 wildtype cells (29). We observed that 10 out of the 14 lines tested (71%) grew in the presence of Nutlin-3 (Figure S7), in agreement with the ~75% of HNSCC carrying inactivating *TP53* mutations (30). For example, N1 organoids (TP53 wildtype) organoids died in the presence of Nutlin-3, whereas tumoroid line T1 did not (Figure 2C). TP53 staining on fixed organoid sections confirmed the TP53 status (Figure 2D). TP53 staining is caused by accumulation of mutant protein, a clinical parameter to determine the presence of mutant TP53 protein (31).

We performed transcriptome analysis of nine normal organoid lines and seven tumoroid lines. As a quality control, two tumor organoid lines (T1 and T3) were sequenced twice in two independent runs. Samples from independent runs clustered together. To determine the contribution of the cancerous state to the total variability in gene expression, principal component analysis (PCA) was performed. PCA revealed segregation of normal and tumor organoids into different clusters, with the exception of tumoroid line T6 (with confirmed mutations in *TP53* and *CDKN2A*) clustering within the normal wildtype organoid group, and normal line N10 not clustering with the other normal samples (Figure 2E). Additionally, we used DESEQ2 analysis to explore the potential to identify or validate tumor biomarkers using HNSCC organoids (32). A search for differentially expressed genes between normal

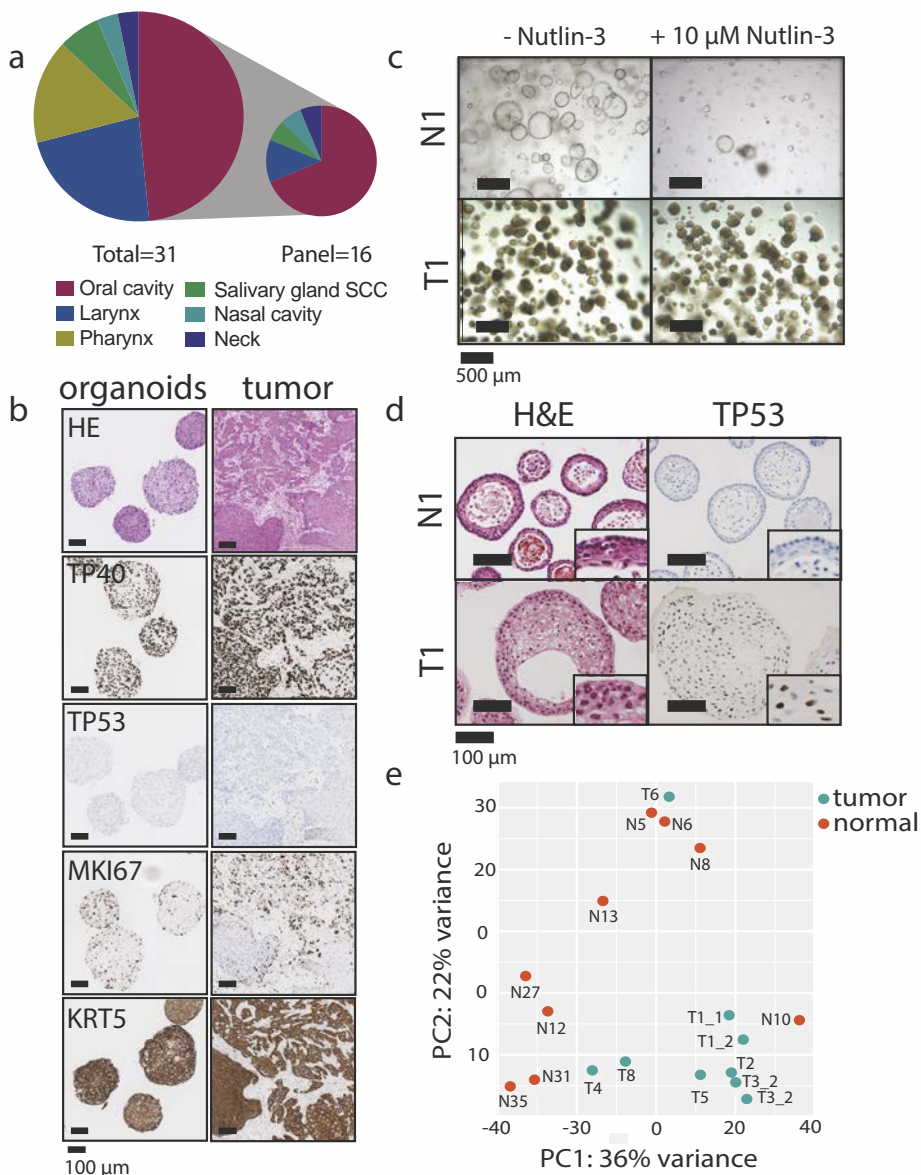
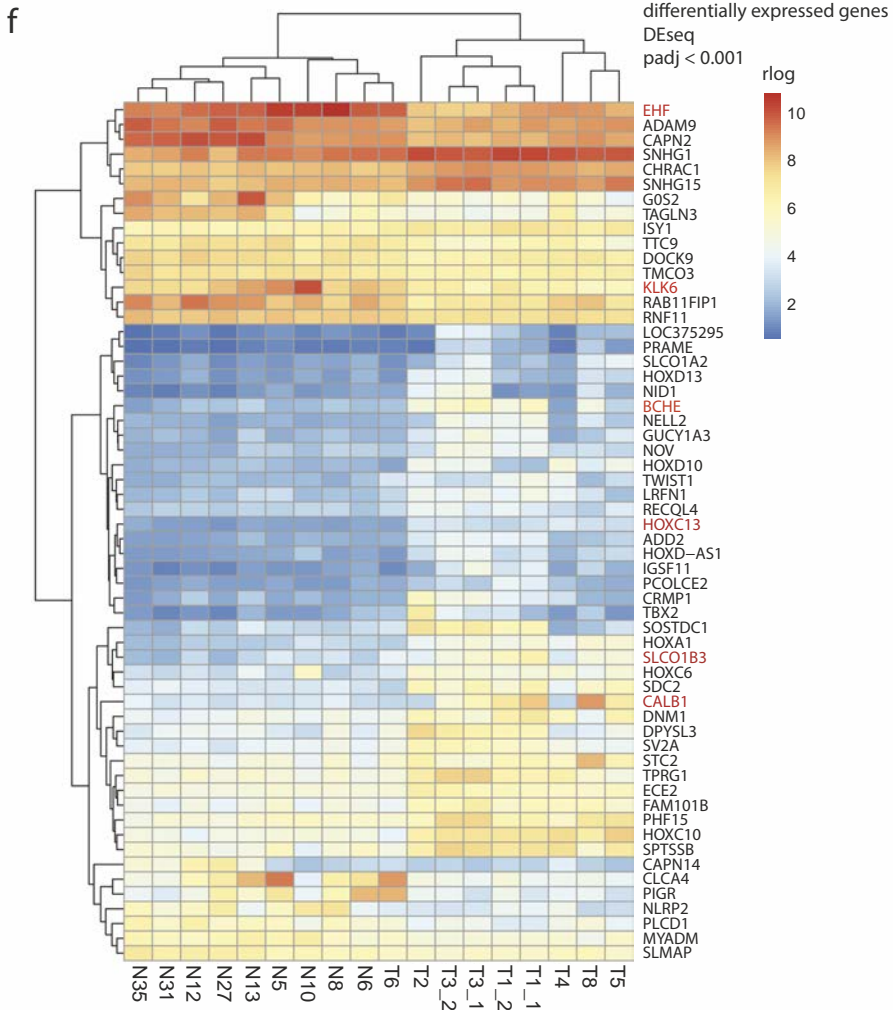


Figure 2. HNSCC organoids can be established and recapitulate functional and morphological characteristics of the tumor. A. Overview of the tumors of which organoids were established in this study and their anatomical location. B. Hematoxylin and eosin (H&E) staining and immunostaining for basal cell marker TP40, tumor suppressor TP53, proliferation marker MKI67 and KRT5 of paraffin-embedded T15 organoids and corresponding tissue. Scalebar, 100 μ m C. Organoids established from HNSCC and corresponding normal tissue of the same patient show a different response to Mdm2 agonist Nutlin-3. Scalebar 500 μ m D. H&E and immunostaining for TP53 performed on sections of paraffin-embedded organoids reveal differences in morphology and TP53 status of the two organoid lines. Scalebar 100 μ m. E. Principal component analysis of RNA sequencing data of 9 normal wildtype



► (orange) and 7 tumor organoid lines (blue). Two tumor samples were sequenced in two independent runs as a quality control. These samples cluster together. Tumor-derived organoid cluster together and away from the normal wildtype-epithelium derived organoids. There are two exceptions to this clustering as N10 and T6 do not cluster together with the other normal- and tumor-derived organoid lines, respectively.-F. Heatmap depicting expression of the 58 differentially expressed genes between normal- and tumor-derived organoids (padj<0.001) in the sequenced organoids. Blue indicates low expression, red indicates high expression. Differential expression was calculated as described in DESeq2 package (32). Genes marked in red are described in the text and were reported by others to be differential expressed in HNSCC. For these genes, Figure S8 shows the expression values relative to normal organoids.

and tumor samples resulted in detection of 857 genes ($p_{adj} < 0.0001$). Amongst the 58 most differentially expressed genes ($p < 0.01$) we found genes of which the expression has been described to be altered in HNSCC including *KLK6*, *SLCO1B3*, *HOXC13*, *CALB1*, *EHF* and *BCHE* (33–38) (Figure 2F, Figure S8, Table S2).

Tumoroids recapitulate genetic alterations found in HNSCC

Targeted sequencing (on a panel of 54 oncogenes or tumor suppressors relevant to HNSCC, in one case an extended oncopanel of 140 genes) ($n=14$, Figure 3A) or whole exome sequencing ($n=2$, Figure 3B) was performed on a subset of the HNSCC organoid lines (Table S3 and S4). The most commonly mutated gene *TP53* was genetically altered in 11 out of the 16 tumor lines (69%). As expected, no *TP53* mutations were detected in the Nutlin3-sensitive lines T8, T9, T10, T20 and T27. *PIK3CA* was altered in 7 of the 16 tumoroid lines. *KRAS* was mutated in four cases, although often mutations were detected at low frequency. *BRAF*, *CDKN2A*, *FAT1* and *PDGFRA* were mutated in two cases. Genes affected in one case include *ABL*, *ATR*, *ESR1*, *FGFR2*, *HRAS*, *MDM2*, *MET* and *VHL*. In three cases (T3, T5 and T8), we sequenced both the original tumor and the tumoroid line (see Figure S9) and observed an enrichment of the variant allele frequency (VAF) of the detected mutations. Most likely, this is due to the purely epithelial character of tumoroids, whereas the primary tumor sample also contains immune cells, vasculature and stromal components in addition to the tumor epithelial cells. As T5 and T8 were subjected to WES, mutations were also detected in genes that were not included in the targeted sequencing panel. Those mutation lists were filtered for those present in genes most commonly affected in HNSCC (39). Using this criterium, we detected pathogenic mutations in twenty (T5) and four (T8) HNSCC cancer-associated genes (Figure 3B). For both tumor organoids, corresponding normal organoids were also sequenced, which confirmed the absence of any of these mutations. Subsequently, we scrutinized all single nucleotide variants (SNVs) and small insertions or deletions (Indels) throughout the genome in the tumor and normal tissue as well as in N5 and T5 organoids (Figure 3C). For both samples, both the tumor tissue and the tumoroids showed SNVs and Indels that were absent from the normal tissue. Moreover, tumoroids largely recapitulated the genetic alterations that were detected in the tumor. Normal organoids and normal tissue lacked these genetic alterations, confirming that these organoids consisted of normal (non-tumor) cells.

HNSCC-derived organoids are chromosomally unstable *in vitro*

Chromosome mis-segregation underlies the aneuploidies frequently observed in human tumors (40). Increased mis-segregation rates result in the phenotype known as chromosomal instability (CIN), which is commonly observed in cancers, including HNSCC (41). To investigate whether CIN was also present in HNSCC tumoroids, we

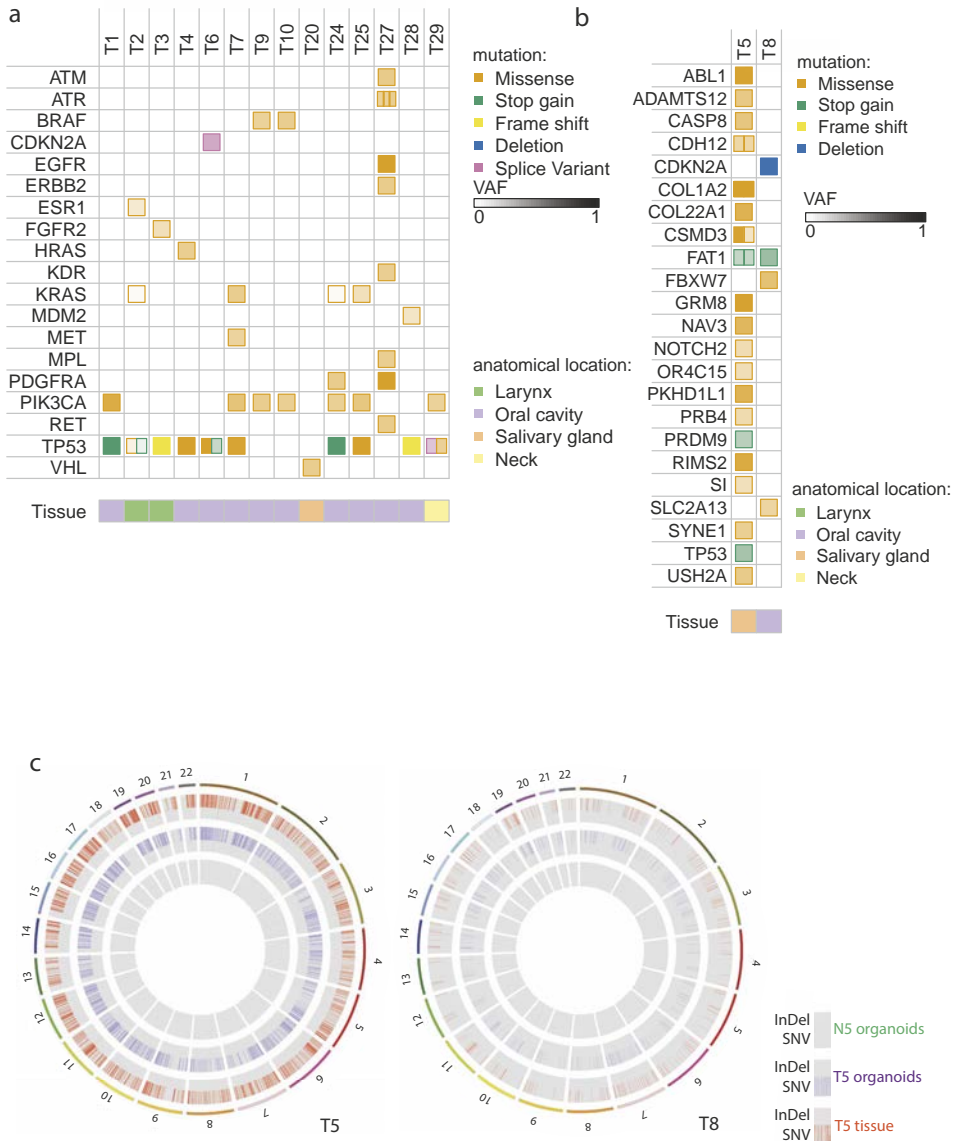


Figure 3. HNSCC-derived organoids recapitulate genetic alterations found in this tumor type.

A and B. Mutations detected in HNSCC-derived organoids that were sequenced using targeted sequencing (A) or WES (B). The color of the square indicates the type of mutation detected: missense (orange), stop/gain (green), frameshift (yellow), deletion (blue), splice acceptor (purple). Color intensities indicate the variant allele frequency (VAF) of the detected genetic alteration. Anatomical source of the organoid line is shown: oral cavity (purple), larynx (green) or parotis (orange). C. Circos plots of T5 and T8, showing the single nucleotide variants (SNV, outer track) and small insertions or deletions (Indels, inner track) for tumor tissue (orange), tumor organoids (purple) and wildtype organoids (green). All variants are shown relative to wildtype tissue.

assessed chromosome segregation in a matched normal and tumor organoid line. Organoids labelled with Histone2B-mNeon were imaged using a spinning-disc confocal microscope to visualize the chromatin during cell division (42). T1 had elevated levels of chromosome segregation errors as compared to its normal counterpart, N1 (Figure 4A, Movie S4 and S5). The majority of cells in N1 showed no signs of chromosome mis-segregation (Figure 4B), whereas T1 showed a variety of segregation errors, including anaphase bridges and a bi-nucleated cells undergoing multipolar division (Figure 4C and 4D, respectively). We conclude that T1 has acquired CIN during oncogenic transformation. CIN can result in aneuploidy, by the loss or gain of (parts of) chromosomes (40). In agreement, quantification of the number of chromosomes in cells of N1 and T1 using metaphase spreads revealed that this number was much more variable in T1 than it was in N1

(Figure 4E). Other tumoroid lines also carried aberrant chromosome numbers, with T3 and T4 being tetraploid (Figure 4F), whereas organoids derived from corresponding normal tissue contained normal numbers of chromosomes.

HNSCC tumoroids recapitulate characteristics of HNSCCs upon xenotransplantation

To assess whether tumorigenic potential of the cultured HNSCC cells was retained, we subcutaneously transplanted tumoroids into mice. Injection of the normal organoids did not result in outgrowth, whereas transplantations of all three tumor lines yielded macroscopically visible tumors after six weeks in at least two out of three mice (n=3 for each organoid line) (Figure 5A). For all tumors, H&E staining revealed stratification and keratinization characteristic of HNSCC (Figure 5B and S10). Staining for human nuclei showed positive, thus proving the origin of the tumors from the injected human-derived organoids. Comparison of proliferating cells, measured by MKI67 staining, revealed differences in proliferation among the distinct organoid lines (Figure 5C). These characteristics were retained between mice that were transplanted with the same organoid line (Figure S10).

The tumor cells displayed levels of atypia that were regarded cancerous (assessed by a pathologist). Tripolar mitotic figures and nuclear pleomorphism were observed (Figure 5D). Moreover, muscle invasion was observed in one case (Figure 5E). Taken together, this shows that HNSCC organoids retain tumorigenic potential in culture and can form HNSCC with features similar to the parental tumor, upon subcutaneous transplantation into mice.

HNSCC tumoroids as a platform for drug-screening

The genetic alterations found in HNSCC are commonly found in other tumor types, and therapies targeting some of these specific mutations exist. Regardless, with the exception of Cetuximab (an anti-EGFR antibody) that is used in treatment of HNSCC, no targeted

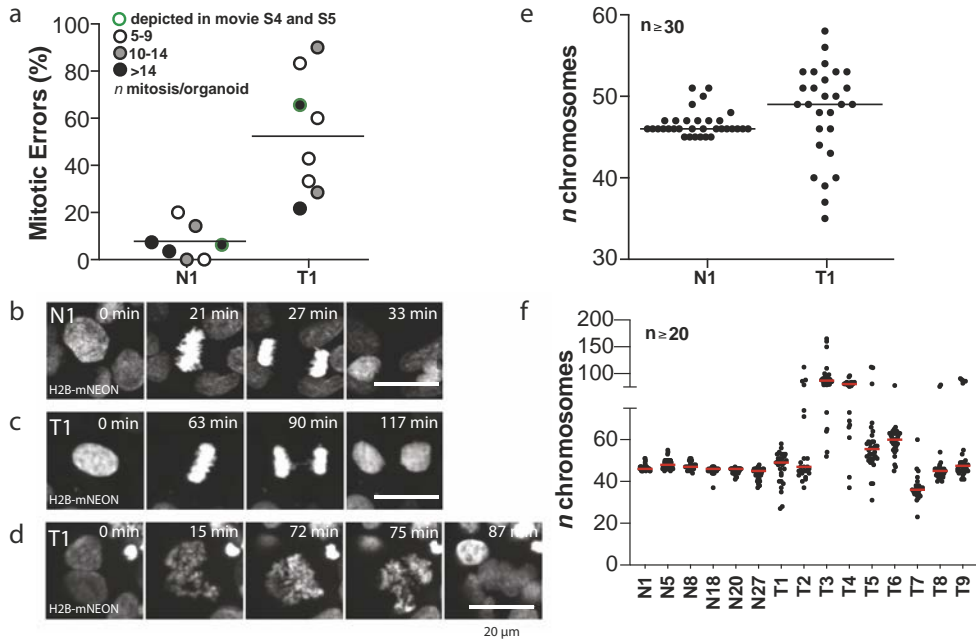


Figure 4. HNSCC-derived organoids are chromosomally unstable *in vitro*. Imaging of H2B-mNEON expressing organoids reveals cell divisions that can be studied and quantified for segregation errors during division. **A.** Quantification of segregation errors observed in N1 and T1. Percentage of mitotic errors per organoids is shown. One dot represents an imaged organoid and the color of the dot indicates the corresponding number of mitoses. Green encircled dots represent the organoids that are shown in movie S4 and S5. **B-D.** Stills taken from time-lapse movies of N1 and T1 organoids. Maximum projections of selected Z-planes are shown. **B** Examples of a correct mitosis observed in N1. **C.** Example of an anaphase bridge formed during mitosis in T1. **D.** Example of a bi-nucleated cell undergoing multipolar division observed in T1. *Scalebar* 20 μ m. **E.** Scatter plot, presenting chromosome number distribution and median, based on organoid metaphase spreads of N1 and T1 cells. **F.** Scatter plot, presenting chromosome number distribution and median.

therapies are currently applied in standard care of these patients (43–46). In recent years, it has become clear that mutation status alone does not provide the required specificity or sensitivity to serve as a predictive marker (47). For this reason, we tested a panel of organoid lines carrying different genetic alterations that are regularly found in HNSCC for their *in vitro* drug sensitivity (Figure S11A).

To refine our *in vitro* drug screening assay, we used Nutlin-3 treatment. Exposure to a concentration series allowed quantitative discrimination between sensitive and non-sensitive lines (Figure 6A). As expected, *TP53* wildtype cells were sensitive to Nutlin-3 exposure, whereas *TP53* mutant organoids were not (Figure 6B). The assay was reproducible ($n = 3$; Fig S11B). To assure quality of the drug-screen data, a Z factor score (a measure of assay quality) was calculated for each drug screen in this study (Figure S11C).

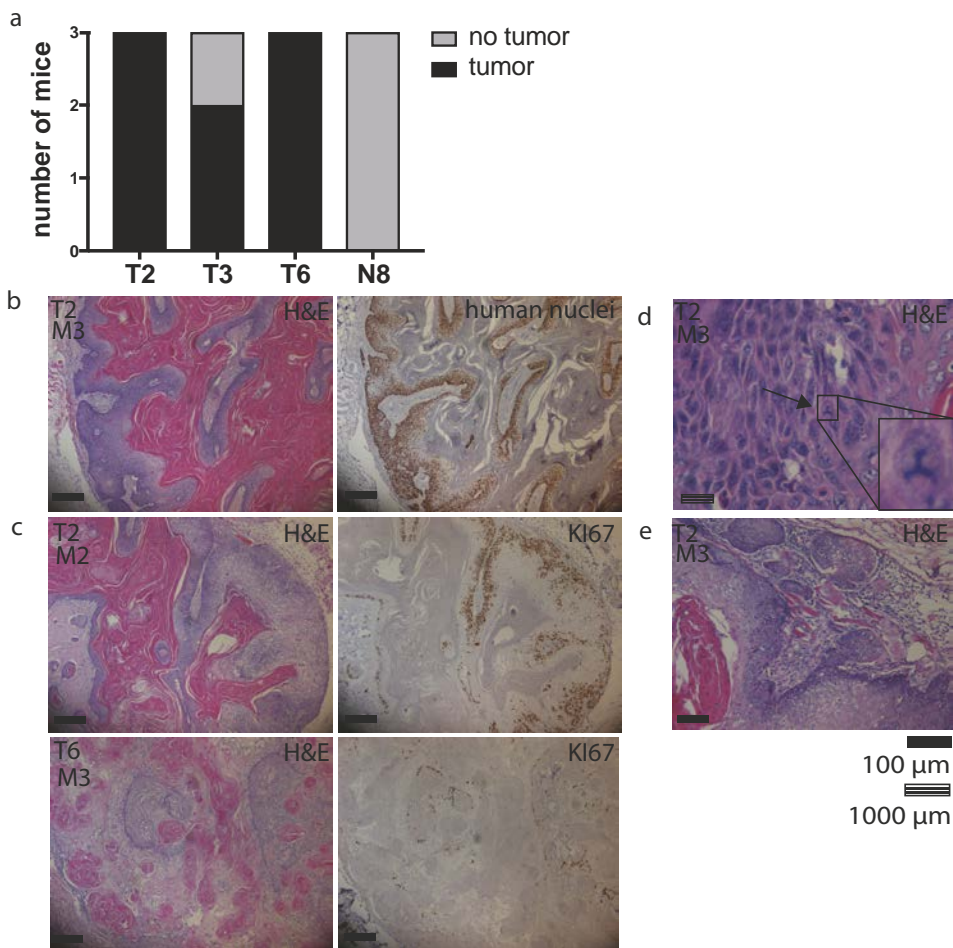


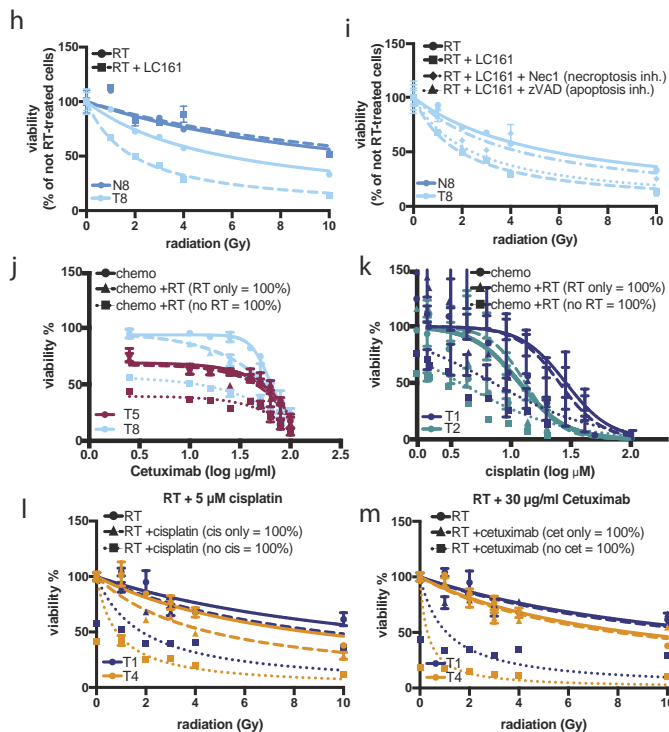
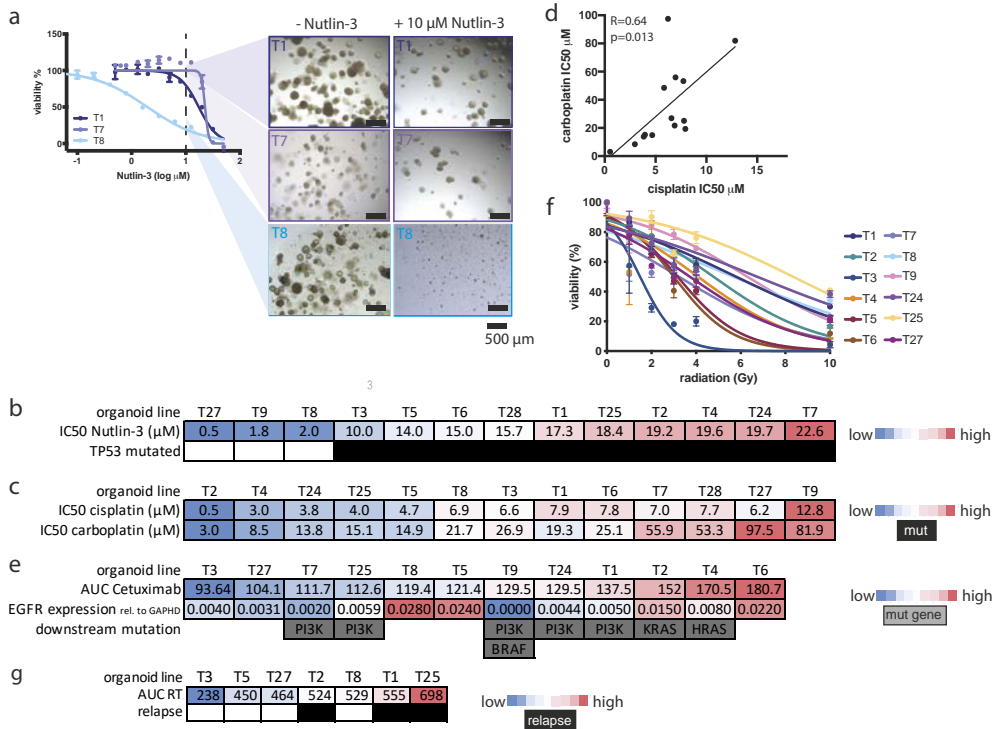
Figure 5. Xenografted HNSCC organoids recapitulate histopathological characteristics of HNSCCs. A. Three independent mice were injected with each organoid line, and the number of mice that developed tumors is depicted. B. Hematoxylin and eosin (H&E) and anti-human nuclei staining of the paraffin-embedded tumor. Left panel, H&E reveals stratification from more basal (dark purple) to more differentiated keratinocytes (light purple) to eventually deposited keratin (pink). Right panel, immunostaining for human nuclei reveals human origin of the squamous epithelial cells observed in the tumor. C. Comparison of two tumors originating from either organoid line T2 or T6. Left panels, H&E reveal different morphology of the different tumors. Right panels, Ki-67 staining shows difference in the number of cells in G1 between the two tumors. D. Example of atypia that can be observed in the tumors. Arrow indicates a tripolar mitotic figure. Throughout the image, nuclear pleomorphism can be observed. E. Squamous cells can invade into the surrounding muscle tissue of the mouse. *Striped scalebar, 10 μ m. black scalebar, 100 μ m.*

Average Z factor score was 0.70 (ranging from 0.30 to 0.92), which is consistent with an experimentally robust assay.

Subsequently, we exposed thirteen fully characterized tumoroid lines (tumoroid lines T10 and T29 did not survive the robotized drug screening procedure) to cisplatin, carboplatin and cetuximab, drugs currently used in the treatment of HNSCC patients. Using *in vitro* concentrations similar to plasma concentrations reached in HNSCC patients (48), we observed differential sensitivity of the organoids to these compounds. Based on the measured IC₅₀, we made a ranking of the tumoroid lines tested for cisplatin and carboplatin (Figure 6C). While IC₅₀ values for cisplatin and carboplatin were different (average IC₅₀^{cisplatin} was 5.91 mM and IC₅₀^{carboplatin} was 44.1 mM), correlation between cisplatin and carboplatin sensitivity was observed (Pearson correlation, $r=0.64$, $p<0.05$. Figure 6D, Figure S12). This correlation has previously been described in ovarian cancer cells (49). *In vitro* platinum-DNA adduct formation has shown that both drugs give rise to the same damage, yet cisplatin does so at lower dose (50). Although the mechanism of action is the same, it is suggested that cisplatin should be preferred over carboplatin as a radiosensitizer in HNSCC (51). We confirm that, for the lines tested here, none showed a higher sensitivity to carboplatin than to cisplatin.

Organoids were also exposed to the anti EGFR-antibody Cetuximab and differential responses were observed (Figure 6E, Figure S12). Recent studies challenge the prognostic value of EGFR overexpression or increased gene copy number for Cetuximab response (47). Here, no correlation between EGFR expression and Cetuximab response was observed. Lastly, we found that organoid lines insensitive to Cetuximab, commonly carried mutations downstream of *EGFR* (*PIK3CA*, *KRAS*, *HRAS* or *BRAF*). This has important implications for patient inclusion for Cetuximab therapy, which currently does not include genetic testing. Of note, RAS/RAF genetic testing is routinely performed in patients with colorectal cancer that are eligible for EGFR-targeting treatments.

Currently, treatment with curative intent of HNSCC patients with advanced disease consists of surgery with adjuvant radiotherapy, with or without chemotherapy, or radiotherapy with or without chemotherapy with the possibility of surgery as salvage treatment in case of residual/recurrent disease (47). Radiotherapy can also be a part of palliative treatment to reduce pain or tumor invasion. Therefore, we tested the sensitivity of the tumoroids to ionizing radiation. We consistently observed differential responses between the tumoroid lines when exposed to radiotherapy. This suggested that clinical correlations could be studied (Figure 6F). To assess if expression profiles could predict responses to these therapies, we performed DEseq analysis, comparing organoid lines with different responses to either cisplatin and carboplatin, Cetuximab or radiotherapy (see Figure S13, Table S5). Although differentially expressed genes could be detected in all comparisons, including those previously described associated with resistance to these



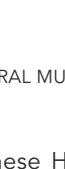
therapies (52–55), no clear indication for resistance mechanisms could be deduced from performing gene enrichment analysis on these gene sets.

Correlation of *In vitro* organoid responses with clinical responses in seven patients that received radiotherapy

2.1

Seven of the patients received (post-operative) radiotherapy, which allowed a correlation with organoid sensitivity to this treatment. Although the number of patients is small, and

◀ **Figure 6. HNSCC organoids as a platform for drug screening.** A. Validation of the drug screen set-up using Nutlin-3 exposure. Drug screen viability is consistent with the Nutlin-3 response observed using brightfield imaging. Scalebar 500 μm . B. Heatmap showing the tumoroids ranked based on Nutlin-3 IC50. Red indicates high IC50 values, blue indicates low IC50 values. IC50 values and *TP53* mutation status are depicted. C. Heatmap showing the organoid lines ranked based on cisplatin and carboplatin sensitivity. Red indicates high IC50 values, blue indicates low IC50 values. D. Correlation between cisplatin sensitivity (x-axis) and carboplatin sensitivity (y-axis) can be observed *in vitro*, Pearson correlation, $r=0.71$, $p<0.05$. Each dot represents one tumoroid line, for which the cisplatin IC50 value is plotted on the x-axis, and the carboplatin IC50 value is plotted on the y-axis. E. Heatmap showing the organoid lines ranked based on Cetuximab sensitivity as measured by area under the curve (AUC). Here, AUC was used instead of IC50 values, because of the curvature of the kill curve, that did not allow for IC50 value calculation. Red indicates high AUC values, blue indicates low AUC values. In this dataset, no correlation between EGFR expression and Cetuximab sensitivity can be observed. Mutations in downstream components of EGFR (*PIK3CA*, *KRAS*, *HRAS* and *BRAF*) confer resistance to Cetuximab. F. Organoids show variable sensitivity to radiation. Cell viability is plotted on the y-axis, for different amounts of radiation, ranging from 0 to 10 Gy (x-axis). G. Heatmap showing the organoids ranked based on radiotherapy sensitivity as measured by area under the curve (AUC). Red indicates high AUC values, blue indicates low AUC values. The row below summarizes the clinical response of patients, where a black box indicates a relapse after completion of radiotherapy treatment. H. radiotherapy (RT) sensitivity of T8 and N8 organoids in the presence (dashed line, square symbols) or absence of 1 μM LC161. For cells exposed to radiation in the presence of LC161, viability was calculated relative to organoids treated with LC161 alone. I. Exposure of T8 cells to RT alone, RT + LC161 and RT + LC161 in the presence of either necroptosis inhibitor Nec1 (diamonds) or apoptosis inhibitor zVAD-FMK (triangles). For cells exposed to RT in the presence of any of the used compounds, viability was calculated relative to organoids treated with these compounds alone. J and K. Chemoradiation therapy of tumoroids. Cisplatin and Cetuximab screens were performed either in the presence ('chemo +RT (no RT = 100%') or absence ('chemo') of radiation. Viability was calculated relative to untreated (no chemo, no RT) organoids, for which viability was set to 100%. To depict the effect of chemotherapy only, in the presence of RT, viability of the radiated tumoroids was calculated relative to tumoroids that were exposed to radiation, but no chemotherapy. This result is depicted by the line 'chemo + RT (RT only = 100%)'. This line shows the effect of chemotherapy in the presence of radiotherapy, corrected for the effect of radiotherapy only, whereas the 'chemo +RT (no RT = 100%)' line shows the overall effect of this combination therapy on tumoroid viability, compared to no treatment. L and M. The effect of chemotherapy (cisplatin or Cetuximab) on radiotherapy sensitivity in organoids. AUC is shown as indicator of organoid sensitivity to *in vitro* radiotherapy. For each line tested, AUC is shown for RT alone, or when combined with chemotherapy. Here, the effect of radiotherapy is corrected for the effect of chemotherapy alone. As such, the green area indicates lines where chemotherapy serves as a radiosensitizer, whereas the red area indicates lines where chemotherapy acts as a radioprotector.



these HNSCC tumors comprise a heterogeneous group (by anatomical location, timing (primary or adjuvant) and total dose of irradiation given), we used this set to explore the potential of HNSCC organoids as predictor for treatment response in the future. All patients described here were given radiotherapy with curative intent. An overview of the treatment details is given in Table S6. Three out of seven patients relapse after undergoing radiotherapy. Indeed, the three corresponding organoid lines are amongst the most resistant when exposed to radiotherapy *in vitro* (Figure 6G). Organoid line T3 showed the highest sensitivity to radiotherapy. Indeed, this patient had a lasting response to palliative radiotherapy. The primary tumor of the larynx received 48 Gy in four weeks and showed no signs of growth upon physical examination up to five months later, corresponding with ongoing local control due to radiotherapy. The patient unfortunately succumbed to lung carcinoma five months later. The patient from which T5 was derived, was treated with adjuvant RT following surgery (stage T4aN0 parotid tumor) because of 2 prognostic factors that predict high risk of relapse of disease: macroscopic residual disease and perineural growth, observed in the resected tissue. The patient received a dose of 66 Gy over a period of six weeks at the parotid area. Nine months after completion of radiotherapy, the patient showed no signs of relapse or progression upon physical examination, showing a clinically good response to radiotherapy. Organoid lines T1 and T2 were not responsive to radiotherapy in the *in vitro* assay. Indeed, the patients corresponding to these lines showed progressive disease shortly after completing the treatment. Patient T1 presented with tongue SCC (stage T2N2b) with extranodal growth and was treated with radiotherapy after resection of the primary tumor with positive margins. The patient received a dose of 66 Gy over the course of 10 weeks. Six months later, the patient complained of pain in the tumor area and loco-regional relapse of disease was eventually diagnosed three months later, leading to death three months after that. Patient T2 presented with a SCC in the larynx (stage T2N0) for which 60 Gy of radiation was given. Four months later the patient presented with complaints. Five months later, a recurrent tumor was diagnosed that invaded the subglottis and required a complete laryngectomy. T25 was the organoid line most resistant to radiotherapy. These *in vitro* findings correlated well with the clinical history of patient T25. This patient presented with a SCC of the floor of mouth (stage T2N1). After receiving surgery for excision of the primary tumor and a selective neck dissection with negative margins, he developed a recurrence in the neck for which he was treated with radiotherapy. A total dose of 52 Gy was delivered to the neck. Only one month later, extensive regional recurrent disease (including skin metastases) in the neck was diagnosed upon physical examination. One month later, the patient succumbed to disease. Patient T27 was diagnosed with a floor of mouth SCC (stage T3N1) for which adjuvant radiotherapy was given after excision of the primary tumor. Indications for adjuvant radiotherapy included close surgical margins and positive sentinel node. The patient received a total dose of ionizing radiation of 56 Gy and was last seen two months after the end of treatment. So far, there are no signs

of recurrence. It is too early to tell if this patient will remain in remission. It will be of interest to see if disease will recur, as based on our *in vitro* findings, radiotherapy should have been effective for this particular tumor. Finally, although T8 appeared resistant to radiotherapy in the *in vitro* assay, patient T8 so far did not show relapse after treatment. The patient received adjuvant radiotherapy after incomplete resection of a gingival SCC (stage T4aN0). A dose of 66 Gy was delivered to the tumor area. Five months later no signs of recurrence were observed upon physical examination. Standard follow up is ongoing. It will be of interest to see if the patient relapses in the coming months, a progression that would be in line with our *in vitro* findings.

Combination of chemo- and radiation therapy in HNSCC-derived organoids allows to study synergistic effects of these therapies

In an attempt to overcome the observed radio resistance, HNSCC organoids that were responding poorly to radiotherapy were re-exposed to radiation, but now in the presence of LC161. LC161 is a Second Mitochondria-derived Activator of Caspase (SMAC) mimetic, described to overcome intrinsic cell death resistance by promoting degradation of clAPs (56). As others have shown an effect of SMAC mimetics in HNSCC cells, either alone or in combination with radiotherapy, we set out to test this in HNSCC organoids (57). Indeed, a radio-sensitizing effect of LC161 was observed in T8. In parallel, T1 and T9 were also tested, but did not show increased sensitivity to radiotherapy in the presence of LC161. In T8 organoids, the addition of SMAC mimetic increased cell death in response to radiation (Figure 6H). Importantly, LC161 did not radio-sensitize the matched N8 organoids; these were more resistant to this treatment. To validate these findings and understand which type of cell death was triggered in response to radiotherapy combined with LC161, the treatment was repeated in the presence of either Z-VAD-FMK (zVAD) or Necrostatin1 (Nec1), which block apoptosis or necroptosis, respectively. It was found that the addition of Nec1, but not zVAD, could prevent the radio-sensitizing effect of the SMAC mimetic (Figure 6I). These findings show that T8 tumor cells, in line with general tumorigenic mechanisms (58), evade apoptosis, yet that this resistance could be overcome by the addition LC161. These results highlight the potential of organoids to explore alternative (sensitizing) therapies on a personalized level.

In addition to determining radio sensitivity of the tumoroids, we set up an *in vitro* screening assay combining chemotherapy with radiotherapy. We exposed organoids to a gradient of chemotherapy in the presence (2 Gy) or absence (0 Gy) of radiation. Previously detected differences in sensitivity for these compounds were confirmed (cetuximab sensitivity T5 > T8, cisplatin sensitivity T2 > T1) (Figure 6J and 6K). We found that combination therapy resulted in increased cell death at lower doses of chemotherapy than when chemotherapy was given as a single agent. To study the effect of chemotherapy in the presence of radiation, we compared organoids treated with chemotherapy and radiotherapy with organoids exposed to radiotherapy alone (T5 and T8 to Cetuximab, T1 and

T2 to Cisplatin (Figure 6J and 6K). It seems that in these cases, the effect of chemotherapy itself is not changed by the presence of radiotherapy, although the combination treatment results in additional cell death.

Using the same approach, we studied the radio sensitizing effect of chemotherapy *in vitro*. In the clinic, such combination therapy is used to treat patient with HNSCC, both in the curative and adjuvant setting. The combination of Cisplatin or Cetuximab with radiotherapy increases relapse-free survival when compared to treatment with radiotherapy alone in clinical trials (59). As radiotherapy and chemotherapy are given concurrently to patients, it is impossible to understand if the effect between these treatments is additive or synergistic. Here, ten organoid lines (T1 to T6, T8, T24, T25 and T27) were exposed to a range of radiotherapy, either in the presence or absence of a toxic dose of cisplatin or Cetuximab. Indeed, the combination of chemotherapy and radiotherapy resulted in increased cell death when compared to single agent treatment. When corrected for the effect of the chemotherapy itself, sensitivity to radiotherapy was increased in the presence of cisplatin in six out of ten tested lines, and in four out of ten when combined with Cetuximab (Figure 6L, 6M and S14A). Although not statistically significant, a correlation between the effect of radiotherapy alone, and radiotherapy combined with cisplatin was observed. Overall, response to radiotherapy improved in the presence of cisplatin, implying a synergistic effect (Figure S14B). Based on the data presented here, this is not the case when radiotherapy is combined with Cetuximab (Figure S14C). This suggests that, although additive (Figure S14D and E), no synergistic effect of Cetuximab and radiotherapy can be observed, at least *in vitro*.

HNSCC organoids as a platform to identify effective targeted therapies

Based on mutations detected in this set of HNSCC-derived tumoroids, we determined the *in vitro* sensitivity for a range of targeted therapies that are not used in the treatment of HNSCC patients. As T1, T7, T9, T10, T24, T25 and T29 carry activating mutations in *PIK3CA*, sensitivity to *PIK3CA* inhibitor Alpelisib was determined for sequenced tumoroid lines eligible for drug screening (Figure S12). *PIK3CA* mutation has been investigated as a biomarker for response to *PIK3CA* inhibitors (60–62). Although some studies imply that activating mutations of *PIK3CA* can serve as a biomarker for good response, others claim the type of mutation can influence response to these therapeutics. We observe no enrichment for *PIK3CA* mutations in the organoid lines more responsive to Alpelisib (Figure 7A). Recently, a study linking genetic alterations to Alpelisib responses in patients showed that patients carrying H1047R *PIK3CA* mutations had a more durable response in the clinic, whereas a negative association was found between E545K mutations and Alpelisib response (62). When testing all *PIK3CA* mutant organoid lines eligible for drug screening, T9 organoids (*PIK3CA* H1047R, IC₅₀ 0.32 μM) showed increased sensitivity to Alpelisib compared to E545 *PIK3CA* mutant organoids T1 (IC₅₀ 3.19 μM) and T7

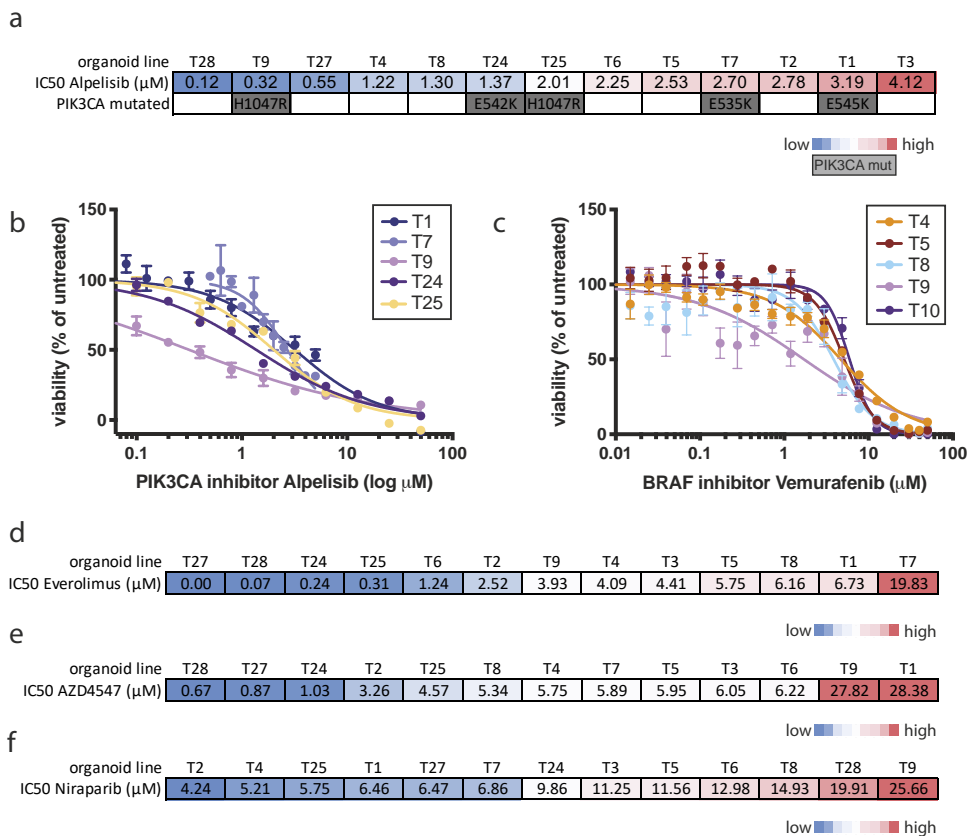
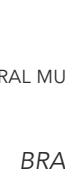


Figure 7. HNSCC organoids as a platform to identify effective targeted therapies. A. Heatmap showing IC₅₀ values of tumoroid lines exposed to PIK3CA inhibitor Alpelisib. Red indicates high IC₅₀ values, blue indicates low IC₅₀ values. Amino acid changes caused by the respective genetic alterations are shown in the row below to highlight that mutation status is not correlating to Alpelisib response. B. Sensitivity of tumoroid lines T1, T7, T9, T24 and T25 for PI3K-inhibitor Alpelisib. C. Sensitivity of tumoroid lines T4, T5, T8 and T9 for BRAF-inhibitor Vemurafenib. T9 (carrying a BRAF V600E activating mutation) shows increased sensitivity to this agent. D. Heatmap showing IC₅₀ values of tumoroid lines exposed to MTOR inhibitor Everolimus. Red indicates high IC₅₀ values, blue indicates low AUC values. E. Heatmap showing IC₅₀ values of tumoroid lines exposed to FGFR inhibitor AZD4547. Red indicates high IC₅₀ values, blue indicates low AUC values. F. Heatmap showing IC₅₀ values of tumoroid lines exposed to PARP inhibitor Niraparib. Red indicates high IC₅₀ values, blue indicates low AUC values.

(IC₅₀ 2.69 μM). However, the IC₅₀ value of organoid line T25, also carrying a H1047R activating mutation in *PIK3CA*, was 2.01 μM (Figure 7B). Although still lower than IC₅₀ values obtained for the E545K mutant organoid lines, this data supports the hypothesis that *PIK3CA* mutation status cannot predict response to PIK3CA inhibitors in all cases, and functional testing might be required to identify responders.



BRAF V600E mutations were detected in T9 and T10. Therefore, we tested a panel of tumoroid lines for sensitivity to vemurafenib, a *BRAF* inhibitor (Figure 7C). As expected, we observed increased sensitivity of *BRAF* mutant T9 when compared to the other tumoroid lines tested in this assay.

Finally, we exposed the panel of tumoroids to PARP-inhibitor Niraparib, mTOR inhibitor everolimus and FGFR-inhibitor AZD4547 (Figure 7D, 7E, 7F). These compounds were selected based on the genetic alterations described in HNSCC (30). Interestingly, although mutations in *PARP*, *MTOR* and *FGFR* were not detected in the characterized tumoroid lines, we observed variable sensitivities to these compounds (Figure S12). For all tested compounds, the difference in response between matched normal and tumor organoids was tested (Figure S15). Responses to therapies remain stable over time (Figure S16). Amongst the lines sensitive to everolimus (Figure 7D) was tumor line T27, which carries a *RET* mutation. Inhibition of mTOR signaling has shown to inhibit the growth of *RET* mutant tumor cells *in vitro* (63). AZD4547 was also found to effectively target tumoroid line T27 (Figure 7E). This response can likely be explained by the mutation in *KDR* (also known as *VEGFR2A*) detected in T27 organoids. Indeed, AZD4547 has been shown to target *KDR* in addition to *FGFR1*, although with lower affinity (64). Taken together, these data reveal differences in sensitivity to all compounds tested between different tumoroid lines, that in some but not all cases can be explained by detected genetic alterations. Thereby, this data illustrates the potential of this technology to guide personalized therapy in the future.

DISCUSSION


We present a protocol for long-term expansion of wildtype oral mucosal epithelia and HNSCC in the form of organoids. The growth factor cocktail that is used in this work differs from that for other epithelia. The addition of the GSK3- β inhibitor CHIR and the growth factor FGF2 appears essential for the successful establishment of these organoids. We characterize HNSCC organoids by histology, gene expression analysis and -in the case of tumoroids- by mutational profiling. Using the technique described here, we can retain normal keratinocytes without the requirement for feeder cells in culture for >15 passages. To document that these organoids are amenable to infectious disease modeling, we performed infection with HSV1 and HPV16. Previous studies have applied 3D models of fibroblasts, vaginal epithelium and melanoma cells to study the interaction of HSV1 with epithelial cells (65,66). Yet to our knowledge, a 3D model to study HSV1 infection in oral mucosa cells has not been reported. Infection with HPV16 has been limited to studies in immortalized cell lines, or to primary cells that can only be cultured briefly (21). Essential for HPV infection is viral access to basal cells of the stratified epithelium, while for virion production, differentiated keratinocytes are essential. A model which retains this stratification *in vitro* and shows productive infection, such as the one described here, should therefore be valuable to research in this field.

We report the initiation of a HNSCC-derived organoid biobank, which is being expanded significantly. Like our other biobanks, these will be made available to the research community. The biobank was used to test sensitivity to a panel of drugs. This drug panel included both drugs currently used in the treatment of HNSCC patients, and targeted drugs that based on their molecular targets appeared relevant to be tested in this setting. The fact that a variable response to cisplatin, carboplatin, cetuximab and radiotherapy was observed *in vitro*, suggests that this method records interindividual differences. This implies that tumor-derived HNSCC organoids hold potential to guide personalized therapy. Vlachogiannis and colleagues recently showed the predictive potential of similar drug screens using organoids derived from metastasized gastrointestinal cancers (23).

The high-take rate and the fast growth rate of the HNSCC tumoroids makes them particularly suited for personalized approaches. In current clinical practice, treatment options for HNSCC are dictated by site, stage and patient factors. There is a need for more tailored treatment. For this reason, we explored the potential to correlate organoid responses to patient outcome. Clinical data was available for five patients that presented with tumors in different anatomical locations. They received different total dosages of radiotherapy, while all were therapy naïve at the start of treatment. Although numbers should still be considered small, we find that clinical response of patients treated with radiotherapy can be correlated to *in vitro* responses of the corresponding organoids. To investigate if such a correlation truly exists, more cases are required, especially considering the heterogeneity of this disease and other variables such as patient outcome (total delivered dose, if surgery is performed and if so, if resection is successful, ability to finish treatment regimen as prescribed etcetera). To follow up on these initial findings, we are embarking on an observational study to link patient outcome to organoid responses *in vitro* (ONCODE-P2018-0003). We anticipate to include around 100 patients. Organoids will be exposed to cisplatin, carboplatin or cetuximab, and combined with irradiation such as occurs in clinical practice. Here, we already show the possibility to combine chemo- and radiotherapy *in vitro*. The observational trial will elucidate if these *in vitro* results hold predictive potential for patient responses.

Cetuximab is used in the treatment of HNSCC patients. 50-90% of tumors overexpress EGFR (47), and 15% carries gene amplification of EGFR (30). Initially, it was expected that differing levels of EGFR expression could explain patient response to anti-EGFR therapy. However, it has been shown that neither EGFR overexpression nor increased gene copy number can serve as a prognostic biomarker for Cetuximab response (47). In agreement, the Cetuximab sensitivity of the tumoroids could not be correlated by their EGFR expression levels. It will be interesting to see if this correlation can be observed in larger panels of patient-derived organoids. A direct, functional test such as offered by patient-derived tumoroids may prove valuable.

As chemo- and radiotherapy are given concurrently to patients, it is difficult to evaluate the effect of these single treatments at the individual patient level. As shown here, organoids



can be used to study both the effect of these treatments as single agents, but also can be used to study how chemotherapy influences radiotherapy efficacy and vice versa. As such, our results implicate that Cetuximab does not act as a radiosensitizer in patient-derived HNSCC cells. Regardless, compared to radiotherapy alone, the combination of Cetuximab and radiotherapy results in increased cell death *in vitro*, fitting with clinical data (67).

In addition, screening for sensitivity to other targeted drugs may be of value when the tumor recurs. The targeted therapies tested in our studies (Everolimus, Niraparib, Alpelisib, AZD4547 and Vemurafenib) yielded differential responses. While phase 1 and 2 clinical trials are ongoing to test a number of these drugs in HNSCC patients (68–70),

implementation remains limited. Organoids might serve as an *in vitro* tool to select the right therapy for the right patient. Alternatively, studying the characteristics of those organoids that are responding in such screens might help identify biomarkers that distinguish responders from not responders. As an example, in this study we show that *PIK3CA* mutant tumoroid lines show variable responses to Alpelisib. *PIK3CA* E545K mutant lines showed a similar response to the other *-PIK3CA* wildtype- tumoroids in our panel, whereas H1047R mutant lines showed increased sensitivity to this agent (although the extent of sensitivity differed for the two H1047R mutant lines tested here). In patients, differences in Alpelisib responses could indeed be linked to the type of *PIK3CA* mutation where H1047R mutant patients showed more durable responses than patients harboring a E545K mutation (62). On the contrary, other studies have implicated *PIK3CA* mutation as a predictor for Alpelisib response, regardless of the specific mutation (60,61). Our data support the hypothesis that the type of *PIK3CA* mutation might be relevant for the response to Alpelisib. In organoids, the presence of *PIK3CA* activating mutations did not correlate with *in vitro* responses to Alpelisib. These differences in sensitivity between lines carrying identical *PIK3CA* mutations might be explained by other genetic alterations, interfering with the dependence on this pathway for cell survival.

In general, *in vitro* responses observed in this study could in some, but not all, cases explained by the genetic alterations detected in the tumoroid lines. For example, the response of tumoroid line T27 to AZD4547 can be explained by the mutation in *KDR*, as AZD4547, designed as a FGFR inhibitor, is known to also target *KDR* with high affinity (64).

Interestingly, in the panel tested here, there are tumoroid lines showing comparable sensitivity to this therapeutic agent, although we, at this point, cannot identify genetic alterations explaining this sensitivity. These results indicate that, at least in some cases, functional tests such as those performed in here, might be more informative than genetic screening to predict response to therapeutic agents.

In an attempt to detect general therapy resistance mechanisms, we performed differential gene expression on a panel of organoid lines that either responded well or poorly to cisplatin/carboplatin, Cetuximab or radiotherapy. Under current conditions (sequencing depth, number of samples included in the analysis etc.), no indications for resistance mechanisms could be deduced from this data by gene enrichment analysis.

Differently expressed gene lists did contain genes previously described to be associated with therapy resistance. For example, genes enriched in radiotherapy-resistant organoid lines included *PGK1* and *GPX3*. For both genes, high expression has previously been associated with poor response to radiotherapy or DNA damaging therapies (52,53). Expression of *IGFBP5* and *SLC16A3* expression, both enriched in Cetuximab-resistant organoid lines, have previously been reported to be biomarkers for poor response to Cetuximab (54,55).

Finally, extension of this system to the generation of immune-tumoroids, tumor-derived organoids combined with immune cells, might make this system suitable to test responses to immunomodulating antibodies. Such drugs are currently evaluated in HNSCC patients (71). Again, prognostic biomarkers are largely lacking. Initial studies demonstrate that tumoroids can be cocultured with immune cells (derived either from peripheral blood or tumor microenvironment) and can provide functional read-outs (17,72).

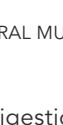
METHODS

Human Material for Organoid Cultures

The collection of patient data and tissue for the generation and distribution of organoids has been performed according to the guidelines of the European Network of Research Ethics Committees (EUREC) following European, national, and local law. The Biobank Research Ethics Committee of the UMC Utrecht (TCBio) approved the biobanking protocol: 12-093 HUB-Cancer according to the UMCU Biobanking Regulation. All donors participating in this study signed informed consent forms and can withdraw their consent at any time, leading to the prompt disposal of their tissue and any derived material, as well as the cessation of data collection. Available organoids will be catalogued at www.hub4organoids.eu and can be requested at info@hub4organoids.eu.

Tissue processing

Patient material was collected from pathology material in Advanced DMEM/F12 (Life Technologies, cat. no. 12634-034), supplemented with 1x GlutaMAX (adDMEM/F12; Life Technologies, cat. no. 12634-034), Penicillin-streptomycin (Life Technologies, cat. no. 15140-122) and 10 mM HEPES (Life Technologies, cat. no. 15630-056). This medium was named Advanced DMEM +/+/. For collection of patient material, 100 µg/ml Primocin (Invivogen, cat. no. ant-pm1) was added to the +/+ medium. For normal tissue samples, excess fat or muscle tissue was removed to enrich for epithelial cells and tissue was cut into small fragments. Random pieces of approximately 5 mm³ were stored at -20°C for DNA isolation. Some pieces were fixed in formalin for histopathological analysis and immunohistochemistry, and the remainder was processed for organoid derivation. Fragments were incubated at 37 °C in 0.125% Trypsin (Sigma, cat. no. T1426) in +/+ until digested. Every 10 minutes, the tissue suspension was sheared using 1 ml pipette.



Digestion was monitored closely to prevent excess incubation in trypsin. Incubation was performed for a maximum of 60 minutes. When complete, Trypsin was diluted by addition of 10 ml +/+/. Suspension was strained over a 100 µm EasyStrainer filter (Greiner, cat. no. 542000) and centrifuged at 1000 rpm. The resulting pellet was resuspended in ice-cold 70% 10 mg·ml⁻¹ cold Cultrex growth factor reduced BME type 2 (Trevigen, 3533-010-02) in organoid medium. Droplets of approximately 10 µl were plated on the bottom of pre-heated suspension culture plates (Greiner, cat. no. M9312). After plating, plates were inverted and put at 37 °C for 30 minutes to let the BME solidify. Subsequently, prewarmed organoid medium was added to the plate. For the first week, 10 µM Rho-associated kinase (ROCK) inhibitor Y-27632 (Abmole Bioscience, cat. no. M1817) was added to the medium to aid outgrowth of organoids for the primary tissue. For mouse-derived organoids, tongue tissue was obtained from control mice used under IvD approved projects. Subsequent processing of tissue was identical to processing of human tissue.

Organoid culture

HNSCC and normal epithelium-derived organoids were grown in Advanced DMEM +/+/. Organoid medium contained 1x B27 supplement (Life Technologies, cat. no. 17504-044), 1,25 mM N-acetyl-L-cysteine (Sigma-Aldrich, cat. no. A9165), 10 mM Nicotinamide (Sigma-Aldrich, cat. no. N0636), 50 ng/ml human EGF (PeproTech, cat. no. AF-100-15), 500 nM A83-01, 10 ng/ml human FGF10 (PeproTech, cat. no. 100-26), 5 ng/ml human FGF2 (PeproTech, cat. no. 100-18B), 1 µM Prostaglandin E2 (Tocris Bioscience, cat. no. 2296), 3 µM CHIR 99021 (Sigma-Aldrich, cat. no. SML1046), 1 µM Forskolin (Bio-Techne (R&D Systems) cat. no. 1099), 4% RSPO and 4% Noggin (produced via the r-PEX protein expression platform at U-Protein Express BV). Mouse organoids were maintained similar to human organoids, but were grown in +/+/, containing B27, 25 mM N-acetyl-L-cysteine, 10 mM Nicotinamide, 2% RSPO, 50 ng/ml EGF and 10 ng/ml FGF10. Organoids were split between 7 and 14 days after initial plating. For passaging, organoids were collected from the plate by disrupting the BME droplets with a P1000, collecting and washing in 10 ml +/+/. Pellet was resuspended in 1 ml of TrypLE Express (Life Technologies, cat. no. 12605-010) and incubated at 37°C. Digestion was closely monitored and suspension was pipetted up and down every 5 minutes to aid disruption of the organoids. TrypLE digestion was stopped when organoids were disrupted into single cells by adding 10 ml +/+/. Cells were subsequently resuspended in ice-cold 70% BME in organoid medium and plated at suitable ratios (1:5 to 1:20) to allow efficient outgrowth of new organoids. After splitting, 10 µM Y-27632 was always added to aid outgrowth of organoids from single cells. Medium was changed every 2-3 days and organoids were split once every 1-2 weeks.

RNA collection

Organoids were cultured as normal. For differentiation of the organoids (as shown in Figure 1C), organoids were split to single cells, left to grow one week on organoid medium, and then put on +/+ for one week before collection. On the day of collection, organoids were

collected from tissue culture plates and washed twice in 10 ml +/-/. RNA was extracted using RNeasy mini kit (Qiagen, cat. no. 74104) according to protocol. RNA amount was measured using Nanodrop. For quantification of EGFR expression, organoids were split to single cells, left to grow five days on organoid medium, and then put on organoid medium with lower EGF concentration (0.63 ng/ml).

RNA sequencing

RNA was processed as described previously, following the protocol of CEL-Seq (73,74). Paired-end sequencing was performed on the Illumina Nextseq500 platform, High Output 2x75 bp run mode. Read 1 was used to identify the Illumina library index and CEL-Seq sample barcode. Read 2 was aligned to the hg19 human RefSeq transcriptome using BWA (75). Reads that mapped equally well to multiple locations were discarded. Around 2 million reads were mapped per sample. Samples with low number of reads were removed. Sample annotation and barcodes can be found on the GEO submission of this data. The remaining samples were normalized and analyzed by the DESeq2 package (32). For visual comparison between samples, regularized log transformed (rlog) values were used.

cDNA synthesis and quantitative PCR

For cDNA synthesis, RNA was incubated with 50 µg/ml Oligo (dT) 15 Primer (Promega, cat. no. C1101) in water for 5 minutes at 70 °C. Subsequently GoScript Reverse Transcriptase (Promega, cat. no. A5003) was used according to protocol to produce cDNA. qPCR reactions were performed in 384 well format using IQ SYBR green (Bio-Rad, cat. no 1708880) in the presence of 0,67 µM FW and RV primer and cDNA transcribed from 25 ng RNA. For qPCR, samples were incubated for 2 minutes at 95 °C and for 40 cycles at: 15 seconds at 98 °C, 15 seconds at 58 °C and 15 seconds at 72 °C. Results were calculated by using the $\Delta\Delta C_t$ method. Expression was calculated relative to expression in tongue tissue (total RNA, human normal tongue tissue, AmsBio, cat. no. R1234267). Melt peak analysis was performed to assure that primer had no aspecific binding. Primers used were the following:

Human TP63 FW: GACAGGAAGGCGGATGAAGATAG,
 Human TP63 RV: TGTTTCTGAAGTAAGTGCTGGTGC,
 Human MKI67 FW: GAGGTGTGCAGAAAATCCAAA,
 Human MKI67 RV: CTGTCCCTATGACTTCTGGTTGT,
 Human KRT13 FW: GACCGCCACCATTGAAAACAA,
 Human KRT13 RV: TCCAGGTCAGTCTTAGACAGAG,
 Human KRT4 FW: CTCTTTGAGACCTACCTCAGTGT,
 Human KRT4 RV: GGCTGCTGTGCGTTTGTTG,
 Human EGFR FW: AGGCAGGAGTAACAAGCTCAC,
 Human EGFR RV: ATGAGGACATAACCAGCCACC,
 Human Actin FW: TGCGTGACATTAAGGAGAAG,
 Human Actin RV: TGAAGGTAGTTTCGTGGATG,

Human GAPDH FW: GGAGCGAGATCCCTCCAAAAT,
 Human GAPDH RV: GGCTGTTGTCATACTTCTCATCG.

DNA isolation

DNA was isolated using Reliaprep gDNA tissue miniprep system (Promega, cat. no. A2052) according to protocol. DNA concentration were measured using Nanodrop.

Growth rate analysis

100.000 single cells were plated in 50 μ l of BME. After one week in culture, all organoids were collected and disrupted into single cells. Cells were counted and total cell number was determined. Counting was performed 4 times. By calculating the number of cells at day 7, which all came from the 100.000 cells plated at day 0, a multiplication factor could be determined for each week. Using this, a theoretical total number of cells could be calculated by multiplying the total cell number of the previous week with the multiplication factor of that week. Subsequently, 100.000 cells of the counted single cells were plated in 50 μ l BME. This procedure was repeated for five weeks.

HSV infection and quantification experiments

For imaging experiments, cells were incubated with 10×10^6 PFU HSV-dTomato virus in the culture medium. Virus was a kind gift of Prof. Prashant Desai (John Hopkins University, USA). For DNA quantification, organoids were split using TrypLE. On the third day after splitting, organoids were incubated with 1×10^6 PFU HSV-dTomato virus in suspension for 6 hours. After washing with 10 ml +/+/+, organoids were plated (1500 organoids in 20 μ l BME per well) in 48 well format. Organoids were kept in organoid medium, with or without 10 mM Acyclovir (Sigma). For DNA collection, the BME drop was collected together with culture medium and added to 10 ml +/+/+ in a 15 ml falcon tube. After centrifugation, medium was removed and pellet was stored at -20 until gDNA extraction. For DNA quantification, qPCR reactions were performed in 384 well format using IQ SYBR green mix (Bio-Rad) in the presence of 0,67 μ M FW and RV primer and 2% of total DNA isolated from 1500 organoids. After gDNA extraction, qPCR was performed with the following primers to detect HSV DNA: FW: 5'-ATCAACTTCGACTGGCCCTT-3' and RV: 5'-CCGTACATGTCGATGTTTAC-3'. PCR program used: 2 minutes at 95 $^{\circ}$ C and for 40 cycles at: 15 seconds at 98 $^{\circ}$ C, 15 seconds at 60 $^{\circ}$ C and 15 seconds at 72 $^{\circ}$ C. Increase in DNA content was calculated relative to noninfected wells.

HPV infection and quantification experiments

HPV16 virions were produced as previously described (26). Upon fractionation of the supernatant containing the virus, fractions with highest titer (as determined by quantitative PCR on HPV DNA) were pooled and subsequently used for infection experiments. Organoids were split using TrypLE and plated at a density of 1500 cells/

well, in 20 μ l BME drops. After addition of culture media, HPV containing supernatant was added to the wells. During the course of the experiment, medium was refreshed every 2-3 days. DNA isolation and DNA quantification were performed as described for HSV infections, except primers used were FW: '5-CTACATGGCATTGGACAGGA-3' and RV: 5'-GGTCACGTTGCCATTCACTA-3'. For re-infection experiments, supernatant taken from organoids cultured for 12 days after HPV infection was collected and filtered with 0.45 μ m pore filter. Subsequently, this was added to the uninfected organoids.

Next Generation Sequencing

Oncopanel sample prep and analysis was performed as previously described (76) and sequenced with the mpliSeq Cancer Hotspot Panel V2+ (for details: https://www.umcutrecht.nl/getmedia/c39cd469-a4de-4ae9-9a52-0b8ed6761311/CHPv2Plus_NGS.pdf.aspx). For sample T27, an extended oncopanel was used, where 140 genes were checked with 3817 probes targeting a region of 1,080,437 bp. For library preparation, SureSelectXT Library Prep Kit was used following the SureSelectXT Target Enrichment System for Illumina Version B.2 protocol. For cluster generation, the library is loaded into a flow cell where fragments are captured on a lawn of surface-bound oligos complementary to the library adapters. Each fragment is then amplified into distinct, clonal clusters through bridge amplification. Total reads were above 50,000,000 (52 < GC% > 50).

Whole exome sequencing data were mapped against human reference genome GRCh37 and variants were called using the IAP pipeline (<https://github.com/UMCUGenetics/IAP>). To obtain high-quality somatic mutation catalogs, we filtered out variants with evidence in their corresponding normal samples, overlaps with the Single Nucleotide Polymorphism Database v137.b3730, and the variants did not reach our quality measurements (base coverage of 10x, variant allele frequency (VAF) of 0.1, GATK phred-scaled quality score of 100 for base substitutions, 250 for indels and mapping quality (MQ) of 60 for indels). Indels that were present within 100 bp of a called variant in the control were excluded. Only autosomal variants were considered. The scripts used for the filtering are available at: <https://github.com/UMCUGenetics/SNVFI>, and <https://github.com/ToolsVanBox/INDELFI>. Non-synonymous mutations (missense mutation, start loss, stop gain, inframe insertion/deletion and frame shift) in the genes checked in the OncoPanel were reported as driver mutations. Whole-exome sequence data will be deposited in the European Genome-Phenome Archive (EGA; <https://www.ebi.ac.uk/ega/home>); EGA study ID EGAS00001003628

In vitro drug screen

Two days prior to start of the drug screen, organoids were passaged and disrupted into single cells using TrypLE. Single cells were plated in 70% BME in organoid medium as for regular splitting. Two days later, organoids were collected from the BME by addition

of 1mg/ml dispase II (Sigma-Aldrich, cat. no. D4693) to the medium of the organoids. Organoids were incubated for 30 min at 37°C to digest the BME. Subsequently, organoids were filtered using a 70 mm nylon cell strainer (Falcon), counted and resuspended in 5% BME/growth medium (12.500 organoids/ml) prior plating in 40 µl volume (Multi-drop Combi Reagent Dispenser, Thermo Scientific, cat. no.5840300) in 384-well plates (Corning, cat. no. 4588).

The drugs were added 1 hour after plating the organoids using the Tecan D300e Digital Dispenser (Tecan). Nutlin-3 (Cayman Chemical, cat. no. 10004372), Niraparib (Selleckchem, cat. no. S2741), AZD4547 (ApeXbio, cat. no. A8250), Everolimus (LC laboratories, cat no. E4040), Vemurafenib (Selleckchem, cat. no. S1267) and Alpelisib (LC laboratories, cat. no A4477) were dissolved in DMSO. Cisplatin (Sigma, cat. no C2210000), Carboplatin (Sigma, cat. no. C2538) and Cetuximab (obtained from hospital pharmacy) were dissolved in PBS containing 0.3% Tween-20, which was required to dispense these drugs using the HP printer. All wells were normalized for solvent used. DMSO percentage never exceeded 1%, PBS/Tween-20 percentage never exceeded 2%. Drug exposure was performed in triplicate for each concentration shown. For a lay-out of the drug screen, see supplementary Figure S12.

120 hours after adding the drugs, ATP levels were measured using the CellTiter-Glo 3D Reagent (Promega, cat. no. G9681) according to the manufacturer's instructions and luminescence was measured using a Spark multimode microplate reader (Tecan). Results were normalized to vehicle (100%) and baseline control (Staurosporin 1 µM), (0%). For each line, when viability did not go above 70% or below 30%, an additional screen was performed for that particular drug with an adjusted dose of this drug for this organoid line. Screen quality was determined by checking Z factor scores for each plate following this formula:

$$Z \text{ factor} = 1 - \frac{3 * \text{standard deviation}(\text{negative control}) + 3 * \text{standard deviation}(\text{positive control})}{\text{average}(\text{negative control}) - \text{average}(\text{positive control})}$$

Drug screens with a Z factor of < 0.3 were not used and repeated. Kill curves were produced using GraphPad software and lines were fitted using the option 'log (inhibitor) vs normalized response -variable slope'.

Radiation of organoids

Organoids were disrupted into single cells using TrypLE, and plated at a density of 6000 single cells in 30 µl BME drops in a 48-well plate. Two days later, cells were irradiated. For each radiation dose, a separate plate was used. Plates were sealed air-tight and irradiated with a single fraction of 0-8 Gy using a linear accelerator (Elekta Precise Linear Accelerator 11F49, Elekta, Crawley, United Kingdom). The plates were positioned on top of 2 cm

polystyrene and submerged in a 37 °C water bath. After radiation, medium was changed. Four days later, read-out was performed as previously described.

Chemoradiation therapy in organoids

For testing a range of chemotherapy concentrations in the presence or absence of radiotherapy, drug screens were performed as described in section 'In vitro drug screen'. Two identical plates of organoids were treated with the desired chemotherapy. One day after the start of treatment, one of these plates was irradiated with a total dose of 2 Gy. This dose was chosen as a sublethal dose based on the radiotherapy only experiments that were previously performed.

To test a range of radiation doses in the presence or absence of cisplatin, Cetuximab, LC161, zVAD-FMK or Necrostatin 1, organoids were disrupted into single cells using TrypLe, and plated at a density of 6000 organoids per 20 µl BME in 96 wells plates. One day later, chemotherapy treatment was started. Based on chemotherapy screens that were previously performed, the sublethal doses of 5 µM cisplatin and 30 µg/ml Cetuximab were chosen. Based on literature, 1 µM LC161, 10 µM zVAD and 10 µM Necrostatin were used. One day later, cells were irradiated as described above. Four days later, read-out was performed.

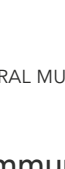
Live-cell imaging and lentiviral infection

Organoids were infected with lentivirus encoding mNeon-tagged histone 2B and a puromycin-resistance cassette (77). After selection, organoids were plated in BME in glass-bottom 96-well plates and mounted on an inverted confocal laser scanning microscope (Leica SP8X), which was continuously held at 37 °C and 5.0% CO₂. Over 16–20 h, ~10 H2B-mNeon-expressing organoids were imaged simultaneously in XYZT-mode using a ×40 objective (N.A. 1.1), using minimal amounts of 506 nm laser excitation light from a tunable white light laser. Time interval was approximately 3 min (2:30–3:20 min). Cell divisions were scored, judged and counted manually.

Transplantations

For all *in vivo* work, ethical approval was gained prior to the start of this project by the Central Authority for Scientific Procedures on Animals (CCD) and the local animal experimental committee at the Hubrecht Institute (IvD-HI-KNAW-HI 17.10.11). Five days before transplantation, organoids were disrupted to single cells and plated as usual. On the day of transplantation, organoids were disrupted into single cells and resuspended in 50% BME/organoid medium at a density of 33.33 million cells per ml. 2.5 million cells were subcutaneously injected in *NOD.Cg-Prkd^{scid} Il2rg^{tm1Wjl}/SzJ* mice, between 6 and 12 weeks of age. Six weeks after injection, mice were sacrificed by cervical dissociation and tumors were excised and fixed overnight in 4% formaldehyde.

Immunohistochemistry



Tissues or organoids were fixed in 4% paraformaldehyde overnight, dehydrated and embedded in paraffin. Sections were subjected to H&E as well as immunohistochemical staining. The details on primary antibodies used for immunohistochemical staining on organoids and primary tissue are given in Table S7. Staining for TP40, TP53, MKI67 and KRT5 on the tumoroids (Figure 2) were performed at the pathology department of the UMCU.

Karyotyping

Two days after splitting, organoids were treated with 0.1 $\mu\text{g ml}^{-1}$ Colcemid (Gibco 15212012) for 17 h in organoid medium. After that, organoids were disrupted into single cells using TrypLE and processed as previously described (78). Metaphase spreads were mounted with DAPI-containing vectashield (Vector laboratories, cat. no. H-1200) and imaged on a DM6000 Leica microscope.

Scanning electron microscopy (SEM)

Organoids were collected and BME was removed using Cell Recovery Solution (Corning). To fix organoids, 1 ml of 1% (v/v) glutaraldehyde (Sigma-Aldrich, G5882) in PBS was added. Following o/n fixation at 4°C, organoids were transferred onto 12 mm coverslips (Corning, cat. no. 354085). Samples were dehydrated by consecutive 10 min incubations in 2 ml of 10% (v/v), 25% (v/v) and 50% (v/v) ethanol-PBS, 75% (v/v) and 90% (v/v) ethanol-H₂O (2x) followed by 50% ethanol-hexamethyldisilazane (HMDS) and 100% HMDS (Sigma-Aldrich, cat. no 379212). Coverslips were removed from the 100% HMDS, air-dried overnight at room temperature and mounted onto 12 mm specimen stubs (Agar Scientific). Following gold-coating to 1 nm using a Q150R sputter coater (Quorum Technologies), samples were examined with a Phenom PRO table-top scanning electron microscope (Phenom-World).

Transmission Electron Microscopy (TEM)

Organoids were placed in BME on 3 mm diameter and 200 mm depth standard flat carriers for high pressure freezing and immediately cryoimmobilized using a Leica EM high-pressure freezer (equivalent to the HPM10), and stored in liquid nitrogen until further use. They were freeze-substituted in anhydrous acetone containing 2% osmium tetroxide 0.1% uranyl acetate at -90 °C for 72 hours and warmed to room temperature, 5°C per hour (EM AFS-2, Leica, Vienna, Austria). The samples were kept 2h at 4°C and 2h more at room temperature. After acetone rinses (4 x 15 min), Epon resin infiltration was performed during 2 days (acetone: resin 3:1- 3h; 2:2 – 3h; 3:1 – overnight; pure resin- 6h + overnight + 6h + overnight + 3h). Resin was polymerized at 60°C during 96 hours. Leica Ultracut UC6 ultramicrotome was used to cut sections which were mounted on Formvar-coated copper grids and stained with 2% uranyl acetate. Sections were observed in a Tecnai T12 Spirit

equipped with an Eagle 4kx4k camera (FEI Company, The Netherlands) and large EM overviews were collected using the principles and software described by Ravelli et al (79).

AUTHOR CONTRIBUTIONS

E.D. designed, performed and analyzed the research, assisted by S.K and S.S. J.E and V.G assisted in establishment of the organoid lines. S.M.W., L.A.D., and R. de B. were essential for input from clinical perspective and, together with O.K. aided patient inclusion. S.M.W. was responsible for Oncopanel Sequencing, together with P.S and D.T. E.R. performed IHC staining on tumoroids. J.K. performed xenotransplantation of organoids in mice. H.B. performed IHC staining on HSV-infected organoids. K.L. performed HPV-infection experiments, together with E.D. G.H. advised on experiments involving SMAC mimetics. R.O., supervised by R. van B., analyzed and interpreted Exome Sequencing data. R.J., supervised by G.K. imaged and analyzed H2B-mNeon infected organoids to study chromosomal segregation. J.V prepared samples for RNA sequencing, M.M. analyzed and interpreted the RNA sequencing data, supervised by A. van A. M.Z. S.K. and E.D. designed and performed radiation experiments in organoids. A.H. assisted during SEM of organoids. N.I, supervised by P.P performed, analyzed and interpreted TEM data of organoids. E.D. and H.C. wrote the manuscript.

ACKNOWLEDGEMENTS

We thank Tulay Bayram for supporting of ethical regulatory affairs. We acknowledge Anneta Brousalı, Petra van der Groep, Alexander Constantinides and Anne Snelting of the Utrecht Platform for Organoid Technology (U-PORT; UMC Utrecht) for patient inclusion and tissue acquisition. We would like to thank the molecular diagnostics department of the UMCU, department of pathology. Special thanks to Marja Blokland, Carmen Vooijs and Wendy de Leng for help with targeted sequencing of the organoids. We thank Prof. Prashant Desai of the John Hopkins University, US for contributing fluorescently labelled HSV virus. We thank Prof. Dohun Pyeon and Sharon Kuss-Duerkop of the Michican State University for contributing HPV16 virus, and their guidance while setting up these infections. We would like to acknowledge the members of the Microscopy Core Lab at M4I Maastricht University for their scientific and technological support regarding high pressure freezing and sample preparation for electron microscopy, with a special mention to Carmen López-Iglesias and Hans Duimel. We thank Yorick Post, Frans Schutgens, and Joep Beumer for critically reading this manuscript.

REFERENCES

1. Squier C, Kremer M. Biology of oral mucosa and esophagus. *J Natl Cancer Inst Monogr.* 2001;29:7–15.
2. Fitzmaurice C, Allen C, Barber RM, Barregard L, Bhutta ZA, Brenner H, et al. Global, Regional, and National Cancer Incidence, Mortality, Years of Life Lost, Years Lived With Disability, and Disability-Adjusted Life-years for 32 Cancer Groups, 1990 to 2015: A Systematic Analysis for the Global Burden of Disease Study. *JAMA Oncol. United States;* 2017;3:524–48.
3. Leemans CR, Snijders PJF, Brakenhoff RH. The molecular landscape of head and neck cancer. *Nat Rev Cancer. Nature Publishing Group;* 2018;18:269–82.
4. Argiris A, Karamouzis M V, Raben D, Ferris RL. Head and neck cancer. *Lancet (London, England).* 2008;371:1695–709.
5. Barretina J, Caponigro G, Stransky N, Venkatesan K, Margolin AA, Kim S, et al. The Cancer Cell Line Encyclopedia enables predictive modelling of anticancer drug sensitivity. *Nature.* 2012;483:603–7.
6. Smits JPH, Niehues H, Rikken G, Van Vlijmen-Willems I, Van De Zande G, Zeeuwen PLJM, et al. Immortalized N/TERT keratinocytes as an alternative cell source in 3D human epidermal models. *Sci Rep.* 2017;7:11838.
7. Mery B, Rancoule C, Guy J-B, Espenel S, Wozny A-S, Battiston-Montagne P, et al. Preclinical models in HNSCC: A comprehensive review. *Oral Oncol. England;* 2017;65:51–6.
8. Laban S, Steinmeister L, Gleißner L, Grob TJ, Grénman R, Petersen C, et al. Sorafenib sensitizes head and neck squamous cell carcinoma cells to ionizing radiation. *Radiother Oncol.* 2013;109:286–92.
9. Maushagen R, Reers S, Pfannerstill AC, Hahlbrock A, Stauber R, Rahmzadeh R, et al. Effects of paclitaxel on permanent head and neck squamous cell carcinoma cell lines and identification of anti-apoptotic caspase 9b. *J Cancer Res Clin Oncol.* 2016;142:1261–71.
10. Voskoglou-Nomikos T, Pater JL, Seymour L. Clinical predictive value of the in vitro cell line, human xenograft, and mouse allograft preclinical cancer models. *Clin Cancer Res.* 2003;9:4227–39.
11. Johnson JI, Decker S, Zaharevitz D, Rubinstein L V., Venditti JM, Schepartz S, et al. Relationships between drug activity in NCI preclinical in vitro and in vivo models and early clinical trials. *Br J Cancer.* 2001;84:1424–31.
12. Kross KW, Heimdal JH, Olsnes C, Olofsson J, Aarstad HJ. Co-culture of head and neck squamous cell carcinoma spheroids with autologous monocytes predicts prognosis. *Scand J Immunol.* 2008;67:392–9.
13. Kohno N, Ohnuma T, Truog P. Effects of hyaluronidase on doxorubicin penetration into squamous carcinoma multicellular tumor spheroids and its cell lethality. *J Cancer Res Clin Oncol.* 1994;120:293–7.
14. Braakhuis BJ, Sneeuwloper G, Snow GB. The potential of the nude mouse xenograft model for the study of head and neck cancer. *Arch Otorhinolaryngol.* 1984;239:69–79.
15. Smith LP, Thomas GR. Animal models for the study of squamous cell carcinoma of the upper aerodigestive tract: a historical perspective with review of their utility and limitations. Part A. Chemically-induced de novo cancer, syngeneic animal models of HNSCC, animal models of transplanted xenogeneic human tumors. *Int J cancer. United States;* 2006;118:2111–22.
16. Tanaka N, Osman AA, Takahashi Y, Lindemann A, Patel AA, Zhao M, et al. Head and neck cancer organoids established by modification of the CTOS method can be used to predict in vivo drug sensitivity. *Oral Oncol.* 2018;87:49–57.
17. Neal JT, Li X, Zhu J, Giangarra V, Grzeskowiak CL, Ju J, et al. Organoid Modeling of

- the Tumor Immune Microenvironment. *Cell*. United States; 2018;175:1972–1988.e16.
18. Clarkson E, Mashkoo F, Abdulateef S. Oral Viral Infections: Diagnosis and Management. *Dent Clin North Am*. 2017;61:351–63.
 19. Sayers CL, Elliott G. Herpes Simplex Virus 1 Enters Human Keratinocytes by a Nectin-1-Dependent, Rapid Plasma Membrane Fusion Pathway That Functions at Low Temperature. *J Virol*. 2016;90:10379–89.
 20. D'Souza G, Kreimer AR, Viscidi R, Pawlita M, Fakhry C, Koch WM, et al. Case-Control Study of Human Papillomavirus and Oropharyngeal Cancer. *N Engl J Med*. 2007;356:1944–56.
 21. Griffin LM, Cicchini L, Xu T, Pyeon D. Human Keratinocyte Cultures in the Investigation of Early Steps of Human Papillomavirus Infection. *Methods Mol Biol*. 2014;219–238.
 22. Drost J, Clevers H. Organoids in cancer research. *Nat Rev Cancer*. England; 2018;18:407–18.
 24. Vlachogiannis G, Hedayat S, Vatsiou A, Jamin Y, Fernández-mateos J, Khan K, et al. Patient-derived organoids model treatment response of metastatic gastrointestinal cancers. *Science (80-)*. 2018;926:920–6.
 25. Etienne L, Joshi P, Dingle L, Huang E, Grzesik P, Desai PJ. Visualization of herpes simplex virus type 1 virions using fluorescent colors. *J Virol Methods*. 2017;241:46–51.
 26. Gillison ML, Lowy DR. A causal role for human papillomavirus in head and neck cancer. *Lancet*. 2004;363:1488–9.
 27. Pyeon D, Lambert PF, Ahlquist P. Production of infectious human papillomavirus independently of viral replication and epithelial cell differentiation. *Proc Natl Acad Sci*. 2005;102:9311–6.
 28. Van De Wetering M, Francies HE, Francis JM, Bounova G, Iorio F, Pronk A, et al. Prospective derivation of a living organoid biobank of colorectal cancer patients. *Cell*. Elsevier Inc.; 2015;161:933–45.
 29. Fujii M, Shimokawa M, Date S, Takano A, Matano M, Nanki K, et al. A Colorectal Tumor Organoid Library Demonstrates Progressive Loss of Niche Factor Requirements during Tumorigenesis. *Cell Stem Cell*. 2016;18:827–38.
 30. Vassilev LT, Vu BT, Graves B, Carvajal D, Podlaski F, Filipovic Z, et al. In Vivo Activation of the TP53 Pathway by Small-Molecule Antagonists of MDM2. *Science (80-)*. 2004;303:844–8.
 32. The Cancer Genome Atlas Network. Comprehensive genomic characterization of head and neck squamous cell carcinomas. *Nature*. 2015;517:576–82.
 33. Freed-Pastor WA, Prives C. Mutant TP53: One name, many proteins. *Genes Dev*. 2012;26:1268–86.
 35. Love MI, Huber W, Anders S. Moderated estimation of fold change and dispersion for RNA-seq data with DESeq2. *Genome Biol*. 2014;15:550.
 36. Schrader CH, Kolb M, Zaoui K, Flechtenmacher C, Grabe N, Weber KJ, et al. Kallikrein-related peptidase 6 regulates epithelial-to-mesenchymal transition and serves as prognostic biomarker for head and neck squamous cell carcinoma patients. *Mol Cancer*. 2015;14:107.
 37. Zolk O, Schnepf R, Muschler M, Fromm MF, Wendler O, Traxdorf M, et al. Transporter Gene Expression in Human Head and Neck Squamous Cell Carcinoma and Associated Epigenetic Regulatory Mechanisms. *Am J Pathol*. 2013;182:234–43.
 38. Castillo-González AC, Nieto-Cerón S, Pelegrín-Hernández JP, Montenegro MF, Noguera JA, López-Moreno MF, et al. Dysregulated cholinergic network as a novel biomarker of poor prognostic in patients with head and neck squamous cell carcinoma. *BMC Cancer*. 2015;15:385.
 39. Bhosale PG, Cristea S, Ambatipudi S, Desai RS, Kumar R, Patil A, et al. Chromosomal Alterations and Gene Expression Changes Associated with the Progression of Leukoplakia to

- Advanced Gingivobuccal Cancer. *Transl Oncol.* 2017;10:396–409.
40. Yan L, Zhan C, Wu J, Wang S. Expression profile analysis of head and neck squamous cell carcinomas using data from The Cancer Genome Atlas. *Mol Med Rep.* 2016;13:4259–65.
 41. Gonzalez HE, Gujrati M, Frederick M, Henderson Y, Arumugam J, Spring PW, et al. Identification of 9 genes differentially expressed in head and neck squamous cell carcinoma. *Arch Otolaryngol Head Neck Surg.* United States; 2003;129:754–9.
 42. Stransky N, Egloff AM, Tward AD, Kostic AD, Cibulskis K, Sivachenko A, et al. The mutational landscape of head and neck squamous cell carcinoma. *Science.* 2011;333:1157–60.
 43. van Jaarsveld RH, Kops GJPL. Difference Makers: Chromosomal Instability versus Aneuploidy in Cancer. *Trends in cancer.* United States; 2016;2:561–71.
 44. Lengauer C, Kinzler KW, Vogelstein B. Genetic instability in colorectal cancers. *Nature.* 1997;384:623–7.
 45. Koo BK, Stange DE, Sato T, Karthaus W, Farin HF, Huch M, et al. Controlled gene expression in primary Lgr5 organoid cultures. *Nat Methods.* 2012;9:81–3.
 46. Cavalieri S, Perrone F, Miceli R, Ascierio PA, Locati LD, Bergamini C, et al. Efficacy and safety of single-agent pan-human epidermal growth factor receptor (HER) inhibitor dacomitinib in locally advanced unresectable or metastatic skin squamous cell cancer. *Eur J Cancer.* Elsevier Ltd; 2018;97:7–15.
 47. Soulières D, Faivre S, Mesía R, Remenár É, Li SH, Karpenko A, et al. Buparlisib and paclitaxel in patients with platinum-pretreated recurrent or metastatic squamous cell carcinoma of the head and neck (BERIL-1): a randomised, double-blind, placebo-controlled phase 2 trial. *Lancet Oncol.* 2017;18:323–35.
 48. Machiels JPH, Haddad RI, Fayette J, Licitra LF, Tahara M, Vermorken JB, et al. Afatinib versus methotrexate as second-line treatment in patients with recurrent or metastatic squamous-cell carcinoma of the head and neck progressing on or after platinum-based therapy (LUX-Head & Neck 1): An open-label, randomised phase 3 trial. *Lancet Oncol.* 2015;16:583–94.
 49. Machiels JP, Bossi P, Menis J, Lia M, Fortpied C, Liu Y, et al. Activity and safety of afatinib in a window preoperative EORTC study in patients with squamous cell carcinoma of the head and neck (SCCHN). *Ann Oncol.* 2018;29:985–91.
 50. Bossi P, Resteghini C, Paielli N, Licitra L, Pilotti S, Perrone F. Prognostic and predictive value of EGFR in head and neck squamous cell carcinoma. *Oncotarget.* 2016;7:74362–79.
 51. Andersson A, Fagerberg J, Lewensohn R, Ehrsson H. Pharmacokinetics of cisplatin and its monohydrated complex in humans. *J Pharm Sci.* 1996;85:824–7.
 52. Perez RP, O'Dwyer PJ, Handel LM, Ozols RF, Hamilton TC. Comparative cytotoxicity of CI-973, cisplatin, carboplatin and tetraplatin in human ovarian carcinoma cell lines. *Int J Cancer.* 1991;48:265–9.
 53. Atsushi H, Shuji S, Kosuke A, Takafumi K. A comparison of in vitro platinum-DNA adduct formation between carboplatin and cisplatin. *Int J Biochem.* 1994;26:1009–16.
 54. Guan J, Li Q, Zhang Y, Xiao N, Chen M, Zhang Y, et al. A meta-analysis comparing cisplatin-based to carboplatin-based chemotherapy in moderate to advanced squamous cell carcinoma of head and neck (SCCHN). *Oncotarget.* 2016;7:7110–9.
 55. Sun W, Yan H, Qian C, Wang C, Zhao M, Liu Y, et al. Cofilin-1 and phosphoglycerate kinase 1 as promising indicators for glioma radiosensitivity and prognosis. *Oncotarget.* Impact Journals LLC; 2017;8:55073–83.

58. Pelosof L, Yerram S, Armstrong T, Chu N, Danilova L, Yanagisawa B, et al. GPX3 promoter methylation predicts platinum sensitivity in colorectal cancer. *Epigenetics*. Taylor & Francis; 2016;12:540–50.
59. Lenarduzzi M, Hui ABY, Alajez NM, Shi W, Williams J, Yue S, et al. MicroRNA-193b Enhances Tumor Progression via Down Regulation of Neurofibromin 1. *PLoS One*. 2013;8:e53765.
60. Castle JC, Loewer M, Boegel S, de Graaf J, Bender C, Tadmor AD, et al. Immunomic, genomic and transcriptomic characterization of CT26 colorectal carcinoma. *BMC Genomics*. BioMed Central; 2014;15:190.
61. Fulda S, Vucic D. Targeting IAP proteins for therapeutic intervention in cancer. *Nat Rev Drug Discov*. 2012;11:331.
62. Eytan DF, Snow GE, Carlson S, Derakhshan A, Saleh A, Schiltz S, et al. SMAC mimetic birinapant plus radiation eradicates human head and neck cancers with genomic amplifications of cell death genes FADD and BIRC2. *Cancer Res*. 2016;76:5442–54.
63. Hanahan D, Weinberg RA. Hallmarks of cancer: The next generation. *Cell*. 2011;144:646–74.
64. Seiwert TY, Salama JK, Vokes EE. The chemoradiation paradigm in head and neck cancer. 2007;4:156–71.
65. Fritsch C, Huang A, Chatenay-Rivauday C, Schnell C, Reddy A, Liu M, et al. Characterization of the Novel and Specific PI3K Inhibitor NVP-BYL719 and Development of the Patient Stratification Strategy for Clinical Trials. *Mol Cancer Ther*. 2014;13:1117–29.
66. Juric D, Rodon J, Tabernero J, Janku F, Burris HA, Schellens JHM, et al. Phosphatidylinositol 3-Kinase α -Selective Inhibition With Alpelisib (BYL719) in PIK3CA -Altered Solid Tumors: Results From the First-in-Human Study. *J Clin Oncol*. 2018;36:1291–9.
67. Mayer IA, Abramson VG, Formisano L, Balko JM, Estrada M V, Sanders ME, et al. A Phase Ib Study of Alpelisib (BYL719), a PI3K α -specific Inhibitor, with Letrozole in ER+/HER2-Negative Metastatic Breast Cancer. *Clin Cancer Res*. 2017;23:26–34.
68. Gild ML, Landa I, Ryder M, Ghossein RA, Knauf JA, Fagin JA. Targeting mTOR in RET mutant medullary and differentiated thyroid cancer cells. *Endocr Relat Cancer*. 2013;20:659–67.
69. Gavine PR, Mooney L, Kilgour E, Thomas AP, Al-Kadhimi K, Beck S, et al. AZD4547: An orally bioavailable, potent, and selective inhibitor of the fibroblast growth factor receptor tyrosine kinase family. *Cancer Res*. 2012;72:2045–56.
70. Zhu X, Ding X. Study on a 3D Hydrogel-Based Culture Model for Characterizing Growth of Fibroblasts under Viral Infection and Drug Treatment. *SLAS Discov*. 2017;22:626–34.
71. Valyi-Nagy T, Fredericks B, Ravindra A, Hopkins J, Shukla D, Valyi-Nagy K. Herpes simplex virus type 1 infection promotes the growth of a subpopulation of tumor cells in 3D uveal melanoma cultures. *J Virol*. United States; 2018;92:e00700-18.
72. Bonner J a, Harari PM, Giralt J, Azarnia N, Shin DM, Cohen RB, et al. Radiotherapy plus cetuximab for squamous-cell carcinoma of the head and neck. *N Engl J Med*. 2006;354:567–78.
73. Cai Y, Doodia S, Su GH. Dysregulations in the PI3K pathway and targeted therapies for head and neck squamous cell carcinoma. *Oncotarget*. 2017;8:22203–17.
74. Munster P, Elkabets M, Gilbert J, Razak ARA, Ahn M-J, Yen C-J, et al. Abstract A46: Inhibition of PIK3CA with BYL719 can overcome resistance to cetuximab in squamous cell carcinoma of the head and neck (SCCHN). *Mol Cancer Ther*. 2015;14:A46–A46.
75. Ho A, Chau N, Brana Garcia I, Ferte C, Even C, Burrows F, et al. Preliminary

- results from a phase 2 trial of tipifarnib in HRAS-mutant head and neck squamous cell carcinomas. *Int J Radiat Oncol Biol Phys.* 2018;100:1367.
80. Economopoulou P, Perisanidis C, Giotakis EI, Psyri A. The emerging role of immunotherapy in head and neck squamous cell carcinoma (HNSCC): anti-tumor immunity and clinical applications. *Ann Transl Med.* 2016;4:173–173.
 81. Dijkstra KK, Cattaneo CM, Weeber F, Chalabi M, van de Haar J, Fanchi LF, et al. Generation of Tumor-Reactive T Cells by Co-culture of Peripheral Blood Lymphocytes and Tumor Organoids. *Cell.* Elsevier; 2018;174:1586–98.
 82. Hashimshony T, Wagner F, Sher N, Yanai I. CEL-Seq: single-cell RNA-Seq by multiplexed linear amplification. *Cell Rep.* United States; 2012;2:666–73.
 83. Simmini S, Bialecka M, Huch M, Kester L, van de Wetering M, Sato T, et al. Transformation of intestinal stem cells into gastric stem cells on loss of transcription factor Cdx2. *Nat Commun.* England; 2014;5:5728.
 84. Li H, Durbin R. Fast and accurate long-read alignment with Burrows-Wheeler transform. *Bioinformatics.* England; 2010;26:589–95.
 85. Hoogstraat M, Hinrichs JWJ, Besselink NJM, Radersma-Van Loon JH, De Voijis CMA, Peeters T, et al. Simultaneous detection of clinically relevant mutations and amplifications for routine cancer pathology. *J Mol Diagnostics.* 2015;7:10–8.
 86. Shaner NC, Lambert GG, Chammas A, Ni Y, Cranfill PJ, Baird MA, et al. A bright monomeric green fluorescent protein derived from *Branchiostoma lanceolatum*. *Nat Methods.* 2013;10:407–9.
 87. Huch M, Dorrell C, Boj SF, van Es JH, Li VSW, van de Wetering M, et al. In vitro expansion of single Lgr5+ liver stem cells induced by Wnt-driven regeneration. *Nature.* 2013;494:247–50.
 88. Faas FGA, Avramut MC, van den Berg BM, Mommaas AM, Koster AJ, Ravelli RBG. Virtual nanoscopy: generation of ultra-large high resolution electron microscopy maps. *J Cell Biol.* United States; 2012;198:457–69.

SUPPLEMENTARY DATA

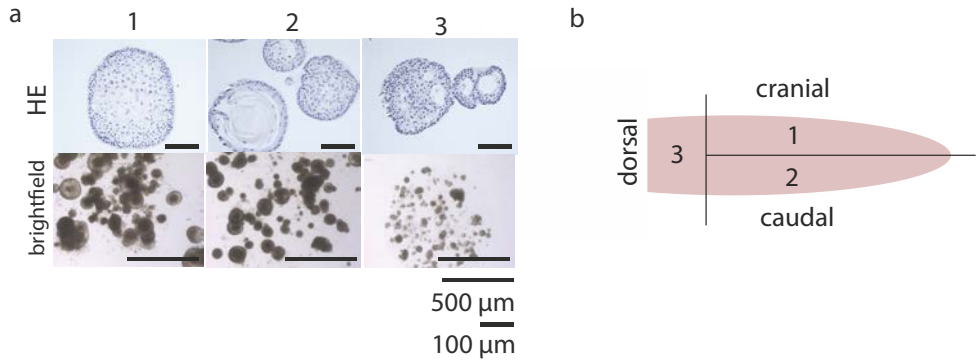
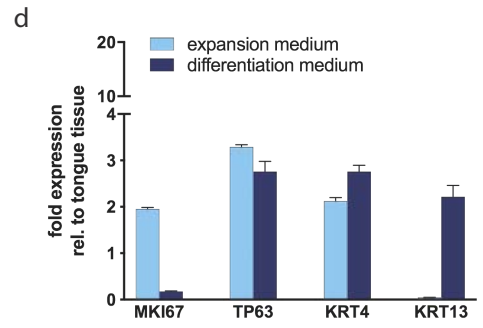
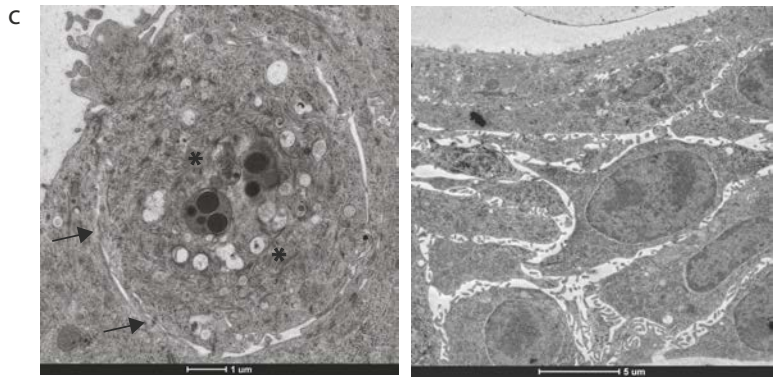
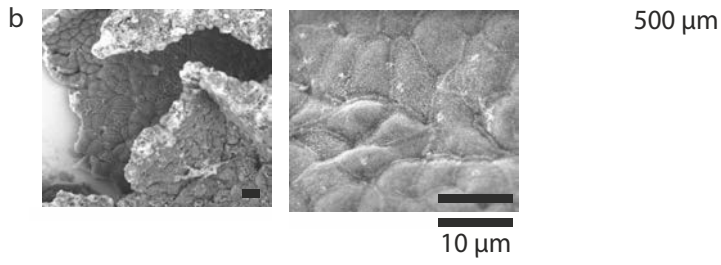
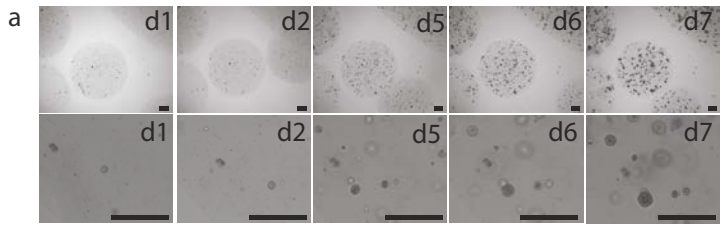
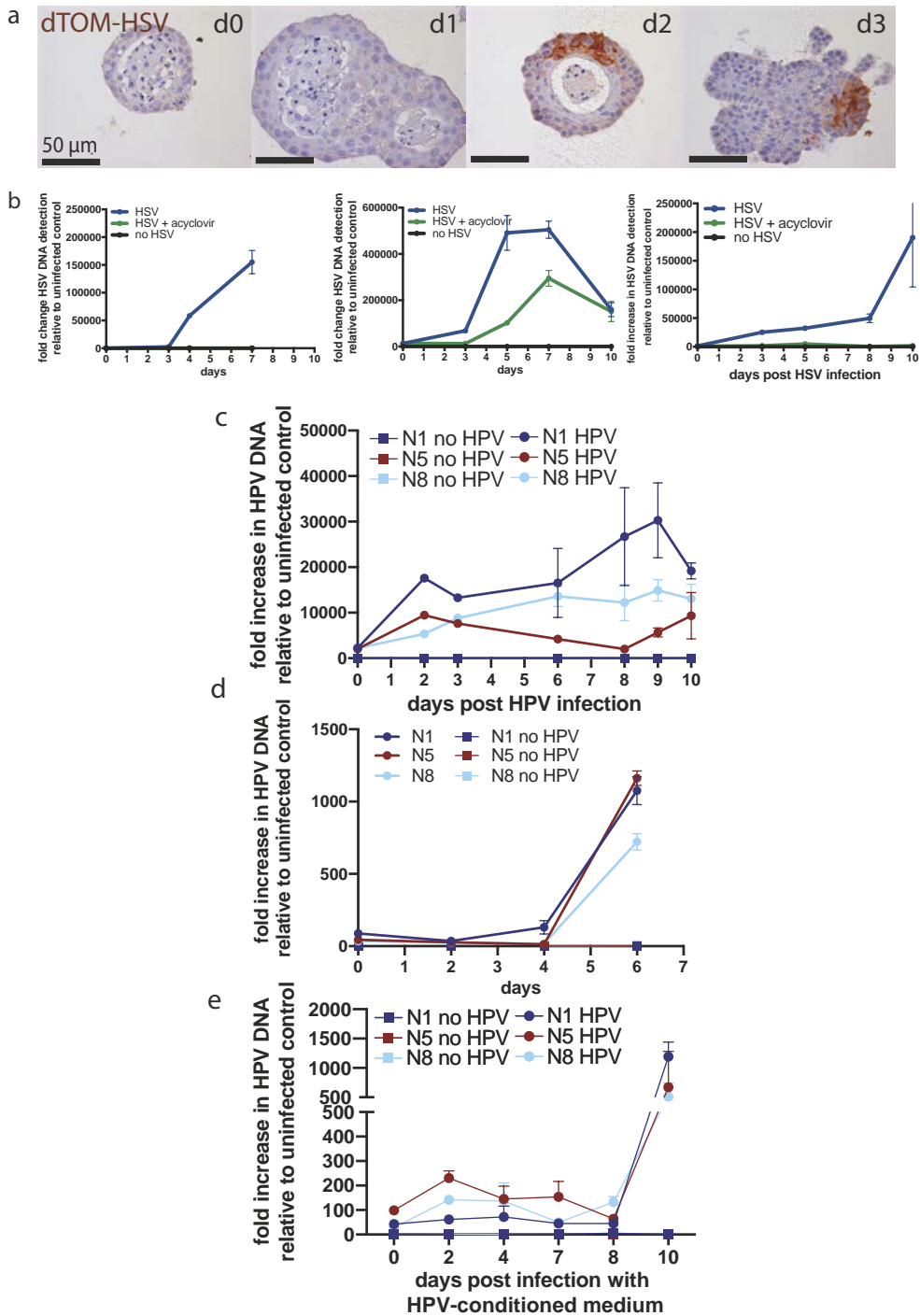


Figure S1. Oral mucosa organoids can be established from mouse tongue epithelium, related to Figure 1. A. brightfield microscopy images and H&E staining of paraffin-embedded organoid sections of organoids established from different regions of the mouse tongue (annotated 1, 2 and 3, see schematic in B) B. Organoids keratinize at larger sized, revealed by darker centers in the brightfield images or acellular parts in the H&E staining. Scalebar top panels 100 μm, scalebar bottom panels 500 μm. B. Schematic of locations annotated 1, 2 and 3 in figure S1A.



◀ **Figure S2. Outgrowth of human oral mucosa organoids and characterization using scanning electron microscopy and transmission electron microscopy, related to Figure 1.** A. Organoid outgrowth can be observed from human primary tissue when put in culture. Representative images of establishment of an organoid culture. Starting one day after initial plating of the tissue, images of the same BME drop with human cells were taken on day 1, 2, 5, 6 and 7 to show outgrowth of organoids from primary tissue. Scalebar 500 μm . B. Scanning electron microscopy of human oral mucosa organoids. First panel: an organoid that broke open during processing shows the apical surface of organoid cells. Most cells have a smooth surface, whereas some cells have a folded apical surface. Second panel: zoom in of the apical surface of an organoid, showing multiple keratinocytes forming tight connections. Scalebar 10 μm . C. Transmission electron microscopy images of human oral mucosa organoids. First panel: a single keratinocyte shows properties characteristic for keratinocytes, such as abundant tonofilament formation (asterixes) and tight junctions (arrows) connecting it to neighboring cells. Second panel: cross section spanning the apical part of the organoid wall. Cells located more towards the outside of the organoids are bigger, more rounded and have intact nuclei. Moving more towards the inside of the organoid, cells seem to flatten out, and lose their nucleus. Third panel, cross section showing the inside of an organoid, where cell fragments are still present. One keratinocyte is being shed into the inside of the structure. Scalebars are shown below each individual panel. E. Quantitative PCR of a normal oral mucosa organoid line (N8) for proliferation marker MKI67, basal cell marker TP63 and KRT13. Prior to RNA collection, growth factors were withdrawn from the medium to induce differentiation. Expression levels are calculated using $\Delta\Delta\text{Ct}$ method. For each marker, fold change in expression is made relative to expression of this markers in human primary tongue tissue, which is set to 1. $n=3$, individual data points are shown, bars represent average.



◀ **Figure S3. Oral mucosa organoids can be productively infected with Herpes Simplex Virus and Human Papilloma Virus, related to Figure 1.** A. Quantification of HSV DNA after infection of oral mucosa organoids derived from three different donors. Quantitative PCR of DNA obtained from oral mucosa organoids infected with HSV and kept in culture for 10 days. HSV can replicate in oral mucosa organoids, and this replication can be inhibited by the addition of acyclovir. Fold increase in DNA content is calculated relative to Ct values of the uninfected control at day 0, using the ΔCt method. Datapoints represent the average of three technical replicates, error bars represent the SEM. Blue, organoids infected with HSV. Green, organoids infected with HSV and cultured in the presence of $1\mu\text{M}$ acyclovir. Black, organoids not infected with HSV. B. Immunohistochemical staining for dTomato was performed on organoids infected with dTomato labelled HSV (dTOM-HSV). Organoids were collected on day 0, 1, 2 and 3. *Scalebar* $50\mu\text{m}$. C. Quantification of HPV DNA after splitting of HPV-infected organoids. 10 days after initial infection (results shown in Figure 2F), organoids were split and plated to follow HPV DNA over time. Increase in HPV DNA could be observed six days after splitting in all three organoid lines. D and E. Quantitative PCR for HPV on DNA obtained from oral mucosa organoids infected with HPV (D) or HPV-conditioned medium (E) and kept in culture for a maximum 10 days. Fold increase in DNA content is shown relative to uninfected control at day 0. Data points represent the average of three technical replicates, error bars represent the SEM.

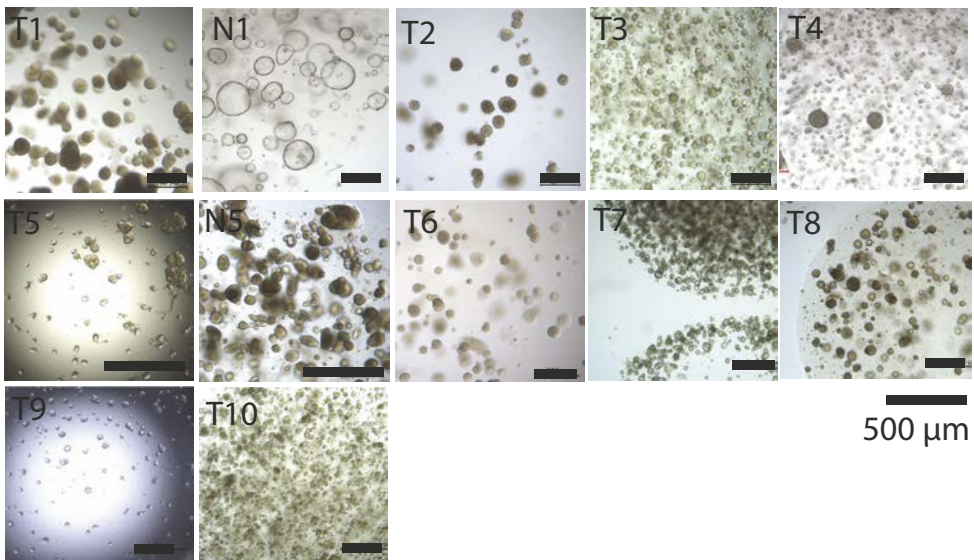


Figure S4. Brightfield images of HNSCC-derived organoid lines, related to Figure 3. For all organoid lines characterized in this work, images are shown of organoids in culture. *Scalebar*, $500\mu\text{m}$.

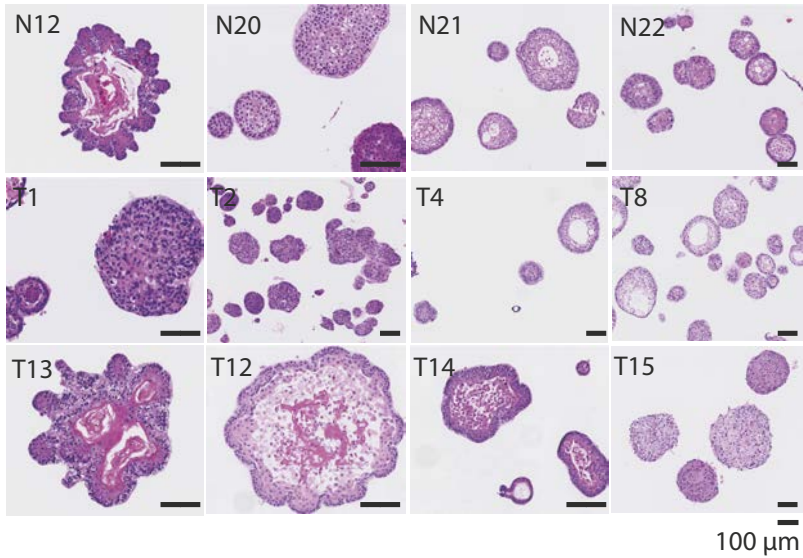


Figure S5. H&E staining of HNSCC-derived organoids reveals differences in morphology between different organoid lines, related to Figure 3. H&E staining performed on sections of paraffin-embedded organoids. Here, H&E staining of four normal and eight tumor lines are shown.

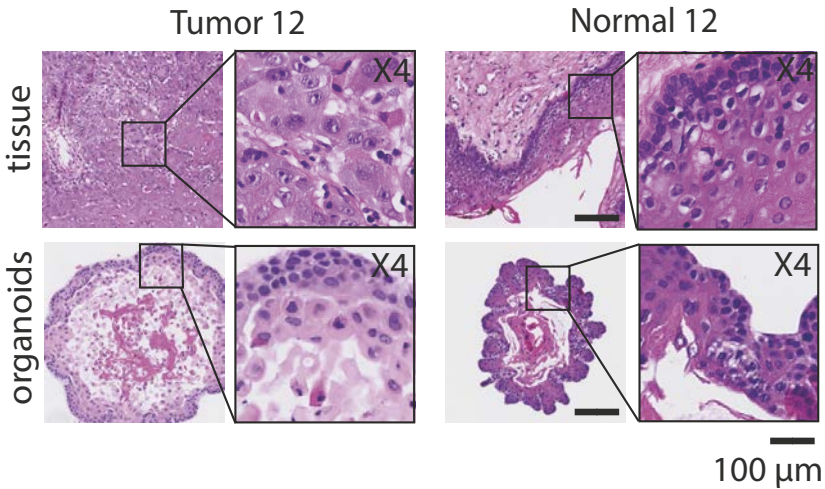


Figure S6. Normal and tumor organoids derived from the same patient show different morphology, related to Figure 3. Organoids were derived from both tumor tissue and adjacent normal tissue from the same patient. H&E staining of organoids are shown and reveal different morphology of the two organoid lines.

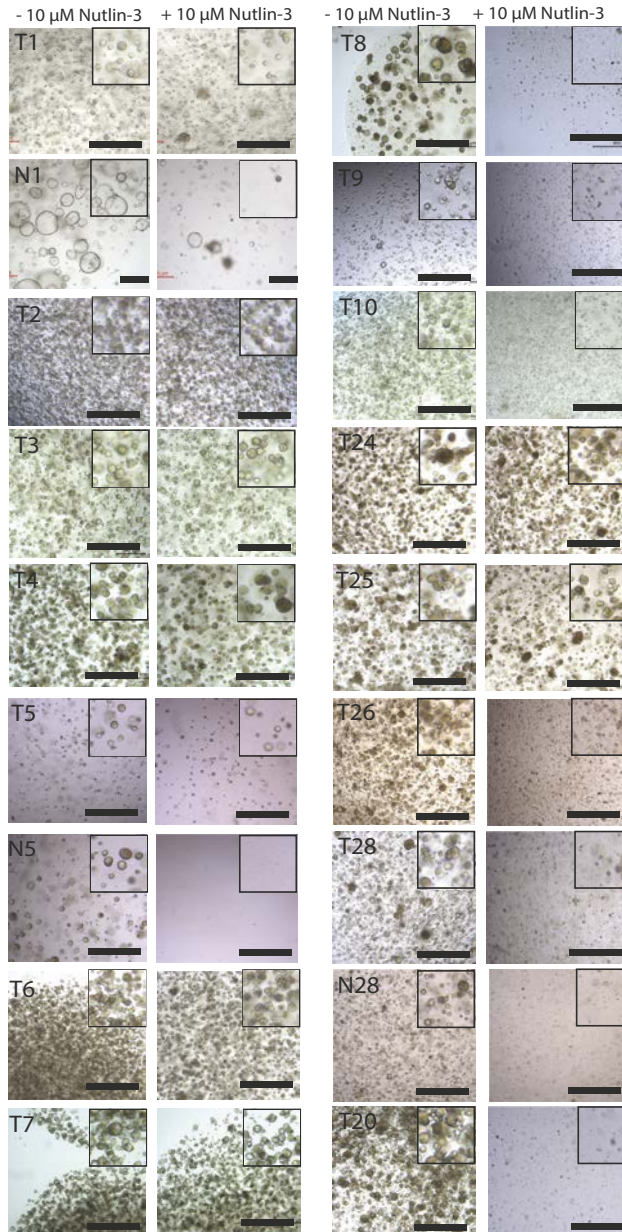


Figure S7. HNSCC-derived organoid show differences in sensitivity to Nutlin-3, related to Figure 3. Organoids were cultured for three passages in the presence of 10 μM Nutlin-3 and passaged weekly. Left panels, organoid cultured in the absence of Nutlin-3. Right panels, organoids cultured in the presence of Nutlin-3. All tumor lines, except T8, T9 and T10 are resistant to these compounds. Both normal lines (N1 and N5, corresponding normal organoids of T1 and T5) show Nutlin-3 sensitivity. Scalebar, 500 μm.

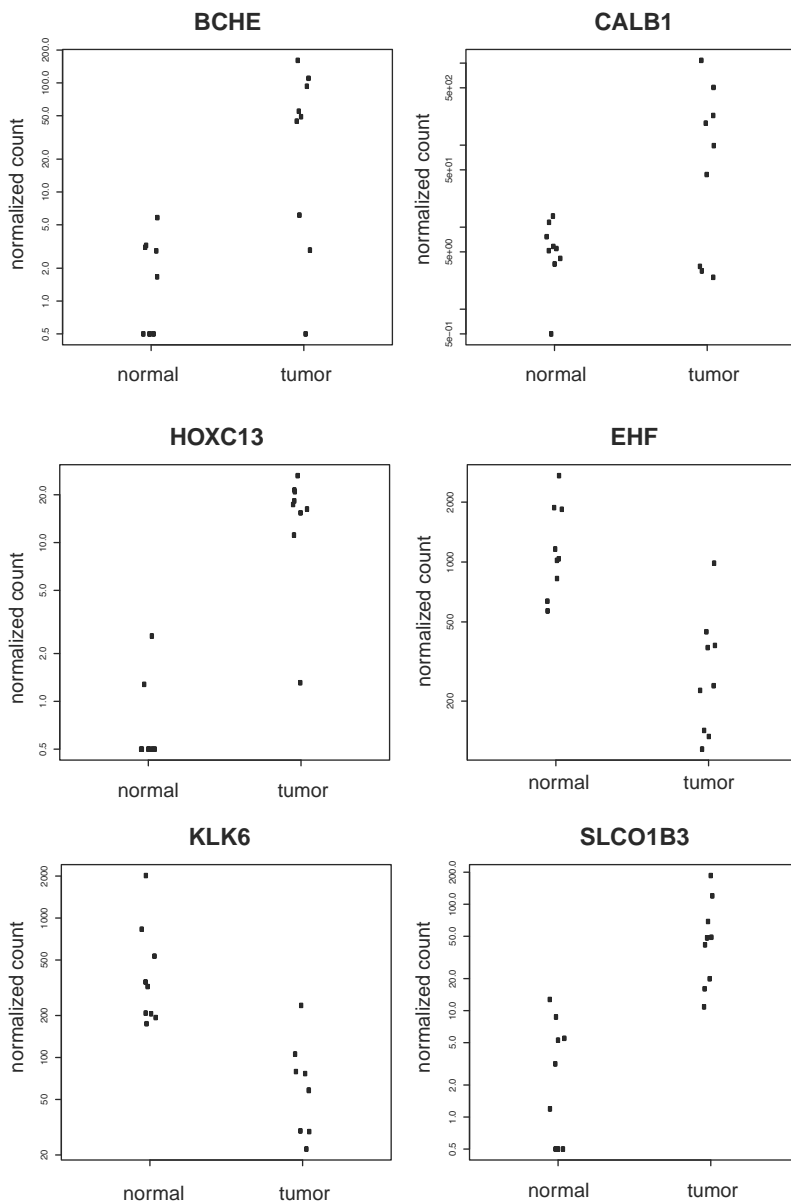
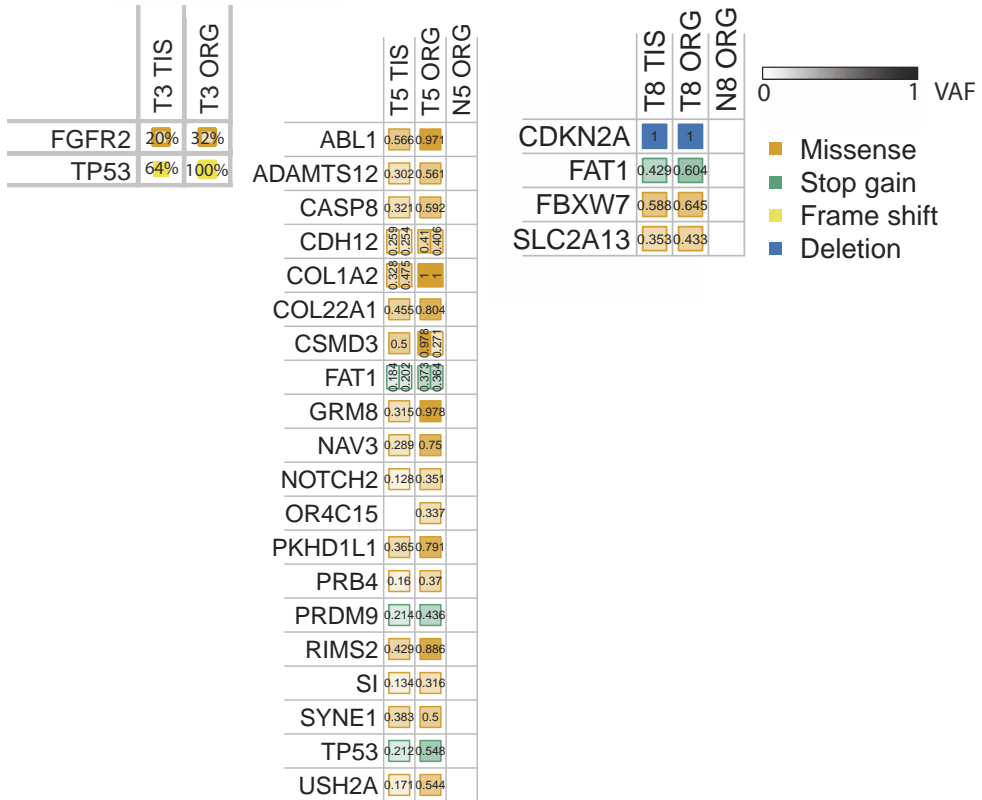


Figure S8. Highlighted genes differentially expressed between normal and tumor organoids , related to Figure 3. Scatterplots of the expression of these seven genes, plotted for each individual gene.



2.1

Figure S9. Comparison of sequencing results of primary tissue and organoid cultures of patient 3, 5 and 8, related to Figure 4. Allele frequency of mutations detected by targeted sequencing (T3) or whole exome sequencing (T5 and T8), performed in both primary tissue and corresponding organoids.

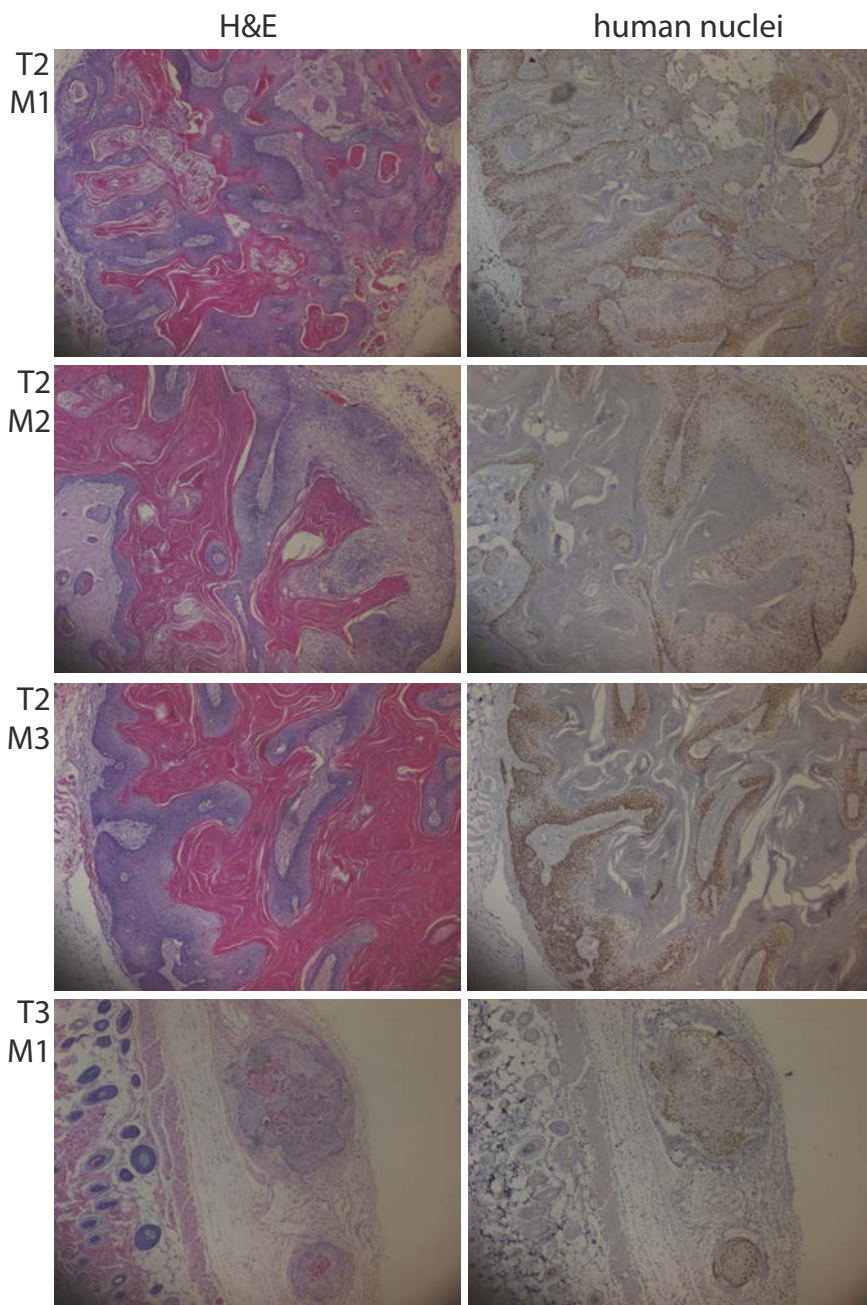
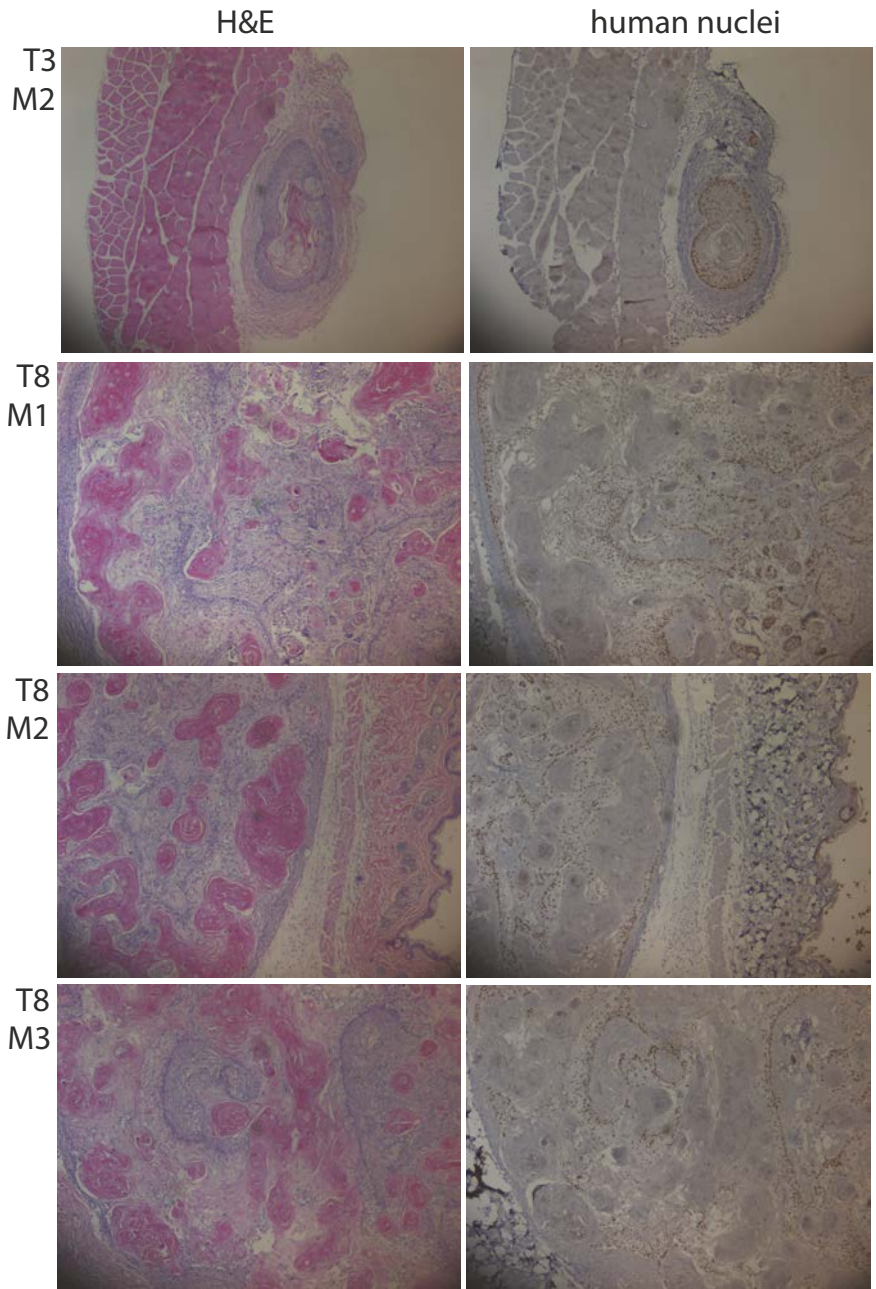
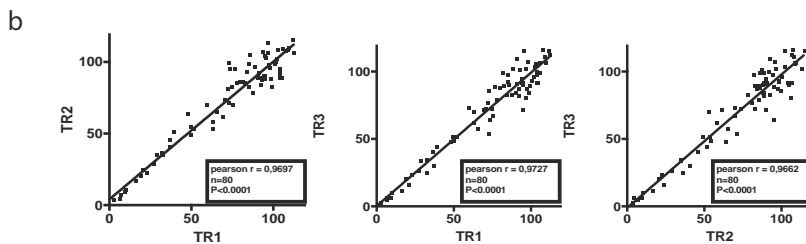
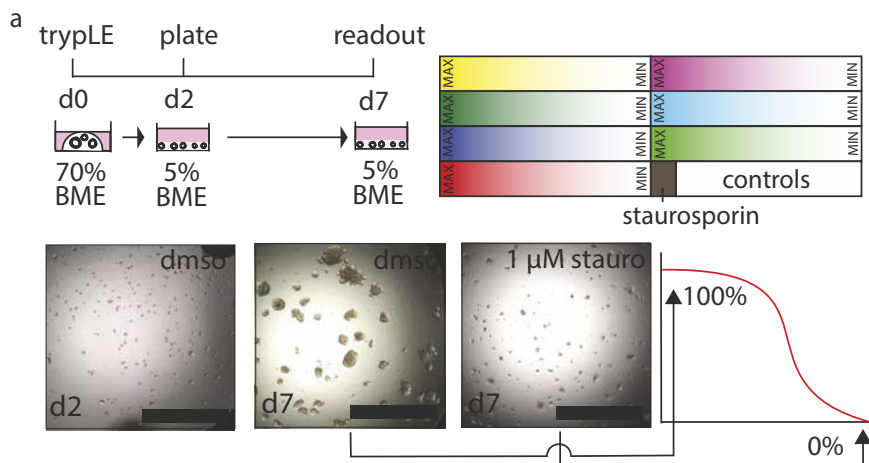


Figure S10. HNSCC-derived organoids result in tumor formation *in vivo*, related to Figure 6. For all transplanted organoid line, three mice were injected. Here, H&E and anti-human nuclei staining for these tumors is shown. As can be seen, histology of tumors originating from the same organoid line matches. Scale bar, 100 μ m.



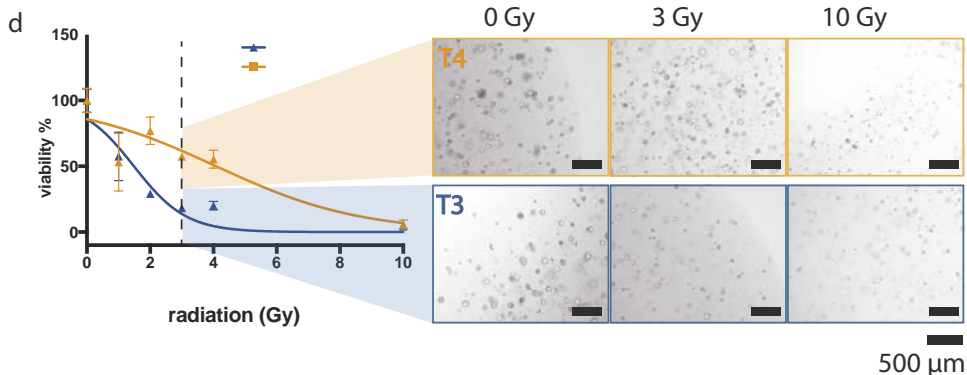
2.1

Figure S10. (continued)



c

Drug used:	T1	T2	T3	T4	T5	T6	T7	T8	T9	T24	T25	T27	T28
Cisplatin	0.72	0.72	0.34	0.77	0.71	0.65	0.71	0.92	0.79	0.82	0.64	0.60	0.57
Carboplatin	0.72	0.67	0.34	0.77	0.71	0.65	0.71	0.92	0.79	0.82	0.64	0.60	0.57
Cetuximab	0.82	0.82	0.63	0.74	0.90	0.72	0.76	0.47	0.59				
Alpelisib	0.67	0.41	0.32	0.71	0.60	0.62	0.81	0.88	0.46	0.96	0.81	0.50	0.70
AZD4547	0.76	0.41	0.85	0.71	0.60	0.78	0.81	0.88	0.46	0.96	0.81	0.50	0.70
Everolimus	0.76	0.41	0.30	0.71	0.70	0.78	0.81	0.88	0.77	0.96	0.81	0.50	0.70
Nutlin	0.76	0.41	0.85	0.71	0.60	0.78	0.81	0.88	0.77	0.96	0.81	0.50	0.70
Niraparib	0.76	0.62	0.85	0.71	0.60	0.78	0.81	0.88	0.46	0.96	0.81	0.50	0.70
Vemurafenib				0.74	0.43				0.59	0.86			



◀ **Figure S11. *In vitro* drug screens in HNSCC-derived organoids, related to Figure 7.** A. Schematic layout of the drug screens as performed in this study. Organoids were disrupted into single cells on day 0, and plated to recover for two days. On day 2, organoids were collected from the BME, washed, filtered, counted and plated in 5% BME in organoid medium in 384 well format (500 organoids per well). Subsequently a gradient of drug concentrations was printed in the wells (different drugs are represented by different colors in the figure), and cells were left exposed to the drugs for five days. As positive control, cells were exposed to 1 μ M staurosporin. Solvent volumes were normalized for each plate, so that percentage DMSO or PBS/Tween-20 was identical for each well. Wells with only normalization were used as negative control. Each drug concentration was tested in triplicate. Readout was performed using Cell Titer Glow. B. To assess the reproducibility of the assay, the same drug screen was performed three times (technical replicates, named as TR1, TR2 and TR3). Calculated viability for each individual data point was plotted against its replicate value to assess robustness of the assay. C. Z factor scores of the performed drug screens for all drugs and all organoid lines presented in this work. D. *In vitro* radiation sensitivity screen. As an example, brightfield images on the day of readout are shown here for T3 and T4. T3 is more sensitive to radiation when compared to T4, which can be seen also from the number and the size of the organoids when compared to organoids that were not exposed to radiation. Scale bar 500 μ m.

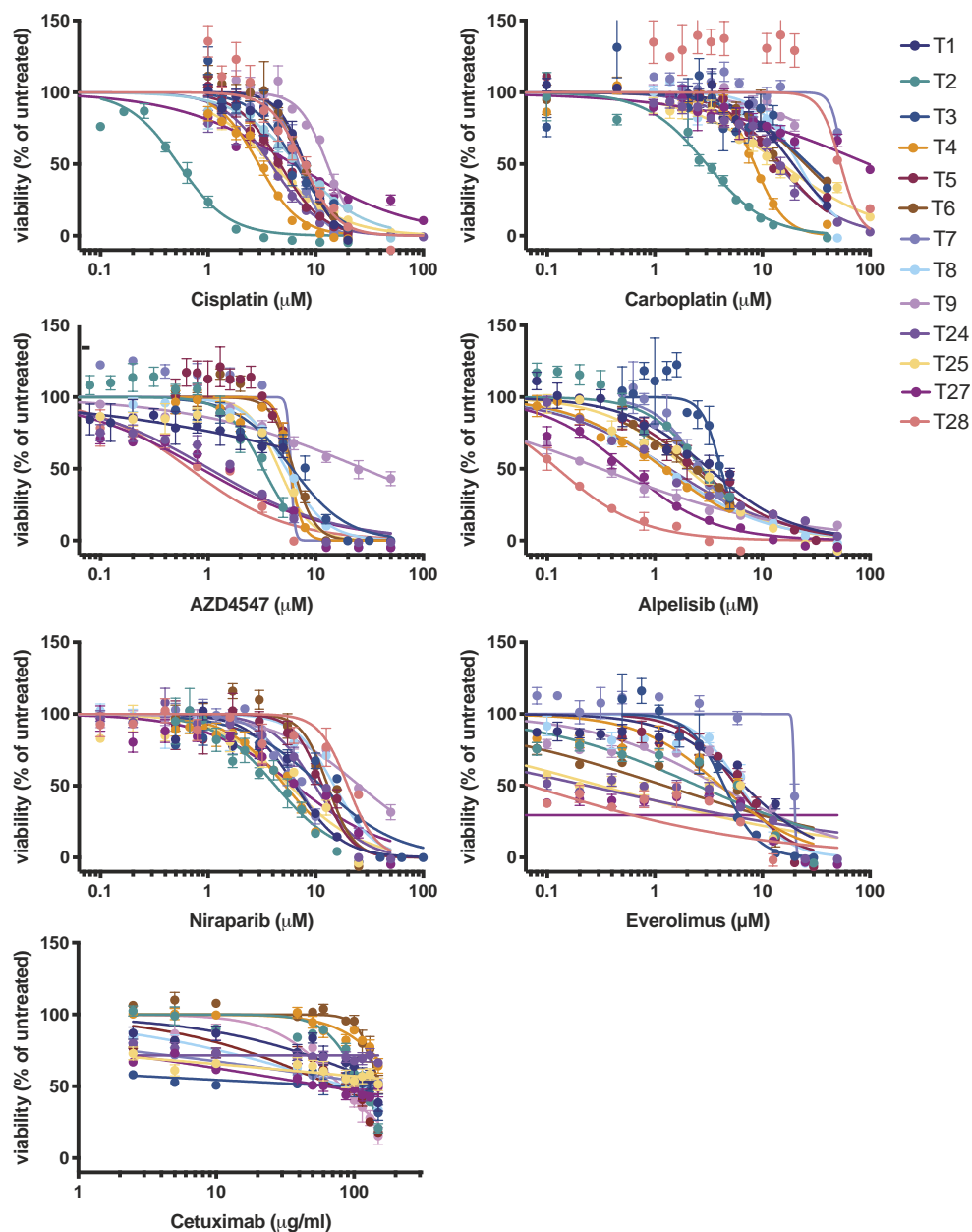
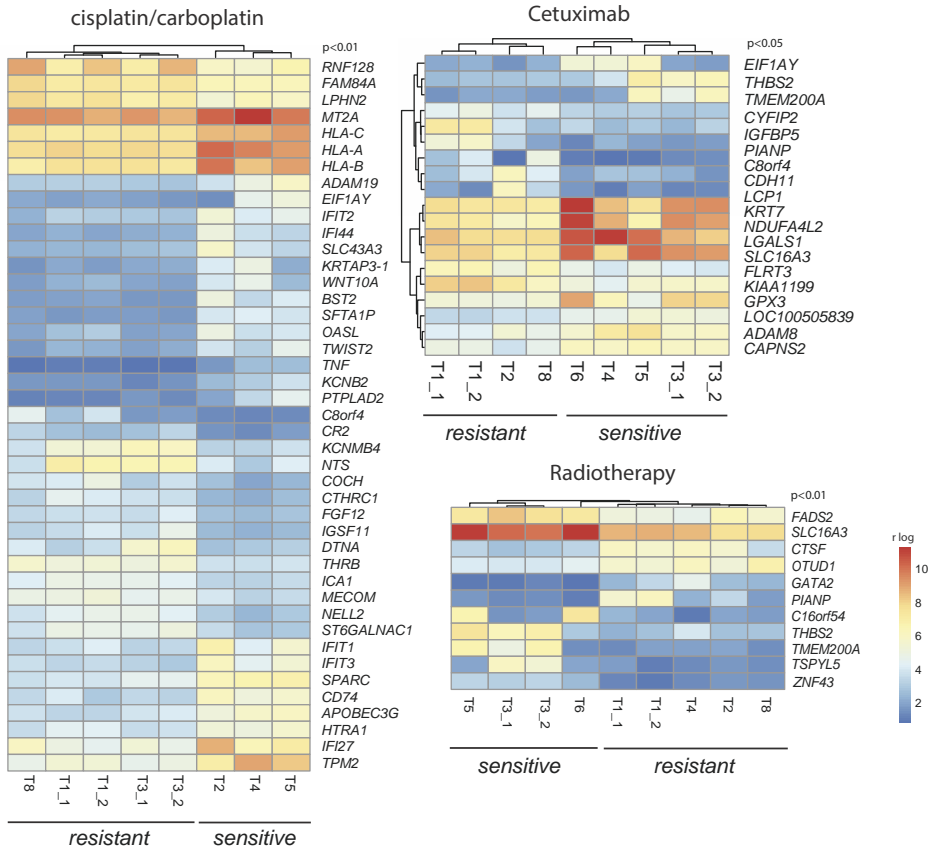


Figure S12. Sensitivity of HNSCC-derived organoids exposed to all compounds used in this study, related to Figure 7. Drugscreen results from organoid lines exposed to Cisplatin, Carboplatin, Cetuximab, AZD4547, Everolimus, Alpelisib and Niraparib.



2.1

Figure S13. Differential gene expression between organoids showing a good or bad respons to cisplatin/carboplatin, cetuximab or radiotherapy. Heatmap showing differentially expressed genes between good and bad responding organoid lines. Only genes with a $p_{adj} < 0.001$ are shown here. DEseq analysis results in identification of genes differentially expressed between lines that are most and least sensitive, respectively. to the therapy of interest. Here, cisplatin/carboplatin, cetuximab and radiotherapy are tested.

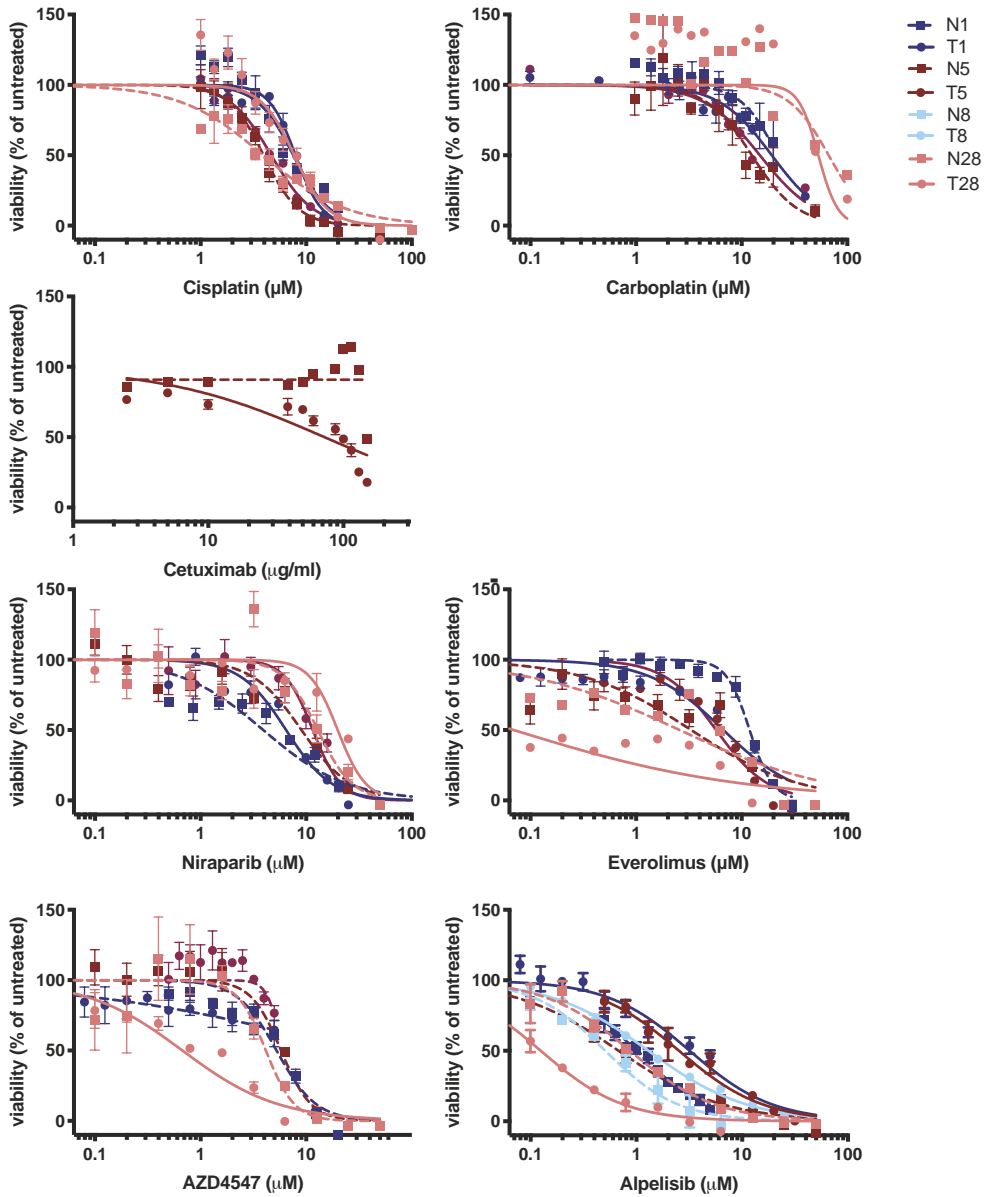


Figure S14. Sensitivity of matched normal and tumor organoids to compounds used in this study, related to Figure 7. Drugscreen results from N1 and T1, N5 and T5 and N8 and T8 organoid lines exposed to cisplatin, carboplatin, cetuximab, AZD4547, everolimus, Alpelisib and niraparib.

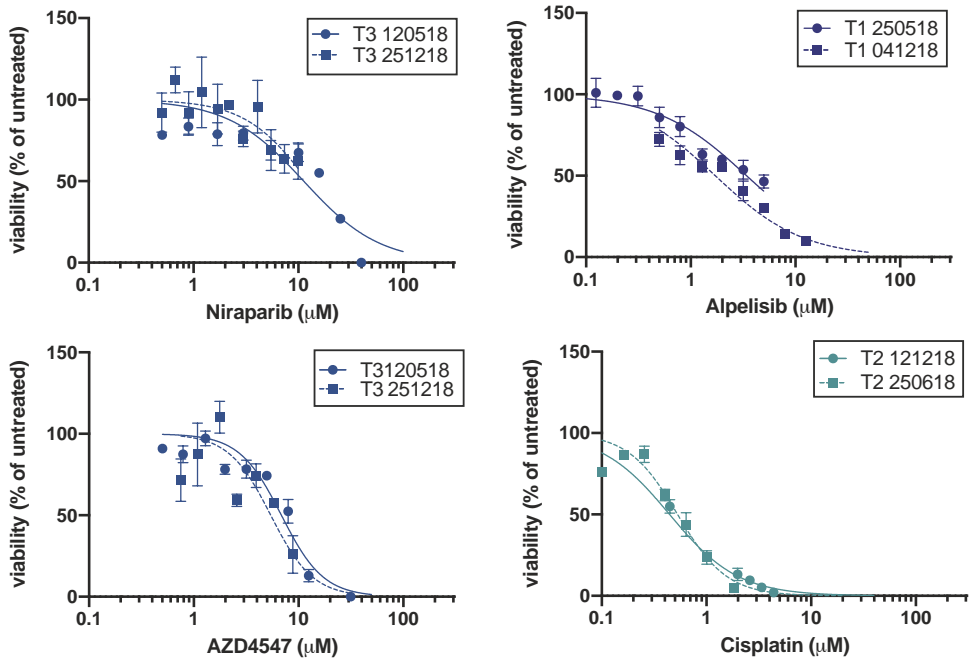


Figure S15. Organoid in vitro drug response remains comparable over time in culture. Four different drug screens were performed with at least 22 weeks of culturing in between, and reveal comparable drug screening results over time. Screens shown are Alpelisib testing in T1, Cisplatin testing in T2 and Niraparib and AZD4547 testing in T3.

Supplemental Movie S1. Time lapse showing organoid outgrowth after plating cells obtained from tissue digestion, related to Figure 1. Movie is a three day timelapse of cultures isolated 24h before the start of the movie for primary tissue.

Supplemental Movie S2. Outgrowth of organoids from single cells or clumps of cells after splitting an established organoid line, related to Figure 1. Movie is a three day timelapse of organoids that were splitted 2 hours prior to the start of imaging with TrypLE.

Supplemental Movie S3. Infection of organoids with dTOM-HSV, related to Figure 2. Movie is a 62 hours timelapse of organoids infected one hour before the start of imaging with dTOM-HSV. *Scalebar 500 μ m.*

Supplemental Movie S4. Example of a timelapse movie of H2B-mNEON N1 organoids, used to quantify segregation errors during mitosis, related to Figure 5. Color in the left panel indicates depth. *Scalebar 20 μ m.*

Supplemental Movie S5. Example of a timelapse movie of H2B-mNEON N1 organoids, used to quantify segregation errors during mitosis, related to Figure 5. Color in the left panel indicates depth. *Scalebar 20 μ m.*

Table S2. DEseq2 analysis results comparing tumoroid samples versus normal wildtype organoids, related to Figure 2.

Table S5. DEseq2 analysis identifying differential gene expression analysis performed on organoids responding well or poorly to cisplatin/carboplatin, cetuximab or radiotherapy, related to Figure 6.

All supplemental movies and tables S2 and S5 can be found at:
http://tiny.cc/Supp_ElseDriehuis

Table S1. Patient data corresponding to the organoid lines presented in this work, related to Figure 3.

#T	gender	birthyear	tumor location	pretreatment	HPV status	sequencing	drugscreen	N/T	No longer in culture
1	male	1955	tongue	no	negative	oncopanel	Yes	N/T	
2	female	1927	larynx	no	negative	oncopanel	Yes	T	
3	female	1934	larynx	no	negative	oncopanel	Yes	T	
4	male	1956	tongue	no	negative	oncopanel	Yes	T	
5	male	1938	parotis SCC	no	negative	exome sequencing	Yes	N/T	
6	male	1935	oral cavity	no	negative	oncopanel	Yes	T	
7	female	1960	floor of mouth	no	negative	oncopanel	Yes	T	
8	female	1948	gingiva	no	negative	exome sequencing	Yes	N/T	
9	male	1948	mandibula	no	negative	oncopanel	Yes	T	
10	female	1936	mandibula	no	n.t.	oncopanel	No	T	stopped at p10
11	male	1951	oral cavity	no	n.t.	n.t.	No	T	stopped at p20
12	male	1937	gingiva	no	n.t.	n.t.	No	T	
13	male	1946	larynx	no	n.t.	n.t.	No	T	
14	female	1962	larynx	no	n.t.	n.t.	No	T	stopped at p4
15	male	1954	pharynx	no	n.t.	n.t.	No	T	
16	male	1959	pharynx	no	n.t.	n.t.	No	T	
17	male	1939	floor of mouth	no	n.t.	n.t.	No	N	
18	male	1949	larynx	no	n.t.	n.t.	No	N	
19	male	1949	oropharynx	no	n.t.	n.t.	No	T	
20	male	1954	salivary gland SCC	no	n.t.	oncopanel	No	N/T	
21	female	1947	larynx	no	n.t.	n.t.	No	T	stopped at p5
22	male	73	pharynx	no	negative	n.t.	No	T	
23	male	1970	floor of mouth	no	n.t.	n.t.	No	T	
24	male	1941	oral cavity	no	n.t.	oncopanel	Yes	T	
25	male	1946	floor of mouth	no	n.t.	oncopanel	Yes	T	
26	male	1947	nasal cavity	no	n.t.	oncopanel*	no	T	
27	female	1958	oral cavity	no	n.t.	oncopanel	Yes	N/T	
28	male	1935	oral cavity	no	n.t.	oncopanel	Yes	N/T	



Table S1. (continued)

#T	gender	birthyear	tumor location	pretreatment	HPV status	sequencing	drugscreen	N/T	No longer in culture
29	male	1943	neck	no	n.t.	oncopanel	Yes	N/T	
30	male	1947	hypopharynx	no	n.t.	n.t.	No	T	
31	female	1932	tongue	no	n.t.	n.t.	No	N	
32	female	1939	larynx	no	n.t.	n.t.	No	T	
34	female	1972	larynx	no	n.t.	n.t.	No	T	stopped at p5
35	male	1965	oral cavity	no	n.t.	n.t.	No	N	stopped at p6

No mutations were detected by the 54 gene covering oncopanel. WGS will be performed to validate the tumor origin of this organoid line.

Table S3. Details of mutation detected by (targeted) sequencing of the organoid lines, related to Figure 4.

organoid line	gene	DNA	protein	variant effect	external status
T1	PIK3CA	1633G>A	Glu545Lys	missense	COSM763
T1	TP53	586C>T	Arg196*	stop gained	COSM10705
T2	KRAS	204G>T	Arg68Ser	Missense	COSM183929
T2	ESR1	1138G>A	Glu380Lys	Missense	
T2	TP53	406C>T	Gln136*	Stop gained	COSM11166
T2	TP53	374C>T	Thr125Met	Missense	COSM44988
T3	TP53	102delC	Leu35Cysfs*9	Frameshift	COSM2745164
T3	FGFR2	1576A>G	Lys526Glu	Missense	rs121918507
T4	HRAS	37G>C	Gly13Arg	Missense	COSM486
T4	TP53	578A>G	His193Arg	Missense	COSM10742
T6	CDKN2A	151G>A		splice acceptor	COSM13694
T6	TP53	637C>T	Arg213*	stop gained	COSM10654
T6	TP53	856G>A	Glu286Lys	Missense	COSM10726
T7	KRAS	35G>C	Gly12Arg	Missense	COSM522
T7	PIK3CA	1633G>A	Glu545Lys	Missense	COSM763
T7	MET	504G>T	Glu168Asp	Missense	COSM706
T7	TP53	830G>A	Cys277Tyr	Missense	COSM43737
T9	BRAF	1799T>A	Val600Glu	Missense	COSM476
T9	PIK3CA	3140A>G	His1047Arg	Missense	COSM775
T10	BRAF	1799T>A	Val600Glu	Missense	COSM476
T10	PIK3CA	3140A>G	His1047Arg	Missense	COSM775
T20	VHL	74C>T	Pro25Leu	Missense	COSM36211
T24	KRAS	34G>C	Gly12Arg	Missense	COSM518
T24	TP53	586C>T	Arg196*	Missense	COSM10705
T24	PIK3CA	1624G>A	Glu542Lys	Missense	COSM760
T24	PDGFRA	827C>T	Thr276Met	Missense	COSM1540243
T25	KRAS	34G>C	Gly12Arg	Missense	COSM518
T25	PIK3CA	3140A>G	His1047Arg	Missense	COSM775



Table S3. (continued)

	organoid line	gene	DNA	protein	variant effect	external status
T25	TP53		694A>T	Ile232Phe	Missense	COSM562650
T27	ATM		5558A>T	Asp1853Val	Missense	COSM3752120
T27	ATR		2875G>A	Val959Met, Lys764Glu, Val316Ile	Missense	COSM1579027
			2290A>G			COSM5020937
			946G>A			COSM1579030
T27	EGFR		G761A	Arg254Lys	Missense	COSM5830713
T27	ERBB2		1960A>G	Ile654Val	Missense	COSM6854579
T27	KDR		889G>A	Val297Ile	Missense	COSM1131107
T27	MPL		340G>A	Val144Met	Missense	COSM3996746
T27	PDGFRA		1432T>C	Ser478Pro	Missense	
T27	RET		166C>A	Lys56Met	Missense	COSM6493950
T28	MDM2		428G>A	Asp140Asn	Missense	
T28	TP53		836_848delGGAGAGACCGGCG	Gly279AlafsTer62	Frameshift	
T29	PIK3CA		1633G>C	Glu545Gln	COSM27133	COSM27133
T29	TP53		375G>T		Splice region	COSM381996
T29	TP53		825T>A	Val272Glu	Missense	COSM44580

Table S4. Patient information for correlation between in vitro organoid response to RT and patient clinical response.

organoid/ patient	tumor location	tumor stage	primary surgery	primary / adjuvant RT	indication for adjuvant RT
T1	tongue	T2N2b	excision of primary tumor, selective neck dissection level I-IV right and reconstruction with free radial forearm flap	adjuvant	positive resection margins, multiple lymph node metastases with extranodal extension
T2	larynx	T2N0		primary	
T3	larynx	T3N0		primary	
T5	parotid gland	T4aN0	parotidectomy	adjuvant	positive margins
T8	gingiva	T4aN0	excision of primary tumor with marginal mandibula resection and selective neck dissection level I-III left	adjuvant	positive margins
T25	floor of mouth	T2N1	excision of primary tumor, selective neck dissection level I-III both sides and reconstruction with free radial forearm flap	adjuvant after complete neck dissection because of neck recurrence	recurrence neck
T27	floor of mouth	T3N1	excision of primary tumor and sentinel node biopsy	adjuvant	close surgical margins and positive sentinel node

* limited RT dose because of diagnosis of second primary lung adenocarcinoma

RT dose	last check of response (after end RT)	timing of first indication of relapse after RT	details	organoid sensitive for RT	match organoid response/patient response
66 Gy	12 months	6 months	succumbed to locoregional and distant disease 12 months after RT completion	no	yes
60 Gy	18 months	4 months	total laryngectomy for recurrence, thereafter no evidence of disease	no	yes
48 Gy*	5 months	n.a.	succumbed to lung adenocarcinoma 5 months after end of RT without signs of laryngeal recurrence	yes	yes
66 Gy	11 months	n.a.	no evidence of disease	yes	yes
66 Gy	6 months	n.a.	no evidence of disease	no	no
52 Gy	2 months	1 month	succumbed to metastases neck, skin, lungs and liver	no	yes
56	2 months	n.a.	no evidence of disease	yes	yes

Table S6. Patient information for correlation between *in vitro* organoid response to RT and patient response, related to Figure 6.

organoid/ patient	tumor anatomical location	tumor stage	primary surgery	primary / adjuvant RT	indication for adjuvant RT	RT dose	last check of response (after finishing RT treatment)	timing of first indication of relapse after finishing RT	details	organoid sensitive for RT	match organoid response/ patient response
T1	tongue	T2N2b	excision of primary tumor selective neck dissection level I-IV right and reconstruction with free radial forearm flap	adjuvant	positive resection margins, multiple lymph node metastases with extranodal extension	66 Gy	12 months	6 months	succumbed to locoregional and distant disease 12 months after RT completion	no	yes
T2	larynx	T2N0		primary		60 Gy	18 months	4 months	total laryngectomy for recurrence, thereafter no evidence of disease	no	yes
T3	larynx	T3N0		primary		48 Gy*	5 months	n.a.	succumbed to lung adenocarcinoma 5 months after end of RT	yes	yes
T5	parotid gland	T4aN0	parotidectomy	adjuvant	positive margins	66 Gy	11 months	n.a.	no evidence of disease	yes	yes
T8	gingiva	T4aN0	excision of primary tumor with marginal mandibula resection and selective neck dissection level I-III left	adjuvant	positive margins	66 Gy	6 months	n.a.	no evidence of disease	no	no

* limited RT dose because of diagnosis of second primary lung adenocarcinoma


Table S7. Antibodies used for immunohistochemistry

protein	Supplier	Ordernumber	Host Species	Clone	Lotnumber	Dilution	Pretreatment
KRT5	Novocastra	NCL-L-CK5	Mouse	XM26	6027941	Ventana 1:200	CC1 24' (EDTA) Ventana
MKI67	Monosan	MONX10293	Mouse	MM1	10293	1:2000	Citrate autoclave
TP40	Abcam	ab172731	Rabbit	BC28	GR322490-1	Ventana 1:50	CC1 48'/ 32'AB
P53	DAKO	M7001	Mouse	DO-7	95381	Ventana 1:6000	CC1 24' (EDTA) Ventana
P63	Abcam	AB735	Mouse	4AB	AB735	1:800	Citrate
Human nuclei	Millipore	MAB1281	Mouse	235-1	1281	1:1000	Citrate autoclave
KRT13	Progen	10523	Mouse	1C7	10523	1:100	Citrate
dTOM	Rockland	600-401-379	Rabbit			1:1000	Citrate

**HOW TO PROCEED:
IN VITRO SCREENINGS FOR
THE ONCODE CLINICAL TRIAL
(ONCODE-P2018-0003)**

2.2

ABSTRACT



In the first part of Chapter 2, we have described how organoids derived from head and neck squamous cell carcinomas (HNSCC) can be used for personalized drug screening. Here, we summarize those findings that are relevant for the future Oncode clinical trial. This trial will assess the potential of HNSCC organoids to predict therapy responses of patients diagnosed with cancer. Using organoid cultures, we observe that *in vitro* therapy responses remain stable over time in culture and can be reproducibly obtained using our *in vitro* screening approach. However, when organoids are kept in culture long-term, selection of genetically distinct tumor clones is observed. Although numbers are small, these results indicate that: 1) screens should be performed as quickly as possible after establishment of the culture and 2) a comparison between primary tissue and corresponding organoid cultures is required before correlation can be tested. Lastly, we advise on the clinical parameters relevant to assess to correlate patient responses to *in vitro* organoid responses.

Else Driehuis, Maurice M.J.M. Zandvliet, Hans Clevers

INTRODUCTION

In the remainder of this chapter we would like to discuss what, in our opinion, are the next steps required to properly prepare for the Oncode Clinical trial. For this trial, *in vitro* screens that determine sensitivity to radiotherapy, chemotherapy or chemoradiation therapy will be performed. As described earlier in this chapter, a panel of patient-derived organoid lines was already exposed to chemoradiation therapy. These experiments were performed to: 1) assess reproducibility of organoid screens and 2) to expand our dataset of organoids exposed to this combination therapy, to see if and to what extent, chemotherapeutics can serve as radio sensitizing agents. Here, we would like to describe these results, as we believe these are relevant for the future clinical trial.

Testing a correlation between *in vitro* organoid responses and patient responses: how to proceed?

It is essential to keep in mind that to study correlation between patient response in the clinic and organoid response in the lab, other variables that influence the chance of relapse need to be controlled. Among those, success of tumor removal is the most obvious one, although total dose of ionizing radiation given (which can vary depending on anatomical tumor location), drug pharmacodynamics and kinetics and tumor characteristics (such as stage, specific mutations etc.) might also influence this outcome. Therefore, in the upcoming trial, we aim to measure these variables if possible, so that we can control for these when determining the predictive potential of HNSCC-derived organoids for the treatment of HNSCC patients. This also means that, in order to arrive at a conclusion about the predictive potential of this approach, we need to include a large enough number of patients. In the coming two years, we aim to include 80 patients diagnosed with HNSCC, of which organoid lines will be established from surgical resection or biopsy material. As efficiency of HNSCC organoid outgrowth is 60%, we anticipate we will establish about 50 HNSCC-organoid lines. Here, response to chemotherapy, radiation or both of the organoids will be compared to patients' clinical response. In a pilot experiment, a panel of patient-derived organoid lines was exposed to chemoradiation therapy, following the protocol described previously. These experiments were performed to: 1) assess reproducibility of organoid screens and 2) to expand our dataset of organoids exposed to this combination therapy, to see if, and to what extent, chemotherapeutics serve as radio sensitizing agents.

Comparison of radiotherapy screens performed over time

First, we compared the result of radiotherapy screens of a panel of ten organoid lines that were performed at different moments in time (Figure 1A and 1B). The time between the two screens was for the different tested lines. For T1, T2, T3, T4, T6 and T8, the screens were performed six months apart, whereas for T24, T25 and T27, the interval was one month. Overall, the results of the two screens were comparable, where lines such as T3, T4 and T6, that showed high sensitivity to radiotherapy in the first screen, still did so in the later

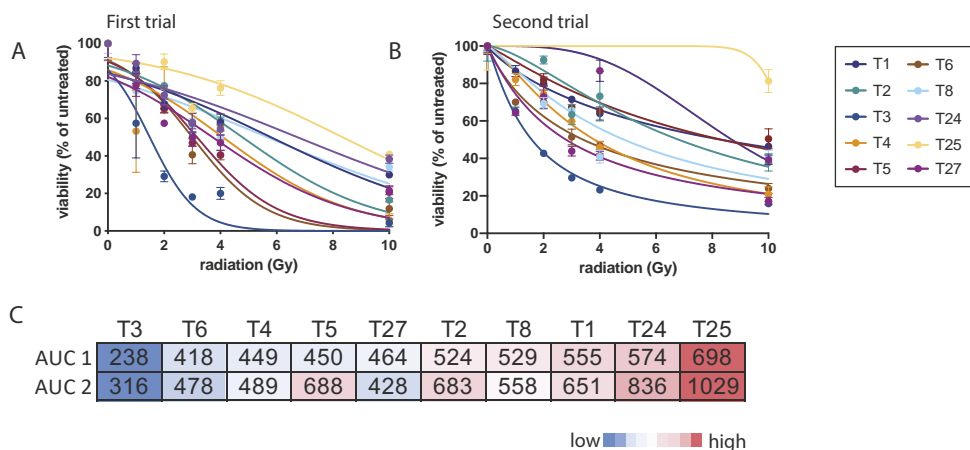


Figure 1. Comparison of organoid sensitivity to radiotherapy, as screened 1 to 6 months later. A. Results of first trial, depicted in viability curves of all individual organoid lines tested. Viability was calculated relative to cells not exposed to radiation. B. Results of second trial, depicted in viability curves of all individual organoid lines tested. Viability was calculated relative to cells not exposed to radiation. C. Heatmap comparing the results of the first and second *in vitro* radiotherapy screen. Area under the curve (AUC) was used as an indication of radiotherapy sensitivity. AUC values of the first and second trial are depicted below each other. Blue indicates low AUC values, Red indicates high AUC values.

screen. The same held true for the most resistant lines tested here. As such, although differences were detected, the ranking of organoid lines from sensitive to resistant by area under the curve (AUC) did not drastically change over time (Figure 1C).

Technical and biological variance between screens

The absolute AUC values were higher in the second screen, indicating overall survival was better in the second screen. This can also be appreciated by the data points indicating the exposure to 10 Gy of radiation, where survival was much better in the second screen than it was in the first screen. These differences might have a technical or biological cause. For example, this difference might be explained by a different location of the screening plate relative to the radiation source when the cells were irradiated. To overcome technical variance, we would recommend to include a control organoid line as a reference for overall toxicity of the radiation. This line should be expanded and frozen down. For each screen, this line (which should be at a fixed passage when tested) should be taken along on the screening plate as an internal control. As such, inter-screen variability can be assessed and potentially corrected for.

Additionally, it cannot be excluded that clonal selection within the lines is responsible for (part of) the difference in sensitivity observed between the two screens. For example,

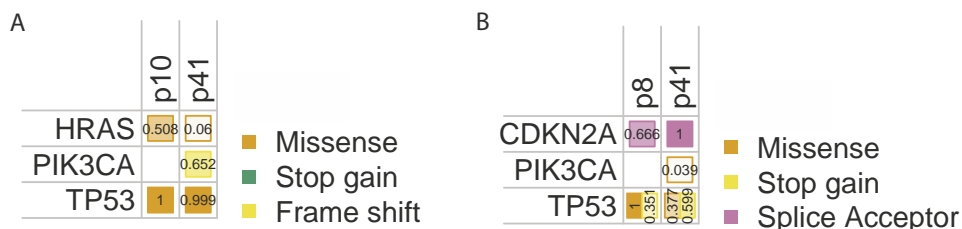


Figure 2. Clonal selection in patient-derived organoids line over time. Mutations detected by targeted sequencing in both passage 10 (p10) and passage 41 (p41) in organoid line T4 (A), and passage 8 (p8) and passage 41 (p41) of organoid line T6 (B). Allele frequency of detected mutations is given by the values. Different mutation types are depicted by different colors, see legend.

T5 shows a decrease in sensitivity to radiotherapy when comparing the earlier screen with the later screen. As organoids were cultured in between the two sensitivity screens, it cannot be excluded that clonal selection within the lines is responsible for (part of) the difference in sensitivity observed between the two screens. Although only assessed in two organoid lines, we have observed clonal selection over time in culture (Figure 2A and 2B). This has to be kept in mind when a correlation between organoid response and clinical outcome is studied. Screens should be performed as soon as enough material is obtained, and sequencing of DNA isolated from both organoid culture at the time of the therapy screen and primary tumor tissue should be performed to exclude data obtained with organoid lines that are not genetically recapitulating the primary tumor. Potential clonal selection is also why we stress to freeze a large batch of the control organoid line that should be always screened at a fixed passage.

Translation of *in vitro* sensitivities to predict a response to combination therapy: where to start?

Ultimately, the goal of the Oncode proof of principle clinical trial is to assess predictive potential of organoids for the patients' response to the therapy applied in the clinic. This therapy can be either radiotherapy alone, or radiotherapy combined with cisplatin, carboplatin or cetuximab. Currently, it is unknown if and which *in vitro* organoid response is most predictive for clinical response. For example, is the response to chemotherapy equally important as the response to radiotherapy? Or is it ultimately the radio sensitizing potential of the applied chemotherapeutic that determines patient outcome? Does it differ per patient which component of the therapy is most important? Or is this uniform over all patients? For example, if a patient-derived organoid line responds well to radiotherapy but poorly to cisplatin, and the patient receives a therapy consisting of the combination of the latter, would we expect a response? Or should only the *in vitro* response to the combination therapy be considered?

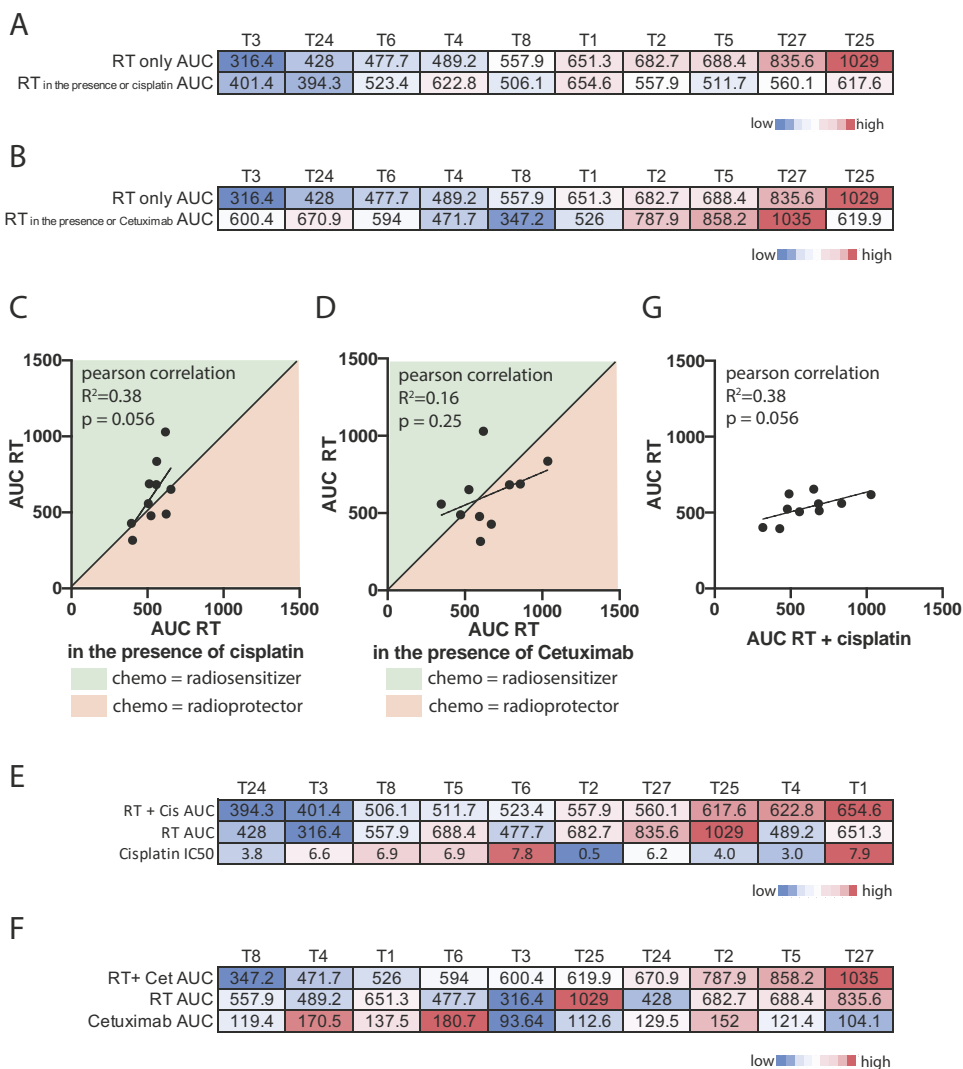


Figure 3. Comparison of organoid response to single or combination therapies. A. Heatmap depicting the AUC values for RT alone, or when given together with cisplatin. To study the synergistic effect of cisplatin, cell viability is corrected for the effect of cisplatin alone. B. Heatmap depicting the AUC values for RT alone, or when given together with Cetuximab. To study the synergistic effect of cisplatin, cell viability is corrected for the effect of cisplatin alone. C. The effect of cisplatin on radiotherapy sensitivity in organoids. AUC is shown as indicator of organoid sensitivity to *in vitro* radiotherapy. For each line tested, AUC is shown for RT alone, or when combined with cisplatin. Here, the effect of radiotherapy is corrected for the effect of chemotherapy alone. As such, the green area indicates lines where cisplatin serves as a radiosensitizer, whereas the red area indicates lines where cisplatin acts as a radioprotector. D. The effect of Cetuximab on radiotherapy sensitivity in organoids. AUC is shown as indicator of organoid sensitivity to *in vitro* radiotherapy. For each line tested, AUC is shown for RT alone, or when combined with Cetuximab. Here, the effect of radiotherapy is corrected for the effect of chemotherapy alone. As such, the green area indicates lines where Cetuximab serves

- ▶ as a radiosensitizer, whereas the red area indicates lines where Cetuximab acts as a radioprotector. E. Heatmap depicting the AUC values for RT alone, or when given together with cisplatin. In contrast to figure B, here we focus on additive effects of radiotherapy and cisplatin. Therefore here, the effect of 'RT + cisplatin' is not corrected for the effect of a single therapy. F. Heatmap depicting the AUC values for RT alone, or when given together with Cetuximab. In contrast to figure B, here we focus on additive effects of radiotherapy and Cetuximab. Therefore here, the effect of 'RT + Cetuximab' is not corrected for the effect of a single therapy. G. Correlation plot showing the sensitivity of 10 organoid lines for 'RT alone' or RT + cisplatin (not corrected for the effect of cisplatin alone). Correlation indicates that the effect of RT alone can predict for the response to 'RT + cisplatin'.

Radiosensitizing effect of cisplatin and Cetuximab in a panel of ten patient-derived organoid lines

We have shown that it is possible to combine chemo- and radiotherapy to assess the effect of each of these therapies either in the absence/presence of the other one. Here, we repeated these experiments in a larger number of organoid lines (Figure 3). These experiments gave us the opportunity to study the radio sensitizing potential of chemotherapeutics in tumor cells derived from different patients. As previously explained, we define an agent as radio sensitizing when the effect of radiotherapy itself, when corrected for the decrease in viability as a consequence of the chemotherapeutic, improves in response to treatment with the chemotherapeutic. To assess whether a radio sensitizing effect could be observed in the organoid lines, area under the curve (AUC) of radiotherapy alone was compared to the AUC of radiotherapy in the presence of chemotherapy, corrected for the effect of chemotherapy itself. If the AUC of radiotherapy becomes smaller in the presence of chemotherapy, this implies that the presence of the chemotherapeutic itself changes the effect of radiotherapy. As such, we identified six lines in which cisplatin had a radio sensitizing effect (T2, T3, T5, T8, T25 and T27, Figure 3A) and four where the presence of Cetuximab improved the response to radiotherapy (T1, T4, T6 and T25, Figure 3B).

Although not statistically significant, a correlation was observed between the *in vitro* response to radiotherapy as a single agent and the response to radiotherapy when combined with cisplatin (Figure 3C). The six organoid lines that responded better to radiotherapy in the presence of cisplatin (even though the effect of cisplatin itself was corrected for), fall above the identity line, indicating that here, cisplatin acts as a radiosensitizer. For Cetuximab, such a correlation was less pronounced (Figure 3D) and Cetuximab only improved the response to radiotherapy in three lines.

It is important to note that this analysis only provides information on how chemotherapy potentiates radiotherapy, as the effect of chemotherapy itself is corrected for. As such, although the effect of radiotherapy is not improved by the presence of cisplatin in the other lines (the organoid lines plotted below the identity line), this does not indicate a lack of effect of combination treatment as a whole. In all ten lines tested, the combination treatment resulted in more cell death than both treatments given as single agents

(Figure 4).

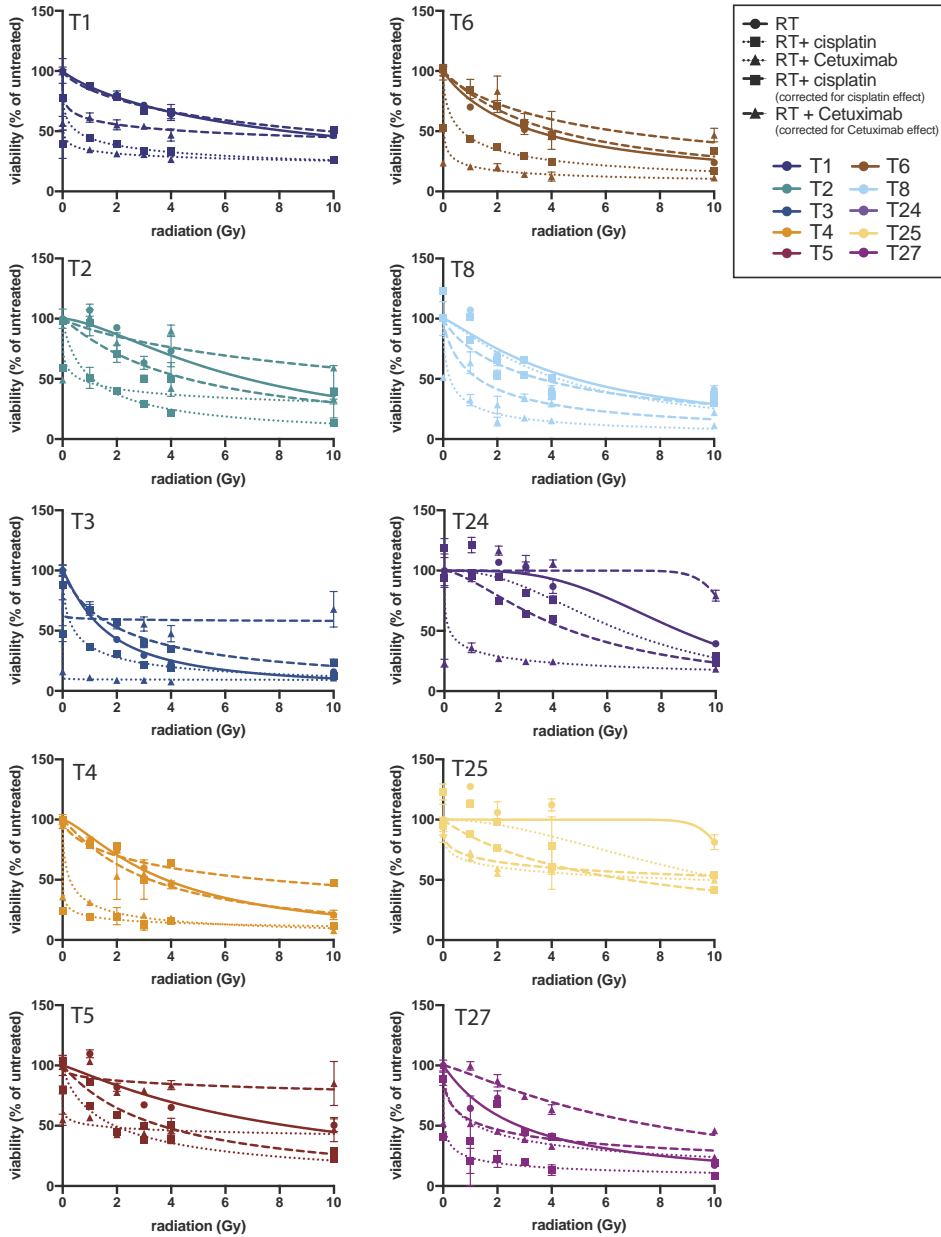


Figure 4. Chemoradiation therapy tested in 10 lines. Viability curves of all ten tested organoid lines for RT alone, RT + cisplatin, either with or without correction for the effect of cisplatin alone, and RT + Cetuximab, either with or without correction for the effect of Cetuximab alone.

Additive effects of chemoradiation therapy

As chemo- and radiotherapy are concurrently given to patients, the contribution of each individual therapy to the total effect cannot be determined in the clinic. To assess if chemo- and radiotherapy contribute equally to the total effect of combinational therapy, we investigated if there was a correlation between the effect of combination therapy and the effect of the individual therapies. Here, the effect of combination therapy was not corrected for the effect of the individual therapies. For both therapies, no correlation was observed between the effect of chemoradiation and chemotherapy alone (Figure 3E and 3F). For Cetuximab, no clear correlation was observed between AUC of Cetuximab and AUC of radiotherapy combined with this chemotherapeutic agent. For cisplatin, the additive effect of chemoradiation therapy did correlate with the effect of radiotherapy alone, although the correlation was not statistically significant (Figure 3G). This suggests that here, radiotherapy contributes more to the total effect of combinational treatment than cisplatin.

CONCLUSION

Taken together, this method allows to distinguish synergistic and additive effects of chemo- and radiation therapy when combined. This is not feasible in patients, as these treatments are given concurrently. Therefore, these experiments could aid understanding of how the individual agents of which combination treatments, exert their effect. Cisplatin acts as a radiosensitizer that, more often than Cetuximab, increases the response to radiotherapy in HNSCC organoids. Importantly, even when chemotherapeutics did not increase response to radiotherapy, chemoradiation therapy resulted in more cell death in all organoid lines tested here. Therefore, this data confirms that combination treatment is more effective than single agent therapy, regardless of whether the interaction is synergistic or additive.

CHAPTER

**PATIENT-DERIVED HEAD AND
NECK CANCER ORGANIDS
RECAPITULATE CLINICALLY
RELEVANT EGFR EXPRESSION
LEVELS AND ARE RESPONSIVE
TO EGFR-TARGETED
PHOTODYNAMIC THERAPY**

3 Y

ABSTRACT

Patients diagnosed with head and neck squamous cell carcinoma (HNSCC) are currently treated with surgery and/or radiotherapy with or without chemotherapy. Despite these therapeutical interventions, up to 40% of patients relapse, urging the need for more effective therapies. In photodynamic therapy (PDT), a photosensitizer is locally activated by light of a specific wavelength. In contact with oxygen, the activated photosensitizer produces reactive oxygen species, ultimately leading to cell death. Targeted PDT, using a photosensitizer that is conjugated to tumor-targeting molecules, is currently explored in clinical trials. Organoids are self-organizing three-dimensional structures that can be grown from patient material. Recently, we have shown that organoids can be established from HNSCC. Here, we explore the potential of HNSCC-derived organoids as an *in vitro* model to evaluate Epidermal Growth Factor Receptor (EGFR) targeted PDT. We find that organoids closely recapitulate EGFR expression levels detected on patient material. EGFR expression levels differ between organoid lines derived from different donors and was found to correlate with the response to EGFR-targeting PDT. Organoids grown from surrounding normal tissues showed lower EGFR expression levels than their tumor counterparts, and were not affected by PDT. In general, nanobody-targeted PDT was more effective than antibody-targeted PDT. Taken together, we present HNSCC-derived organoids as a novel 3D model for *in vitro* PDT, that better recapitulates the *in vivo* situation than currently used models.

Else Driehuis^{1†}, Sacha Spelier^{1,2†}, Irati Beltrán Hernández³, Emma J. de Rooter⁴, Remco de Bree⁵, Stefan M. Willems⁴, Hans Clevers^{1,6}, Sabrina Oliveira^{2,3*}

¹ Oncode Institute, Hubrecht Institute, Royal Netherlands Academy of Arts and Sciences (KNAW) and University Medical Center Utrecht, The Netherlands

² Cell Biology, Department of Biology, Faculty of Science, Utrecht University, Utrecht, The Netherlands

³ Pharmaceutics, Department of Pharmaceutical Sciences, Faculty of Science, Utrecht University, The Netherlands

⁴ Department of Pathology, University Medical Center Utrecht, The Netherlands

⁵ Department of Head and Neck Surgical Oncology, University Medical Center Utrecht, The Netherlands

⁶ Princess Maxima Center, Utrecht, The Netherlands

† These authors contributed equally to this work

* Corresponding author

INTRODUCTION

Head and neck squamous cell carcinoma (HNSCC) is a collective term used for tumors of the stratified epithelium that lines the oral cavity, pharynx and larynx (1). Depending on anatomical tumor location, tumor stage, patient's age, performance and comorbidities, the treatment of HNSCC can consist of surgery, radiotherapy and chemotherapy (either alone or in combination). While surgery and radiotherapy are applied locally, these therapies may compromise important functions such as mastication and swallowing, significantly decreasing patients' quality of life. Commonly used chemotherapeutics cisplatin and carboplatin serve as radiosensitizer, and are therefore given concurrently with radiotherapy. Although effective in a subset of patients, these treatments bring about severe side-effects (2). As EGFR is overexpressed in 50-90% of HNSCC and 15% of tumors carries EGFR gene amplification, the EGFR-targeting antibody cetuximab was introduced as an alternative treatment strategy for patients not eligible for treatment with cisplatin or carboplatin (3–6). Despite these interventions, relapse rates remain around 50% for advanced stage HNSCC (8).

The limited efficacy and side-effects of current treatments emphasize the need for more selective treatment strategies for HNSCC. As tumors are often accessible and surgery is a main component of HNSCC treatment, targeted photodynamic therapy (PDT) could enable such a targeted and local effect. Conventional PDT begins with the administration of a photosensitizer (PS), that after 2-4 days is excited by locally applied light. Activated PS subsequently converts oxygen to reactive oxygen species (ROS) that can damage DNA, proteins and lipids, ultimately resulting in cell death (9–11). In addition, PDT has been shown to contribute to tumor vasculature destruction and activation of the immune system (12). Side-effects of conventional PDT (using hydrophobic PS) are common, and include damage to normal surrounding tissues and skin photosensitivity. By conjugation of the PS to a tumor-targeting molecule such as an antibody, PDT can be made more tumor-specific. Although encouraging results have been obtained using this approach, targeted PDT has only recently entered clinical testing (13). The development of a water soluble PSs such as the silicon phthalocyanine derivative IRDye700DX has contributed greatly to this, rendering the antibody-PS conjugate more stable, without the need for spacers between antibody and PS (14). Cetuximab-IRDye700DX conjugate is currently tested in advanced stage HNSCC (NCT02422979) (15). First results indicate that patient respond well to this targeted PDT therapy with limited side-effects.

We have recently introduced nanobody-targeted PDT as an alternative to antibody-targeted PDT (16,17). Nanobodies are the variable domain of a subset of antibodies that consist only heavy chain, and are found in only a small subset of animals, including camelids (18). As nanobodies are approximately ten times smaller than conventional antibodies, they allow for a quicker and more homogenous tissue penetration and a faster systemic clearance when left unbound (16). When used conjugated to a PS, this is expected to result in shorter time intervals between administration and light application (1 or 2 hours, instead

of day(s)), more extensive tumor damage, and a decrease of skin photosensitivity. We have shown that nanobody-targeted PDT is selective for cells with high EGFR expression *in vitro* (16), and induces extensive tumor damage in an orthotopic HNSCC model (17).

Although results obtained in these studies are promising, it is unclear whether the expression level of the cell lines employed represents the expression of EGFR in human samples (19). As such, it remains uncertain if these findings can be translated to the clinic. Moreover, 2D cell lines do not recapitulate the 3D structure of a tumor, which is essential to consider when studying the distribution of PS-conjugates. Lastly, considering personalized approaches to identify patients eligible for EGFR-targeted PDT, studies indicate that 2D cell lines hold limited predictive potential (20,21). To address these points, we set out to characterize expression of EGFR and subsequently test EGFR-targeted PDT on HNSCC-derived tumor organoids. Organoids are 3D self-organizing structures that can be grown in the laboratory from stem cells, and recapitulate the organization, histological features and -to some extent- functional characteristics of epithelial tissues (22). Moreover, organoids can be established with high efficiency from patient-derived material such as surgical resections or tumor biopsies, and allow for the expansion of patient-derived tumor cells *in vitro*. Recent data shows that organoids hold predictive potential in the therapeutic context (23–26). We recently developed a organoid model for HNSCC which recapitulates morphological and genetic characteristics of this tumor type, and is found to be eligible for *in vitro* drug testing (26). In addition, this technology creates the opportunity to establish cultures from both tumor and wildtype tissue, derived from the same patient. Here, we have employed the same organoid model, which we have characterized for EGFR expression and subsequently used to evaluate EGFR-targeted PDT.

RESULTS

EGFR expression differs between patient-derived organoid lines and recapitulates endogenous (clinical) EGFR levels

HNSCC-derived organoid lines were established from patient material (Table S1) and cultured as previously described (26). To assess EGFR expression levels in HNSCC organoids, quantitative PCR and FACS analysis were performed. EGFR messenger RNA was detectable in all tested organoid lines, although expression varied between lines derived from different donors (Figure S1A). Interestingly, lowering the level of EGF in organoid culture medium to the levels detected in human serum (hereafter called 'physiological EGF'), resulted in upregulation of EGFR expression in all but two lines (Figure S1B). This finding was in line with the fact that EGFR protein on organoids could initially not be detected by flow cytometry, whereas it was detectable on control cell lines overexpressing EGFR. Indeed, EGFR protein levels were increased upon culture of organoids in physiological EGF medium (Figure 1A). EGFR protein levels were assessed for a panel of HNSCC organoids. In line with variable EGFR expression in primary

tumors (27), EGFR expression varied between organoid lines derived from different donors (Figure 1B). EGFR protein levels detected on HNSCC-derived organoids were lower than those observed on EGFR overexpressing cell lines (namely A431 and 14C). As organoid culture allows for the expansion of corresponding normal tissue in culture, EGFR levels of organoids grown from surrounding normal tissues were also compared. For three donors, EGFR levels on both normal and tumor organoids were compared. In all cases, EGFR protein levels detected on tumor cells were higher than on matched normal organoids (Figure 1C). Importantly, EGFR expression levels in organoids were comparable to those detected in primary patient material (Figure 1C). Also in primary patient material, average EGFR expression was lower in normal tissue than in its tumor counterpart. The observed differences in EGFR expression between normal and tumor organoids were confirmed using immunohistochemistry (Figure 1D).

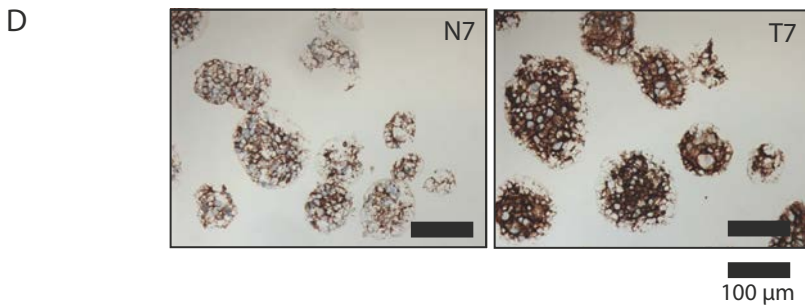
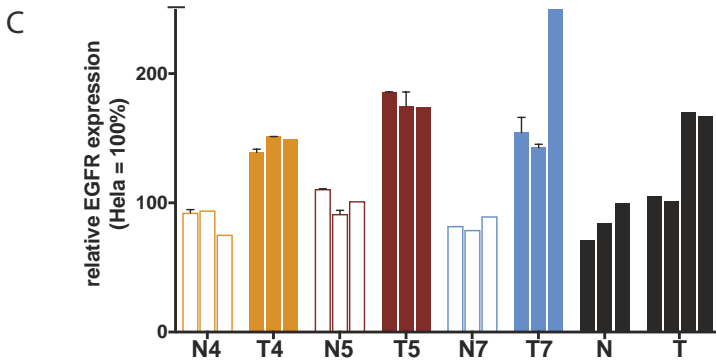
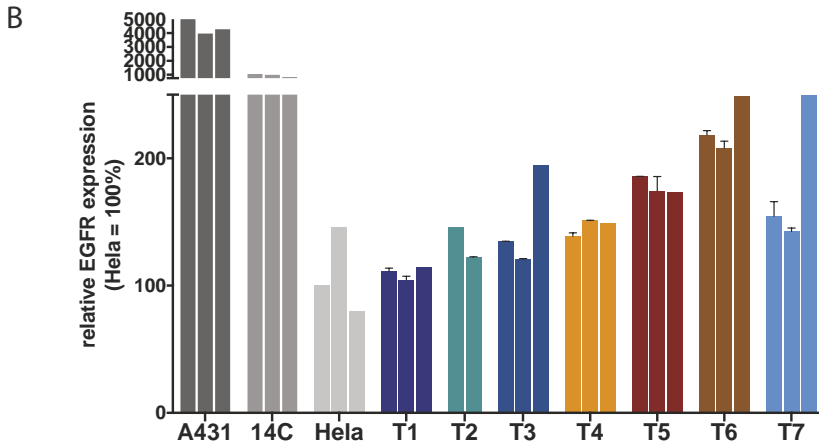
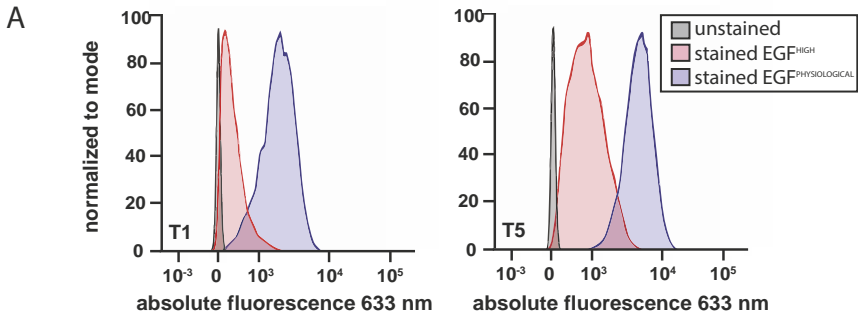
Organoid response to EGFR-targeted PDT is donor-dependent and tumor-specific

We set out to adopt existing PDT protocols of 2D cell lines to make them suitable for organoid screens (Figure 2A depicts the experimental set-up of these experiments). All experiments were performed with cetuximab-PS, which is currently tested in the clinic, and the nanobodies-PS conjugates 7D12-PS and 7D12-9G8-PS and that were used in our previous studies (16,17). 7D12 is a monovalent EGF-competing nanobody, whereas 7D12-9G8-PS is a biparatopic nanobody, consisting of two linked monomeric nanobodies targeting two different epitopes. *In vitro*, biparatopic nanobodies have been shown to be more potent than monovalent nanobodies (16), as they can carry more PS per nanobody and can activate receptor clustering, which leads to faster EGFR endocytosis (28).

When exposing organoids to EGFR-targeting PDT, organoids were killed by concentrations of PS-conjugate that did not cause any toxicity without light exposure (Figure 2B, shown for 7D12-9G8-PS but found for all used conjugates). As expression levels are lower in patient-derived organoids than in the cell lines that were used so far for PDT research (16), these findings are encouraging.

Tumor and wildtype organoids established from the same patient were subjected in parallel to EGFR-targeting PDT. In all pairs tested, tumor organoids were found to be more sensitive to PDT than their wildtype counterparts (Figure 2C). Although numbers are limited, these findings are encouraging and provide the first proof that cancer cells derived from patient material can be selectively killed by targeted PDT, leaving normal cells unaffected.

For all organoids tested, the effect of nanobody-conjugated PS was more pronounced than that of cetuximab-PS. In most cases, treatment with the biparatopic nanobody 7D12-9G8-PS was most effective, which is in line with previous observations in 2D cell lines (16).



Organoid response to EGFR-targeted correlates with EGFR expression levels

Organoid lines derived from different patients showed variable responses to EGFR-targeted PDT. Comparison of EGFR protein levels and response to EGFR-targeted PDT revealed a positive correlation between these two variables, confirming results previously obtained in 2D cell lines (16). Organoids that expressed higher protein levels of EGFR were more sensitive to EGFR-targeted PDT, regardless of the PS-conjugate used (Figure 2A). The fact that this correlation could be validated in patient-derived organoids that express endogenous or physiological levels of EGFR is clinically relevant, as it indicates that EGFR levels could be a predictor for EGFR-targeting PDT. The response of all individual lines to the three used PS-conjugates is shown in Figure S1.

Induction of EGFR expression increases sensitivity to EGFR-targeting PDT

Based on the observed correlation between EGFR expression and PDT response, we set out to verify whether an increase in EGFR expression would result in increased sensitivity to EGFR-targeted PDT. For this, a doxycycline-inducible EGFR expression construct was introduced into two HNSCC organoid lines using lentiviral infection (Figure 4A). After selection of infected cells, induction resulted in expression of GFP (of which the coding sequence was cloned after EGFR), indicating that induction was effective (Figure 4B). After doxycycline treatment, EGFR expression increased in both lines (Figure 4C). Lastly, EGFR overexpression resulted in increased sensitivity to targeted PDT (Figure 4D). This data confirms that EGFR-targeted PDT is most effective in organoids that show high EGFR protein levels, thereby, showing a causal relation between EGFR levels and sensitivity to PDT.

-
- ◀ **Figure 1. EGFR expression differs between patient-derived organoid lines and recapitulates endogenous EGFR levels.** A. EGFR protein expression measured by flow cytometry. EGFR expression of organoids grown in either physiological EGF (blue peak) or high EGF (red peak). An unstained control is shown in black. B. EGFR protein expression measured by flow cytometry in organoid lines derived from HNSCC patients. Experiment was performed in technical duplicate (error bars) and biological triplicate (individual bars). EGFR expression was stable over time, as biological replicates were measured 2 months apart. EGFR protein levels are shown relative to HeLa cell line, a line considered to have physiological levels of EGFR expression. For reference, expression in A431 cells and 14 C cells is shown, as these were previously used to test EGFR-targeted PDT *in vitro*. C. EGFR protein expression measured by flow cytometry in matched wildtype organoids and tumor organoids of three patients. EGFR protein expression levels on patient-derived primary tissue is shown as a reference. For primary tissue, each bar represents EGFR expression on tissue derived from an individual patient. D. EGFR immunohistochemical staining performed on N7 and T7 organoids derived from the same donor. Scalebar = 100 μ m
-

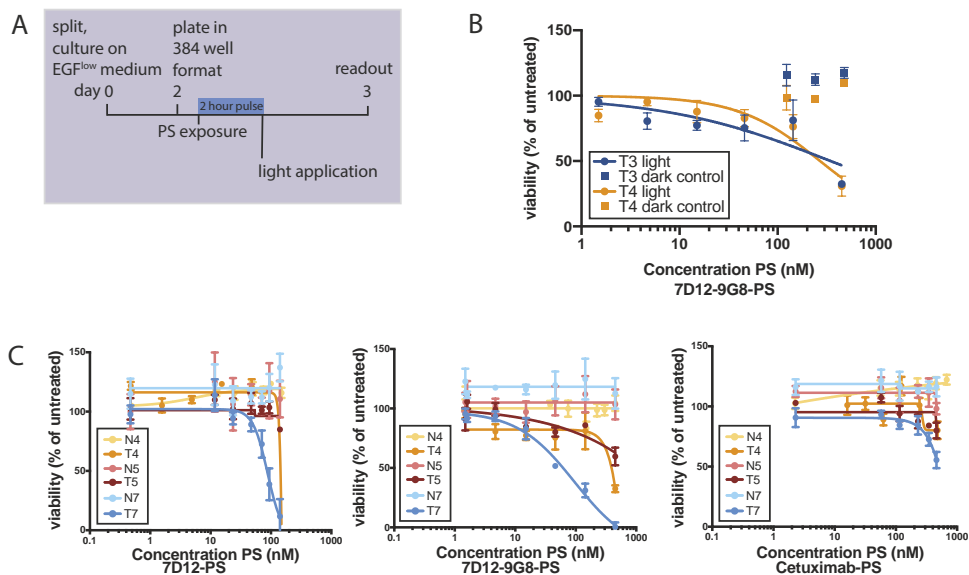


Figure 2. Organoid response to *in vitro* EGFR-targeted PDT is donor-dependent and tumor-specific **A.** Schematic outline of the experimental set-up of organoid *in vitro* PDT. Organoids are disrupted into single cells, recovered for two days on medium containing physiological EGF, and subsequently filtered, counted and plated into a 384 well format. A two hour exposure to EGFR-targeting nanobody-PS or antibody-PS conjugates was followed by a light-dose activating the PS. Twentyfour hours later, cell viability was assessed. **B.** EGFR-targeting conjugates used in this study did not show toxicity without activation of the PS. Here, toxicity of 7D12-9G8 in T3 and T4 is shown as an example. **C.** Response to EGFR-targeting PDT of matched normal and tumor organoid pairs. Response to 7D12-9G8-PS and 7D12-PS and 7D12-9G8 is shown for N4 and T4 (orange), N5 and T5 (red) and N7 and T7 (blue). Normal organoids are depicted in a lighter shade of the same color than their tumor counterparts.

DISCUSSION

The aim of this study was to characterize EGFR expression in HNSCC-derived tumor organoids and, subsequently, test EGFR-targeted PDT in this model. Organoid EGFR levels were found to recapitulate clinically relevant EGFR expression, in contrast to commonly used cell lines that overexpress EGFR at non-physiological levels. Using this model, EGFR-targeted PDT was shown to be effective in these patient-derived organoids. Tumor organoids were more sensitive to PDT than their corresponding wildtype organoids, suggesting that this therapy will likely not damage normal epithelium surrounding the tumor. EGFR levels between organoid lines varied, and correlated with response to EGFR-targeted PDT. The direct effect of EGFR expression levels on PDT response was verified by inducible EGFR overexpression, which resulted in increased responses to PDT. To our knowledge, this is the first report on *in vitro* targeted PDT performed on patient-

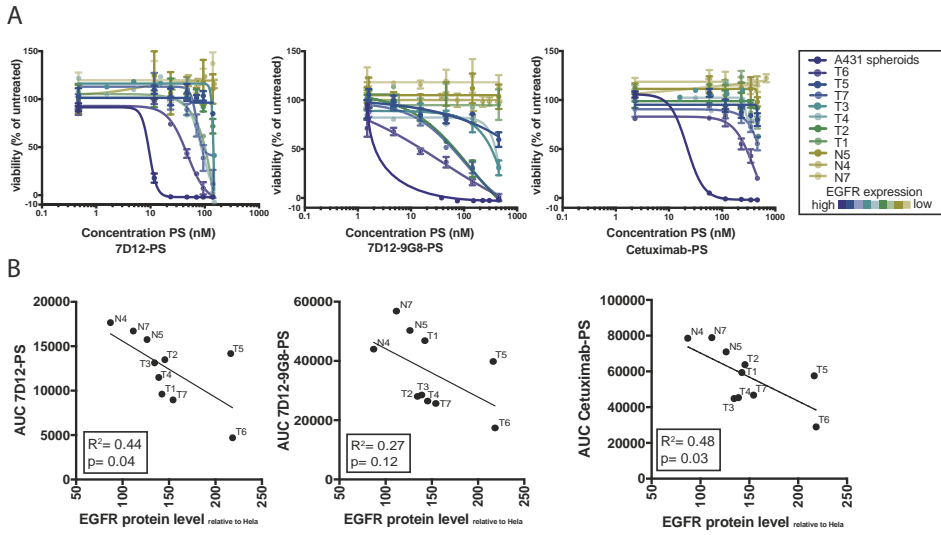


Figure 3. Organoid response to in vitro EGFR-targeted PDT correlates with EGFR expression levels. A. Sensitivity of HNSCC organoids with variable EGFR expression to PDT using conjugates 7D12-PS (first panel), 7D12-9G8-PS (second panel) and cetuximab-PS (third panel). Color of the lines indicate the relative EGFR expression level detected by FACS analysis (blue = highest expression, yellow = lowest expression). B. Correlation plots showing the relation between EGFR expression on the x-axis and response to PDT therapy as indicated by area under the curve (AUC) on the y-axis. First panel shows the AUC for 7D12-PS, second panel for 7D12-9G8-PS and the third panel for cetuximab-PS.

derived material, in a 3D format. The findings we report here hold clinical implications, including the validation of EGFR expression as a potential biomarker for response to EGFR-targeted PDT.

The efficiency of organoid culture allows for the establishment of matching organoid pairs, where corresponding normal oral mucosa tissue can be grown in parallel to the adjacent tumor tissue. This allowed for the comparison of therapy responses between wildtype and tumor cells of the same patient. Here, we tested three pairs of organoids, and found in all cases that wildtype organoids showed no response to EGFR-targeted PDT. This is likely due to the lower EGFR expression levels detected on wildtype cells, although others have shown that tumor cells also produce more ROS than wildtype cells, which might also influence PDT responses (29,30).

In this work, we confirmed the correlation that was previously observed between EGFR expression and response to EGFR-targeting PDT. Here, we show this correlation in material that is patient-derived and shows endogenous EGFR expression. These findings suggest that high EGFR expression in tumor tissue might be used as a predictive marker for response to EGFR-targeted PDT. The potential of EGFR expression as a biomarker for

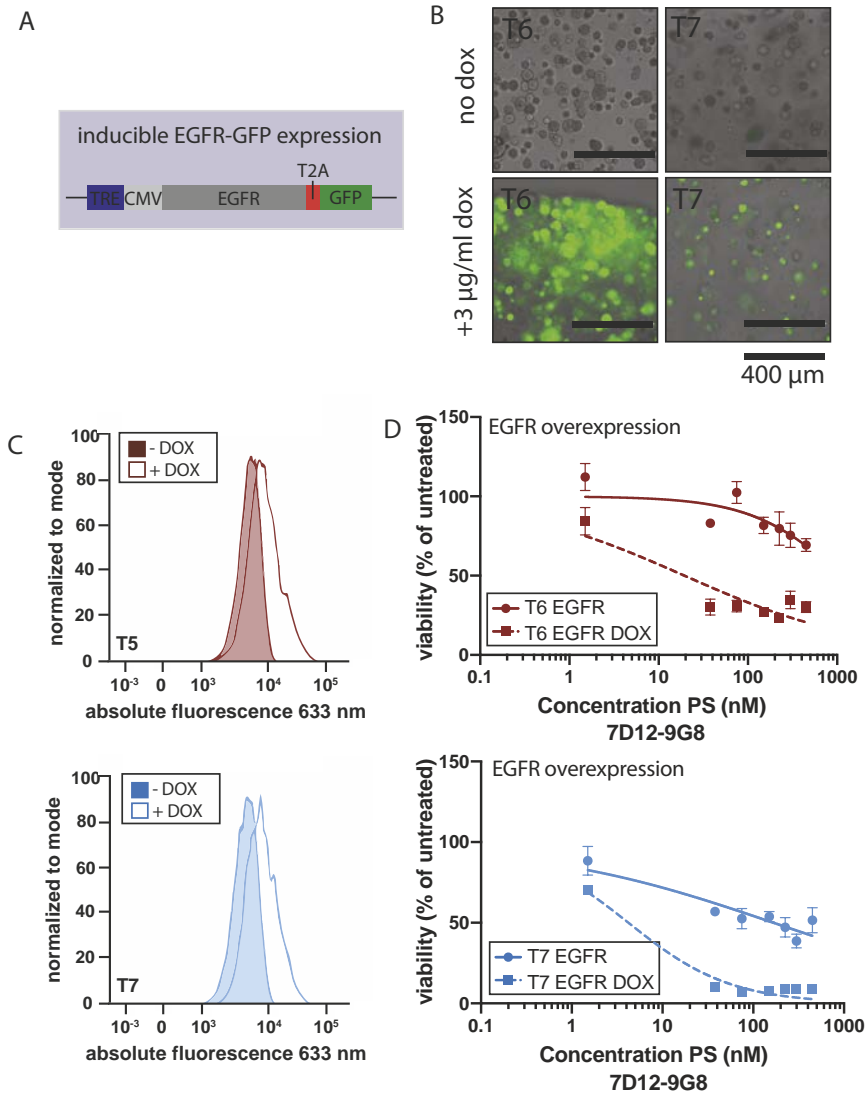


Figure 4. Induced EGFR expression enhances the response to EGFR-targeted PDT. A. Schematic outline of lentiviral vector used to create organoid lines that can inducibly overexpress EGFR (TRE: tetracycline responsive element, CMV: cytomegalovirus promotor). The TRE and CMV promotor precede the open reading frame encoding EGFR and GFP, separated by a T2A sequence, assuring generation of separate mRNA molecules for EGFR and GFP. B. Merged brightfield and immunofluorescence images of organoids after two day administration of doxycycline, scalebar 400 µm. C and D. Effect of doxycycline-mediated EGFR overexpression on EGFR protein levels in organoid lines T6 and T7. Color peaks indicate uninduced expression, lined peaks indicate induced expression. E and F. PDT using nanobody 7D12-PS in EGFR overexpressing organoid lines T6 and T7. Organoids were either doxycycline induced (squared symbols, dashed line) or not induced (round symbols, solid line) and exposed to PDT as previously described.

other EGFR-targeted therapies was previously investigated. Such studies found that EGFR expression levels could not predict response to the EGFR blocking antibody cetuximab (3). However, this is likely explained by downstream mutations in the EGFR pathway, that are commonly found in HNSCC (4). The presence of such mutations will negate the effect of cetuximab competing with EGF for EGFR binding, even in EGFR overexpressing tumors. In contrast, the effect of EGFR-targeted PDT is independent from EGFR downstream signaling. As such, it is not influenced by the commonly found mutations downstream of EGFR. Therefore, EGFR expression could potentially be a good biomarker for response to EGFR-targeted PDT.

Gene amplification of EGFR is reported in 15% of HNSCC patients (4), although EGFR protein overexpression has been reported in up to 90% of tumors (3). Here, tumor cells showed increased EGFR expression levels compared to their wildtype counterparts, despite the fact that no gene amplification of EGFR could be detected in these lines (26). These findings are in line with previously mentioned statistics and support the hypothesis that EGFR protein overexpression is not only driven by gene amplification. It would be of interest to test EGFR-targeted PDT in organoids derived from a tumor carrying EGFR amplification, to see if responses are comparable to those observed in the organoids reported here.

In this study, we used two different nanobodies: monovalent 7D12 and bipolaratopic 7D12-9G8. *In vitro*, bipolaratopic nanobodies have been shown to be more potent than monovalent nanobodies (16), as they can carry more PS per nanobody, and their binding to EGFR results receptor clustering, leading to faster EGFR endocytosis (28). The internalization of nanobody-PS (10) and also of antibody-PS has been correlated with increased cellular damage (31,32). However, *in vivo*, only small differences have been observed thus far between these two nanobody formats, where 7D12-PS has shown more reproducible tumor damage than 7D12-9G8-PS. As 7D12 is smaller than 7D12-9G8, tissue penetration of this nanobody is suggested to be more rapid and more homogenous, and secondly it may bring the PS in closer proximity to the cell membrane when bound to EGFR (17). When compared to treatment with antibody-PS, nanobody-PS results in less variation in the extent of damage induced and in an increase in tumor damage (17). These results have been correlated to the larger size of the antibody, hampering an homogenous distribution *in vivo*. In organoids, cetuximab-PS was indeed found to be less effective than any of the two nanobodies in all tested lines (Figure S2). Moreover, we found that overall, when corrected for the amount of PS conjugated to the carrier molecule, the bipolaratopic nanobody more effectively killed HNSCC cells than the monovalent nanobody (Figure S2). This is likely explainable by the small dimensions of the organoids employed, and the fact that this set up does not reflect systemic distribution. Nevertheless, organoids are gaining increasingly more attention as realistic representations of tumors that enable effective screens.

Cetuximab-targeted PDT is currently tested in clinical trials (NCT02422979). Initial findings are encouraging and show responses to therapy, with limited side effects (15).

Here, no inclusion criteria were applied based on EGFR expression levels. It would be very interesting to see to what extent EGFR levels can explain differential responses to therapy in this patient cohort. To determine if organoids can aid personalized decision making, it would be interesting to establish organoids from patients receiving EGFR-targeted PDT. As such, it would be possible to compare *in vitro* organoid responses to corresponding patient responses and see if organoids hold predictive potential in EGFR-targeted PDT.

The known clinical need for effective and selective local treatment of HNSCC, and the current complexity of conventional PDT protocols used in the clinic, encourages many researches dedicated to developing targeted PDT. This study complements others that have shown promising results for selective and extensive tumor damage, with a unique approach using patient derived tumor and normal tissues.

CONCLUSION

EGFR expression levels on HNSCC patient derived organoids closely recapitulated EGFR expression in primary tissue. *In vitro* PDT showed efficacy in these patient-derived organoids. HNSCC organoids were responsive to EGFR-targeting PDT using both antibody-PS and nanobody-PS, and response to EGFR-targeting PDT could be correlated to EGFR expression levels. Indeed, a causal relation between EGFR expression levels and response to EGFR-targeted PDT could be shown by overexpression of EGFR.

METHODS

Human Material for Organoid Cultures

The collection of patient data and tissue for the generation and distribution of organoids was performed according to the guidelines of the European Network of Research Ethics Committees (EUREC) following European and national law. The Biobank Research Ethics Committee of the UMC Utrecht (TCBio) approved the biobanking protocol: 12-093 HUB-Cancer according to the UMCU Biobanking Regulation. All donors participating in this study signed informed consent forms and can withdraw their consent at any time. Available organoids will be catalogued at www.hub4organoids.eu and can be requested at info@hub4organoids.eu.

Tissue processing

Patient material was collected from pathology material in Advanced DMEM/F12 (Life Technologies, cat. no. 12634-034), supplemented with 1x GlutaMAX (adDMEM/F12; Life Technologies, cat. no. 12634-034), Penicillin-streptomycin (Life Technologies, cat. no. 15140-122) and 10 mM HEPES (Life Technologies, cat. no. 15630-056). This medium was named Advanced DMEM +/+ medium. For collection of patient material, 100 µg/ml Primocin (Invivogen, cat. no. ant-pm1) was added to the +/+ medium. For normal tissue

samples, excess fat or muscle tissue was removed to enrich for epithelial cells and tissue was cut into small fragments. Random pieces of approximately 5 mm³ were stored at -20°C for DNA isolation. Some pieces were fixed in formalin for histopathological analysis and immunohistochemistry, and the remainder was processed for organoid derivation. Fragments were incubated at 37 °C in 0.125% Trypsin (Sigma, cat. no. T1426) in +/+ medium until digested. Every 10 minutes, the tissue suspension was sheared using 1 ml pipette. Digestion was monitored closely to prevent excess incubation in trypsin. Incubation was performed for a maximum of 60 minutes. When complete, Trypsin was diluted by addition of 10 ml +/+ medium. Suspension was strained over a 100 µm EasyStrainer filter (Greiner, cat. no. 542000) and centrifuged at 1000 rpm. The resulting pellet was resuspended in ice-cold 70% 10 mg/ml cold Cultrex growth factor reduced BME type 2 (Trevigen, 3533-010-02) in organoid medium. Droplets of approximately 10 µl were plated on the bottom of pre-heated suspension culture plates (Greiner, cat. no. M9312). After plating, plates were inverted and put at 37 °C for 30 minutes to let the BME solidify. Subsequently, prewarmed organoid medium was added to the plate. For the first week, 10 µM Rho-associated kinase (ROCK) inhibitor Y-27632 (Abmole Bioscience, cat. no. M1817) was added to the medium to aid outgrowth of organoids for the primary tissue.

Organoid culture

HNSCC and normal epithelium-derived organoids were grown in Advanced DMEM +/+ medium. Organoid medium contained 1x B27 supplement (Life Technologies, cat. no. 17504-044), 1,25 mM N-acetyl-L-cysteine (Sigma-Aldrich, cat. no. A9165), 10 mM Nicotinamide (Sigma-Aldrich, cat. no. N0636), 50 ng/ml human EGF (PeproTech, cat. no. AF-100-15), 500 nM A83-01, 10 ng/ml human FGF10 (PeproTech, cat. no. 100-26), 5 ng/ml human FGF2 (PeproTech, cat. no. 100-18B), 1 µM Prostaglandin E2 (Tocris Bioscience, cat. no. 2296), 3 µM CHIR 99021 (Sigma-Aldrich, cat. no. SML1046), 1 µM Forskolin (Bio-Techne (R&D Systems) cat. no. 1099), 4% RSPO and 4% Noggin (produced via the r-PEX protein expression platform at U-Protein Express BV). Organoids were split between 7 and 14 days after initial plating. For passaging, organoids were collected from the plate by disrupting the BME droplets with a P1000 pipette, collecting and washing in 10 ml +/+ medium. Pellet was resuspended in 1 ml of TrypLE Express (Life Technologies, cat. no. 12605-010) and incubated at 37°C. Digestion was closely monitored and suspension was pipetted up and down every 5 minutes to aid disruption of the organoids. TrypLE digestion was stopped when organoids were disrupted into single cells by adding 10 ml +/+ medium. Cells were subsequently resuspended in ice-cold 70% BME in organoid medium and plated at suitable ratios (1:5 to 1:20) to allow efficient outgrowth of new organoids. After splitting, 10 µM Y-27632 was always added to aid outgrowth of organoids from single cells. Medium was changed every 2-3 days and organoids were split once every 1-2 weeks.

Cell line culture

Human vulvar squamous cell carcinoma A431 (CRL-1555), human cervical carcinoma cell line HeLa (CCL-2) and human embryonal kidney cell line HEK293T (CRL-3216) were purchased from the American Type Culture Collection (ATCC, LGC Standards, Germany). Human head and neck squamous cell carcinoma cell line UM-SCC-14C (14C) was kindly provided to the lab of Oliveira by Prof. Dr. T.E. Carey (University of Michigan, USA). All cell lines were cultured in advanced DMEM/F12 (Life Technologies, cat. no. 12634-034), supplemented with 10% fetal calf serum (FCS), 100 µg/ml penicillin and 100 µg/ml streptomycin (Life Technologies, cat. no. 15140-122). Cells were cultured at 37°C with 5% CO₂ in a humidified atmosphere, and split with TrypLE Express for 10 minutes at 37°C (Life Technologies) after washing away all remaining medium with PBS.

RNA collection

Organoids were cultured as normal. For quantification of EGFR expression, organoids were split to single cells, left to grow five days on organoid medium, and then put on organoid medium with low EGF concentration (0.63 ng/ml), that was otherwise left unchanged. After five days on EGF low medium, organoids were collected and washed twice with 10 ml +/+ medium. RNA was extracted using RNeasy mini kit (Qiagen, cat. no. 74104) according to protocol. RNA amount was measured using Nanodrop.

cDNA synthesis and quantitative PCR

For cDNA synthesis, RNA was incubated with 50 µg/ml Oligo(dT) 15 Primer (Promega, cat. no. C1101) in water for 5 minutes at 70°C. Subsequently GoScript Reverse Transcriptase (Promega, cat. no. A5003) was used according to protocol to produce cDNA. qPCR reactions were performed in 384 well format using IQ SYBR green (Bio-Rad, cat. no 1708880) in the presence of 0.67 µM FW and RV primer and cDNA transcribed from 25 ng RNA. For qPCR, samples were incubated for 2 minutes at 95°C and for 40 cycles at: 15 seconds at 98°C, 15 seconds at 58°C and 15 seconds at 72°C. Results were calculated by using the $\Delta\Delta C_t$ method. Melt peak analysis was performed to assure that primer had no aspecific binding. Primers used were the following:

Table 1.

Primer	Sequence
Human EGFR FW	AGGCAGGAGTAACAAGCTCAC
Human EGFR RV	ATGAGGACATAACCAGCCACC
Human GAPDH FW	GGAGCGAGATCCCCTCCAAAAT
Human GAPDH RV	GGCTGTTGCATACTTCTCATCG

PS conjugation

Monovalent NB 7D12, binding domain III on EGFR, and biparatopic NB 7D12-9G8, binding domains II and III on EGFR, were produced as previously described (16). mAB cetuximab, binding domain III on EGFR, was purchased at the local hospital pharmacy. As the original ligand of EGFR, EGF, also binds domain III 7D12, 7D12-9G8 and cetuximab all compete with EGF (16). IRDye® 700DX NHS Ester (Licor, P/N 929-70010) was conjugated to cetuximab, 7D12 and 7D12-9G8 as previously described (16), thus with molar ratio for conjugation of 1:4 for all conjugates. Alexa Fluor™ 647 NHS Ester (ThermoFisher A20006) was similarly conjugated to cetuximab. All conjugates were checked on gel after conjugation to determine the percentage of free dye, and to confirm the conjugates were not degraded they were checked on gel every 3-4 weeks after conjugation. Conjugates were solely used when free dye percentage was less than 10%. Additionally, to confirm that binding affinity was not affected after conjugation, new conjugates were tested in a binding assay on A431 as previously described (16).

EGFR flow cytometry

Organoids used for flow cytometry analysis were grown in physiological EGF medium. Organoids were collected 7 days after splitting and disrupted into single cells using TrypLE. Cells were washed once with 10 ml +/+ medium, counted and subsequently incubated in FACS buffer (PBS with 5% serum, 2 mM EDTA) containing 19 nM cetuximab-Alexa647 for one hour on ice (100 µl FACS buffer for 100.000 cells). After incubation, cells were washed once using 10 ml +/+ medium and resuspended in 100 µl FACS buffer for analysis. Just before measurements, 1 µg/ml DAPI was added to allow the identification of dead cells, that were excluded from the analysis. Unstained controls were taken along for each line and A431, 14C and Hela served as positive controls. Measurements were carried out on the BD FACSCanto II (BioRad) with standard filter sets, and fluorescence intensity of cetuximab-Alexa647 was measured on the 633 nm channel. FlowJo software was used for analysis.

Immunohistochemistry

Organoids were cultured for one week on complete medium, followed by one week on physiological EGF medium. Subsequently, organoids were collected, washed twice with +/+ medium to remove BME and incubated for at least 2 hours at room temperature in 4% PFA. Organoids were subsequently processed for paraffin embedding. Paraffin sections were stained with H&E and the EGFR antibody (Invitrogen, clone 31G7, dilution 1:40, pretreatment citrate). All stainings were performed at the pathology department of the University Medical Center Utrecht (UMCU).

***In vitro* PDT assay on HNSCC organoids**

Organoids were disrupted into single cells using TrypLE and manual shearing using a p1000 pipette. Single cells were subsequently plated in BME and cultured on low EGF medium. Two days later, BME drops were mechanically disrupted by pipetting and 1 mg/ml dispase II (Sigma-Aldrich, cat. No. D4693) was added to the medium to disrupt BME. Culture plates were incubated at 37°C for 40 minutes to digest the BME. Subsequently, organoids were collected, washed with cold DMEM +/+/+, filtered using a 70 µm nylon cell strainer. Organoids were counted and resuspended in 5% BME/low EGF medium without NAC. A431 spheroids were resuspend in 5% BME/2D medium. 500 organoids were plated in a volume of 40 µL in 384 well format using the multi-drop Combi Reagent Dispenser (Thermo Scientific, cat. no. 584030). PS conjugates were added using HP Tecan D300e Digital Dispenser. Conjugates were dissolved in PBS containing 0.3% Tween-20. Each concentration was tested in triplicate. After addition of the conjugates, organoids were incubated for 2 hours. Thereafter, light was applied with a 690 nm laser (Modulight, Finland) with a light fluence rate of 5 mW/cm² (measured by an Orion Laser power monitor) and a total light dose of 26 J/cm². After illumination, the plates were incubated for 24 hours, after which cell viability was measured using CellTiter-Glo 3D Reagent (Promega, cat. No. G9681). Luminescence readout was carried out using a Spark multimode microplate reader (Tecan). Viability of wells that only received PBS/Tween for normalization was set at 100%. Viability of organoids exposed to 10 µM staurosporin was set at 0%. A separate dark control plate was made, in which for each line the highest concentration of the conjugate was added in triplicate. GraphPad software was used to create kill curves and lines were fitted by means of the nonlinear fit option 'log (inhibitor) vs. response -variable slope'. Concentration of NB/AB-PS was corrected for the DOC of the conjugate in order to plot on the y-axis the total amount of PS, the actual drug.

EGFR overexpression construct and lentivirus production

cDNA was obtained from A431 cells. EGFR open reading frame was amplified using PCR (FW primer 5'→3': GCT AGCGCCACCATGGACTACAAGGATGACGATGACAAGATGCGA CCCTCCGGGACGGC, Reverse primer 5'→3': CACGCGTTGCTCCAATAAATTCAGTCTTT. PCR product was ran on a 1% agarose gel and purified using gel extraction. Restriction digest using Nhe1 and Mlu1 allowed ligation of the EGFR open reading frame into the Addgene plasmid #50661. Production of lentivirus was performed in HEK293T cells which were transduced with packaging plasmids and the created EGFR construct. Transduction was performed using a mixture of 300 µL PEI, 25 µg EGFR construct and 5 ml Optimem (Thermo-Fisher, cat. Nr. 11058021). This was added to 15 ml of DMEM with 10% serum and left on cells for 8 hours, after which medium was replaced by DMEM with 10% FBS. Supernatant was collected, filtered and collected using ultracentrifugation (20.000 x g, 2 hours, 4°C). Virus derived from one 15 cm dish of HEK293T cells was resuspended in 500 µl organoid medium and stored at -80°C until use.

Organoid infection and doxycycline-mediated induction of EGFR expression

Organoids were disrupted into single cells using TrypLE, washed and incubated with 100 μ l of the created virus suspension. Virus/cell mixture plus 1 μ g/ml polybrene was incubated for 6 hours in a 48 well plate. After incubation, organoids were washed with 10 ml +/-/+ medium and plated in BME as regular. Three days later, selection using puromycin was commenced using organoid medium supplemented with 1 μ g/ml puromycin (InvivoGen, cat. Nr. 58-58-2). Organoids were kept on puromycin containing medium for two weeks, after which successful infection was validated using doxycycline induction. PDT was performed as previously described, except the addition of 3 μ g/ml doxycycline after splitting of organoids two days prior to PDT. Doxycycline was also added during the PDT assay. For FACS analysis, organoids were cultured for one week in the presence of doxycycline.

ACKNOWLEDGEMENTS

We thank Folkert Morsink of the department of Pathology at the UMCU for his help with performing immunohistochemical stainings. We would like to thank Sigrid Kolders for her help with drug screens. We thank Anne Snelting and Anneta Brousalı for their help with patient inclusion. Thanks to Stefan van der Elst for his help with FACS analysis. This research was partly supported by the European Research Council (ERC) under the European Unions Horizon 2020 Research and Innovation Program (Grant agreement No. 677582).

DECLARATION OF INTEREST

H.C. is inventor on several patents related to organoid technology. E.D. is inventor on a patent related to the culturing of HNSCC organoids.

REFERENCES

1. Squier C, Kremer M. Biology of oral mucosa and esophagus. *J Natl Cancer Inst Monogr.* 2001;29:7–15.
2. Guan J, Li Q, Zhang Y, Xiao N, Chen M, Zhang Y, et al. A meta-analysis comparing cisplatin-based to carboplatin-based chemotherapy in moderate to advanced squamous cell carcinoma of head and neck (SCCHN). *Oncotarget.* 2016;7:7110–9.
3. Bossi P, Resteghini C, Paielli N, Licitra L, Pilotti S, Perrone F. Prognostic and predictive value of EGFR in head and neck squamous cell carcinoma. *Oncotarget.* 2016;7:74362–79.
4. The Cancer Genome Atlas Network. Comprehensive genomic characterization of head and neck squamous cell carcinomas. *Nature.* 2015;517:576–82.
5. Mandic R, Rodgarkia-Dara CJ, Zhu L, Folz BJ, Bette M, Weihe E, et al. Treatment of HNSCC cell lines with the EGFR-specific inhibitor cetuximab (Erbiximab®) results in paradox phosphorylation of tyrosine 1173 in the receptor. *FEBS Lett.* Wiley Online Library; 2006;580:4793–800.
6. Bonner JA, Harari PM, Giralt J, Azarnia N, Shin DM, Cohen RB, et al. Radiotherapy plus cetuximab for squamous-cell carcinoma of the head and neck. *N Engl J Med.* 2006;354:567–78.
7. Eriksen JG, Steiniche T, Askaa J, Alsner J, Overgaard J. The prognostic value of epidermal growth factor receptor is related to tumor differentiation and the overall treatment time of radiotherapy in squamous cell carcinomas of the head and neck. *Int J Radiat Oncol Biol Phys.* 2004.
8. Argiris A, Karamouzis M V., Raben D, Ferris RL. Head and neck cancer. *Lancet (London, England).* 2008;371:1695–709.
9. Plaetzer K, Krammer B, Berlanda J, Berr F, Kiesslich T. Photophysics and photochemistry of photodynamic therapy: fundamental aspects. *Lasers Med Sci.* Springer; 2009;24:259–68.
10. Trachootham D, Alexandre J, Huang P. Targeting cancer cells by ROS-mediated mechanisms: a radical therapeutic approach? *Nat Rev Drug Discov.* Nature Publishing Group; 2009;8:579.
11. Curtin JF, Donovan M, Cotter TG. Regulation and measurement of oxidative stress in apoptosis. *J Immunol Methods.* Elsevier; 2002;265:49–72.
12. Agostinis P, Berg K, Cengel KA, Foster TH, Girotti AW, Gollnick SO, et al. Photodynamic therapy of cancer: an update. *CA Cancer J Clin.* Wiley Online Library; 2011;61:250–81.
13. Mew D, Wat C-K, Towers GH, Levy JG. Photoimmunotherapy: treatment of animal tumors with tumor-specific monoclonal antibody-hematoporphyrin conjugates. *J Immunol.* Am Assoc Immunol; 1983;130:1473–7.
14. van Dongen GAMS, Visser GWM, Vrouenraets MB. Photosensitizer-antibody conjugates for detection and therapy of cancer. *Adv Drug Deliv Rev.* Netherlands; 2004;56:31–52.
15. Cognetti D, Curry JM, Gillenwater AM, William WN, Kochuparambil ST, McDonald D, et al. A Phase 2a, Multicenter, Open-Label Study of RM-1929 Photoimmunotherapy in Patients With Recurrent Head And Neck Cancer. *Int J Radiat Oncol • Biol • Phys.* Elsevier; 2018;100:1368.
16. Heukers R, van Bergen en Henegouwen PMP, Oliveira S. Nanobody-photosensitizer conjugates for targeted photodynamic therapy. *Nanomedicine Nanotechnology, Biol Med.* Elsevier; 2014;10:1441–51.
17. Van Driel PBAA, Boonstra MC, Slooter MD, Heukers R, Stammes MA, Snoeks TJA, et al. EGFR targeted nanobody-photosensitizer conjugates for photodynamic therapy in a pre-clinical model of head and neck cancer. *J Control Release.* Elsevier; 2016;229:93–105.

18. Hamers-Casterman C, Atarhouch T, Muyldermans S, Robinson G, Hammers C, Songa EB, et al. Naturally occurring antibodies devoid of light chains. *Nature*. 1993;
19. Carpenter G, Cohen S. Epidermal growth factor. *Annu Rev Biochem*. Annual Reviews 4139 El Camino Way, PO Box 10139, Palo Alto, CA 94303-0139, USA; 1979;48:193–216.
20. Voskoglou-Nomikos T, Pater JL, Seymour L. Clinical predictive value of the in vitro cell line, human xenograft, and mouse allograft preclinical cancer models. *Clin Cancer Res*. 2003;9:4227–39.
21. Johnson JI, Decker S, Zaharevitz D, Rubinstein L V., Venditti JM, Schepartz S, et al. Relationships between drug activity in NCI preclinical in vitro and in vivo models and early clinical trials. *Br J Cancer*. 2001;84:1424–31.
22. Kretzschmar K, Clevers H. Organoids: Modeling Development and the Stem Cell Niche in a Dish. *Dev Cell*. Elsevier Inc.; 2016;38:590–600.
23. Dekkers JF, Wiegerinck CL, de Jonge HR, de Jong NWM, Bijvelds MJC, Nieuwenhuis EES, et al. A functional CFTR assay using primary cystic fibrosis intestinal organoids. *J Cyst Fibros*. Nature Publishing Group; 2012;11:S32.
24. Sachs N, de Ligt J, Kopper O, Gogola E, Bounova G, Weeber F, et al. A Living Biobank of Breast Cancer Organoids Captures Disease Heterogeneity. *Cell*. United States; 2018;172:373-386.e10.
25. Vlachogiannis G, Hedayat S, Vatsiou A, Jamin Y, Fernández-mateos J, Khan K, et al. Patient-derived organoids model treatment response of metastatic gastrointestinal cancers. *Science* (80-). American Association for the Advancement of Science; 2018;926:920–6.
26. Driehuis E, Kolders S, Spelier S, Lohmussaar K, Willems SM, Devriese LA, et al. Oral mucosal organoids as a potential platform for personalized cancer therapy. *Cancer Discov*. 2019;CD-18-1522.
27. Kalyankrishna S, Grandis JR. Epidermal growth factor receptor biology in head and neck cancer. *J Clin Oncol*. American Society of Clinical Oncology; 2006;24:2666–72.
28. Heukers R, Vermeulen JF, Fereidouni F, Bader AN, Voortman J, Roovers RC, et al. EGFR endocytosis requires its kinase activity and N-terminal transmembrane dimerization motif. *J Cell Sci*. 2013;
29. Schumacker PT. Reactive oxygen species in cancer cells: live by the sword, die by the sword. *Cancer Cell*. Elsevier; 2006;10:175–6.
30. Szatrowski TP, Nathan CF. Production of large amounts of hydrogen peroxide by human tumor cells. *Cancer Res*. AACR; 1991;51:794–8.
31. Carcenac M, Dorvillius M, Garambois V, Glaussel F, Larroque C, Langlois R, et al. Internalisation enhances photo-induced cytotoxicity of monoclonal antibody-phthalocyanine conjugates. *Br J Cancer*. 2001;85:1787–93.
32. Vrouwenraets MB, Visser GWM, Stigter M, Oppelaar H, Snow GB, Van Dongen GAMS. Targeting of aluminum (III) phthalocyanine tetrasulfonate by use of internalizing monoclonal antibodies: Improved efficacy in photodynamic therapy. *Cancer Res*. 2001;61:1970-5.

SUPPLEMENTARY DATA

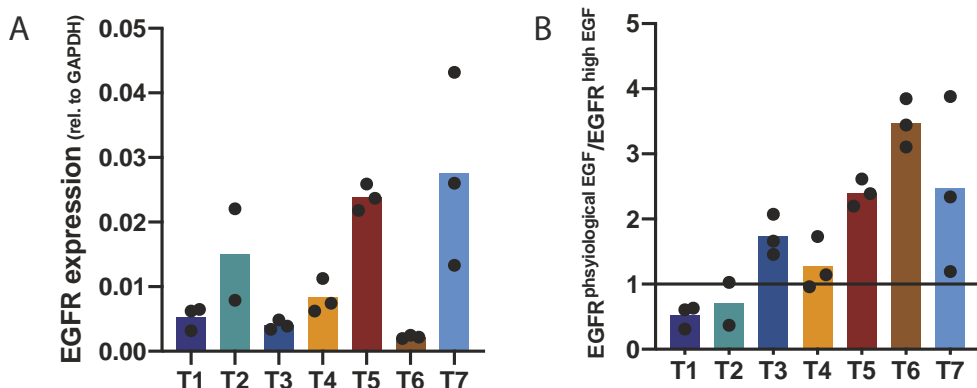


Figure S1. EGFR mRNA expression differs between patient-derived organoid lines and is increased upon medium change to physiological EGF levels. A. EGFR mRNA expression levels measured in organoid lines derived from different HNSCC patients. Expression is calculated relative to housekeeping gene GAPDH. Experiment was performed in technical triplicate. B. Culturing organoids under physiological EGF resulted in an increase in EGFR mRNA levels in 4/7 lines. EGFR expression is depicted as the ratio of EGFR in medium containing physiological EGF levels, versus EGFR expression in organoid cultured in high EGF medium. When this ratio is > 1, EGFR expression is increased in response to physiological EGF levels.

Figure S2. Comparison of different PS carriers in EGFR-targeted PDT. Results of *in vitro* PDT screens performed with 7D12-PS, 7D12-G98-PS and cetuximab-PS in eight patient-derived HNSCC organoid lines. Results of 7D12-PS are depicted in dashed lines and squared symbols, results of 7D12-9G8-PS in dotted lines and triangular symbols, and cetuximab-PS in solid lines and circular symbols. Color coding of the different samples is identical to that applied in the main figures.

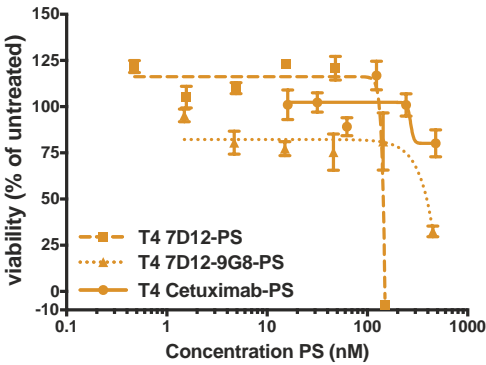
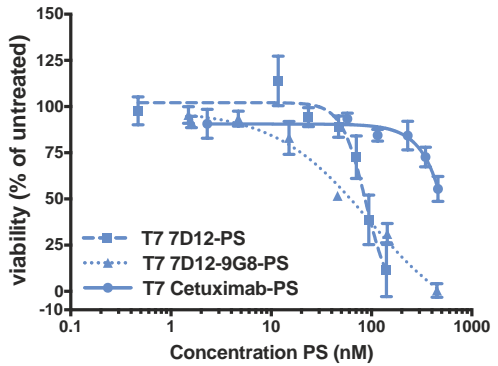
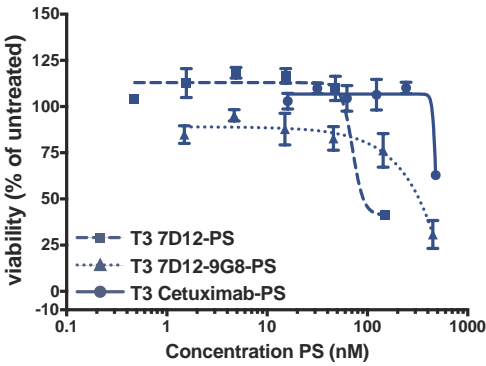
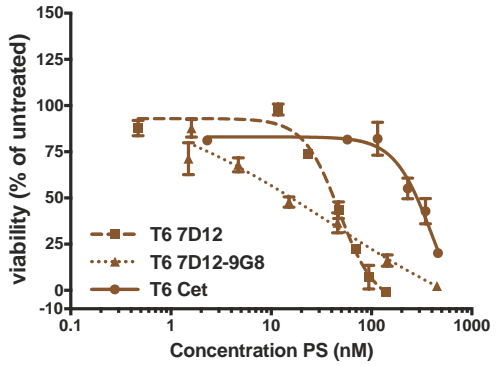
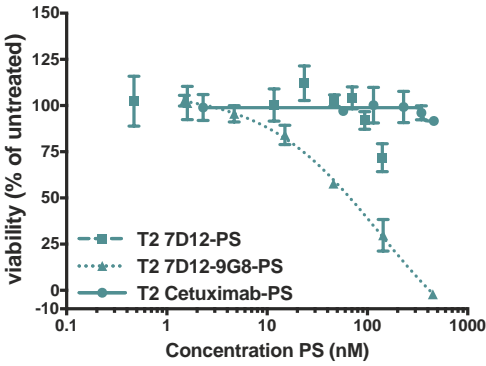
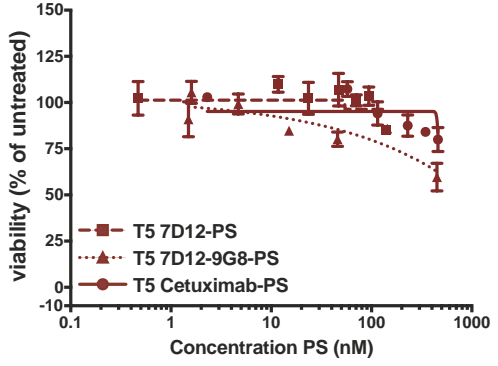
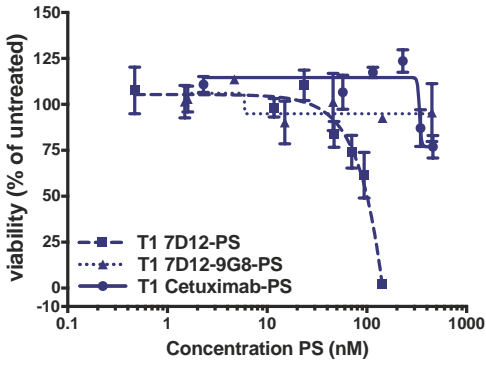


Table S1. Patient information.

#T	gender	age	tumor location	pretreatment	HPV status	sequencing	N/T
1	male	61	tongue	no	negative	oncopanel	T
2	female	90	larynx	no	negative	oncopanel	T
3	female	83	larynx	no	negative	oncopanel	T
4	male	60	tongue	no	negative	oncopanel	N/T
5	male	80	parotid gland	no	negative	exome sequencing	N/T
6	male	82	oral cavity	no	negative	oncopanel	T
7	female	70	gingiva	no	negative	exome sequencing	N/T

Patient information of organoid lines used in this study is given. From left to right, columns indicate: patient gender, patient age at diagnosis, tumor location, pretreatment, HPV status of tumor, type of DNA sequencing used to confirm tumor status of the organoid line, and availability of organoid lines from only tumor (T) or both tumor and corresponding normal (N/T) epithelium.



CHAPTER

PATIENT-DERIVED ORAL MUCOSA ORGANOIDS AS AN *IN VITRO* MODEL FOR METHOTREXATE- INDUCED TOXICITY

4



ABSTRACT

Methotrexate (MTX) is an important chemotherapeutic compound in pediatric acute lymphoblastic leukemia (ALL) therapy. Folinic acid (leucovorin, LV) rescue therapy is administered to reduce toxicity after high-dose MTX courses. Despite this intervention, side-effects are common and 20% of patients present with severe oral mucositis, resulting in hospitalization and chemotherapy delays. *In vitro* models to study the effect of MTX and LV on healthy oral mucosa epithelial cells are non-existent. Recently, we reported a method to establish patient-derived oral mucosa organoids. Here, we showed that these organoids express proteins essential for MTX uptake and intracellular retention and show MTX-induced cell death *in vitro*. In line with what is observed in the clinic, the extent of MTX-induced cytotoxicity differed between organoids derived from different donors, and was decreased by treatment with LV. The effect of LV on MTX-induced toxicity was both timing- and concentration-dependent. We found that a one day LV pre-treatment prior to MTX exposure reduced oral mucosa toxicity. Even though such a LV pre-treatment decreased MTX cytotoxicity on B-cell and T-cell leukemia cell lines, this effect was less pronounced in leukemia cells than in oral mucosa cells. Taken together, we present the first *in vitro* model for MTX-induced cell death in proliferating, human oral mucosa cells. Our findings underscore the relevance of the clinically applied LV regimen and highlight the potential of this model to further optimize modifications in dosing and timing on oral mucosa cells.



E. Driehuis^{1†}, N. Oosterom^{2†}, S. G. Heil³, I.B. Muller⁴, M. Lin⁴, S. Kolders¹, G. Jansen⁵,
R. de Jonge⁴, R. Pieters², H. Clevers^{1,2}, M. M. van den Heuvel-Eibrink^{2*}

¹ Oncode Institute, Hubrecht Institute, Royal Netherlands Academy of Arts and Sciences (KNAW) and University Medical Center Utrecht, The Netherlands

² Princess Maxima Center for Pediatric Oncology, Utrecht, The Netherlands

³ Erasmus MC, University Medical Center Rotterdam, Department of Clinical Chemistry, Rotterdam, The Netherlands

⁴ Amsterdam UMC, Department of Clinical Chemistry, Amsterdam, The Netherlands.

⁵ Amsterdam Rheumatology and immunology Center, Department of Rheumatology, Amsterdam UMC, Amsterdam, The Netherlands

[†] These authors contributed equally to this work.

* Corresponding author

INTRODUCTION

High-dose methotrexate (HD-MTX) is an important antifolate chemotherapeutic agent used in pediatric acute lymphoblastic leukemia (ALL) therapy. Currently, five-year survival rates of pediatric ALL have reached 90% in developed countries (1-4). However, patients often suffer from toxicity of chemotherapeutic regimens such as MTX. Despite administration of folinic acid (Leucovorin - LV) after HD-MTX infusion, 20% of patients develop severe MTX-induced oral mucositis leading to chemotherapy delays and an impaired quality of life (5-7). The development of oral mucositis is a complex process, of which therapy-induced epithelial cell death is one of the main features (8,9).

After HD-MTX, clinical practice guidelines advise to administer LV (5-formyltetrahydrofolate) to reduce toxicity. MTX enters the cell through the reduced folate carrier 1 (RFC1), the proton-coupled folate transporter (PCFT) and membrane folate receptors (MFR) (10,11). MTX is subsequently polyglutamated (PG) by folylpolyglutamate synthetase (FPGS). This polyglutamation is essential, as it increases intracellular MTX retention and augments its pharmacological activity (12). MTX-PG can inhibit DNA and RNA synthesis by depleting intracellular reduced folate levels through inhibition of the enzymes dihydrofolate reductase (DHFR), thymidylate synthase (TS) and aminoimidazole carboxamide ribonucleotide transformylase (AICARTFase) (Figure S1) (13). Ultimately, this results in apoptosis in leukemic cells. However, healthy cells with a high cell turnover, including bone marrow and the epithelial lining of the gastrointestinal tract and oral mucosa, are also affected by MTX therapy.

LV is a reduced folate, that reactivates DHFR and purine/pyrimidine biosynthesis, thereby restoring the intracellular folate pool after HD-MTX therapy (14,15). In mice, a decrease in MTX-induced damage to the jejunal- and oral mucosa was observed after LV administration (16-19). Importantly, when administered 12 to 24 hours after MTX, LV did not compromise the anti-leukemic activity of MTX (16-19). In line with this, a selective mechanism of action for MTX and LV in tumor cells versus normal cells has been proposed. A higher level of MTX-PG accumulation in leukemia and solid tumor cell lines compared to normal intestinal and bone marrow precursor cells has been reported both *in vitro* and *in vivo* (20-26). Retrospectively, these preclinical studies provided a biochemical rationale for the LV rescue regimens introduced in the clinic in the 1960s. While it is nowadays generally accepted that LV decreases toxicities such as oral mucositis after antifolate therapy, the optimal LV dosing- and timing- regimen to reduce oral mucositis rates, without interfering with the efficacy of leukemia treatment, remains unknown.

Further compromising our understanding of the mechanism of action of LV, is the absence of efficacy and selectivity studies of MTX and LV in healthy human oral mucosa cells. The effect of MTX and LV on intestinal epithelium has been studied in 2D tumor cell lines or intestinal mouse tissue (20,22). Although valuable, it is recognized that both 2D models and mouse models cannot always be used to reliably predict clinical utility of therapies (27,28). As such, there is a need for models that more closely recapitulate the *in*

vivo situation. Ideally, MTX and LV effects on healthy mucosal epithelia should be studied in normal, not immortalized, human cells.

Organoids are 3D structures grown from stem cells, that recapitulate histological and functional characteristics of their tissue of origin (29). Since the discovery that organoids could be established from adult stem cells of the mouse gut, organoid technology has quickly evolved (30). Nowadays, organoids can be grown from many different epithelia (30-42). These 'mini-organs' can be established from both tumor and normal primary patient material with high (60-70%) efficiency. Data supporting the translational potential of this technology is accumulating. For example, *in vitro* therapy response of tumor organoids was shown to predict the responses of corresponding patients (43,44). When derived from Cystic Fibrosis (CF) patients, organoids were also found to predict patient response *in vitro* (45) and could be used to find effective therapies for CF patients (46). The organoids recapitulated disease phenotype and were shown to be a useful tool to predict response to therapy (45).

Recently, we described an organoid model derived from healthy oral mucosa (34). The resulting patient-derived structures consist of a functional stratified squamous epithelium that can be maintained in culture over six months. Taken that others have shown that organoids are a proper model for body physiology, we set out to test the potential of different dosing- and timing- regimens of LV in search for the most optimal regimen to 'rescue' mucosal toxicity during treatment with HD-MTX in patient-derived oral mucosal organoids.

RESULTS

Human normal oral mucosa organoids can be used to model MTX-induced toxicity *in vitro*

Organoid lines used in this study were derived from tumor-adjacent normal epithelium of patients with head and neck squamous cell carcinoma (Table S1). Oral mucosa organoids grew as dense structures consisting of epithelial cells that recapitulate the histological organization of the oral mucosal epithelium *in vivo* (Figure 1A and 1B). Keeping in mind their origin and the potential risk of cancer cell contamination, the wildtype status of the organoids was confirmed by whole exome sequencing. Using normal epithelial tissue as a reference, a low number of mutations was detected in these lines (two in N1, none in N2), with no mutations found in common cancer driver genes (Figure 1C, Table S2).

As previously mentioned, MTX transport by either RFC1, PCFT and/or MFR into the cell, and its subsequent polyglutamylolation by FPGS, is essential for MTX effectivity and toxicity. MTX inhibits DHFR, TS and AICARTFase, resulting in inhibition of DNA- and RNA-synthesis. Expression of these genes was confirmed by quantitative PCR (Figure 1D). In addition, we assessed catalytic activity of FPGS as compared with a reference human T-cell leukemia cell line CCRF-CEM, revealing a 5.5-fold lower FPGS activity in oral

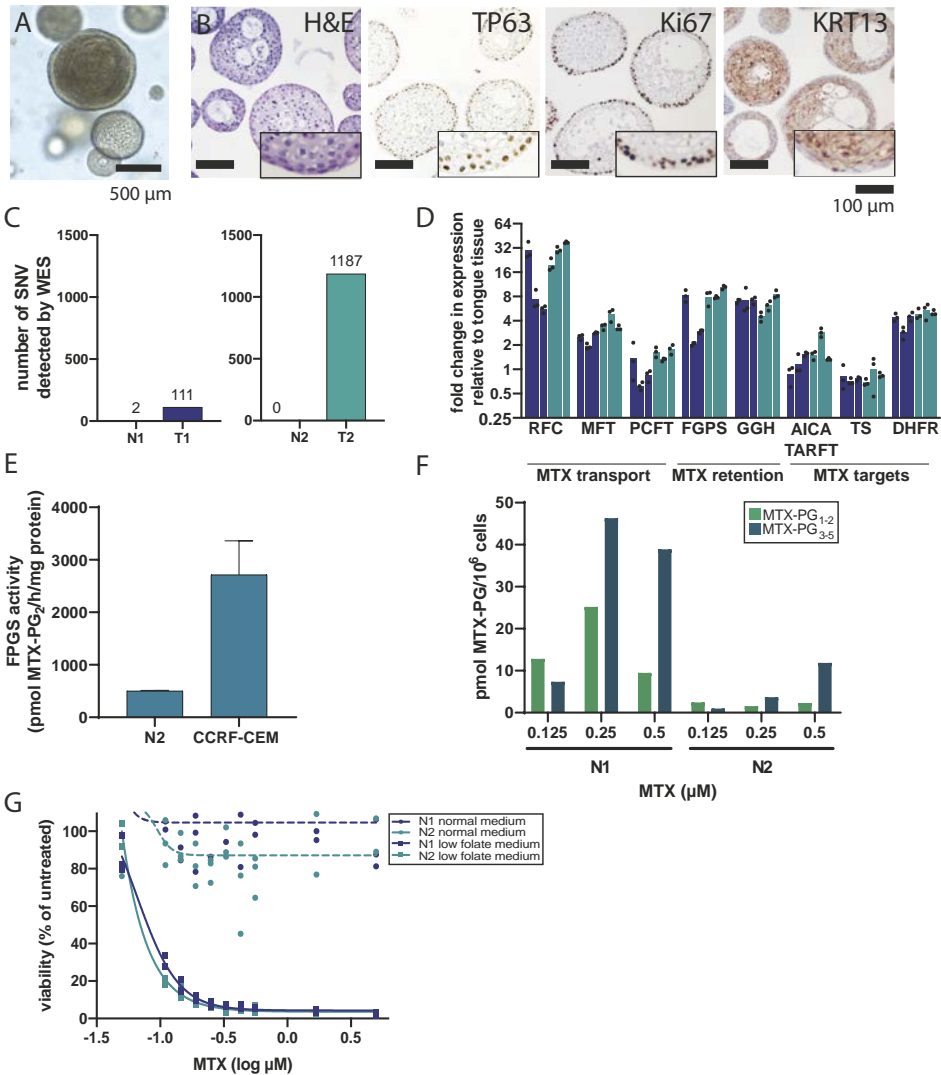


Figure 1. Human normal oral mucosa organoids can be used to model MTX-induced toxicity

in vitro. A. Oral mucosa organoids as seen through a brightfield microscope. The cells form multicellular round structures with keratinized centers. Scalebar, 500 μm . B. Immunohistochemical stainings performed on paraffin-embedded oral mucosa organoids show that organoids resemble the histological characteristics of *in vivo* epithelium. Top panel: human oral mucosa epithelium, lower panel: oral mucosa organoids. Hematoxylin and eosin, TP63 staining, Ki67 staining and KRT13 staining are shown from left to right. P63 positive basal cells are located on the outside of the structure, where they are in contact with the BME, an *in vitro* basal lamina mimic. Proliferation, marked by Ki67 staining, occurs in the basal cells. More differentiated keratin 13 positive keratinocytes are located in the center of the organoids. Scalebar, 100 μm . C. Oral mucosa organoids are derived of human normal cells, and not cancer cells. Number of mutations detected by whole exome sequencing in the healthy oral mucosa organoids used in this study, and their corresponding tumor organoids. Mutational load is low (2 for N1, 0 for T1), especially when compared to the tumor organoids. D. Expression of

- ▶ genes important for MTX transport, metabolism and toxicity was tested in low folate medium using quantitative qPCR. All the genes checked expressed at detectable levels in our system. E. FPGS activity (in pmol MTX-PG₂/h/mg) in organoid line versus CCRF-CEM reference leukemia cell line. F. Short chain MTX-PG_{1,2} and long-chain MTX-PG_{3,5} accumulation in two oral mucosa organoid lines in increasing doses of MTX. G. MTX exposure induces toxicity (cell death) in oral mucosa organoids grown in low folate medium, but not in normal oral mucosa medium. Organoids were exposed for five days to MTX and viability was quantified relative to untreated organoids. Reproducible killing at physiological doses of MTX can be obtained only in low folate medium (dashed lines, circle data points), not in normal organoid medium (straight lines, square data points).



mucosa organoids than in CCRF-CEM cells (501 versus 2715 pmol MTX-PG₂/h/mg protein) (Figure 1E).

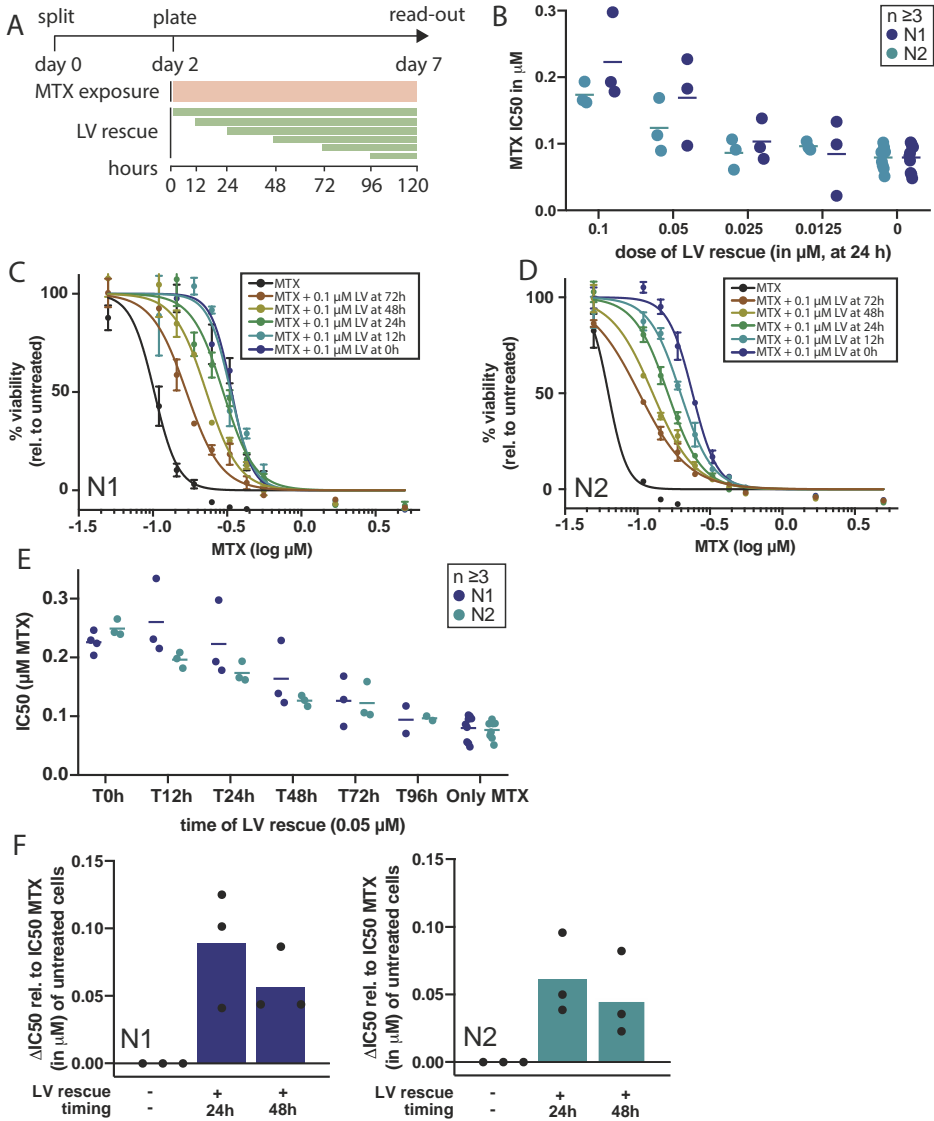
Subsequently, oral mucosa organoids were exposed to MTX *in vitro* for five days. MTX polyglutamates (MTX-PG_{1,5}) accumulated intracellularly in oral mucosa organoids in a dose-dependent way (Figure 1F), suggestive of functional MTX metabolism. Total intracellular levels of MTX-PG differed between donors, in line with the large variation in MTX-PG levels detected in patients. We showed that the higher the MTX concentration, the higher total intracellular MTX-PG levels, and especially of long-chain MTX-PG_{3,5}.

MTX-induced cell death was only observed when organoids were grown in medium containing physiological folate levels and lacking hypoxanthines and thymidines, which are normally present in standard organoid culture medium (Figure 1G). Indeed, also in 2D tumor cell lines, more prominent MTX toxicity was observed when cells were cultured in media containing physiological folate levels (47,48). Organoids grew at similar speed in this folate-deprived medium when compared to normal medium, and showed similar morphology (Figure S2). All subsequent drug screens were therefore performed in folate-deprived medium.

MTX-induced toxicity in oral mucosa organoids can be partly rescued by LV and is time- and concentration-dependent

Normal human oral mucosa organoids were exposed to a clinically relevant concentration range of MTX for five days, either in the presence or absence of LV that was added at fixed timepoints after the start of MTX treatment (Figure 2A). All drug screens in this project were performed in technical and biological triplicates. Drug screens showed high technical quality as measured by Z-scores (median 0.82; range 0.33 – 0.98, Table S3). Administration of LV resulted in a decrease of MTX-induced cell death in a concentration-dependent manner (Figure 2B).

In clinics, the timing of LV administration after MTX differs per treatment protocol, and is initiated at timepoints ranging from 24 to 42 hours after MTX infusion. LV administration is usually not continued after 54 hours post MTX infusion as MTX plasma levels of have dropped by then. To model LV rescue therapy *in vitro*, organoids were exposed to LV



4

Figure 2. MTX-induced toxicity in oral mucosa organoids can be rescued by LV, and is both timing- and dosing-dependent. A. Schematic outline showing the experimental set-up used in this study to perform MTX drug screens with LV rescue of different dosages (shades of green) and timing (length of LV bars). Organoids were split on day 0, left to recover for two days and filtered, counted and plated in 384 well format to be exposed to MTX for five days (with or without LV). On day 7, viability readout was performed. B. MTX-induced toxicity can be decreased by LV rescue. Here we focus on LV rescue that was initiated 24 hours after the start of MTX treatment. IC50 values of MTX are depicted for all tested dosages of LV (0.1 µM, 0.05 µM, 0.025 µM and 0.0125 µM) and was compared to IC50 values obtained when no LV rescue was performed. All experiments are performed at least three times, and each dot indicates the result of one experiment which was performed in technical triplicate. C. Timing of LV rescue influences its effect of MTX-induced toxicity in organoid line N1. As ▶

- ▶ an example, kill curves are shown for MTX treatment alone, or combined with LV rescue of 0.1 μM (started at 0, 24 and 48 hours after initiation of MTX treatment). D. Timing of LV rescue influences its effect of MTX-induced toxicity in organoid line N2. E. Quantification of drugscreens as shown Figure 3C and 3D. Each kill curve is summarized in an IC50 value, and timepoints of LV rescue are extended to 0, 12, 24, 48, 72 and 96 hours after the start of MTX treatment. All experiments are performed at least three times, and each dot indicates the result of one experiment which was performed in technical triplicate. An increase in viability (higher IC50 values) is observed when LV is given at an earlier timepoint). F. Delta IC50 values of N1 and N2 organoids lines when LV was added at T24 and T48 compared to the condition where only MTX was administered without LV rescue. G. The effect of LV rescue was also studied after removal of MTX, to model the effect of LV rescue once MTX-induced damage has already been induced. Compared to continued exposure over five days, MTX-induced toxicity is less when cells are only exposed for two days (circles compared to squared). However, in both cases, the effect of LV was retained in both situations (yellow dashed lines compared to continuous blue lines), suggesting that LV also exerts an effect on MTX-induced damage when MTX is removed.



at different timepoints after the start of MTX treatment. The extent of LV rescue was dependent on the timing of LV addition; the earlier LV was administered, the higher the overall cell viability (Figures 2C and 2D). LV administration decreased MTX toxicity up to 72 hours after the start of MTX treatment (Figure 2E). Indeed, MTX IC50 values were 25 – 35% higher for mucosa cells that received LV rescue at 24 hours after the start MTX treatment, when compared to those receiving LV at 48 hours (Figure 2F). Moreover, LV administration later than 54 hours still affected oral mucosa cell viability. Hence, these findings indicate that LV administration at later timepoints than those currently applied in the clinic, could still contribute to prevent or decrease MTX-induced damage to the oral mucosa.

A one day pre-treatment of oral mucosa cells with LV prior to MTX treatment results in potentiation of the LV rescue effect

MTX-induced oral mucositis occurs most frequently after the first cycle of HD-MTX and LV courses, and is less likely to occur after subsequent cycles (49). This observation has resulted in the hypothesis that intracellular LV from previous administrations remains available intracellularly, and prevents toxicity during subsequent MTX and LV courses. To model this *in vitro*, organoids were exposed to LV one day prior to the start of MTX treatment. At the start of MTX treatment, LV was removed and toxicity was assessed as previously described (Figure 3A). In organoid line N1, LV pre-treatment did not significantly alter the response to MTX, although MTX IC50 values marginally increased (Figure 3B and 3C). However, in organoid line N2, a clear rescue effect of the pre-incubation with LV was observed (Figures 3D and 3E). Pre-treatment with LV increased the viability of N2 organoids when exposed to MTX for all LV rescue timepoints tested (range 5 – 30% increase in cell viability based on which timepoint assessed). When pre-treated, the rescue effect of LV rescue administered at 72 hours resulted in a cell survival similar to a LV rescue that would have been given at 0 hours without pre-treatment. This suggests that pre-

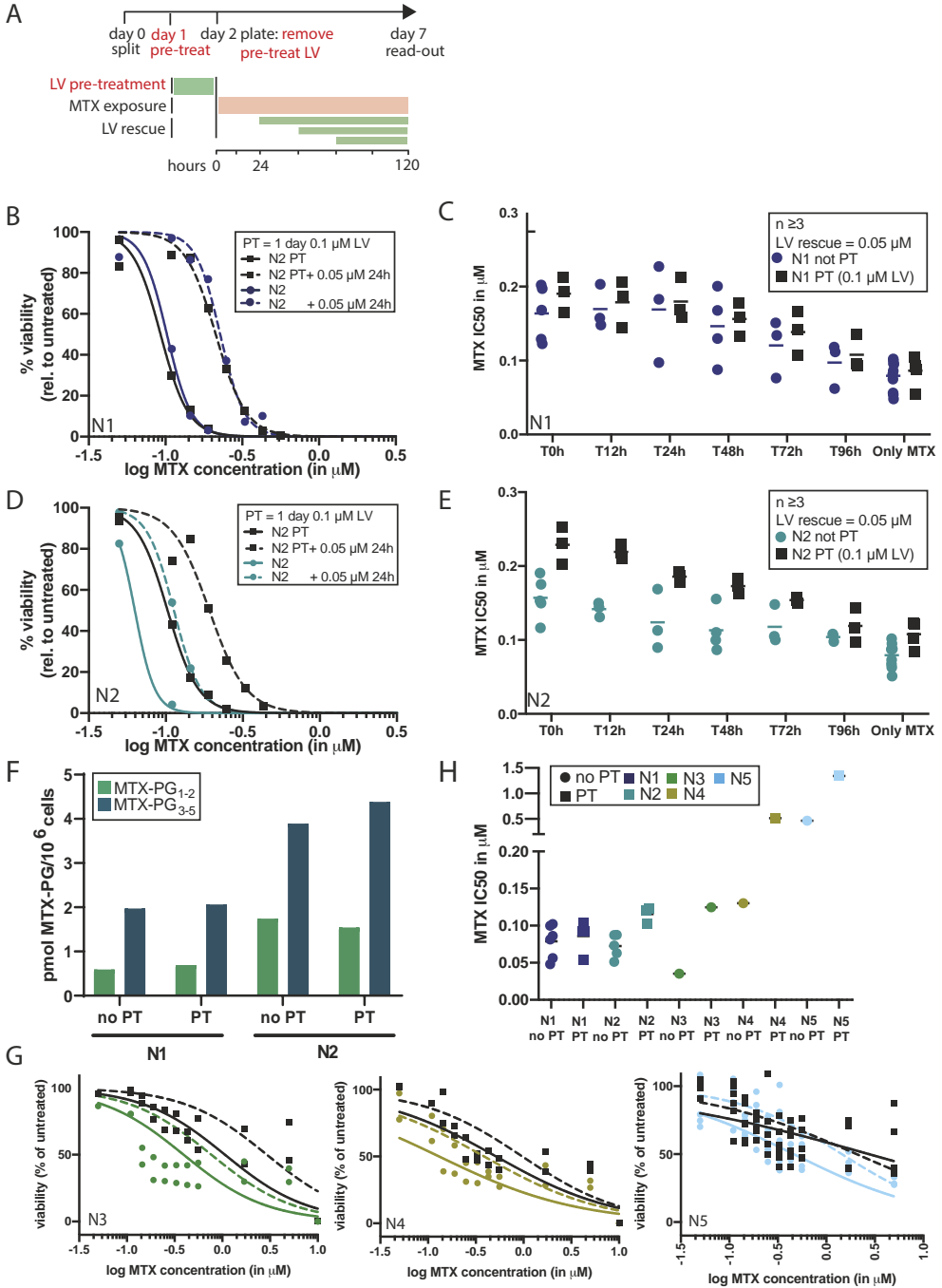
treatment might increase the timeframe in which LV rescue rescues MTX toxicity in oral mucosa cells. After 24 hours of MTX exposure, we did not observe significant differences in accumulation of intracellular MTX-PG levels between not pre-treated and pre-treated N1 and N2 organoids (Figure 3F).

As the effect of LV pre-treatment was dependent on the donor of which the organoids were derived, we exposed organoids derived from three additional donors to the same treatment regimen. We observed that in all other lines tested, pre-treatment increased oral mucosa cell survival upon exposure to MTX (Figures 3G and 3H). Taken together, we conclude that a one day pre-treatment with LV decreases MTX-induced mucosal toxicity in 4/5 tested donors. This implies that LV pre-treatment may reduce the risk of oral mucositis. However, it is crucial to investigate the effect of such a pre-treatment on leukemia cells, before any claims can be made on clinical testing of such an intervention.

Effect of MTX and LV therapy on leukemia cell lines

To assess the effect of LV pre-treatment on leukemia cells, both T cell ALL (Jurkat, MOLT16, HSB2) and B cell ALL (Nalm6, REH) cell lines were exposed to MTX, either in the presence or absence of LV pre-treatment (Figures 4A - 4E). Although LV pre-treatment increased MTX IC50 values in the leukemia cell lines tested, the effect was less pronounced than in oral mucosa cells (Figure 4F). In an attempt to estimate the effect of LV pre-treatment when administered systemically, we compared the effect of this treatment on both oral mucosa cells and leukemia cells at a concentration of 0.1 μM MTX (Figure 4G). This concentration of MTX was chosen as this is a level reached in all patients (median at T48 0.38 μM , range 0.1 – 22 μM) (49). LV pre-treatment decreases the toxicity of MTX on oral mucosa cells, but does not influence the effect of MTX on leukemia cells. Here, the only exception is the Jurkat T-ALL cell line, that showed IC50 values comparable to those observed for oral mucosa organoids. The finding that T-cell lines are less sensitive to MTX than B-cell lines are in line with the results of others (50,51). MTX-PG levels in two B-ALL leukemia cell lines (REH; Nalm6) were around 3-fold higher (Figure 4H) when compared to MTX-PG levels in oral mucosa organoids (3F). MTX-PG levels in two T-ALL leukemia cell lines (Jurkat; HSB2) differed with high MTX-PG levels in Jurkat cells (~3-fold higher than organoids) and low MTX-PG levels in HSB-2 cells (same range as organoids).

We conclude that pre-treatment with LV decreases the effect of MTX on leukemia cells. However, as leukemia cells are much more sensitive to MTX than oral mucosa cells, the pretreatment does not influence the effect of MTX at these concentrations. Regardless, the effect of LV pre-treatment should be explored with caution. Potentially, a local LV application might be a more feasible approach. Such a local application at the oral mucosa would not interfere with the systemic MTX effect on leukemia cells.



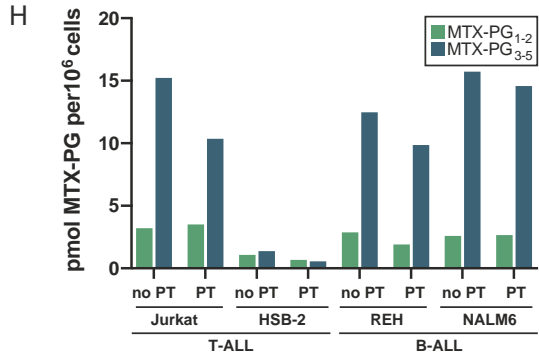
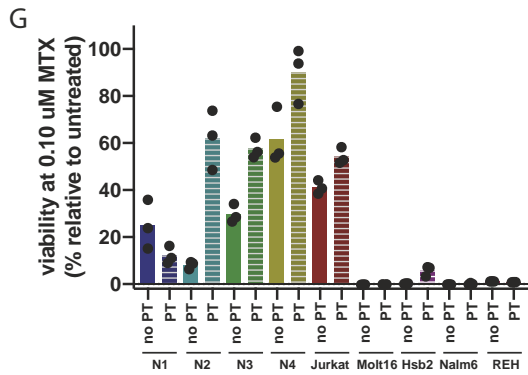
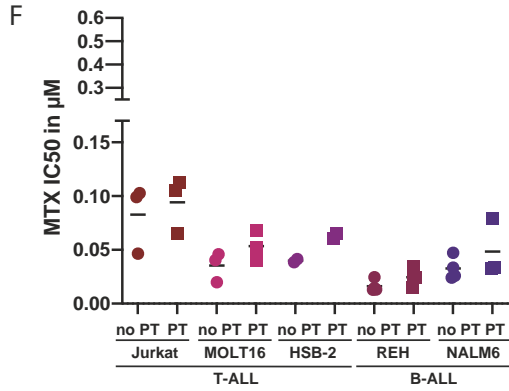
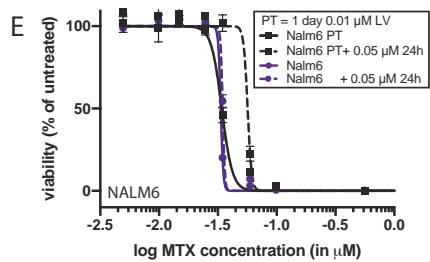
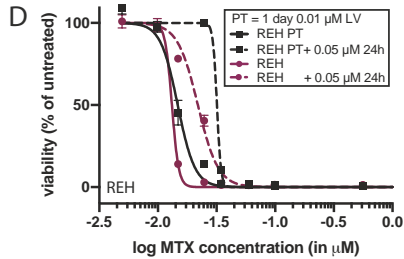
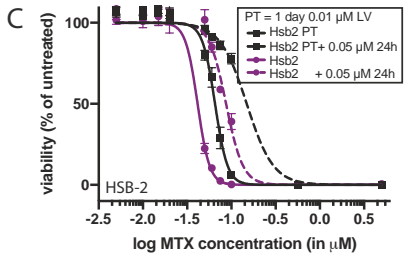
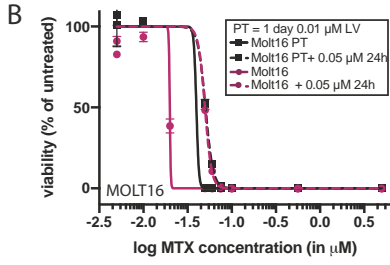
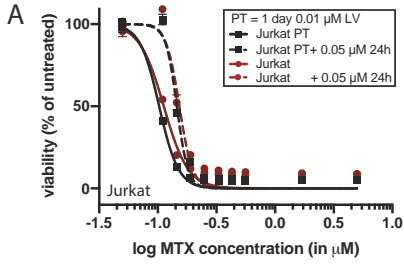
DISCUSSION

Using a 3D *in vitro* model of primary human oral mucosa organoids, we show a concentration- and time-dependent 'rescue' effect of LV on MTX-induced mucosal toxicity. Using this model, mimic the clinical situation, where pediatric ALL patients receive HD-MTX followed by LV rescue therapy. Our findings indicate that LV administration at earlier timepoints, such as 24 hours after start of MTX, would reduce mucositis-associated toxicity. In addition, we found that in 4/5 cases tested, LV pre-treatment increased the potential of LV rescue therapy in mucosal cells.

To our knowledge, this is the first *in vitro* study that investigates the effect of MTX and LV on normal human oral mucosa cells. We show that, using the right culture conditions, oral mucosa cells show sensitivity to MTX and LV at plasma levels that are reached in patients. Limited MTX-induced cell death was observed in the regular organoid medium based on advanced DMEM/F12 (supplemented with 6 μ M folic acid, 15 μ M hypoxanthine and 1.5 μ M thymidine). Most likely, these high concentrations result in rescue of MTX toxicity *in vitro*, as previously described (52).

We show that both higher concentrations and earlier timing of LV rescue decrease the extent of MTX-induced damage in oral mucosa cells. These data confirm that LV rescue, already applied in patients, is a sound approach to reduce the development and severity of mucositis. Although it is generally accepted that LV decreases the chance of oral mucositis after HD-MTX, it is unclear if an increased dose or altered timing of LV administration is beneficial to the patient. Consequently, this has resulted in the introduction of different LV dosing- and timing- regimens in international treatment protocols. LV after HD-MTX is usually initiated 36 or 42 hours after HD-MTX, although in some protocols, LV is already applied at 24 hours post MTX infusion. LV rescue therapy is often not administered beyond the timepoint of 54 hours after start of MTX. Even though it is essential to further

-
- ◀ **Figure 3. A one day pre-treatment of oral mucosa cells with LV before MTX treatment results in potentiation of the LV rescue effect.** A. Schematic outline showing the experimental set-up used to perform MTX drug screens with or without LV rescue started 24 hours after the start of MTX treatment, with or without a one day LV pre-treatment. B and D. Effect of LV pre-treatment (PT) on viability of N1 and N2 organoids, respectively. Dark squares indicate PT conditions, colored circles indicate cells that did not receive PT. Dashed lines indicate viability when a LV rescue is performed 24 hours after start of MTX treatment. C and E. Effect of PT quantified for different LV rescue timepoints. IC50 values are shown on the y-axis. All experiments were performed in technical and biological triplicate. F. Effect of PT on MTX-PG levels in oral mucosa organoid lines derived from two different donors. G. Effect of LV pre-treatment (PT) on viability of N3, N4 and N5 organoids, respectively. Dark squares indicate PT conditions, colored circles indicate cells that did not receive PT. Dashed lines indicate viability when a LV rescue is performed 24 hours after start of MTX treatment. H. MTX IC50 values of oral mucosa organoids tested here, either pre-treated (PT) or not (no PT). In 4/5 cases, an increase in MTX IC50 value can be observed in response to pre-treatment. Here, IC50 values are shown when no LV rescue is performed.
-



investigate the effect of changes to the LV rescue regimen on leukemic cells, we anticipate the following two main findings of our work have potential clinical implications.

First, we find that LV rescue at earlier timepoints than currently used in most treatment protocols (such as at 24 hours) decreases MTX-induced toxicity. Despite the fact that there might be differences in MTX toxicity *in vitro* and *in vivo*, our findings indicate that an earlier start of LV rescue decreases the risk and extent of MTX-induced mucositis. Second, we show that pre-incubation of oral mucosa organoids with LV decreased mucosal cell death upon subsequent exposure to MTX. We did not observe large differences in intracellular MTX-PG levels between pre-treated and not pre-treated organoids, suggesting that the rescue effect was not hampered by competition for cellular transport or polyglutamylation mechanisms. Future studies to assess how optimal timing of pre-treatment with LV contributes to an increased rescue effect would be of value.

The extent of MTX-induced cell death was found to differ per patient. Moreover, the extent of rescue after LV administration also was found to vary between organoid lines. This variation is in line with the fact that only a subset of patients presents with mucositis, suggesting some patients are more sensitive to MTX treatment than others. Although beyond the scope of this work, oral mucosa organoids create the opportunity to study the molecular differences between sensitive and resistant lines. Unravelling these differences might aid the identification of patients at risk, or contribute to alternative treatment strategies to decrease the incidence of oral mucositis.

To assess the effect of LV pre-treatment on leukemia cells, leukemia-derived cell lines were exposed to the same pre-treatment to study the effect on MTX toxicity. Here, the effect of pre-treatment and LV rescue was also present, but less pronounced than in oral mucosa cells. These differences in response observed between leukemia cells and other healthy tissues have been observed before, as several pre-clinical studies discussed that MTX-PG levels accumulated to high levels in leukemia cell lines, whereas only low levels of MTX-PG accumulated in normal intestinal and bone marrow precursor cells, supporting a selective mechanism of action for MTX and LV (14,15,20-26). In line with these results, we showed that in general MTX-PG accumulation in oral mucosa organoids was lower than in leukemia cell lines. This suggests a different level of activity of the FPGS

-
- ◀ **Figure 4. LV pre-treatment influences MTX toxicity in leukemia cell lines.** A to E. Effect of LV pre-treatment (PT) on viability of leukemia cell lines. Both T-ALL and B-ALL cell lines are tested here. Dark squares indicate PT conditions, colored circles indicate cells that did not receive PT. Dashed lines indicate viability when LV rescue is performed 24 hours after start of MTX treatment. F and G. MTX IC50 values of all leukemia cell lines tested here, either pre-treated (PT) or not (no PT). In all cases, an increase in MTX IC50 value can be observed in response to pre-treatment. Here, IC50 values are shown when no LV rescue is performed. H. Effect of PT on MTX-PG levels in two B-ALL and two T-ALL cell lines.
-

and GGH enzymes in leukemic blasts versus oral mucosal cells. In line with these results, we are the first to present that FPGS activity in human oral mucosa cells is indeed 5.5-fold lower than in leukemia cell lines. Previous studies showed that FPGS activity in primary leukemia cells is higher than in a reference leukemia cell line, which is consistent with the notion that FPGS activity is linked to the proliferation and differentiation status of cells (53,54). Taken together, these observations support the fact that primary patient-derived ALL cells (especially B-ALL when compared to T-ALL) are highly sensitive to MTX due to a high proliferation rate and high FPGS activity and thus might be less affected by LV pre-treatment than oral mucosa cells (26).

Despite the fact that the LV pre-treatment rescue effect on leukemia cells was less pronounced *in vitro*, in future studies, it could be investigated whether *local* oral application of LV instead of *systemically* administered LV decreases the incidence or severity of oral mucositis. Even though we do not prove that local administration does not impact leukemia treatment, it is unlikely that the low LV plasma concentration reached after of local application will affect MTX toxicity in leukemia cells.

Oral mucositis is a complex process of which cell death is only one of the hallmarks (8,55). In 2004, Sonis *et al.* proposed a more complicated model of oral mucositis, where the generation of Reactive Oxygen Species (ROS) and pro-inflammatory cytokines were also hallmarks of the clinical phenotype in addition to therapy-induced cell death (8). Furthermore, it has been suggested that the bacterial microbiome might play a role in developing oral mucositis. It would be of interest to study the effect of these factors in future models (8). Co-cultures of organoids and immune cells and co-cultures of bacteria and organoids are feasible and have been described (56,57). Therefore, this model holds the potential to be extended to recapitulate the clinical phenotype of 'oral mucositis' in more detail.

CONCLUSION

Although applied in clinic for many years, the effect of LV rescue therapy to reduce oral mucositis after MTX treatment has not been shown in representative models before. Here, we report the use of normal human oral mucosa organoids that recapitulate functional and histological characteristics of this epithelium, to study the potential of LV to reduce MTX-induced toxicity. As such, we present the first *in vitro* model to test MTX toxicity in proliferating normal oral mucosa epithelial cells. Oral mucosa organoids showed sensitivity to clinically relevant doses of MTX, and MTX-induced toxicity could be reduced by the addition of LV after the start of MTX treatment. The extent of this rescue is concentration- and timing-dependent. Using this system, we find that locally administered LV at earlier timepoints might benefit patients. Moreover, a pre-exposure with LV of the oral mucosa before the start of MTX treatment significantly potentiates the effect of LV rescue. These findings support the LV rescue protocol that is currently applied in the clinic and,

moreover, highlight the potential of this model to study the effect of modifications of this protocol on oral mucosa cells.

METHODS

Establishment and culture of human organoid lines

Tissue for the generation of organoids from adult normal human oral keratinocytes was obtained from tissue biopsies in the oral cavity during ear/nose/throat surgery. Obtaining these tissues was compliant with the guidelines of the European Network of Research Ethics Committees (EUREC) and European and national laws, and informed consent was obtained from all donors. The Biobank Research Ethics Committee of the UMC Utrecht approved the biobanking protocol (12-093 HUB-Cancer). Oral mucosa organoids were generated as previously described (Supplemental Methods) (34).

4

Modification of culture conditions for MTX drug screens

For the purpose of this study, organoids were transferred to medium containing a more physiological concentration of folate rather than media with supra-physiological concentrations of folic acid usually present in regular media. We used RPMI 1640 without folic acid (Thermofisher, cat.no. 27016021) supplemented with the same supplements as in organoid medium supplemented with 5 nM folinic acid (Sigma-Aldrich, cat.no. 47612-250MG; racemic mixture of d- and l-stereoisomer of folinic acid) as sole folate source. This medium was referred to as low folate medium. Medium was changed every 2-3 days and organoids were split once every 1-2 weeks. Organoids were cultured for at least two weeks in this folate-deprived state before starting experiments. All drug screens were performed in this modified, low folate medium.

Quantitative PCR for expression of MTX metabolism genes

For quantitative PCR, IQ SYBR green (Bio-Rad, cat.no. 1708880) was used in a 384-well format. Methods to describe RNA and cDNA synthesis are described in the Supplemental Methods. Per well, 7.5 μ l SYBR Green was used, mixed with 1 μ l 10 μ M FW primer and 1 μ l 10 μ M RV primer, 3 μ l cDNA mix and 2.5 μ l water. For each reaction, it was estimated that 25 ng of cDNA was loaded. For qPCR, samples were incubated for 2 minutes at 95°C and for 40 cycles at: 15 seconds at 98°C, 15 seconds at 58°C and 15 seconds at 72°C. Results were calculated by using the $\Delta\Delta$ Ct method. Expression was calculated relative to expression in tongue tissue (total RNA, human normal tongue tissue, AmsBio, cat.no. R1234267). Melt peak analysis was performed to assure that primer had no aspecific binding. Primers used are described in Table S4.

Whole exome sequencing

DNA was isolated using Reliaprep gDNA tissue miniprep system (Promega, cat. no. A2052) according to protocol. Whole exome sequencing of oral mucosa organoids was previously performed (34). In this study, these data were reported to show the difference in number of detected mutations in both the normal human organoids used in this study compared to the tumor tissue derived from the same patient.



MTX drug screens (384-well format)

Two days prior to start of the drug screen, organoids were passaged and disrupted into single cells using TrypLE. Single cells were plated in 70% BME in organoid medium. Two days later, organoids were collected from the BME by addition of 1mg/mL dispase II (Sigma-Aldrich, cat.no. D4693) to the medium of the organoids. Organoids were incubated for 30 minutes at 37 °C to digest the BME. Subsequently, organoids were washed, filtered using a 70 mm nylon cell strainer (Falcon), counted and resuspended in 5% BME/growth medium (12.500 organoids/mL) prior to plating in 40 µl volume (Multi-drop Combi Reagent Dispenser, Thermo Scientific, cat.no. 5840300) in 384-well plates (Corning, cat.no. 4588). As such, 1000 organoids were plated per well. Drugs were added 1 hour after plating the organoids using the Tecan D300e Digital Dispenser (Tecan).

Methotrexate (Sigma-Aldrich, cat.no. M1000000) was dissolved in DMSO and was used in a concentration range between 5 µM–0.05 µM. Folinic acid (Sigma-Aldrich, cat. no. 47612-250MG) was dissolved in PBS containing 0.3% Tween-20, which was required to dispense the drug using the HP printer, and was used at set concentrations of 0.0125 µM–0.025 µM–0.05 µM–0.1 µM. We based our concentration range of MTX based on median MTX plasma level measured in pediatric ALL patients at T48h (0.38 µM, range 0.1 – 22 µM). The ratio LV:MTX in clinics is around 1:100 (~50 mg/m² : 5000 mg/m²), which was the rationale to focus on a lower range of LV concentrations (for instance 5 µM MTX versus 0.05 µM LV. All wells were normalized for solvent used. DMSO and percentage PBS/Tween-20 never exceeded 1%. Drug exposure was performed in technical triplicate and biological replicates of at least three for each concentration shown. For a lay-out of the drug screen and morphology of the organoid lines during a drugscreen, see supplementary Figure S3.

LV was added at different time points after start of MTX incubation. LV was dispensed using the Tecan Dispenser on top of plates previously started on MTX incubation. No medium change was performed (as organoids are in 5% BME, medium removal is impossible) and LV was dispensed into the medium that contained different concentrations of MTX. LV rescue was performed at 0, 12, 24, 48, 72 and 96 hours.

120 hours after adding the drugs, ATP levels were measured using the CellTiter-Glo 3D Reagent (Promega, cat.no. G9681) according to the manufacturer's instructions and luminescence was measured using a Spark multimode microplate reader (Tecan). Results were normalized to vehicle (no drugs - 100% cell viability) and baseline control (Staurosporin

1 μM - 0% cell viability). Kill curves were produced using GraphPad software and lines were fitted using the option 'log(inhibitor) versus normalized response -variable slope'. IC50 values were calculated for separate experiments. As a quality check for the performed assays, Z-values were calculated for each individual screen. Screens with Z-values below 0.3 were excluded from analysis (Table S2).

MTX-polyglutamate analysis by UHPLC-MS/MS

MTX-polyglutamate measurements were performed as previously described (Supplemental Methods) (58). Organoids were plated at a density of 100.000 per 4 mL in a 6-well non-repellent plate (Greiner) in low folate medium. Leukemia cell lines were cultured at a density of 10^4 cells per 20 mL low folate medium supplemented with 10% fetal calf serum (FCS). Organoids or leukemia cell lines were cultured without MTX or with MTX 0.5 μM . After a 24h incubation, cells were collected and washed twice with 15 mL medium (organoids) or PBS (cell lines). After centrifugation, cells were resuspended in 1 mL, counted and then snap frozen. Before counting organoids, they were incubated at 37°C in 0.125% Trypsin (Sigma, cat.no. T1426) until digested to be able to count single cells.

4

FPGS activity analysis

FPGS catalytic activity analysis in leukemic cell lines and organoids was performed essentially as described by Muller *et al.* (54) In short, FPGS-mediated conversion of MTX-PG₁ to MTX-PG₂ was determined in cell extracts containing 250 μM MTX-PG₁ and 4 mM ¹⁵N-labeled L glutamic acid (Sigma-Aldrich, cat.no. 332143-100MG) as enzyme substrates. After 2 hour incubation at 37°C, amounts of MTX-(¹⁵N)PG₂ formed were measured by UHPLC-MS/MS as described above. FPGS activity was expressed as pmol MTX-(¹⁵N)PG₂ formed/hr/mg protein.

ACKNOWLEDGEMENTS

We acknowledge Onno Kranenburg, Anneta Brousalı, Petra van der Groep, Alexander Constantinides and Anne Snelting of the Utrecht Platform for Organoid Technology (U-PORT; UMC Utrecht) for patient inclusion and tissue acquisition. We thank HUB Organoids for help with regulatory affairs regarding informed consent. We would like to thank Sacha Spelier for her help with organoid experiments. We acknowledge Eduard Struys for technical support in FPGS activity and MTX-PG level measurements. We thank the groups of Monique den Boer and Jules Meijerink at the Princess Maxima Center for providing us with leukemia cell lines.

DECLARATION OF INTEREST

H.C. is an inventor on several patents related to organoid technology. E.D. is inventor on a patent related to the culturing of organoids derived of normal and tumor tissue of the head and neck area.

FINANCIAL SUPPORT

Funded by the Oncode Institute (partly financed by the Dutch Cancer Society), by the gravitation program CancerGenomiCs.nl from the Netherlands Organization for Scientific Research (NWO) and by a Stand Up to Cancer International Translational Cancer Research Grant, a program of the Entertainment Industry Foundation administered by the AACR (SU2C-AACR-DT1213) and a ZonMw grant (116.006.103)



REFERENCES

1. Hunger SP, Lu X, Devidas M, Camitta BM, Gaynon PS, Winick NJ, et al. Improved survival for children and adolescents with acute lymphoblastic leukemia between 1990 and 2005: a report from the children's oncology group. *Journal of clinical oncology : official journal of the American Society of Clinical Oncology* 2012;30:1663-9
2. Pui CH, Carroll WL, Meshinchi S, Arceci RJ. Biology, risk stratification, and therapy of pediatric acute leukemias: an update. *Journal of clinical oncology : official journal of the American Society of Clinical Oncology* 2011;29:551-65
3. Kamps WA, van der Pal-de Bruin KM, Veerman AJ, Fiocco M, Bierings M, Pieters R. Long-term results of Dutch Childhood Oncology Group studies for children with acute lymphoblastic leukemia from 1984 to 2004. *Leukemia* 2010;24:309-19
4. Pieters R, de Groot-Kruseman H, Van der Velden V, Fiocco M, van den Berg H, de Bont E, et al. Successful Therapy Reduction and Intensification for Childhood Acute Lymphoblastic Leukemia Based on Minimal Residual Disease Monitoring: Study ALL10 From the Dutch Childhood Oncology Group. *Journal of clinical oncology : official journal of the American Society of Clinical Oncology* 2016;34:2591-601
5. Ackland SP, Schilsky RL. High-dose methotrexate: a critical reappraisal. *Journal of clinical oncology : official journal of the American Society of Clinical Oncology* 1987;5:2017-31
6. Bertino JR. Karmofsky memorial lecture. Ode to methotrexate. *Journal of clinical oncology : official journal of the American Society of Clinical Oncology* 1993;11:5-14
7. Howard SC, McCormick J, Pui CH, Buddington RK, Harvey RD. Preventing and Managing Toxicities of High-Dose Methotrexate. *The oncologist* 2016;21:1471-82
8. Sonis ST. The pathobiology of mucositis. *Nature reviews Cancer* 2004;4:277-84
9. Villa A, Sonis ST. Mucositis: pathobiology and management. *Current opinion in oncology* 2015;27:159-64
10. Zhao R, Diop-Bove N, Visentin M, Goldman ID. Mechanisms of membrane transport of folates into cells and across epithelia. *Annual review of nutrition* 2011;31:177-201
11. Gonen N, Assaraf YG. Antifolates in cancer therapy: structure, activity and mechanisms of drug resistance. *Drug resistance updates: reviews and commentaries in antimicrobial and anticancer chemotherapy* 2012;15:183-210
12. Raz S, Stark M, Assaraf YG. Foly|poly-gamma-glutamate synthetase: A key determinant of folate homeostasis and antifolate resistance in cancer. *Drug resistance updates : reviews and commentaries in antimicrobial and anticancer chemotherapy* 2016;28:43-64
13. Zhao R, Goldman ID. Resistance to antifolates. *Oncogene* 2003;22:7431-57
14. Goldman ID, Matherly LH. Biochemical factors in the selectivity of leucovorin rescue: selective inhibition of leucovorin reactivation of dihydrofolate reductase and leucovorin utilization in purine and pyrimidine biosynthesis by methotrexate and dihydrofolate polyglutamates. *NCI monographs : a publication of the National Cancer Institute* 1987:17-26
15. Matherly LH, Barlowe CK, Phillips VM, Goldman ID. The effects on 4-aminoantifolates on 5-formyltetrahydrofolate metabolism in L1210 cells. A biochemical basis of the selectivity of leucovorin rescue. *J Biol Chem* 1987;262:710-7
16. Goldin A, Mantel N, Greenhouse SW, Venditti JM, Humphreys SR. Estimation of the antileukemic potency of the antimetabolite aminopterin, administered alone and in combination

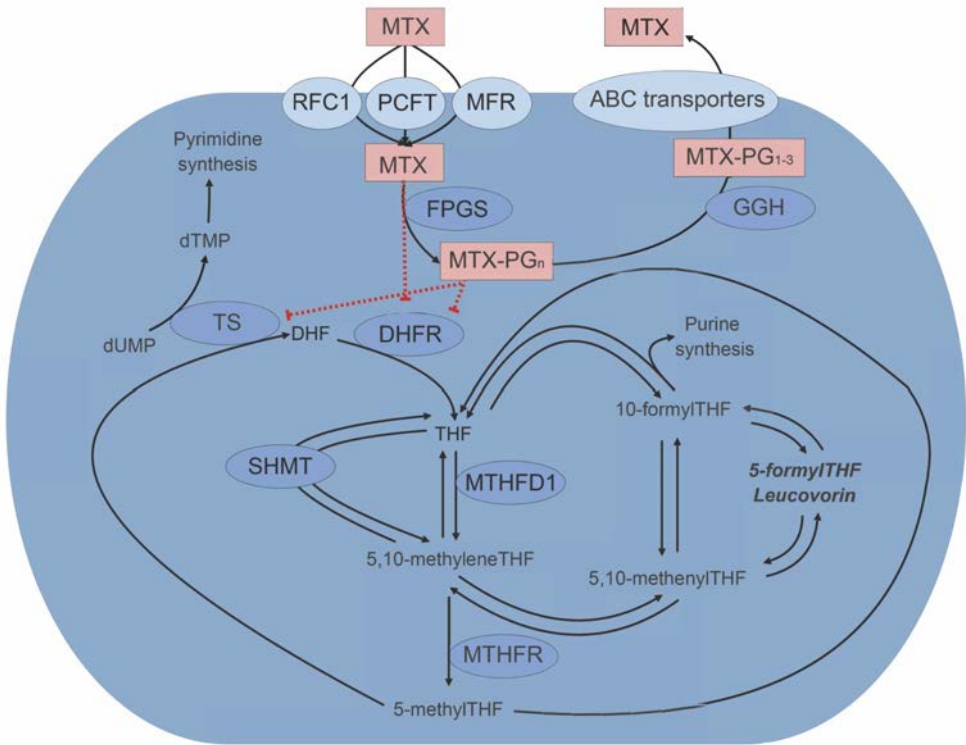
- with citrovorum factor or folic acid. *Cancer research* 1953;13:843-50
17. Goldin A, Venditti JM, Kline I, Mantel N. Eradication of leukaemic cells (L1210) by methotrexate and methotrexate plus citrovorum factor. *Nature* 1966;212:1548-50
 18. Berry CL, Germain J, Looker T. The effect of methotrexate on DNA synthesis and its reversal by folinic acid. *Journal of embryology and experimental morphology* 1972;28:601-5
 19. Sandberg JS, Goldin A. The use of leucovorin orally in normal and leukemic L1210 mice to prevent the toxicity and gastrointestinal lesions caused by high doses of methotrexate. *Cancer research* 1970;30:1276-80
 20. Fry DW, Anderson LA, Borst M, Goldman ID. Analysis of the role of membrane transport and polyglutamation of methotrexate in gut and the Ehrlich tumor *in vivo* as factors in drug sensitivity and selectivity. *Cancer research* 1983;43:1087-92
 21. Fabre I, Fabre G, Goldman ID. Polyglutamylation, an important element in methotrexate cytotoxicity and selectivity in tumor versus murine granulocytic progenitor cells *in vitro*. *Cancer research* 1984;44:3190-5
 22. Poser RG, Sirotiak FM, Chello PL. Differential synthesis of methotrexate polyglutamates in normal proliferative and neoplastic mouse tissues *in vivo*. *Cancer research* 1981;41:4441-6
 23. Koizumi S, Curt GA, Fine RL, Griffin JD, Chabner BA. Formation of methotrexate polyglutamates in purified myeloid precursor cells from normal human bone marrow. *The Journal of clinical investigation* 1985;75:1008-14
 24. Matherly LH, Barlowe CK, Goldman ID. Antifolate polyglutamylation and competitive drug displacement at dihydrofolate reductase as important elements in leucovorin rescue in L1210 cells. *Cancer research* 1986;46:588-93
 25. Rothenberg SP, Iqbal MP, da Costa M. Effect of folate compounds on the accumulation of methotrexate and the activity of dihydrofolate reductase in liver, kidney and small intestine of the mouse. *The Journal of pharmacology and experimental therapeutics* 1982;223:631-4
 26. Rots MG, Pieters R, Peters GJ, Noordhuis P, van Zantwijk CH, Kaspers GJ, et al. Role of folylpolyglutamate synthetase and folylpolyglutamate hydrolase in methotrexate accumulation and polyglutamylation in childhood leukemia. *Blood* 1999;93:1677-83
 27. Voskoglou-Nomikos T, Pater JL, Seymour L. Clinical predictive value of the *in vitro* cell line, human xenograft, and mouse allograft preclinical cancer models. *Clinical cancer research : an official journal of the American Association for Cancer Research* 2003;9:4227-39
 28. Johnson JI, Decker S, Zaharevitz D, Rubinstein LV, Venditti JM, Schepartz S, et al. Relationships between drug activity in NCI preclinical *in vitro* and *in vivo* models and early clinical trials. *British journal of cancer* 2001;84:1424-31
 29. Kretzschmar K, Clevers H. Organoids: Modeling Development and the Stem Cell Niche in a Dish. *Developmental cell* 2016;38:590-600
 30. Sato T, Vries RG, Snippert HJ, van de Wetering M, Barker N, Stange DE, et al. Single Lgr5 stem cells build crypt-villus structures *in vitro* without a mesenchymal niche. *Nature* 2009;459:262-5
 31. Barker N, Huch M, Kujala P, van de Wetering M, Snippert HJ, van Es JH, et al. Lgr5(+ve) stem cells drive self-renewal in the stomach and build long-lived gastric units *in vitro*. *Cell Stem Cell* 2010;6:25-36
 32. Tadokoro T, Wang Y, Barak LS, Bai Y, Randell SH, Hogan BL. IL-6/STAT3 promotes regeneration of airway ciliated cells from basal stem cells. *Proceedings of the National Academy of Sciences of the United States of America* 2014;111:E3641-9

33. Lee SH, Hu W, Matulay JT, Silva MV, Owczarek TB, Kim K, et al. Tumor Evolution and Drug Response in Patient-Derived Organoid Models of Bladder Cancer. *Cell* 2018;173:515-28 e17
34. Driehuis E KS, Spelier S, Lohmussaar K, Willems SM, Devriese LA, de Bree R, de Ruiter EJ, Korving J, Begthel H, van Es JH, Geurts V, He GW, van Jaarsveld RH, Oka R, Muraro MJ, Vivie J, Zandvliet MMJM, Hendrickx APA, Iakobachvili N, Stridevi P, Kranenburg O, van Boxtel R, Kops GJPL, Tuveson DA, Peters PJ, van Oudenaarden A, Clevers H. Oral mucosal organoids as a potential platform for personalized cancer therapy. *Cancer Discov* 2019
35. Kopper O, de Witte CJ, Lohmussaar K, Valle-Inclan JE, Hami N, Kester L, et al. An organoid platform for ovarian cancer captures intra- and interpatient heterogeneity. *Nat Med* 2019;25:838-49
36. DeWard AD, Cramer J, Lagasse E. Cellular heterogeneity in the mouse esophagus implicates the presence of a nonquiescent epithelial stem cell population. *Cell Rep* 2014;9:701-11
37. Huch M, Dorrell C, Boj SF, van Es JH, Li VS, van de Wetering M, et al. In vitro expansion of single Lgr5+ liver stem cells induced by Wnt-driven regeneration. *Nature* 2013;494:247-50
38. Karthaus WR, laquinta PJ, Drost J, Gracanin A, van Boxtel R, Wongvipat J, et al. Identification of multipotent luminal progenitor cells in human prostate organoid cultures. *Cell* 2014;159:163-75
39. Kessler M, Hoffmann K, Brinkmann V, Thieck O, Jackisch S, Toelle B, et al. The Notch and Wnt pathways regulate stemness and differentiation in human fallopian tube organoids. *Nature communications* 2015;6:8989
40. Linnemann JR, Miura H, Meixner LK, Irmeler M, Kloos UJ, Hirschi B, et al. Quantification of regenerative potential in primary human mammary epithelial cells. *Development* 2015;142:3239-51
41. Nanduri LS, Baanstra M, Faber H, Rocchi C, Zwart E, de Haan G, et al. Purification and ex vivo expansion of fully functional salivary gland stem cells. *Stem Cell Reports* 2014;3:957-64
42. Ren W, Lewandowski BC, Watson J, Aihara E, Iwatsuki K, Bachmanov AA, et al. Single Lgr5- or Lgr6-expressing taste stem/progenitor cells generate taste bud cells ex vivo. *Proceedings of the National Academy of Sciences of the United States of America* 2014;111:16401-6
43. Vlachogiannis G, Hedayat S, Vatsiou A, Jamin Y, Fernandez-Mateos J, Khan K, et al. Patient-derived organoids model treatment response of metastatic gastrointestinal cancers. *Science (New York, NY)* 2018;359:920-6
44. Sachs N, de Ligt J, Kopper O, Gogola E, Bounova G, Weeber F, et al. A Living Biobank of Breast Cancer Organoids Captures Disease Heterogeneity. *Cell* 2018;172:373-86 e10
45. Berkers G, van Mourik P, Vonk AM, Kruijselbrink E, Dekkers JF, de Winter-de Groot KM, et al. Rectal Organoids Enable Personalized Treatment of Cystic Fibrosis. *Cell Rep* 2019;26:1701-8 e3
46. Dekkers JF WC, de Jonge HR, Bronsveld I, Janssens HM, de Winter-de Groot KM, Brandsma AM, de Jong NW, Bijvelds MJ, Scholte BJ, Nieuwenhuis EE, van den Brink S, Clevers H, van der Ent CK, Middendorp S, Beekman JM. A functional CFTR assay using primary cystic fibrosis intestinal organoids. *Nat Med* 2013;19:939-45
47. van der Laan BF JG, Kathmann GA, Westerhof GR, Schornagel JH, Hordijk GJ. In vitro activity of novel antifolates against human squamous carcinoma cell lines of the head and neck with inherent resistance to methotrexate. *Int J Cancer* 1992;51:909-14
48. Jansen G, Mauritz R, Drori S, Sprecher H, Kathmann I, Bunni M, et al. A structurally altered human reduced folate carrier with increased folic acid

- transport mediates a novel mechanism of antifolate resistance. *J Biol Chem* 1998;273:30189-98
49. den Hoed MA, Lopez-Lopez E, te Winkel ML, Tissing W, de Rooij JD, Gutierrez-Camino A, et al. Genetic and metabolic determinants of methotrexate-induced mucositis in pediatric acute lymphoblastic leukemia. *The pharmacogenomics journal* 2015;15:248-54
 50. Galpin AJ, Schuetz JD, Masson E, Yanishevski Y, Synold TW, Barredo JC, et al. Differences in folylpolyglutamate synthetase and dihydrofolate reductase expression in human B-lineage versus T-lineage leukemic lymphoblasts: mechanisms for lineage differences in methotrexate polyglutamylolation and cytotoxicity. *Molecular pharmacology* 1997;52:155-63
 51. Pauley JL, Panetta JC, Crews KR, Pei D, Cheng C, McCormick J, et al. Between-course targeting of methotrexate exposure using pharmacokinetically guided dosage adjustments. *Cancer chemotherapy and pharmacology* 2013;72:369-78
 52. Rots MG, Pieters R, Kaspers GJ, van Zantwijk CH, Noordhuis P, Mauritz R, et al. Differential methotrexate resistance in childhood T- versus common/preB-acute lymphoblastic leukemia can be measured by an *in situ* thymidylate synthase inhibition assay, but not by the MTT assay. *Blood* 1999;93:1067-74
 53. Barredo J, Moran RG. Determinants of antifolate cytotoxicity: folylpolyglutamate synthetase activity during cellular proliferation and development. *Molecular pharmacology* 1992;42:687-94
 54. Muller IB LM, Struys EA, Heydari P, Hebing RCF, Nurmohamed MT, van der Laken C, Lems WF, Cloos J, Jansen G, de Jonge R. Development and validation of a sensitive UHPLC-MS/MS-based method for the analysis of folylpolyglutamate synthetase enzymatic activity in peripheral blood mononuclear cells as application in rheumatoid arthritis and leukemia patients. *Ther Drug Monit* 2019
 55. Sonis ST. Regimen-related gastrointestinal toxicities in cancer patients. *Current opinion in supportive and palliative care* 2010;4:26-30
 56. Blutt SE, Crawford SE, Ramani S, Zou WY, Estes MK. Engineered Human Gastrointestinal Cultures to Study the Microbiome and Infectious Diseases. *Cellular and molecular gastroenterology and hepatology* 2018;5:241-51
 57. Noel G, Baetz NW, Staab JF, Donowitz M, Kovbasnjuk O, Pasetti MF, et al. A primary human macrophage-enteroid co-culture model to investigate mucosal gut physiology and host-pathogen interactions. *Scientific reports* 2017;7:45270
 58. den Boer E, Meesters RJ, van Zelst BD, Luijckermans TM, Hazes JM, Heil SG, et al. Measuring methotrexate polyglutamates in red blood cells: a new LC-MS/MS-based method. *Analytical and bioanalytical chemistry* 2013;405:1673-81



SUPPLEMENTARY DATA



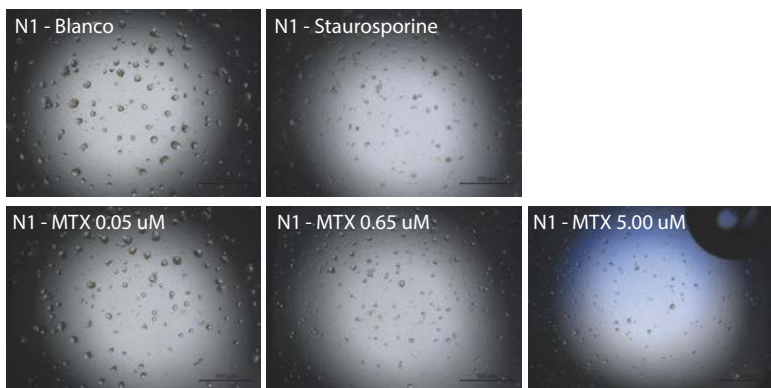
4

Figure S1. Mechanism of action of MTX treatment. Leucovorin (5-formylTHF) is represented in bold/italic. MTX enters the cell mainly through the Reduced Folate Carrier 1 (RFC1), Proton Coupled Folate Transporter (PCFT), Membrane Folate Transporters (MFR) or by passive diffusion through the cell membrane. While circulating, MTX contains one polyglutamate group (MTX-PG₁). Once inside the cell, MTX is polyglutamated by Folylpolyglutamate Synthetase (FPGS) with up to seven polyglutamate groups. Long-chain MTX-PG's (MTX-PG_{4,7}) can not be transported out of the cell before de-polyglutamation by Gamma-Glutamyl Hydrolase (GGH). Short-chain MTX-PG's (MTX-PG_{1,3}) will be actively transported out of the cell by ABCC1-4, ABCB1 and ABCG2 transporters. MTX is cytotoxic as it impairs purine- and pyrimidine synthesis by inhibiting the enzymes Dihydrofolate Reductase (DHFR) and Thymidylate Synthase (TYMS). Abbreviations: ABCB1 - ATP Binding Cassette Subfamily B Member 1; ABCC1-4 - ATP Binding Cassette Subfamily C Member 1 - 4; ABCG2 - ATP Binding Cassette Subfamily G Member 2; DHFR - Dihydrofolate Reductase; FPGS - Folylpolyglutamate Synthetase; GGH - Gamma-Glutamyl Hydrolase; MFR - Membrane Folate Transporter; MTHFR - Methylene tetrahydrofolate reductase; MTHFD1 - Methylene tetrahydrofolate Dehydrogenase, Cyclohydrolase And Formyltetrahydrofolate Synthetase 1; PCFT - Proton-Coupled Folate Transporter; RFC1 - Reduced Folate Carrier; SHMT - Serine hydroxymethyltransferase; TS - Thmidylate Synthase. Created with Biorender.com©.

A

		MTX range concentrations: 5.00 μ M to triplicate																											
		2	3	4	5	6	7	8	9	10	11	12	13	14	15	16	17	18	19	20	21	22	23	24					
K	Block 1	5.00	2.99	1.79	1.06	0.64	0.39	0.22	0.13	0.08	0.05	Stauroporine	5.00	2.99	1.79	1.06	0.64	0.39	0.22	0.13	0.08	0.05	Block 5						
L	MTX only	5.00	2.99	1.79	1.06	0.64	0.39	0.22	0.13	0.08	0.05		5.00	2.99	1.79	1.06	0.64	0.39	0.22	0.13	0.08	0.05	+ LV T48h						
M		5.00	2.99	1.79	1.06	0.64	0.39	0.22	0.13	0.08	0.05		5.00	2.99	1.79	1.06	0.64	0.39	0.22	0.13	0.08	0.05							
N	Block 2	5.00	2.99	1.79	1.06	0.64	0.39	0.22	0.13	0.08	0.05	Blanco	5.00	2.99	1.79	1.06	0.64	0.39	0.22	0.13	0.08	0.05	Block 6						
O	+ LV T0h	5.00	2.99	1.79	1.06	0.64	0.39	0.22	0.13	0.08	0.05		5.00	2.99	1.79	1.06	0.64	0.39	0.22	0.13	0.08	0.05	+ LV T72h						
P		5.00	2.99	1.79	1.06	0.64	0.39	0.22	0.13	0.08	0.05		5.00	2.99	1.79	1.06	0.64	0.39	0.22	0.13	0.08	0.05							
Q	Block 3	5.00	2.99	1.79	1.06	0.64	0.39	0.22	0.13	0.08	0.05		5.00	2.99	1.79	1.06	0.64	0.39	0.22	0.13	0.08	0.05	Block 7						
R	+ LV T12h	5.00	2.99	1.79	1.06	0.64	0.39	0.22	0.13	0.08	0.05		5.00	2.99	1.79	1.06	0.64	0.39	0.22	0.13	0.08	0.05	+ LV T96h						
S		5.00	2.99	1.79	1.06	0.64	0.39	0.22	0.13	0.08	0.05		5.00	2.99	1.79	1.06	0.64	0.39	0.22	0.13	0.08	0.05							
T	Block 4	5.00	2.99	1.79	1.06	0.64	0.39	0.22	0.13	0.08	0.05		5.00	2.99	1.79	1.06	0.64	0.39	0.22	0.13	0.08	0.05							
U	+ LV T24h	5.00	2.99	1.79	1.06	0.64	0.39	0.22	0.13	0.08	0.05		5.00	2.99	1.79	1.06	0.64	0.39	0.22	0.13	0.08	0.05							
V		5.00	2.99	1.79	1.06	0.64	0.39	0.22	0.13	0.08	0.05		5.00	2.99	1.79	1.06	0.64	0.39	0.22	0.13	0.08	0.05							
W		5.00	2.99	1.79	1.06	0.64	0.39	0.22	0.13	0.08	0.05		5.00	2.99	1.79	1.06	0.64	0.39	0.22	0.13	0.08	0.05							
X		5.00	2.99	1.79	1.06	0.64	0.39	0.22	0.13	0.08	0.05		5.00	2.99	1.79	1.06	0.64	0.39	0.22	0.13	0.08	0.05							
Y		5.00	2.99	1.79	1.06	0.64	0.39	0.22	0.13	0.08	0.05		5.00	2.99	1.79	1.06	0.64	0.39	0.22	0.13	0.08	0.05							
Z		5.00	2.99	1.79	1.06	0.64	0.39	0.22	0.13	0.08	0.05		5.00	2.99	1.79	1.06	0.64	0.39	0.22	0.13	0.08	0.05							

B



C

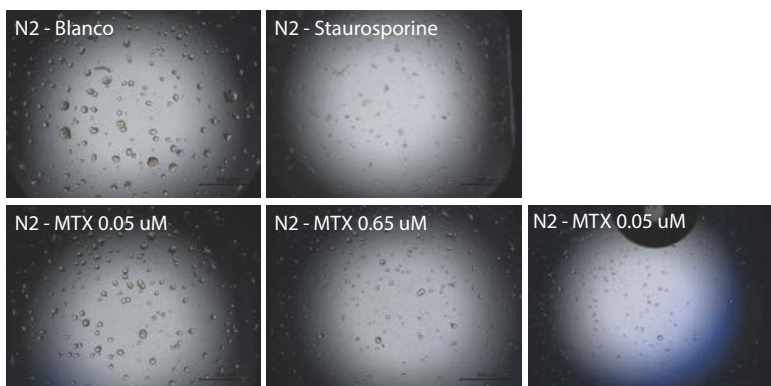


Figure S3. Technical details of drugscreen performed in this study. A. Schematic layout of a drug screen plate as used in this study. The gradient of MTX is depicted using a color gradient (red indicates high concentration, green indicates low concentration). Here, the MTX concentrations used for organoids are depicted. Each concentration is tested in technical triplicate. Different blocks receive LV rescue at different timepoints after the start of MTX treatment, as indicated. Staurosporine treated wells are used as positive controls and are set to 0% viability, wells only receiving drug solvent are used is negative controls, and are set to 100% viability. B. Brighfield microscopy images showing the morphology of N1 organoids in drug screening plates on the day of readout. C. Brighfield microscopy images showing the morphology of N2 organoids in drug screening plates on the day of readout.

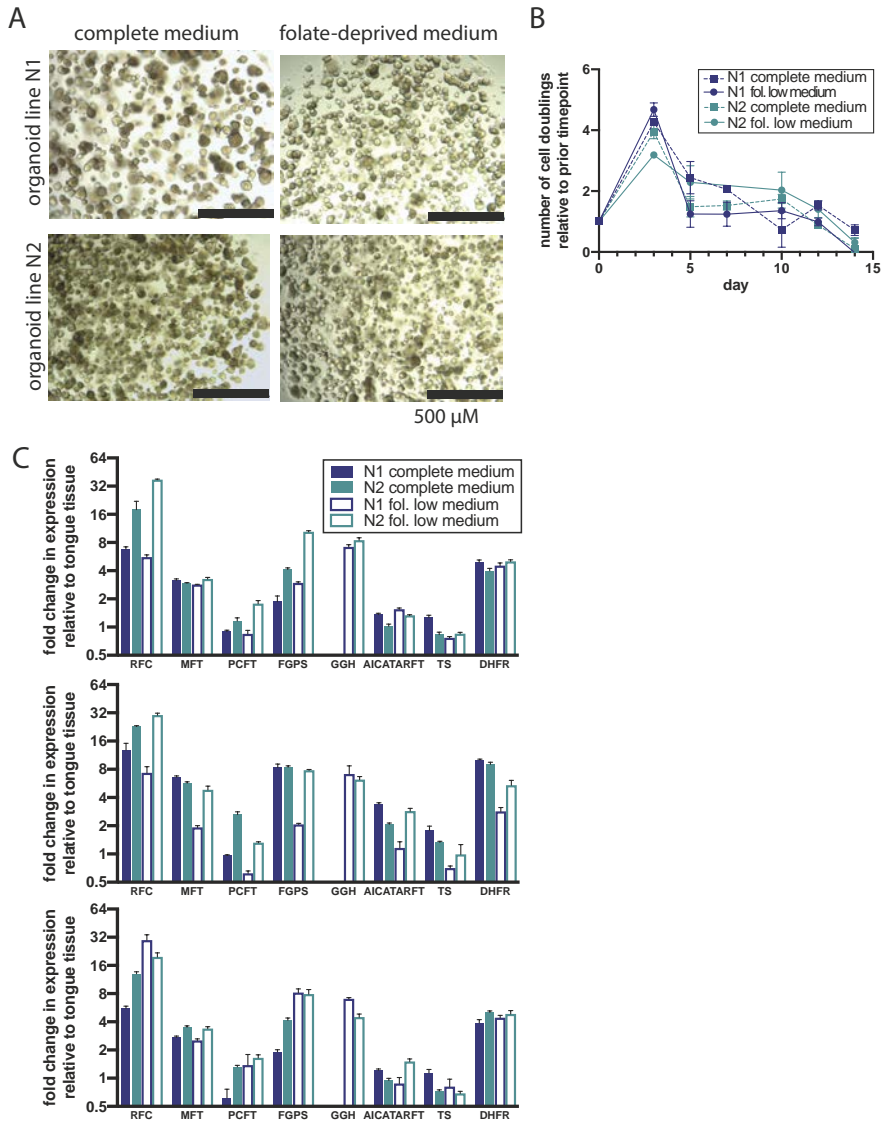


Figure S2. Organoid cultures retain their morphology and growth speed when grown in folate deprived medium. A. Brightfield microscopy images of organoid line N1 and N2, grown in either complete medium, or folate deprived medium. Scalebar, 500 μ m. Growth speed of organoid cultures in both media. Growth was assessed by collection of cell pellets at day 0, 3, 5, 7, 10 and 14. Cell number was assessed by cell titer glow and values were made relative to day 0. C. Quantitative PCR assessing expression of genes relevant for methotrexate metabolism. Experiment was performed in triplicate, results of all three experiments are shown here.

Table S1. Clinical information of patients. Relevant clinical information is given on the patient that participated in this study, and from whose tissue organoids were derived.

name	gender	age at diagnosis	tumor location
N1	male	80	parotis SCC
N2	female	70	gingiva
N3	male	68	larynx
N4	male	65	salivary gland SCC
N5	female	60	oral cavity



Table S2. Comparison of mutations detected by WES in matching normal and tumor organoid lines. All mutation detected in organoid line N1, T1, N2 and T2 are shown. Here, normal tissue was used as a reference.

Table S2. can be found at: http://tiny.cc/Supp_ElseDriehuis

Table S3. Z-scores of drugscreens performed in this study.

Organoid line / Leukemia cell line	Z-scores			
N1	0.6465	0.7194	0.4499	0.3539
N1 - PT	0.4956	0.6276	0.3304	0.8192
N2	0.3644	0.8923	0.8424	0.4888
N2 - PT	0.5608	0.7385	0.7172	0.5921
N3	0.7360			
N3 - PT	0.9172			
N4	0.6484			
N4 - PT	0.6074			
N5	0.9296			
N5 - PT	0.4788			
Jurkat	0.9285	0.8396	0.8985	
Jurkat - PT	0.9782	0.9413	0.9545	
NALM6	0.8172	0.7597	0.5932	
NALM6 - PT	0.8708	0.9015	0.6629	
REH	0.9743	0.7067	0.8949	
REH - PT	0.8998	0.8019	0.6656	
HSB2	0.9202	0.9193	0.8629	
HSB2 - PT	0.9312	0.8975	0.8973	
MOLT16	0.8955	0.9439	0.7531	
MOLT16 - PT	0.9415	0.8294	0.6990	
Median	0.8182			
Minimum	0.3304			
Maximum	0.9782			

Table S4. Sequences of primers used for quantitative PCR. 5' to 3' sequences of primers used to assess gene expression by quantitative PCR in this study.

primer name	primer sequence	length of product
PCFT RT F	5'-CACTCTACCCAGCCACTCTGAAC-3'	127 bp
PCFT RT R	5'-GATCAGCCTTTTCCAGCATCC-3'	
RFC F	5'-ACCATCATCACTTTCATTGTCTC-3'	97 bp
RFC R	5'-ATGGACAGGATCAGGAAGTACA-3'	
MFT F	5'-GCCGTGAGTGATGGATTGGAA-3'	102 bp
MFT R	5'-TCCTTGATAAAGTCCCCGTAGT-3'	
DHFR F	5'-ATGCCTTAAACTTACTGAACAACCA-3'	81 bp
DHFR R	5'-TGGGTGATTCATGGCTTCCT-3'	
TS F	5'-TCCCGAGACTTTTTGGACAGC-3'	166 bp
TS R	5'-TGATGGTGTCAATCACTCTTTGC-3'	
AICARTF F	5'-ACCTGACCGCTTTGGTTTG-3'	171 bp
AICARTF R	5'-TACGAGCTAGGATTCCAGCAT-3'	
FPGS F	5'-CCGAGCATGGAGTACCAGGA-3'	80 bp
FPGS R	5'-GCGCTTACCTGCTCCAG-3'	
GGH F	5'-GCGAGAGTTGTACCAGTAAGGC-3'	118 bp
GGH R	5'-CATAATCTGAGCGTCTGAGGTC-3'	



CHAPTER

**PANCREATIC CANCER
ORGANOIDS RECAPITULATE
DISEASE AND
ALLOW PERSONALIZED
DRUG SCREENING**

5



ABSTRACT

We report derivation of 30 Patient-Derived Organoid lines (PDOs) from tumors arising in the pancreas and distal bile duct. PDOs recapitulate tumor histology and contain genetic alterations that are typical for pancreatic cancer. *In vitro* testing of a panel of 76 therapeutic agents revealed sensitivities currently not exploited in the clinic and underscores the importance of personalized approaches for effective cancer treatment. The PRMT5 inhibitor EZP015556, shown to target *MTAP* (a gene commonly lost in pancreatic cancer) negative tumors, was validated as such, but also appeared to constitute an effective therapy for a subset of *MTAP* positive tumors. Taken together, the work presented here provides a platform to identify novel therapeutics to target pancreatic tumor cells using PDOs.



Statement of significance

This manuscript describes a biobank of patient-derived pancreatic cancer organoids, which are characterized by whole genome DNA sequencing, RNA sequencing and histology. The organoid biobank will be made publicly available and can therefore serve as a resource for others. Pancreatic cancer organoids have been described before. However, here we expose organoids to extensive drug screens to reveal unique drug sensitivity profiles for individual organoid lines. These findings underscore the importance of personalized approaches when using targeted agents to treat cancer in the clinic.

Else Driehuis¹, Arne Hoeck², Sigrid Kolders¹, Hayley E. Francies³,
M. Can Gulersonmez⁴, Edwin C.A. Stigter⁴, Boudewijn Burgering⁴, Veerle Geurts¹, Ana
Granacin⁵, Folkert H. Morsink⁶, Rob Vries⁵, Sylvia Boj⁵, Johan van Es¹,
G. Johan A. Offerhaus⁶, Onno Kranenburg⁷, Mathew J. Garnett³, Edwin Cuppen²,
Lodewijk A.A. Brosens⁶, Hans Clevers^{*1,8}

¹ Oncode Institute, Hubrecht Institute, Royal Netherlands Academy of Arts and Sciences (KNAW) and University Medical Center Utrecht, The Netherlands

² Center for Molecular Medicine and Oncode Institute, University Medical Center Utrecht

³ Wellcome Trust Sanger Institute, Hinxton, United Kingdom

⁴ Department of Molecular Cancer Research, Center Molecular Medicine, Oncode Institute, University Medical Center Utrecht, Utrecht, The Netherlands

⁵ Hubrecht Organoid Technology (HUB), Utrecht, The Netherlands

⁶ Department of Pathology, University Medical Center Utrecht, The Netherlands

⁷ Utrecht Platform for Organoid Technology (U-PORT), Utrecht Medical Center Utrecht, The Netherlands

⁸ Princess Maxima Center, Utrecht, The Netherlands

* corresponding author

INTRODUCTION

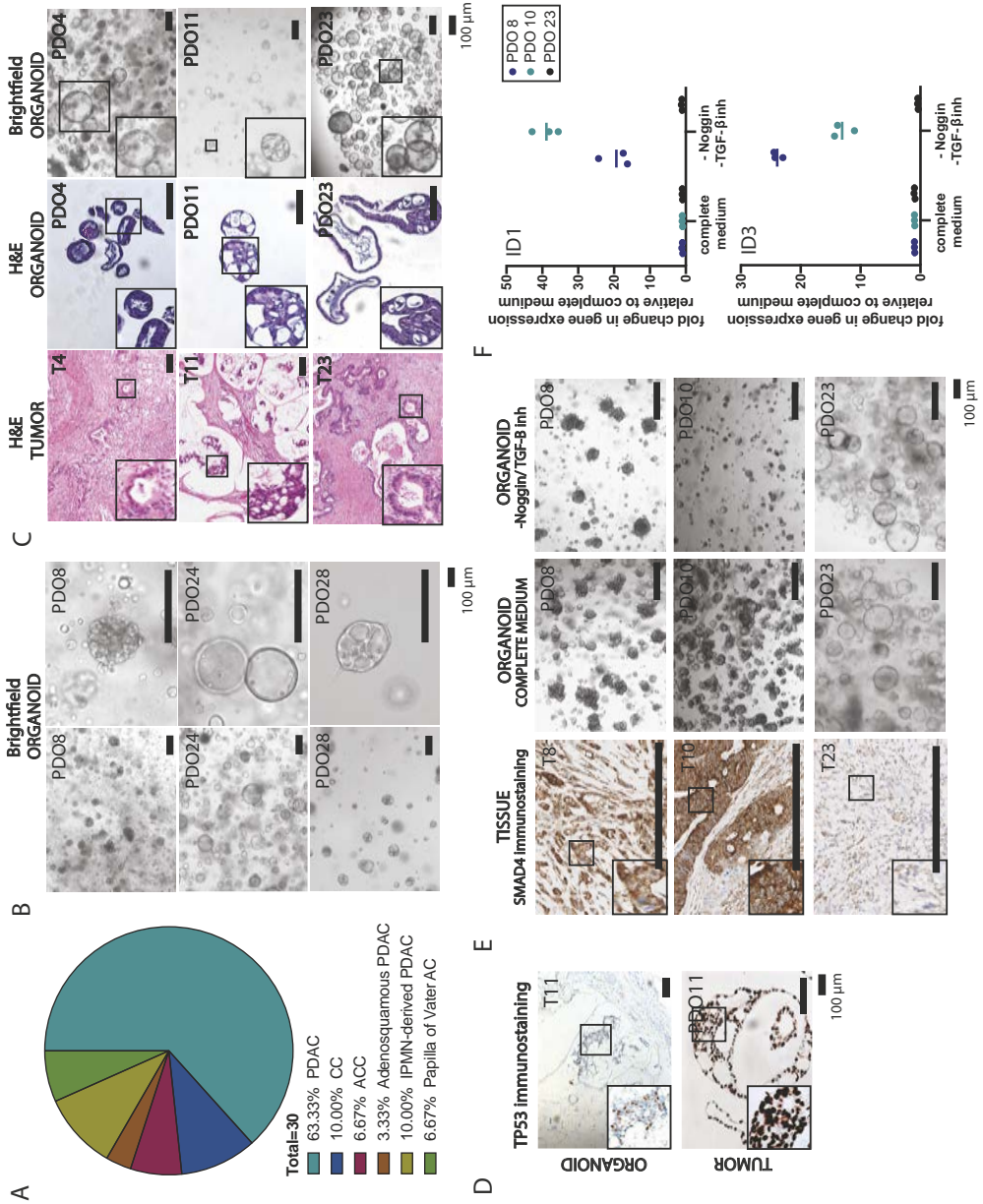
Pancreatic ductal adenocarcinoma (PDAC) accounts for over 7% of all cancer deaths. With an overall survival rate of only 8.5%, it is one of the deadliest forms of cancer, where treatment options are limited (1). Additionally, distal cholangiocarcinomas (dCC), originating from the distal bile duct at the site where it passes through the pancreas, has recently been suggested to be molecularly more similar to pancreatic tumors than to those of the liver (2).

Currently, PDAC is treated with Gemcitabine/nab-Paclitaxel or FOLFIRINOX (5-Fluorouracil, Leucovorin, Irinotecan, Oxaliplatin), combined with surgery when possible (3,4). Despite these interventions, response rates remain poor, with overall survival rates of 6-11 months for patients ineligible for surgery (3,4). As alterations in therapeutically targetable molecular pathways are known to contribute to disease pathogenesis (5–8), agents targeting these pathways hold promise to improve treatment. However, variable responses to these therapeutics are expected, and biomarkers to predict response are lacking. Tools to identify the most effective chemotherapeutic regimens for individual patients, as well as models to develop additional drug treatment strategies, are urgently needed.

Organoid technology allows for the establishment of patient-derived cultures with much higher efficiency than classical 2D cell lines (9). This has resulted in the establishment of a range of tumor-derived organoid biobanks that recapitulate tumor characteristics and can be used to address basic and translational research questions (5,6,10–15). We and others have previously reported the establishment of patient-derived organoids (PDOs) derived from PDAC (5,6,16). Using slightly different protocols, these studies show that PDOs can be established from PDACs with a success rate of 70-73%. Here, we report an additional pancreas tumor biobank and show the feasibility of this model for personalized drug screening. Organoids derived from several non-PDAC tumor types were also included, such as pancreatic acinar cell carcinoma and distal cholangiocarcinoma. Organoids were established from tumor-adjacent normal epithelium when available, allowing for the direct comparison of normal and tumor cells from the same patient.

Patient-derived organoids can be established from different pancreas tumor types and recapitulate the tissue of the original tumor

Biopsies or surgical resections were obtained and digested as previously described (16). Tumor cells were subsequently grown in two types of media, defined here as tumor medium 1 (TM1) and tumor medium 2 (TM2). TM1 contains all components of complete pancreatic medium (CM) except EGF and PGE2, whereas TM2 lacks PGE2, WNT and TGF- β inhibitor A83-01. After initial tumor digestion and plating in extracellular matrix, samples were cultured in both media. If organoids grew out on both media, both cultures were maintained in parallel and compared later on. In total, over the course of three years, 83 tumor samples were received, of which 52 grew out in at least one of



the two used tumor media, resulting in an outgrowth efficiency of 62%. Of these 52 PDOs, 31 were analyzed by whole genome sequencing (WGS), and are described in this study (Figure 1A, Supplementary Table 1). Available organoids are catalogued by Hubrecht Organoid Technology (www.hub4organoids.eu) and can be requested using their assigned HUB codes. With the exception of PDO 30 and 31, which were established from biopsies, all other PDOs were established from surgical resections. Outgrowth efficiency of organoids from biopsies was 31%. For 12 of the 31 established PDOs, tumor samples grew out on both TM1 and TM2 (See Table S1 for information on which sample could be established on which TM). Sato et al. described that the dependence of WNT signaling in PDOs correlates with a basal tumor subtype characterized by GATA6-dependent gene expression (5). In line with these findings, we observed an inverse correlation between GATA6 expression and WNT dependency in PDOs (Figure S1A). This suggests that medium composition may have a selective impact on PDO outgrowth. In cases where tumor material grew out on both media, no difference in GATA6 expression profile was observed between the two lines, indicating that media itself does not directly affect GATA6 expression. This is also shown by the gene expression heatmap where most of the pairs cluster together indicating similarities in gene expression levels (Figure S1B). When available, corresponding tumor-adjacent normal tissue was processed to establish wildtype organoids. We successfully established these matched normal control organoids for 5 patients, corresponding to 7 of the established tumor organoid lines (as in some cases, organoids could be established on both TM1 and TM2). Morphology of tumor organoids differed from cystic (with either a clear or filled lumen) to dense structures (Figure 1B). Comparison of Hematoxylin and

-
- ◀ **Figure 1. Patient-derived organoids can be established from different pancreas tumor types and recapitulate the tissue of the original tumor.** A. Pie-chart depicting the characteristics of the tumor biobank described in this work. PDAD: pancreatic ductal adenocarcinoma; ACC: acinar cell carcinoma; CC: cholangiocarcinoma; IPMN: intraductal papillary mucinous neoplasm. B. Brightfield images of 3 PDO cultures. C. H&E staining performed on tumor tissue and corresponding organoids, of which brightfield images were taken to show organoid morphology in culture. D. Immunohistochemical staining for TP53, performed on tumor tissue and corresponding organoids of patient 11. TP53 staining is consistent with *TP53* mutation status of the tumor and organoids, and corresponds between tumor tissue and organoids. E. IHC for *SMAD4* in tumor tissue and brightfield images of corresponding organoid lines, either grown in complete medium or medium lacking A83-01 and Noggin. Absence of *SMAD4* staining (suggestive of *SMAD4* mutation) was observed in PDO 23, but not PDO 8 and PDO 10. *SMAD4* mutant cells can be functionally selected in organoid cultures by removing TGF- β inhibitors A83-01 and Noggin. This medium induced differentiation in *SMAD4* wildtype PDO 8 and PDO 10, as judged by the change in morphology and loss of the culture over time. *SMAD4* mutant PDO 23 was unaffected by this medium change. F. quantitative PCR for BMP target genes ID1 and ID3. Induction of BMP signaling by the removal of Noggin and A83-01 and the addition of BMP resulted in upregulation of ID1 and ID3 in *SMAD* wildtype PDO 8 and PDO 10, but not in *SMAD* mutant PDO 23. Expression is shown relative to organoids grown in complete medium. This experiment was performed in technical triplicate.
-

Eosin (H&E) staining of PDOs and corresponding tumor tissue showed morphological similarities between PDOs and tumor tissue (Figure 1C).

Organoid culture media composition functionally selects for oncogenic mutations in PDOs

TP53 status of a subset of PDOs and corresponding tumor tissue was determined using immunohistochemistry. Accumulation of mutant *TP53* protein can occur due to conformational changes that result in increased protein half-life (17). Therefore, *TP53* immunohistochemical staining (IHC) is used as a clinical parameter to determine *TP53* mutation status (18). *TP53* IHC staining in organoids correlated with the corresponding tumor tissue results (Figure 1D, where tissue is indicated by 'T' and organoid by 'PDO'). Loss of *SMAD4* is commonly observed in pancreatic tumors (19). Using IHC, the *SMAD4* status of a subset of tumors was assessed. Tumors 8 and 10 stained positive for this marker, indicative of wildtype protein, whereas tumor 23 showed loss of *SMAD4* expression (Figure 1E). In organoids, positive *SMAD4* IHC was never observed. This can potentially be explained by inhibition of BMP/TGF- β signaling, due to the presence of Noggin and A83-01 in the culture medium. Upon further analysis, we did find that loss of *SMAD4* function could be detected in culture, although not by IHC. Withdrawal of A83-01 and Noggin from the media resulted in upregulation of the TGF- β target genes *ID1* and *ID3* in *SMAD4* wildtype PDO 8 and PDO 10 cells and resulted in cessation of growth after two weeks in culture. In contrast, *SMAD4*-mutant PDO 23 was left unaffected by Noggin/A83-01 withdrawal and did not show upregulation of TGF- β target genes (Figure 1E and 1F). Thus, despite the absence of *SMAD4* staining by IHC on organoids, we conclude that the molecular differences between *SMAD4* wildtype and mutant organoid lines were retained in culture. Below, we molecularly confirm that *SMAD4* mutation status of the PDOs indeed fits with their behavior upon Noggin/A83-01 withdrawal. This finding highlights how culture conditions can alter cell behavior, and underscores that these conditions should be considered carefully depending on the application.

We conclude that PDOs retain morphological characteristics of the tissue of origin. Organoids can be manipulated in culture by pharmacological inhibition or removal/addition of certain growth factors to select for cells with tumor-specific genetic alterations. This holds potential to avoid contaminating wildtype cells overgrowing the cultures, a notorious problem when establishing tumor-derived organoids.

Anecdotal expansion of pre-cancerous cells found in 'healthy' pancreas

The selection pressure created by the addition or removal of growth factors allows for enrichment for rare tumor-like cells that can be present in normal pancreas. As an example, organoids derived from normal pancreatic tissue from a patient with pancreatic metastasis of ovarian cancer were established and could be cultured for at least 15

passages on TM1, lacking EGF. This suggested that these cells were independent of EGF ligand for downstream EGFR signaling. Indeed, these organoids were found to carry an activating G12R KRAS mutation, suggesting a (pre-)neoplastic lesion in the pancreas of this individual (Figure S2A). As this mutation was not present in both the ovarian carcinoma tumor tissue and organoids derived thereof, the organoid line was most likely established from a pancreas-derived neoplastic clone such as pancreatic intraepithelial neoplasia (or PanIN), a precursor of PDAC. The established organoid line did respond to Nutlin-3 treatment, indicative of *TP53* wildtype status (Figure S2B). Indeed, this pre-cancerous lesion was detected by pathological assessment of the biopsy (Figure S2C), highlighting the strength of organoid cultures and artificial selection pressures created by the medium to detect and expand rare (pro)tumorigenic cells.

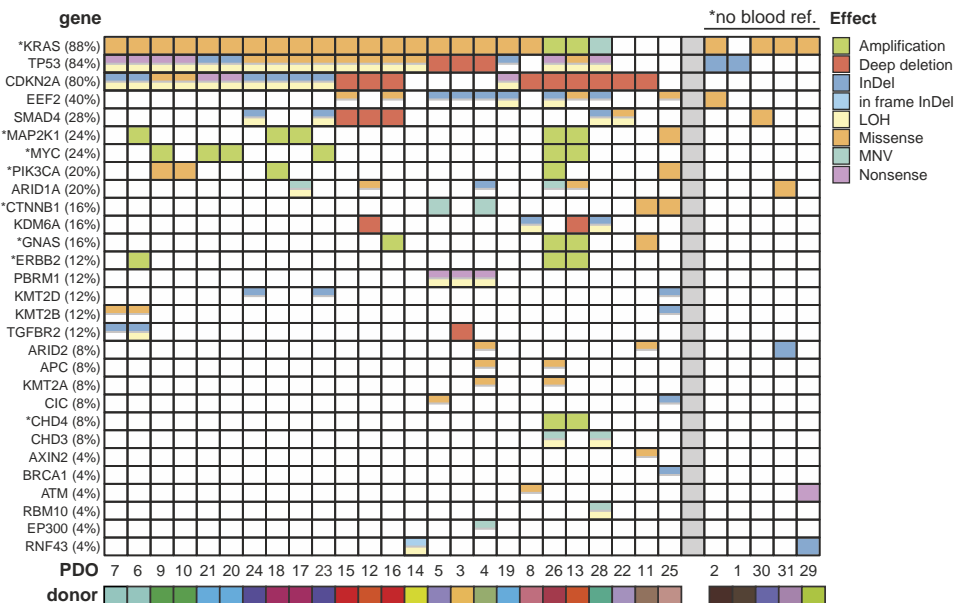
PDOs contain genetic alterations typical for tumor types of which they are derived

31 PDOs were analyzed by WGS. For 26 PDOs, matching germline DNA was available, allowing accurate detection of somatic events. PDO 27 was represented by a low number of mutations and displayed a stable karyotype. As additionally, no oncogenic mutations were detected in this PDO, we assumed that it was derived from wildtype cells present in the primary biopsy and excluded this sample from further analysis. Oncogenic events (protein altering point mutations, indels, amplifications and deep deletions) were characterized in 202 genes previously found to be associated with pancreatic cancer (5–8) (Figure 2A, Table S2). The 5 PDOs for which no germline DNA was available were functionally annotated with COSMIC. The most commonly altered gene *KRAS* was mutated in 22 of the 25 lines (88%), of which 30% were p.G12D, 23% p.G12V, 13% p.G12R, 13% p.Q61H and 6% p.G13D. In the three PDOs without *KRAS* mutation, we detected a p.V600E mutation in *BRAF* in PDO 11 and 25, and a p.G12D *NRAS* mutation in PDO 22. *TP53* was mutated or lost in 84% (21/25) of PDOs. Loss of *CDKN2A* was detected in 80% of the lines (20/25). Other commonly found genetic alterations included loss of *SMAD4*, *EEF2A* mutations, *MYC* amplifications, activating mutations in *PIK3CA*, and *ARID1A* inactivation.

Organoids derived from non-PDAC tumor included PDO 1, 2, 22 and 26. PDO 1, derived from a squamous adenocarcinoma was the only PDO carrying mutations in only one gene (*TP53*) in the panel of genes analyzed. PDO 22, derived from an acinar cell carcinoma, was found to be mutated in *CDKN2A* and *SMAD4*. Lastly, cholangiocarcinoma-derived PDO 2 and PDO 16 also carry mutations in PDAC driver genes, including *TP53*, *CDKN2A*, *EEF2*, *SMAD4*, *GNAS* and *KRAS*.

Next, we compared the genetic landscape of PDOs derived from the same patient in the different media culture conditions. All 8 PDO paired sets showed three to five shared nonsynonymous mutations in cancer genes, which likely reflect the clonal driver events. However, every PDO set also harbored unique genomic events in cancer genes including substantial nonsynonymous mutations in PDO 3, 4 and 5, variation on structural

A



B

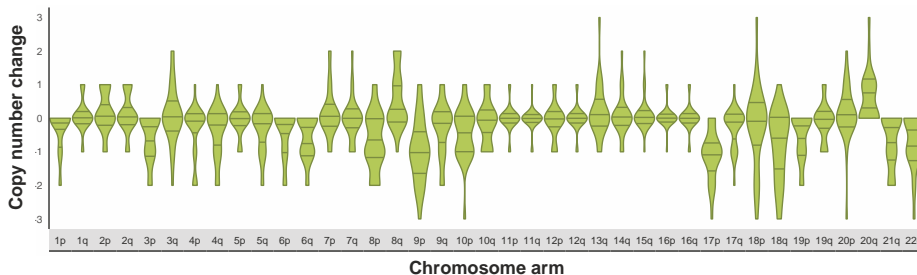
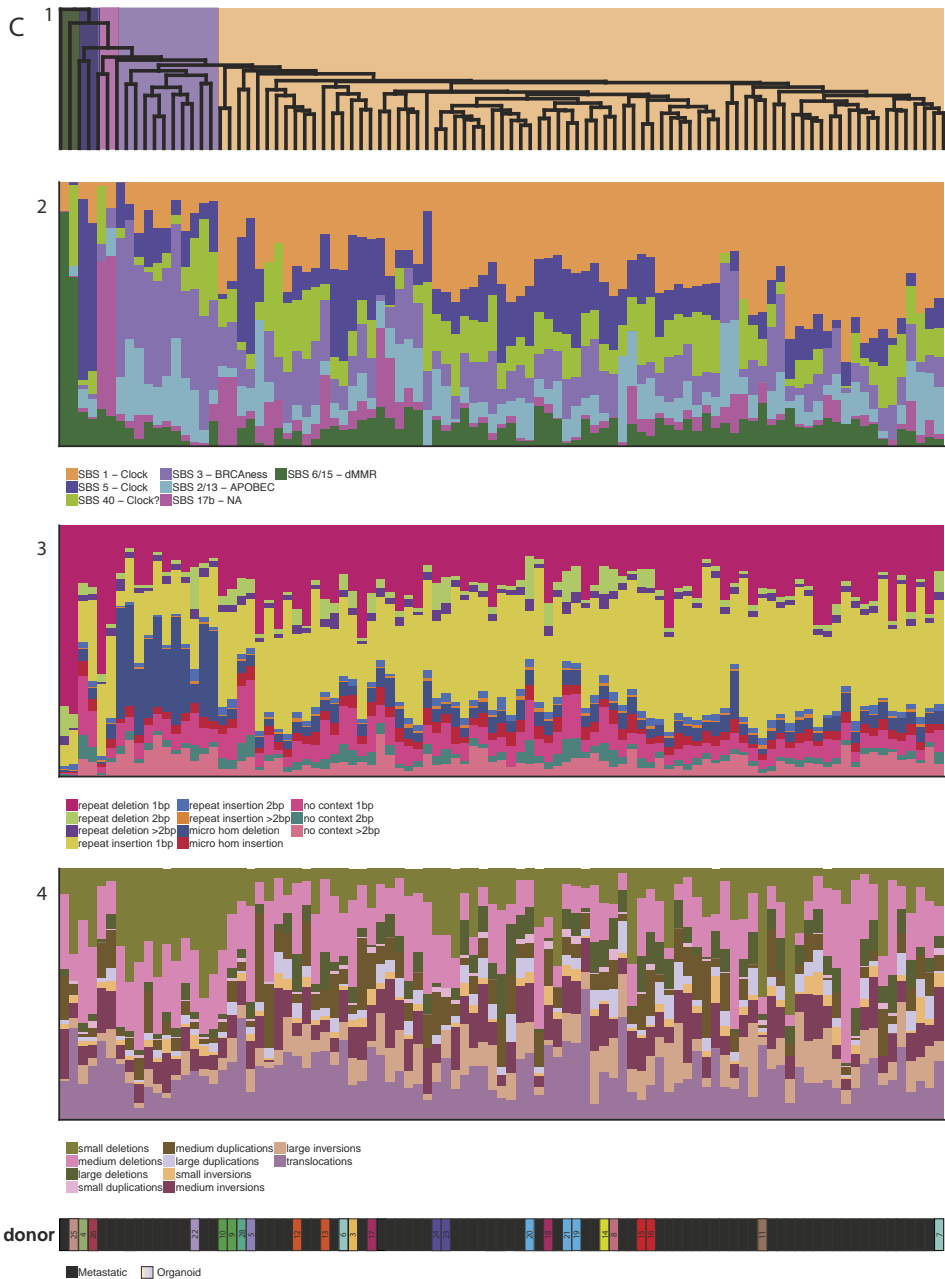


Figure 2. Genomic landscape of pancreatic PDOs recapitulates genetic alterations commonly found in this tumor type. A. Overview of severe somatic events detected in PDOs in genes commonly altered in PDAC. Here, a panel of 220 oncogenic driver genes (marked with an asterisk) and suppressor genes was analyzed for genetic alterations. Different mutation types are depicted with different colors. Five samples lacked a reference DNA, marked with “*no blood ref.,” and pathogenic mutations for these samples were called based on the COSMIC database. Mutation frequency per gene is depicted on the left and is calculated without inclusion of tumor-only samples. In some cases, multiple organoid lines were established from tissue obtained from one patient. Color coding at the bottom of the figure depicts if organoid lines are derived from the same patient. B. Volcano plots showing the common losses and gains of chromosome arms (annotated by the chromosome number, followed by p or q). The gains and losses were normalized against the mean genome ploidy level. C. Unsupervised clustering of distinct genomic profiles in human and organoid pancreas samples. (1) Dendrogram of unsupervised clustering and the main clusters are shown with a different color. 5 main clusters were identified and further explained in the main text. (2) Relative contribution of the *de novo* obtained mutational signatures. All signatures show high consistency to COSMIC ▶



5

- ▶ signatures with known etiology (SBS1, SBS3, SBS2/13, SBS5/15) but also unknown etiology (SBS5, SBS40, SBS17b) (3) Relative contribution of the various INDEL types. Deletions in a repeat context recapitulate microsatellite regions and are highly observed in microsatellite instable tumors. Deletions with microhomology context is typically found in homologous recombination deficient cancer. (4) Relative contribution of the genomic rearrangement signatures. The rearrangements are categorized in type (deletions, insertions, duplications, inversions and rearrangements) as well as length.

level such as *ERBB2* amplification in PDO 6 but not in PDO 7, and *MYC* amplification in PDO 9 but not in PDO 10. Likewise, PDO 13 underwent a whole genome duplication, whereas PDO 12 did not, explaining the amplification events of *GNAS* and *ERBB2* observed in PDO 13. Overall, none of the matched PDOs were genetically identical to their counterparts. This indicates that the different tumor media can be used to capture intra-tumor heterogeneity, which may be of interest in light of drug resistance mechanisms. The finding that none of the matched PDOs were genomically identical to their counterparts underscores the relevance of (intentional or unintentional) *in vitro* selection that can result in enrichment of specific tumor clones. This is in line with the described genetic heterogeneity of PDAC.

DNA copy number analysis revealed aneuploidy in all PDOs, with the exception of PDO 25 (Figure S4). Of these, seven PDOs displayed an overall genome ploidy level of 3 or higher which suggests a whole genome duplication event during tumor development. Next to the chromosomal arm losses as found in Seino et al. (5) (i.e. 6p, 9p, 17p and 18q), we also detected loss of 3p, 6p, 8p, 19p, 21q and 22q, and 20q gain (Figure 2B). Overall, copy number profiles showed a high degree of concordance for PDOs originated from the same patient. This consistency was also observed for other large-scale structural alterations including translocations and inversions (for example in PDO 19, 20 and 21) (Figure S5).

To investigate the mutational processes operating in pancreatic cancer, we applied an unbiased mutational signature analysis on all detected point mutations (18). Seven signatures were identified which show all high consistency to well described signatures in human cancer (19). Of these, signatures SBS1, SBS5 and SBS40 were present in each sample and represent most of the mutations. These three signatures are related to so-called Clock signatures, that result from mutational aging processes that are also seen in healthy cells (Figure S5, Table S3) (20). Unsupervised clustering of PDOs with 71 primary human pancreatic cancer metastasis samples that were previously described (20), revealed five different clusters. Every cluster consisted of both PDOs and human pancreatic samples, indicating that the mutational processes from PDOs recapitulate those found *in vivo* (Figure 2C).

Cluster 1 (green) is characterized by high mutation burden and a strong activity of the mismatch repair deficiency signature in combination with high number of deletions in repeat context. PDO 25, present in this cluster, also displays a near diploid karyotype which are all characteristic features for microsatellite instable tumors (21). Retrospectively, the included patient was diagnosed with an MSI duodenal adenocarcinoma, a tumor located in close proximity to the pancreas. Cluster 2 (blue) represents two human pancreatic samples that show high contribution of SBS5 (a clock signature that currently lacks any etiology). Cluster 3 (pink) exists of two samples that show strong contribution of SBS17. This signature has recently been linked to 5-FU treatment (22). Cluster 4 (purple) is dominated by mutation patterns (SBS3 and deletions with microhomology) highly characteristic for homologous recombination deficiency (23). The final cluster (orange) is

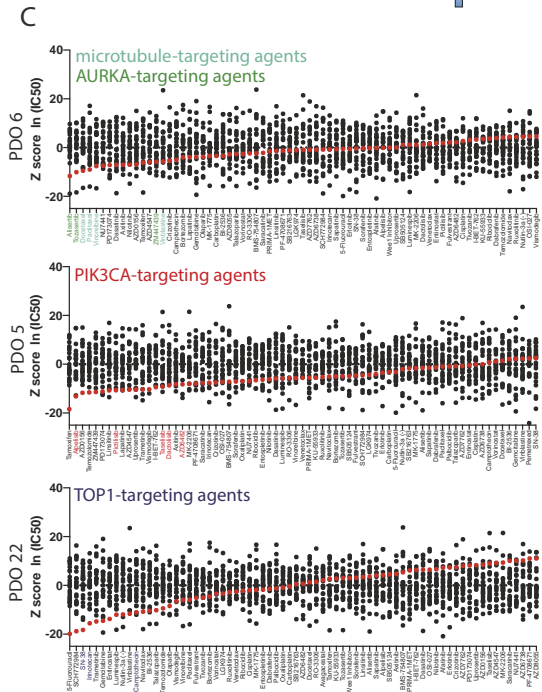
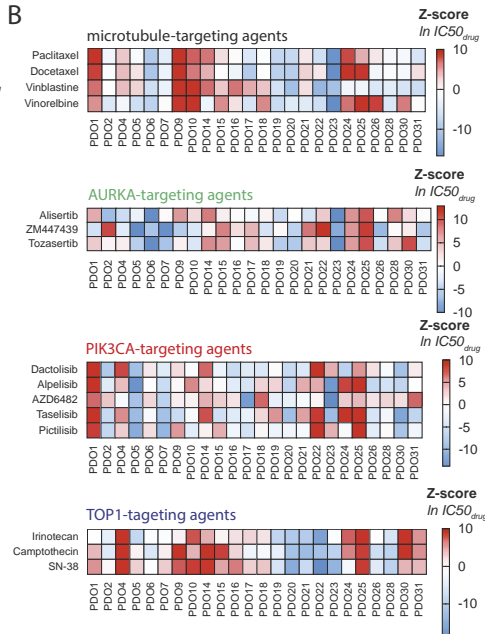
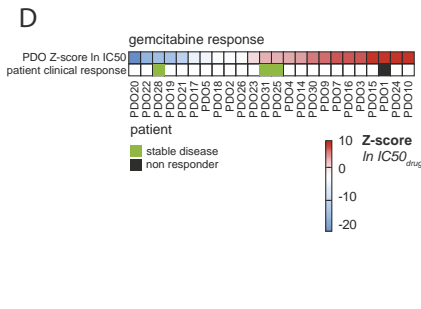
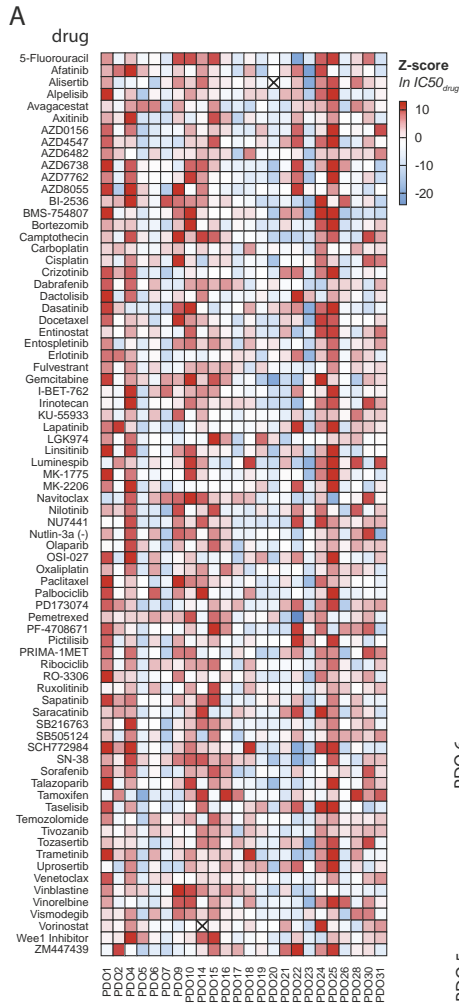
predominantly characterized by the aging signatures (SBS1, SBS5 and SBS40) although some samples also show APOBEC activity (20,24,25).

High-throughput drug screening in PDOs reveals sensitivities to a range of therapeutic agents

To assess the sensitivity of PDOs to a wide range of chemotherapeutic agents, 24 of the established PDOs were exposed to a panel of 76 therapeutics, including chemotherapeutics currently used in the treatment of PDAC. Different responses were observed for organoids derived from different patients (Figure 3A). To validate the results obtained using this screening procedure, we compared the response of organoids when exposed to therapies with similar molecular targets (Figure 3B, Figure S7). As an example, the response to multiple agents targeting either microtubules, Aurora kinase A (AURKA), Phosphatidylinositol-4,5- biphosphate 3-kinase catalytic subunit alpha (PIK3CA) and Topoisomerase-1 (TOP1) are shown (Figure 3B). In general, a similar response was observed for agents targeting the same biological process or molecular pathway. As such, these results indicate that observed *in vitro* responses are indicative for true biological vulnerabilities and are not the consequence of technical variability. For many of the PDOs tested, drugs could be identified for which the individual PDO was more sensitive than all other PDOs tested (Figure 3C, Figure S8). Again, multiple drugs targeting the same molecular pathway were often found amongst the most effective drugs. Together, this supports the hypothesis that specific targeted therapies will only be effective in a subset of patients, and as such, require a personalized approach to select the right drug for each individual patient.

In vitro response of PDOs indicates correlation with clinical patient responses in a limited number of patients

Only for four of the patients, clinical data on given treatment and response was sufficient to assess therapy response. Most patients did not receive treatment at all, or were given treatment in the adjuvant setting (where assessment of therapy response is difficult, since there is no detectable disease at the start of treatment). All four patients were treated with gemcitabine. Patient 1 developed distant metastasis during treatment with this chemotherapeutic agent. Indeed, PDO 1 was highly resistant to treatment with gemcitabine *in vitro*. In contrast, PDO 28 was amongst the most sensitive PDOs upon treatment with gemcitabine. Patient 28 was evaluated as having stable disease with a decrease in distant liver metastasis after gemcitabine treatment, before developing distant metastasis and eventually succumbing to the disease. Also, patient 25 and 31 were evaluated with stable disease after undergoing gemcitabine treatment. PDO 25 and 31 were amongst the intermediate responders in our *in vitro* assays. Although numbers are small, a correlation could be observed between *in vitro* PDO response and clinical patient response (Figure 3D). An overview of relevant patient information is given in Table S4.



◀ **Figure 3. High-throughput drug screening in PDOs reveals sensitivities to a range of therapeutic agents.** A. 76 compounds were tested in 24 PDOs. Here, Z-score calculated from the natural logarithm of obtained IC50 values is depicted in a heatmap. High values (indicating resistance) are depicted in red, low values (indicating sensitivity) in blue. Compounds are ordered alphabetically. B. Response of PDOs to compounds targeting the same biological process or pathway are shown, to highlight similar responses observed between the different compounds. High values (indicating resistance) are depicted in red, low values (indicating sensitivity) in blue. Here response to agents targeting microtubules, AURKA, PIK3CA and TOP1 are shown as an example. C. Compounds arranged from most effective in a particular PDO line. Here, the results for PDO 6, 5 and 22 are shown. Enrichment of compounds that target the same biological process or pathway is observed. Inhibitors targeting the same target are shown in identical colors. Colors are identical to those used in B to identify the pathway. D. Correlation between gemcitabine response of PDOs and corresponding patients. For patient clinical response, green indicates a response to gemcitabine treatment, whereas a black box indicates resistance to treatment. For organoids, similar to Figure 3A and 3B, sensitivity to chemotherapy is indicated by the Z-score of the natural logarithm of IC50 values.

Loss of *MTAP* results in sensitivity to *PRMT5* inhibition

We next focused on a specific therapeutic agent, the selective protein arginine methyltransferase 5 (*PRMT5*) inhibitor EZP01556 (26). The chromosome 9p21 locus, is homozygously deleted in approximately 15% of all human cancers, including pancreatic cancer (27). This locus carries the gene cyclin-dependent kinase Inhibitor 2A (*CDKN2A*), encoding the tumor suppressors alternative reading frame (p19-ARF) and Inhibitor of CDK4 (p16-INK4) (28,29). Upon *CDKN2A* deletion, nearby genes such as methylthioadenosine phosphorylase (*MTAP*) are often co-deleted. Indeed, *MTAP* is deleted in 80-90% of the *CDKN2A*⁻ tumors (30). *MTAP* plays a crucial role in the methionine salvage pathway by recycling its substrate 5'-methylthioadenosine (MTA), ultimately resulting in regeneration of methionine and adenosine (31). A recent search for therapeutic vulnerabilities in *MTAP* deficient cells resulted in the identification of *PRMT5* as a synthetic lethal gene in *MTAP*⁻ cells (32–34). The activity of *PRMT5*, responsible for methylation of a large number of substrates including histones (35), is inhibited by high levels of MTA (32). As MTA accumulates in *MTAP*⁻ cells, exploring the potential of *PRMT5* inhibition in *MTAP*⁻ tumors seems promising (36–38).

CDKN2A and *MTAP* status of the PDOs were determined by DNA and RNA sequencing (Figure 4A and 4B, respectively). DNA and RNA data were concordant for all lines, except for PDO 8 and 11, where the chromosomal breakpoint was found within the *MTAP* gene body. RNA status was in concordance with the result of *MTAP* IHC, performed on a subset of the PDACs (Figure S9). Importantly, tumor 11 showed a positive *MTAP* immunostaining, whereas based on the detected DNA alteration, this detected *MTAP* protein is predicted to be non-functional. To quantify the response to EZP01556, the area under the curve (AUC) of all exposed PDOs was calculated. Indeed, *MTAP*⁻ organoid lines showed increased sensitivity to *PRMT5* inhibition (Figure 4C, Figure S10A). The average IC50 for *MTAP*⁺ lines

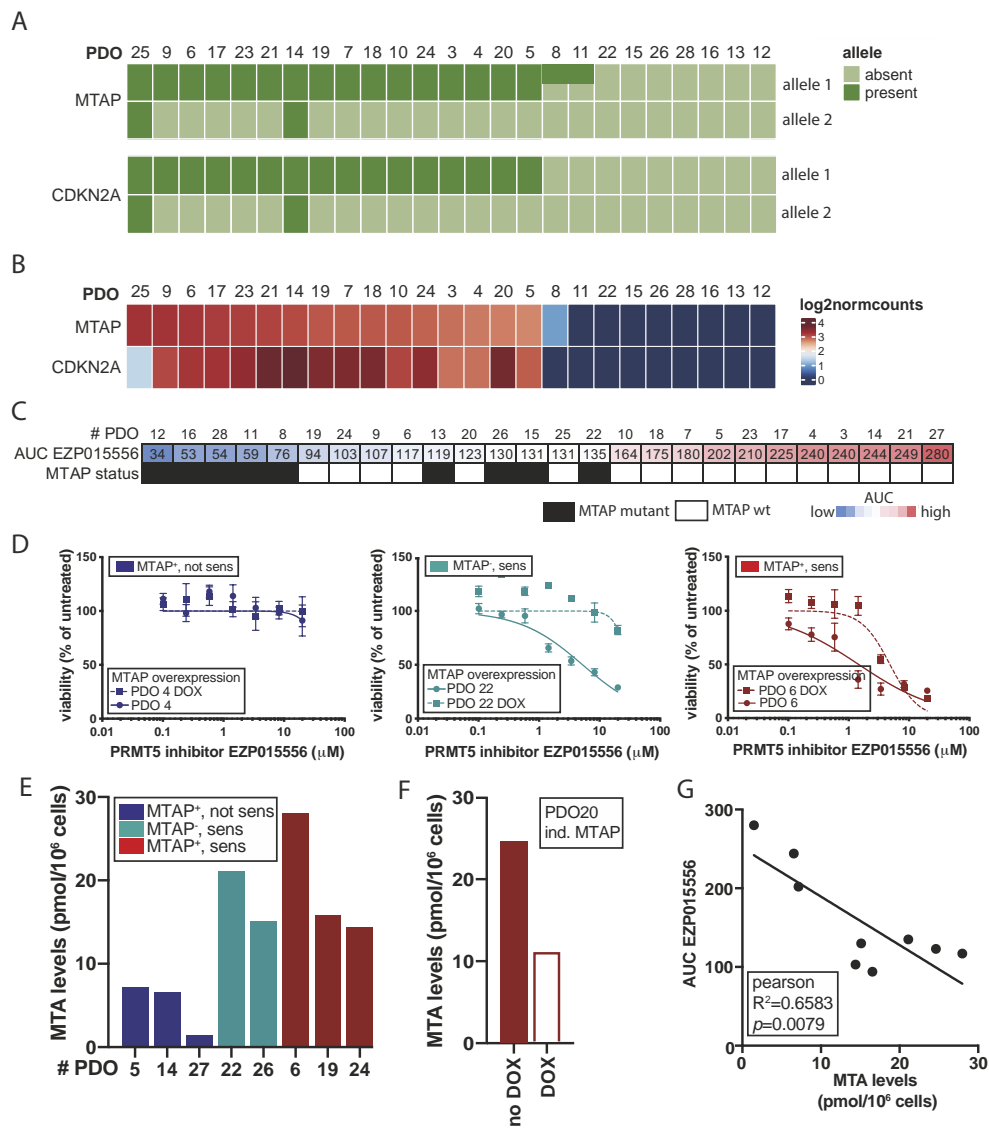


Figure 4. PRMT5 inhibition is effective in a subset of PDOs. A. Detection of CDKN2A and MTAP gene body loss in the 25 tumor-derived PDOs for which reference DNA was available. Dark green indicates loss of gene-coding DNA, light green indicates presence. For both genes, both alleles are shown. B. Expression levels of CDKN2A and MTAP as detected by RNA sequencing in PDOs. Heatmap shows the log2 of normalized counts. Red indicates a high value, blue indicates a low value. C. Heatmap showing AUC of the response to EZP015556 of all tested PDOs and corresponding MTAP DNA status. Low AUC, indicating high sensitivity to PRMT5 inhibition, is depicted in blue. High AUC, indicating low sensitivity to PRMT5 inhibition, is depicted in red. MTAP mutation status is indicated in the row below, where black indicates loss of MTAP and white indicates MTAP wildtype status. D. Induction of MTAP expression in a MTAP⁺ (dark blue), MTAP⁻ (light blue) and MTAP⁺ EZP01556 sensitive line (red). Cells are exposed to EZP015556 either in combination with doxycycline-mediated

- ▶ induction (squared symbols, dashed lines) or without (round symbols, constant line). Experiment was performed in technical triplicate. E. MTA levels measured in PDOs, shown in pmol/10⁶ cells. MTA levels were measured in three *MTAP*⁺, PRMT5 inhibition resistant lines (blue), two *MTAP*⁻, PRMT5 sensitive lines (green), and three *MTAP*⁺, PRMT5 inhibition sensitive lines (red). F. In the case of *MTAP*⁺, PRMT5 inhibition sensitive PDO 20, MTA levels in a were measured in a clone infected with the inducible *MTAP* overexpression construct. MTA levels were measured either in the absence (red bar), or in the presence (white bar, red outline) of DOX, resulting in expression of wildtype *MTAP* protein. G. Correlation plot showing correlation (significant, $p=0.0079$, pearson correlation) between MTA levels (x-axis) and sensitivity to EZP015556, depicted by the AUC (y-axis).

was 19.16 μM , whereas it was 0.68 μM for *MTAP*⁻ organoid lines. Interestingly, a subset of *MTAP*⁺ PDOs also showed sensitivity to PRMT5 inhibition (Figure 4C). *MTAP*⁺ PDO 6, 9, 19, 20, 24 and 25 showed AUC values comparable to those of *MTAP*⁻ organoid lines. These results indicate that PRMT5 inhibition may prove effective in *MTAP*⁻ and in a subset of *MTAP*⁺ tumors. As such, these observations underscore the need for functional testing therapies to identify potentially relevant therapies.

5

Wildtype *MTAP* expression decreases EZP015556 sensitivity in *MTAP*⁺ lines

To test the causal role of *MTAP* dysfunction in sensitivity towards PRMT5 inhibitors, a lentiviral doxycycline-inducible *MTAP* expression vector was introduced in both *MTAP*⁻ and *MTAP*⁺ EZP015556-sensitive organoid lines (Figure S10B). Functionality of the construct was confirmed both by quantitative PCR for *MTAP* transcripts and detection of GFP, whose expression was controlled by the same promoter as *MTAP* in the construct (Figure S10C and S10D). Induction of *MTAP* expression did not change the response of insensitive *MTAP*⁻ lines, but reduced EZP015556 sensitivity in *MTAP*⁻ organoid lines, confirming the causal role of *MTAP* deletion for EZP015556 sensitivity. Moreover, induction of *MTAP* expression decreased EZP015556 sensitivity in *MTAP*⁺ sensitive PDOs, suggestive of defective *MTAP* function in these lines (Figure 4D, Figure S10E).

PDOs sensitive to PRMT5 inhibition are marked by elevated MTA levels

To test whether the underlying mechanism of increased EZP015556 sensitivity was similar in both *MTAP*⁻ and *MTAP*⁺ lines, MTA levels were assessed using proteomics. Elevated MTA levels were detected in *MTAP*⁻ cells, as previously reported (36–38) when compared to EZP015556 insensitive, *MTAP*⁺ lines. In *MTAP*⁺ lines that were sensitive to EZP015556, MTA was detected at levels comparable to that of *MTAP*⁻ lines (Figure 4E). This increase in MTA levels was restored upon overexpression of wildtype *MTAP* (Figure 4F). These results confirmed a comparable mechanism of action of EZP015556 in both subtypes of PDOs, yielding cells vulnerable to EZP015556 treatment. Indeed, a correlation was observed

between MTA levels and EZP015556 sensitivity (Figure 4G). These findings suggest that MTA levels might be a better marker for response to PRMT5 inhibition, than *MTAP* mutation status.

DISCUSSION

Here, a biobank of 30 characterized pancreatic tumor organoids is described and used to explore the translational potential of organoid technology. This was done in two ways. First, by comparing established organoids and corresponding primary tissue for genetic modifications and molecular characteristics. Secondly, after genetic characterization, the established PDOs were exposed to a range of therapeutic agents to identify therapies that effectively kill pancreatic tumor cells.

Morphology of primary tissue and corresponding organoids revealed similarities between the two. Expression of markers currently used in diagnostics was compared between organoids and corresponding primary tissue. It was found that *SMAD4* expression was not detectable by IHC in organoids. As previously mentioned, this is likely due to the presence of BMP/TGF- β -inhibiting molecules Noggin and A83-01 in the organoid medium. This result emphasizes the effect that medium composition can have on cell behavior, a fact that is often overlooked. Despite the absence of *SMAD4* staining, we showed that *SMAD4* wildtype organoids could be distinguished from *SMAD4* mutant ones by using functional selection. These findings highlight the importance of using the correct technique to compare organoids and primary tissue to assess translative potential, and show that IHC might not always be appropriate.

To assess the potential of this system to identify or validate effective therapies for pancreatic cancer, the generated PDO biobank was exposed to a library of both classical chemotherapies and experimental targeted agents. Although highly dependent on the quality and quantity of the primary material, the average time to establish enough organoids for such an extensive screening procedure is expected to be 2-3 months. However, this time can likely be reduced by decreasing the number of compounds tested (for example only focusing on those therapies currently used in first-line treatment).

For most PDOs, we could identify multiple compounds that showed effective tumor killing. Importantly, different drugs killed PDOs derived from different patients. No single therapy could be identified that uniformly resulted in effective tumor killing for all PDOs, indicating that a 'personalized' approach is required when using targeted therapies. In order to identify which therapy is most effective for each individual patient, functional tests such as those described in this study might prove useful. First results indicating that *in vitro* organoid responses can predict clinical outcome have been published, but require further validation before functional testing can be applied in the clinic (6,13,39). It will be interesting to see if this correlation also holds true in pancreatic cancer and, if so, organoids can be used to guide therapy decisions in the clinic.

For four patients, the available clinical data allowed for a comparison of the response to treatment of both the patient and the matching PDO. PDO 1, derived from tumor material of a patient presenting with progressive disease under gemcitabine treatment, was indeed amongst the most resistant PDO in our assays. The three other patients were assessed as having stable disease after receiving gemcitabine treatment. Indeed, matching PDOs showed high or intermediate sensitivity to *in vitro* gemcitabine exposure. Although these results are encouraging, it should be kept in mind that numbers are small, and interpretation of clinical data of patients with pancreatic tumors is difficult, as complications are common and progression is quick. In the future, larger correlation studies should be performed to validate the predictive potential of patient-derived pancreatic organoids.

Finally, we confirmed that PRMT5 inhibition effectively targets *MTAP*⁻ tumors. Moreover, our results indicate that a subset of *MTAP*⁺ tumors might also be susceptible to PRMT5 inhibition. Further research is required to unravel the mechanisms underlying this sensitivity, but our initial results indicate that this is caused by lack of function of the endogenous *MTAP* protein. Potentially, expression analysis of organoids that are undergoing treatment with PRMT5 inhibitors will result in elucidation of the underlying mechanisms. Regardless, these findings highlight the fact that genetic testing might not always be sufficient to identify therapy responders. Currently, clinical trials with PRMT5 inhibitors are ongoing (NCT03573310, NCT02783300, NCT03614728). It will be of interest to see if the *MTAP* (or *CDKN2A*) status of the tumors can be correlated to patient response.

CONCLUSION

Here, we report the establishment of a biobank of patient-derived organoids (PDO) grown from pancreatic cancer and distal cholangiocarcinoma. The organoids were characterized by histology, RNA sequencing, DNA sequencing and drug response. Organoids retain histological features of primary tumors and carried genetic alterations commonly found in this tumor type. High-throughput drug screening using a panel of 76 compounds identified a range of targeted therapies with efficacy in PDOs. In line with personalized medicine approaches, therapy responses differed per PDO. The established PDO model was used to validate PRMT5 inhibition as a potential therapeutic approach for PDAC. We show that PRMT5-inhibitor EZP015556 can be effective in both *MTAP*⁻, and a subset of *MTAP*⁺ PDOs, both characterized by high MTA levels.

METHODS

Human Material for Organoid Cultures

The collection of patient data and tissue for the generation and distribution of organoids has been performed according to the guidelines of the European Network of Research Ethics Committees (EUREC) following European, national, and local law. The Biobank

Research Ethics Committee of the UMC Utrecht (TCBio) approved the biobanking protocol: 12-093 HUB-Cancer according to the UMCU Biobanking Regulation. All donors participating in this study signed informed consent forms and can withdraw their consent at any time, leading to the prompt disposal of their tissue and any derived material, as well as the cessation of data collection. Available organoids will be catalogued at www.hub4organoids.eu and can be requested at info@hub4organoids.eu.

Tissue processing

Patient material was collected from pathology material in Advanced DMEM/F12 (Life Technologies, cat. no. 12634-034), supplemented with 1x GlutaMAX (adDMEM/F12; Life Technologies, cat. no. 12634-034), Penicillin-streptomycin (Life Technologies, cat. no. 15140-122) and 10 mM HEPES (Life Technologies, cat. no. 15630-056). This medium was named +/+/. For collection of patient material, 100 µg/mL Primocin (Invivogen, cat. no. ant-pm1) was added to the +/+ medium. Material was cut into small fragments. Random pieces of approximately 5 mm³ were stored at -20 °C for DNA isolation. A number of pieces were fixed in formalin for histopathological analysis and immunohistochemistry, and the remainder was processed for organoid derivation. Fragments were incubated at 37 °C in 1 mg/mL collagenase (Sigma, C9407) until fully digested. Digested tissue was sheared using 5 ml pipettes. When complete, collagenase was diluted by addition of 10 mL +/+/. The cell suspension was strained over a 100 µm EasyStrainer filter (Greiner, cat. no. 542000) and centrifuged at 300x g. The resulting pellet was resuspended in ice-cold 70% 10 mg·ml⁻¹ cold Cultrex growth factor reduced BME type 2 (Trevigen, 3533-010-02) in organoid medium. Droplets of approximately 10 µL were plated in pre-heated suspension culture plates (Greiner, cat. no. M9312). After plating, plates were inverted and put at 37 °C for 30 minutes to let the BME solidify. Subsequently, prewarmed organoid medium was added to the plate. For the first week, 10 µM Rho-associated kinase (ROCK) inhibitor Y-27632 (Abmole Bioscience, cat. no. M1817) was added to the medium to aid outgrowth of organoids for the primary tissue.

Organoid culture

Organoids were grown in +/+ supplemented with a different subset of growth factors, depending on whether wildtype or tumor organoids were established. For organoids derived from wildtype tissue, medium consisted of Wnt3a-conditioned medium (50% v/v), plus +/+ containing: 1x B27 supplement (Life Technologies, cat. no. 17504-044), 1,25 mM N-acetyl-L-cysteine (Sigma-Aldrich, cat. no. A9165), 10 mM Nicotinamide (Sigma-Aldrich, cat. no. N0636), 50 ng/ml human EGF (PeproTech, cat. no. AF-100-15), 500 nM A83-01, 100 ng/ml human FGF10 (PeproTech, cat. no. 100-26), 1 µM Prostaglandin E2 (Tocris Bioscience, cat. no. 2296), 10 nM Gastrin (R&D, cat. no. 3006), 4% (v/v) RSPO and Noggin (produced via the r-PEX protein expression platform at U-Protein Express BV). This medium was named complete medium (CM). Tumor organoids were grown in parallel in

two types of tumor organoid medium, named tumor medium 1 (TM1) and tumor medium 2 (TM2). TM1 was identical to CM, the only difference being the absence of EGF and PGE2. The difference between TM2 and CM was the absence of PGE2, A83-01 and Wnt3a-conditioned medium.

Organoids were split between 14 and 21 days after initial plating. For passaging, organoids were collected from the plate by disrupting the BME droplets with a P1000, collected and washed in 10 mL +/+/. Pellet was resuspended in 3 mL +/+ and organoids were disrupted using mechanical shearing by pipetting up and down with a glass pipet. For dense tumor organoids not amendable for mechanical shearing, the pellet was resuspended in 1 mL of TrypLE Express (Life Technologies, cat. no. 12605-010) and incubated at 37 °C. Digestion was closely monitored and suspension was pipetted up and down every 2 minutes to aid disruption of the organoids. TrypLE digestion was stopped by adding 10 mL +/+/. Cells were subsequently resuspended in ice-cold 70% BME in organoid medium and plated at suitable ratios (1:2 to 1:5) to allow efficient outgrowth of new organoids. After splitting, 10 µM Y-27632 was added to aid outgrowth of organoids from single cells. Medium was changed every 2-3 days and organoids were split once every 7-10 days.

RNA isolation and RNA sequencing

Total RNA was isolated using the RNeasy mini kit (QIAGEN) from organoids that were passaged 4-6 days prior. Quality and quantity of isolated RNA was checked and measured using Bioanalyzer2100 RNA Nano 6000 chips (Agilent, Cat. 5067-1511). Library preparation was performed with 500 ng of total input RNA using the Truseq Stranded Total RNA kit with Ribo-Zero Human/Mouse/Rat set A and B by Illumina (Cat. RS-122-2201 and RS-122-2202). Library quality was checked using both Bioanalyzer2100 DNA High Sensitivity chips (Cat. 5067-4626) and Qubit (Qubit dsDNA HS Assay Kit, Cat. Q32854). Libraries were pooled to a final concentration of 2 nM. Library pools (1.0-1.4 pM) were loaded and sequenced on the Illumina Nextseq with 2x75bp high output. Samples were sequenced to an average depth of 22.2 million fragments (SD 7.2 million). After quality control, mapping and counting analyses were performed using our in-house RNA analysis pipeline v2.1.0 (<https://github.com/UMCUGenetics/RNASeq>), based on best practices guidelines (<https://software.broadinstitute.org/gatk/documentation/article.php?id=3891>).

RNA isolation, cDNA synthesis and quantitative PCR

Organoids were cultured as normal. On the day of collection, organoids were collected from tissue culture plates and washed twice in 10 mL +/+/. RNA was extracted using RNeasy mini kit (Qiagen, cat. no. 74104) according to protocol. RNA amount was measured using Nanodrop. For cDNA synthesis, RNA was incubated with 50 µg/mL Oligo(dT) 15 Primer (Promega, cat. no. C1101) in water for 5 minutes at 70 °C. Subsequently, GoScript Reverse Transcriptase (Promega, cat. no. A5003) was used according to protocol to produce cDNA.

qPCR reactions were performed in 384-well format using IQ SYBR green (Bio-Rad, cat. no 1708880) in the presence of 0.67 μ M FW and RV primer and cDNA transcribed from 25 ng RNA. For qPCR, samples were incubated for 2 minutes at 95 °C and for 40 cycles at: 15 seconds at 98 °C, 15 seconds at 58 °C and 15 seconds at 72 °C. Results were calculated by using the $\Delta\Delta$ Ct method. Melt peak analysis was performed to assure that primer had no aspecific binding. Primers used were the following:

Table 1.

Primer	Sequence
Human MTAP FW1	ACCACCGCCGTGAAGATTG
Human MTAP RV1	GCATCAGATGGCTTGCCAA
Human MTAP FW2	CAGGCGAACATCTGGGCTTT
Human MTAP RV2	GGACTGAGGTCTCATAGTGGT
Human ID1 FW	CGCATCTTGTGTCGCTGAAG
Human ID1 RV	GAGACCCACAGAGCACGTAA
Human ID3 FW	CTCCGGAACCTGTGCATCTCCA
Human ID3 RV	TGCGTTCTGGAGGTGTCAG
Human Actin	TGCGTGACATTAAGGAGAAG
Human Actin RV	TGAAGGTAGTTTCGTGGATG

Immunohistochemical staining

Tissue and organoids were fixed in 4% paraformaldehyde followed by dehydration, paraffin embedding, sectioning, and standard HE staining. staining on tissue was performed in the UMCU, using a one-hour incubation with either anti-SMAD4 antibody (Santa Cruz sc7966, clone B8, diluted 1:300), anti-TP53 antibody (MS-738-P1, clone D07, diluted 1:2000), or anti-MTAP antibody (Abcam ab126770, clone ERP689, diluted 1:1000), before staining with Brightvision poly-HRP (VWR), followed by development with DAB++ solution (Immunologic, VWRKBS04-110).

SMAD4 signaling detection

To detect the presence of SMAD4, organoids were cultured for two weeks in CM lacking A83-01 and Noggin. In these two weeks, organoids were passaged once. After 14 days, organoids were collected for RNA isolation and cDNA synthesis as described elsewhere.

DNA isolation and KRAS PCR of PDOs

DNA was isolated according to protocol, using the Reliaprep gDNA Tissue Miniprep System (Promega, catalog no. A2052) according to protocol. A PCR for exon 2 of human KRAS was performed using forward primer 5'-ACACGTCTGCAGTCAACTGG-3' and reverse primer 5'- TAACTTGAAACCCAAGGTAC-3'. PCR was performed using GoTaq DNA Polymerase

(Promega, catalog no. M3008) according to protocol, and annealing temperature of 58 °C. A 1% Agarose gel was used to purify PCR product and gel extraction was performed using QIAquick Gel Extraction Kit (Qiagen, catalog no. 28706) according to protocol. DNA was sequenced (using both forward and reverse sequencing primers) by Macrogen.

DNA isolation and WGS of organoid lines

Organoids were dissociated and DNA was isolated using the QiaSymphony DSP DNA mini kit (Qiagen, cat No. 937236). Libraries were prepared using the Truseq DNA nano library prep kit (Illumina, cat. No. 20015964). Paired-end sequencing of the organoid lines was performed (2 x 150 bp) on the generated libraries with 30x coverage using the Illumina HiSeq Xten at the Hartwig Medical Foundation.

5

Somatic mutation calling

Somatic mutation data of the CPCT and DRUP project were kindly shared by HMF on September 1, 2018. To exclude differences in accuracy and sensitivity from somatic calling workflows between human pancreatic data and human pancreatic organoid data, we pulled the HMF somatic mutation workflow from <https://github.com/hartwigmedical/pipeline> and installed the pipeline locally using GNU Guix with the recipe from <https://github.com/UMCUGenetics/guix-additions>. Full pipeline description is explained elsewhere (40). Details and settings of all the tools can be found at their Github page. Briefly, sequence reads were mapped against human reference genome GRCh37 using Burrows-Wheeler Alignment (BWA-MEM) v0.7.5a (41). Subsequently, somatic single base substitutions (SBSs) and small insertions and deletions (INDELS) were determined by providing the genotype and tumor (or organoid for in-vitro analysis) sequencing data to Strelka v1.0.14 (42) with adjustments as described elsewhere (40). For karyoplots and circoplots, pipeline is made available at https://github.com/UMCUGenetics/Pancreas_biobank/.

High throughput drug screens

24 PDOs were screened in the drug screening facility of the Sanger Institute, UK. Organoids were screened in CM to exclude differences in response due to the presence/absence of medium components. This was only done after 100% tumor purity was confirmed, and no change in cell behavior was observed upon this medium change to CM. Organoids were dissociated into single cells and plated as usual to recover for four days. Subsequently, the organoids were transferred into 384-well assay plates within 52 μ L of the complete media using an XRD384 (FluidX) dispenser and left to recover for 24 hours. Prior to dispensing the organoids, 8 μ L of 50:50 BME was added to each well, making the final BME concentration concentration 7% (after the addition of the organoid suspension). Test compounds were added 24 hours later using an Echo555 (Labcyte). Final DMSO concentrations were $\leq 0.1\%$ for single agents and $\leq 0.2\%$ for combinations. Organoids were exposed to therapies for 72 hours. Cell viability was measured by the addition of 15 μ L of

Cell Titer Glo to each well. Readout was performed using a Paradigm (Molecular Devices) plate reader. In parallel with dosing, an additional plate for each cell line was read using the same reagents as above. These plates underwent no treatment and could be used to determine growth estimates over the duration of the assay. MG-132 and Staurosporin were used as positive controls. Plate quality control was performed for each assay plate. Each plate was required to have a control coefficient of variation (CV) below 0.25, which was calculated by dividing of the standard deviation of the negative controls by the standard deviation of the positive controls. Moreover, plates were required to have an NC-0/NC-1 ratio of between 0.8-1.2 calculated using the mean of each negative control, where NC-0 is the value obtained for negative controls that are untreated, and NC-1 the value obtained for negative controls treated with drug solvent, but not drug itself. Z-factors were calculated using the negative control (NC-1) and the Blank positive control (B). Only plates with a Z-Factor above 0.3 were included in analysis. Z-factor was calculated following: $Z\text{-factor} = 1 - 3 \cdot (\sigma_p + \sigma_n) / (\mu_n - \mu_p)$, with σ_n and σ_p the standard deviation of the negative and positive controls, and μ_n and μ_p the mean of the negative and positive controls, respectively.

Drug screen analysis and Z-score calculation

Natural logarithms of IC50 values were normalized to a Z-score, using the formula:

$$\sqrt{(x - \mu) / \left(\frac{\text{stdev}}{n}\right)}$$

where μ is the average of natural logarithm of the IC50 for all PDOs tested, stdev is the standard deviation of the natural logarithm of the IC50 values for all PDOs tested, and n is the number of PDO tested. All calculations were performed with these values, to visual differences in drug response between PDOs, in contrast to differences in IC50 values between different compounds.

PRMT5 inhibitor drug screens

As cells were exposed to PRMT5 inhibitors for 14 days, these screens had to be performed in BME droplets to allow medium change. Cells were passaged and disrupted into single cells using TrypLE. Single cells were counted and plated at 2000 cells/30 μ L BME per well of a round bottom 96-well plate (Greiner). After solidification of the BME, 75 μ L CM was added per well. A gradient of EZP015556 was added to the plate using the using the Tecan D300e Digital Dispenser (Tecan). EZP01556 was dissolved in DMSO, all wells were normalized for solvent used. DMSO percentage never exceeded 1%, which, based on cell viability measurements, did not affect cell survival when compared to wells that were left untreated. Drug exposure was performed in triplicate for each concentration. Medium

was refreshed every 3-4 days. After 14 days, readout was performed. For this, ATP levels were measured using the CellTiter-Glo 3D Reagent (Promega, cat. no. G9681) according to the manufacturer's instructions and luminescence was measured using a Spark multimode microplate reader (Tecan). Results were normalized to vehicle (100%) and baseline control (Staurosporin 1 μ M), (0%). Kill curves were produced using GraphPad software and lines were fitted using the option 'log(inhibitor) vs normalized response -variable slope'.

MTAP overexpression lentivirus production

MTAP open reading frame flanked by restricting digest sequences for Nhe1 and Mlu1 was ordered as a gBlock from Promega. PCR product was purified using gel extraction after running it on a 1% agarose gel. The gBlock was ligated into cloning vector pJET blunt (Thermo Fisher, #K1231) for amplification. Restriction digestion using Nhe1 and Mlu1 allowed ligation of the MTAP open reading frame into Addgene plasmid #50661. Production of lentivirus was performed in HEK293T cells transduced with packaging plasmids and the created construct. Transduction was performed using a mixture of 300 μ l PEI, 45 μ g overexpression construct and 5 ml Optimem (Thermo-Fisher, cat. nr. 11058021). After a 20 minutes incubation, this mixture was added to 15 ml of DMEM with 10% serum and put on a 70% confluent HEK cell mixture. Mixture was left for 8 hours on the cells, and subsequently replaced with fresh culture medium. After 72 hours, supernatant was collected, filtered and collected using ultracentrifugation (20.000 x g, 2 hours, 4 °C). Virus derived from one confluent 15 cm culture dish of HEK293T cells was resuspended in 500 μ L organoid medium and stored at -80 °C until used.

5

Organoid infection with MTAP lentivirus

Organoids were collected, disrupted into small clumps/single cells using TrypLE. After washing with 10 mL +/+/+, the organoid pellet was resuspended in 150 μ L virus suspension, 1 μ g/mL polybrene was added and the mixture was transferred to a 48-well plate. After a 1-hour centrifugation (600 x g, 32 °C) cells were left to incubate for 6 hours with the virus. After that, the organoid pellet was collected, washed twice with 10 mL +/+/+ and plated as usual. After recovery (3 to 5 days), organoids were cultured in the presence of 1 μ g/mL puromycin (InvivoGen, cat. Nr. 58-58-2) to select for infected organoids. Infected organoids were expanded as usual. When ready, organoids were exposed to PRMT5 inhibitor as previously described either in the presence or absence of 3 μ g/ml doxycycline. Doxycycline was kept in the culture medium during the course of the experiment.

Liquid Chromatography Mass Spectrometry (LC-MS) Measurement

Organoids were passaged and cultured for 7 days. On the day of collection, 2 U/mL dispase was added to the wells and left to incubate for 40 minutes at 37 °C. Subsequently, organoids were washed three times in ice-cold PBS and resuspended in 1 mL +/+/+. A 10 μ l sample was taken for cell counting and transferred to a tube containing 1 mL

TrypLE. After 5 minutes incubation, cells were counted. The remaining intact organoids were collected for metabolomic analysis. For this, organoid samples were quenched in 500 μ L of dry-ice cold methanol/water solution (80%/20%; v/v; dry-ice cold), and then stored in -80 °C.

Used chemical standards were MTA (5'-deoxy-5'-(methylthio)adenosine, Sigma-Aldrich), SAM (S-(5'-adenosyl)-L-methionine, Sigma-Aldrich), SAH (S-(5'-adenosyl)-L-homocysteine, Sigma Aldrich), table isotope labelled MTA-d3 (Toronto Research Chemicals), and SAM-d3 (CDN Isotopes). Prior to metabolite extraction, all samples were spiked with 10 μ L of a 20 μ M internal standard mixture and subsequently crushed using zirconium oxide beads in a bullet blender (NextAdvance, USA) for 5 min at 4°C, followed by 10 min centrifugation at 17000x g at 4°C. Supernatants were transferred into clean 1.5 mL tubes and dried using a vacuum concentrator (Labconco, USA). Dried pellets were dissolved in 100 μ L of borate buffer (pH 8.2) and transferred into LC glass vials. The LC-MS measurement was performed using the Thermo Scientific Dionex UltiMate 3000 RS UHPLC system and a Phenomenex Kinetex® F5 column (2.1×150 mm, 1.7 μ m 100Å), which were both kept at 40°C. Column outlet was coupled to a Thermo Scientific Orbitrap XL equipped with an electrospray ion source using positive ion mode. The mass spectrometer was operated in full scan mode between 100-650 *m/z*. The mobile phases consisted of MilliQ/acetonitrile (95%/5%; v/v) (solvent A), and 100% acetonitrile (solvent B), both containing 0.1% formate as mobile phase modifier. The LC gradient program was started upon injection of a 10 μ L sample. A 5 min linear gradient of 0–50% B was started 1 min after the injection of the sample. The gradient was ramped to 100% B between 6-8 min and kept there for 2 min. This process repeated for each subsequent sample. Total runtime was 14 min with a flow rate of 300 μ L per min. Peak detection and integration was performed with Thermo Xcalibur Software (v4.0). Peak area values of MTA and SAM were corrected using internal standards of MTA-d3 and SAM-d3, respectively. Concentrations of MTA and SAM were calculated using a standard curve of both analytes ranging from 10 nM to 10 μ M.

DATA AVAILABILITY

The organoid DNA as well as RNA sequencing data has been deposited at the European Genome-phenome Archive (<http://www.ebi.ac.uk/ega/>) under accession numbers EGAS00001003369. WGS data of metastatic pancreatic cancer patients was obtained from the Hartwig Medical Foundation and can be provided under data request number DR-010. This WGS is freely available for academic use from the Hartwig Medical Foundation through standardized procedures and request forms can be found at <https://www.hartwigmedicalfoundation.nl>.

ACKNOWLEDGEMENTS

We acknowledge all employees of U-PORT; UMC Utrecht for patient inclusion and tissue acquisition. We thank Kim Boonekamp for her help with MTAP experiments and Fjodor Yousef Yengej for his help with qPCR experiments. We would like to thank Jens Puschhof and Maarten Geurts for their valuable input on drug screen analysis. We thank the Genomics of Drug Sensitivity in Cancer screening team. Lastly, we thank the Hartwig Medical Foundation and Barcode for Life for WGS analyses and the Center for Personalized Cancer Treatment for providing the clinical data.

FINANCIAL SUPPORT

Funded by the Onco Institute (partly financed by the Dutch Cancer Society), by the gravitation program CancerGenomiCs.nl from the Netherlands Organization for Scientific Research (NWO) and by a Stand Up to Cancer International Translational Cancer Research Grant, a program of the Entertainment Industry Foundation administered by the AACR (SU2C-AACR-DT1213) and a ZonMw grant (116.006.103). Funding to M. J. Garnett from Wellcome Trust (206194) and CRUK (C44943/A22536). Research of L.A.A. Brosens is funded by the Dutch Digestive foundation (MLDS CDG 14-020).

DECLARATION OF INTEREST

H. Clevers is an inventor on several patents related to organoid technology. H. Clevers is the (unpaid) Chief Scientific Officer of the HUB, co-founder of Surrozen and SAB member of Kallyope (New York), Merus (Utrecht) and Decibel (Boston). H. Clevers is a non-executive board member of Roche and Genentech, and scientific advisor of Life Sciences Partners. E. Driehuis is an inventor on a patent related to organoid technology.

REFERENCES

1. Howlader N, Noone A, Krapcho M, Miller D, Bishop K, Kosary C, et al. Cancer Statistics Review, 1975-2014 - SEER Statistics, National Cancer Institute. SEER Cancer Stat. Rev. 1975-2014. 2016.
2. Schmuck RB, de Carvalho-Fischer C V, Neumann C, Pratschke J, Bahra M. Distal bile duct carcinomas and pancreatic ductal adenocarcinomas: Postulating a common tumor entity. *Cancer Med.* 2016;
3. Conroy T, Desseigne F, Ychou M, Bouche O, Guimbaud R, Becouarn Y, et al. FOLFIRINOX versus gemcitabine for metastatic pancreatic cancer. *N Engl J Med.* United States; 2011;364:1817–25.
4. Von Hoff DD, Ervin T, Arena FP, Chiorean EG, Infante J, Moore M, et al. Increased survival in pancreatic cancer with nab-paclitaxel plus gemcitabine. *N Engl J Med.* United States; 2013;369:1691–703.
5. Seino T, Kawasaki S, Shimokawa M, Tamagawa H, Toshimitsu K, Fujii M, et al. Human Pancreatic Tumor Organoids Reveal Loss of Stem Cell Niche Factor Dependence during Disease Progression. *Cell Stem Cell.* Elsevier; 2018;22:454-467.e6.
6. Tiriac H, Belleau P, Engle DD, Plenker D, Deschênes A, Somerville T, et al. Organoid profiling identifies common responders to chemotherapy in pancreatic cancer. *Cancer Discov.* 2018;
7. Bailey MH, Tokheim C, Porta-Pardo E, Sengupta S, Bertrand D, Weerasinghe A, et al. Comprehensive Characterization of Cancer Driver Genes and Mutations. *Cell.* United States; 2018;173:371-385.e18.
8. Tamborero D, Rubio-Perez C, Deu-Pons J, Schroeder MP, Vivancos A, Rovira A, et al. Cancer Genome Interpreter annotates the biological and clinical relevance of tumor alterations. *Genome Med.* England; 2018;10:25.
9. Drost J, Clevers H. Organoids in cancer research. *Nat Rev Cancer.* England; 2018;18:407–18.
10. Sachs N, de Ligt J, Kopper O, Gogola E, Bounova G, Weeber F, et al. A Living Biobank of Breast Cancer Organoids Captures Disease Heterogeneity. *Cell.* United States; 2018;172:373-386.e10.
11. Van De Wetering M, Francies HE, Francis JM, Bounova G, Iorio F, Pronk A, et al. Prospective derivation of a living organoid biobank of colorectal cancer patients. *Cell.* Elsevier Inc.; 2015;161:933–45.
12. Vlachogiannis G, Hedayat S, Vatsiou A, Jamin Y, Fernández-mateos J, Khan K, et al. Patient-derived organoids model treatment response of metastatic gastrointestinal cancers. *Science (80-). American Association for the Advancement of Science;* 2018;926:920–6.
13. Driehuis E, Kolders S, Spelier S, Lohmussaar K, Willems SM, Devriese LA, et al. Oral mucosal organoids as a potential platform for personalized cancer therapy. *Cancer Discov.* 2019;CD-18-1522.
14. Lee SH, Hu W, Matulay JT, Silva M V, Owczarek TB, Kim K, et al. Tumor Evolution and Drug Response in Patient-Derived Organoid Models of Bladder Cancer. *Cell.* 2018;173:515-528.e17.
15. Kopper O, de Witte CJ, Lohmussaar K, Valle-Inclan JE, Hami N, Kester L, et al. An organoid platform for ovarian cancer captures intra- and interpatient heterogeneity. *Nat Med.* United States; 2019;
16. Boj SF, Hwang C-I II, Baker LA, Chio IIC, Engle DD, Corbo V, et al. Organoid models of human and mouse ductal pancreatic cancer. *Cell.* Elsevier; 2015;160:324–38.
17. Bosari S, Viale G, Roncalli M, Graziani D, Borsani G, Lee AK, et al. p53 gene mutations, p53 protein accumulation and compartmentalization in colorectal adenocarcinoma. *Am J Pathol.* 1995;147:790–8.
18. Freed-Pastor WA, Prives C. Mutant p53: One name, many proteins. *Genes Dev.* 2012;26:1268–86.

19. Bailey P, Chang DK, Nones K, Johns AL, Patch A-M, Gingras M-C, et al. Genomic analyses identify molecular subtypes of pancreatic cancer. *Nature*. 2016;
20. Blokzijl F, De Ligt J, Jager M, Sasselli V, Roerink S, Sasaki N, et al. Tissue-specific mutation accumulation in human adult stem cells during life. *Nature*. 2016;
21. Taylor AM, Shih J, Ha G, Gao GF, Zhang X, Berger AC, et al. Genomic and Functional Approaches to Understanding Cancer Aneuploidy. *Cancer Cell*. United States; 2018;33:676-689.e3.
22. Christensen S, Van der Roest B, Besselink N, Janssen R, Boymans S, Martens J, et al. 5-Fluorouracil treatment induces characteristic T>G mutations in human cancer. *bioRxiv*. 2019;681262.
23. Davies H, Glodzik D, Morganella S, Yates LR, Staaf J, Zou X, et al. HRDetect is a predictor of BRCA1 and BRCA2 deficiency based on mutational signatures. *Nat Med*. 2017;23:517–25.
24. Alexandrov LB, Jones PH, Wedge DC, Sale JE, Campbell PJ, Nik-Zainal S, et al. Clock-like mutational processes in human somatic cells. *Nat Genet*. United States; 2015;47:1402–7.
25. Jager M, Blokzijl F, Kuijk E, Bertl J, Vougioukalaki M, Janssen R, et al. Deficiency of nucleotide excision repair explains mutational signature observed in cancer. *bioRxiv*. 2018;221168.
26. Chan-Penebre E, Kuplast KG, Majer CR, Boriack-Sjodin PA, Wigle TJ, Johnston LD, et al. A selective inhibitor of PRMT5 with in vivo and in vitro potency in MCL models. *Nat Chem Biol*. 2015;
27. Beroukhi R, Mermel CH, Porter D, Wei G, Raychaudhuri S, Donovan J, et al. The landscape of somatic copy-number alteration across human cancers. *Nature*. 2010.
28. Kamijo T, Zindy F, Roussel MF, Quelle DE, Downing JR, Ashmun RA, et al. Tumor suppression at the mouse INK4a locus mediated by the alternative reading frame product p19(ARF). *Cell*. 1997;
29. Serrano M, Hannon GJ, Beach D. A new regulatory motif in cell-cycle control causing specific inhibition of cyclin D/CDK4. *Nature*. 1993;
30. Zhang H, Chen ZH, Savarese TM. Codeletion of the genes for p16INK4, methylthioadenosine phosphorylase, interferon-alpha1, interferon-beta1, and other 9p21 markers in human malignant cell lines. *Cancer Genet Cytogenet*. 1996;
31. Zappia V, Della Ragione F, Pontoni G, Gagnaniello V, Carteni-Farina M. Human 5'-deoxy-5'-methylthioadenosine phosphorylase: kinetic studies and catalytic mechanism. *Adv Exp Med Biol*. United States; 1988;250:165–77.
32. Kryukov G V, Wilson FH, Ruth JR, Paulk J, Tsherniak A, Marlow SE, et al. MTAP deletion confers enhanced dependency on the PRMT5 arginine methyltransferase in cancer cells. *Science*. United States; 2016;351:1214–8.
33. Mavrakis KJ, McDonald ER 3rd, Schlabach MR, Billy E, Hoffman GR, deWeck A, et al. Disordered methionine metabolism in MTAP/CDKN2A-deleted cancers leads to dependence on PRMT5. *Science*. United States; 2016;351:1208–13.
34. Marjon K, Cameron MJ, Quang P, Clasquin MF, Mandley E, Kunii K, et al. MTAP Deletions in Cancer Create Vulnerability to Targeting of the MAT2A/PRMT5/RIOK1 Axis. *Cell Rep*. 2016;
35. Karkhanis V, Hu YJ, Baiocchi RA, Imbalzano AN, Sif S. Versatility of PRMT5-induced methylation in growth control and development. *Trends Biochem. Sci*. 2011.
36. Stevens AP, Spangler B, Wallner S, Kreutz M, Dettmer K, Oefner PJ, et al. Direct and tumor microenvironment mediated influences of 5'-deoxy-5'-(methylthio)adenosine on tumor progression of malignant melanoma. *J Cell Biochem*. 2009;
37. Limm K, Ott C, Wallner S, Mueller DW, Oefner P, Hellerbrand C, et al.

- Deregulation of protein methylation in melanoma. *Eur J Cancer*. 2013;
38. Basu I, Cordovano G, Das I, Belbin TJ, Guha C, Schramm VL. A transition state analogue of 5'-methylthioadenosine phosphorylase induces apoptosis in head and neck cancers. *J Biol Chem*. 2007;
 39. Vlachogiannis G, Hedayat S, Vatsiou A, Jamin Y, Fernández-Mateos J, Khan K, et al. Patient-derived organoids model treatment response of metastatic gastrointestinal cancers. *Science* (80-). American Association for the Advancement of Science; 2018;359:920–6.
 40. Priestley P, Baber J, Lolkema MP, Steeghs N, Bruijn E de, Duyvesteyn K, et al. Pan-cancer whole genome analyses of metastatic solid tumors. *bioRxiv*. 2019;415133.
 41. Li H, Durbin R. Fast and accurate short read alignment with Burrows-Wheeler transform. *Bioinformatics*. England; 2009;25:1754–60.
 42. Saunders CT, Wong WSW, Swamy S, Becq J, Murray LJ, Cheetham RK. Strelka: accurate somatic small-variant calling from sequenced tumor-normal sample pairs. *Bioinformatics*. England; 2012;28:1811–7.



SUPPLEMENTARY DATA

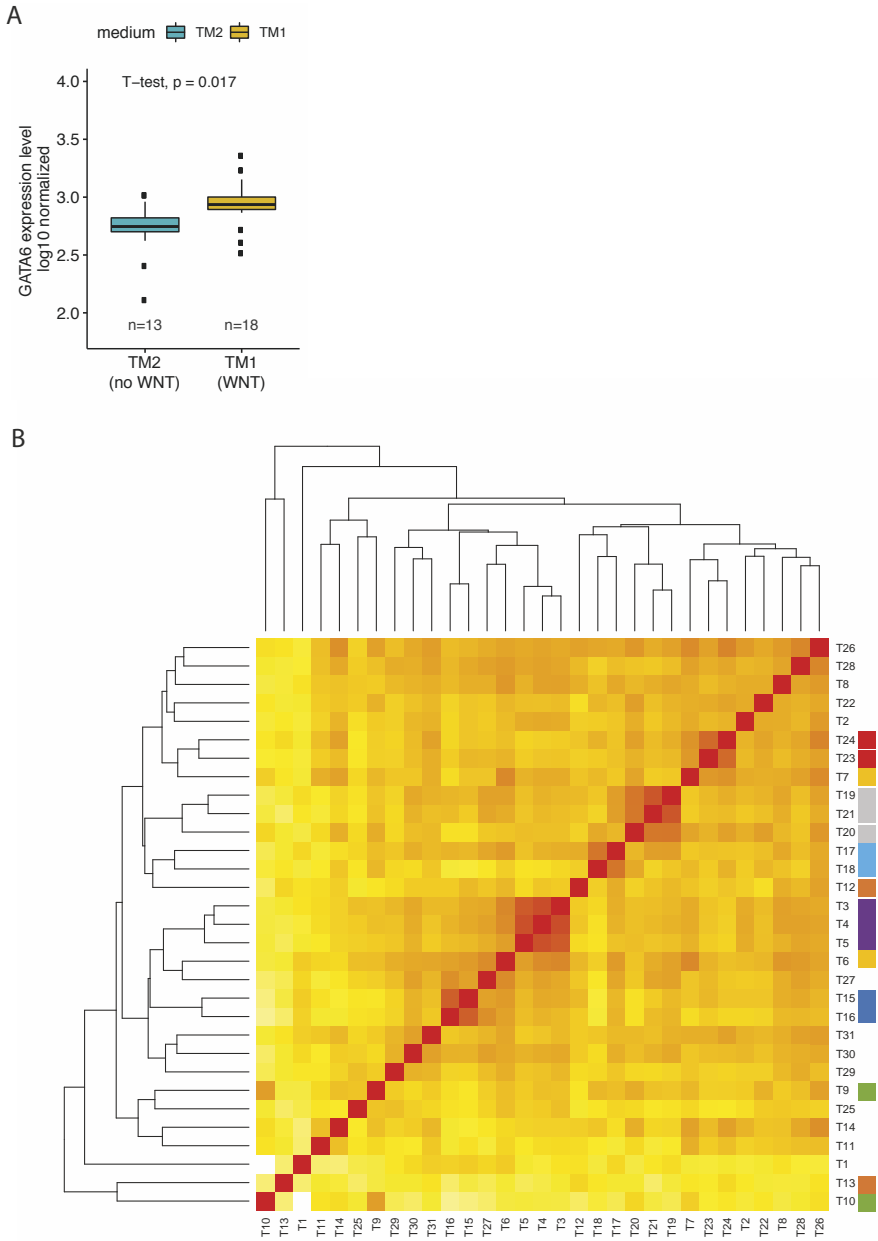


Figure S1. WNT dependency is linked to GATA6 expression in PDOs. A. Boxplot comparing GATA6 expression in PDOs established and grown on TM2 (lacking WNT, blue bar) and TM1 (containing WNT, yellow bar). B. correlation heatmap showing the unsupervised clustering of PDO based on expression profiles. Organoids derived from the same donor are indicated by identical colors.

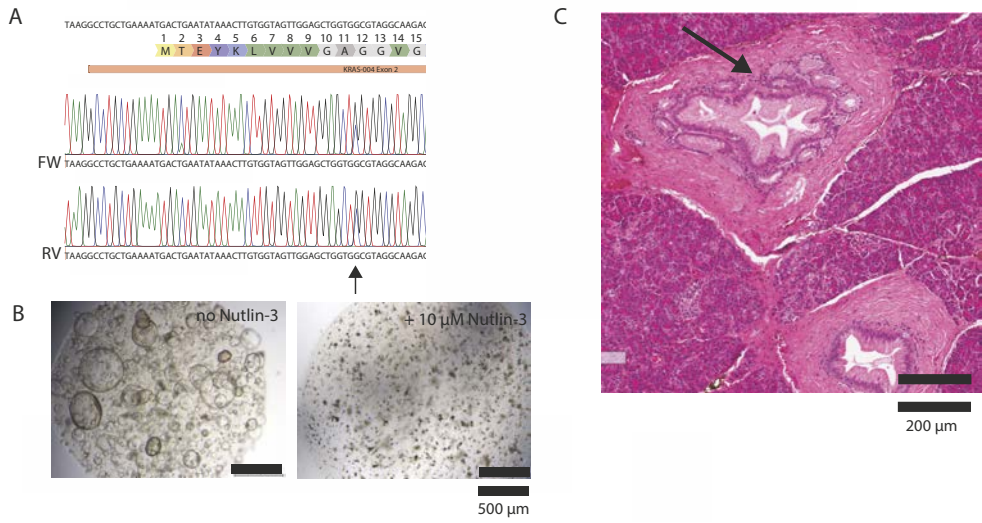


Figure S2. Anecdotal expansion of pre-cancerous cells found in 'healthy' pancreas. A. Sequencing results of the PCR fragment that amplifies exon 2 of *KRAS*. A heterozygous G>C mutations results in a G12R amino acid change in the *KRAS* protein. Here, sequencing results obtained with both forward and reverse primer are shown. The mutation is indicated with an arrow. B. Appearance of the established organoid line as seen by brightfield microscopy. Organoids were cultured in the presence of MDM2-agonist Nutlin-3 for one week. Cells could not survive this treatment (second panel) indicative of wildtype TP53 status. C. H&E of the pancreatic intraepithelial neoplasia identified in the patient upon pathological assessment of the removed pancreatic tissue. The PanIn lesion is indicated with an arrow.

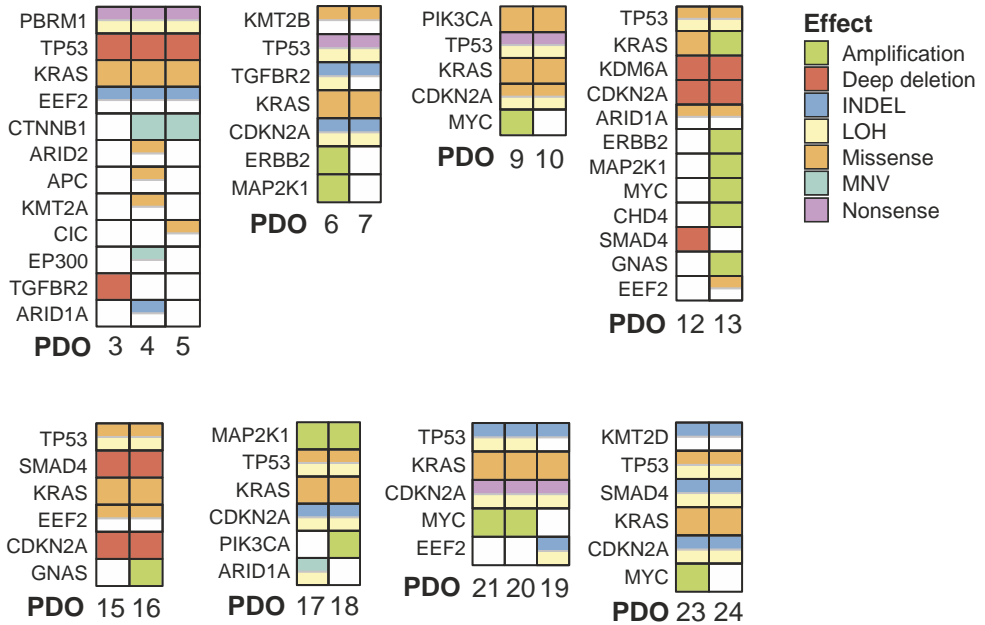


Figure S3. Genomic landscape of pancreatic PDOs established from the same resection sample, but grown on different media. For all matched PDO sets (established from the same resection specimen but put on different tumor media), a separate figure depicts the different genetic alterations detected in the PDOs using WGS. Different mutation types are depicted with different colors, as indicated.

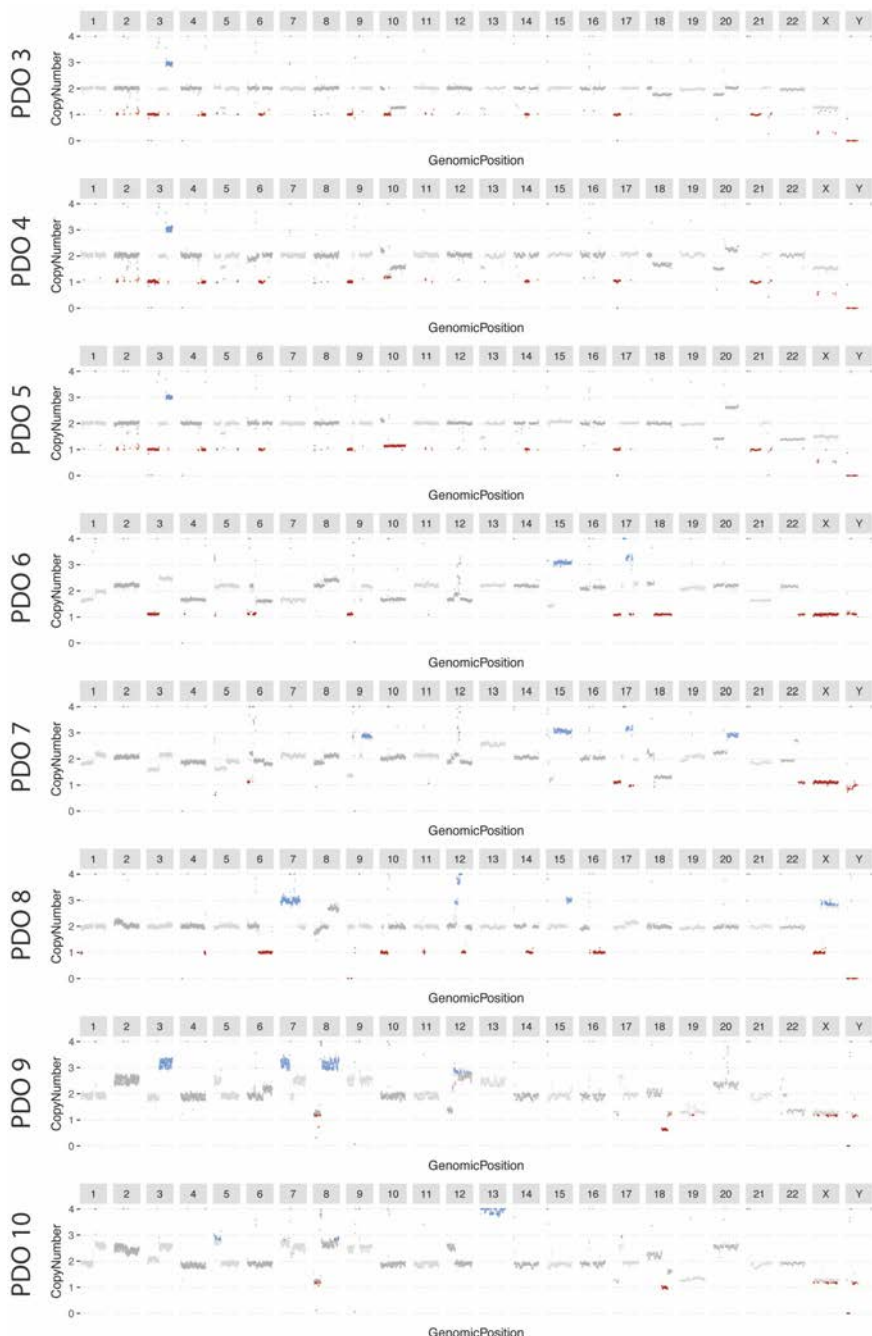
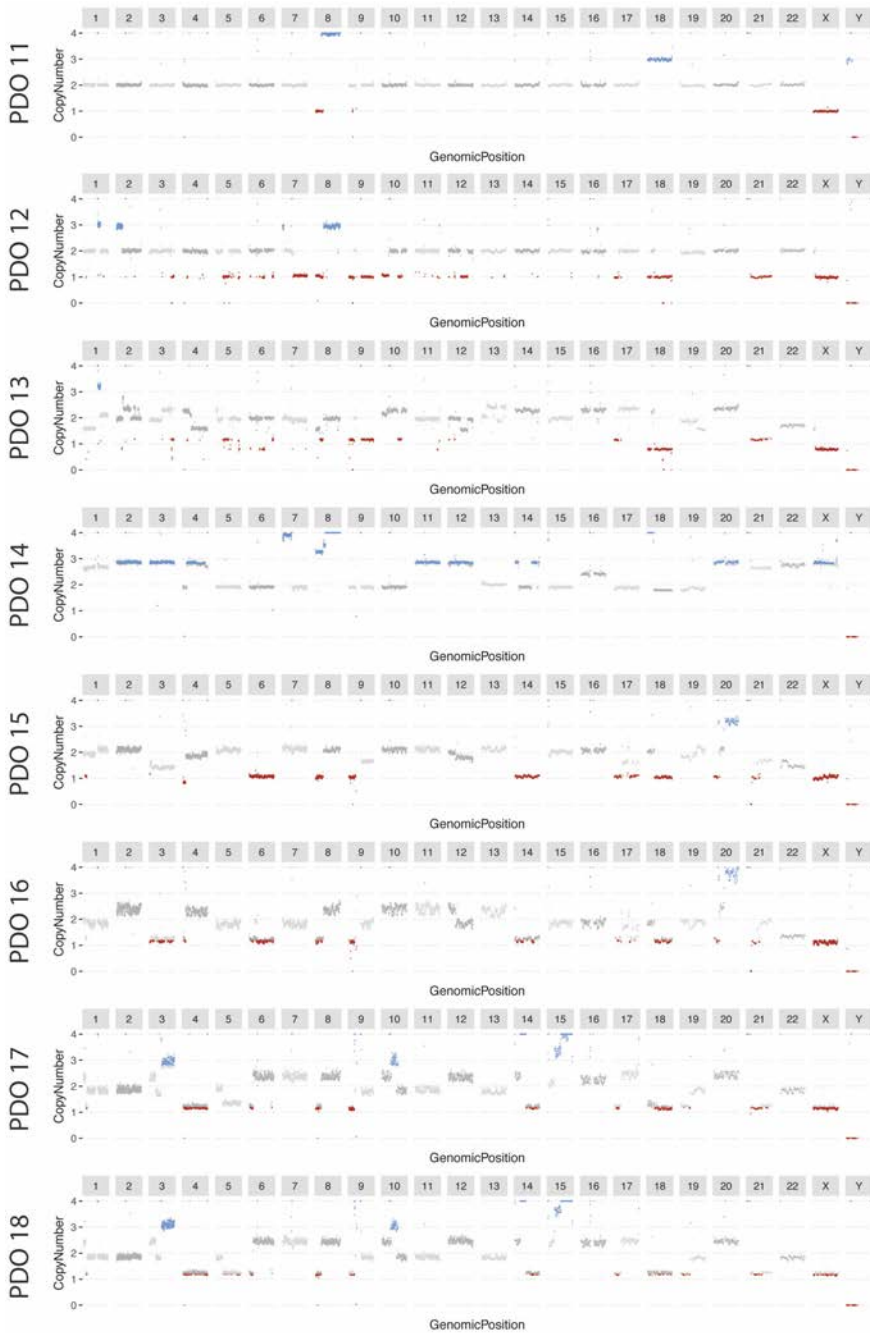


Figure S4. Karyograms of patient-derived organoids. For all PDOs for which reference DNA was available, karyograms were assembled based on WGS. Changes in the DNA content are shown relative to the average DNA amounts. Increase in DNA content is shown in blue, decrease in red.



5

Figure S4. (continued)

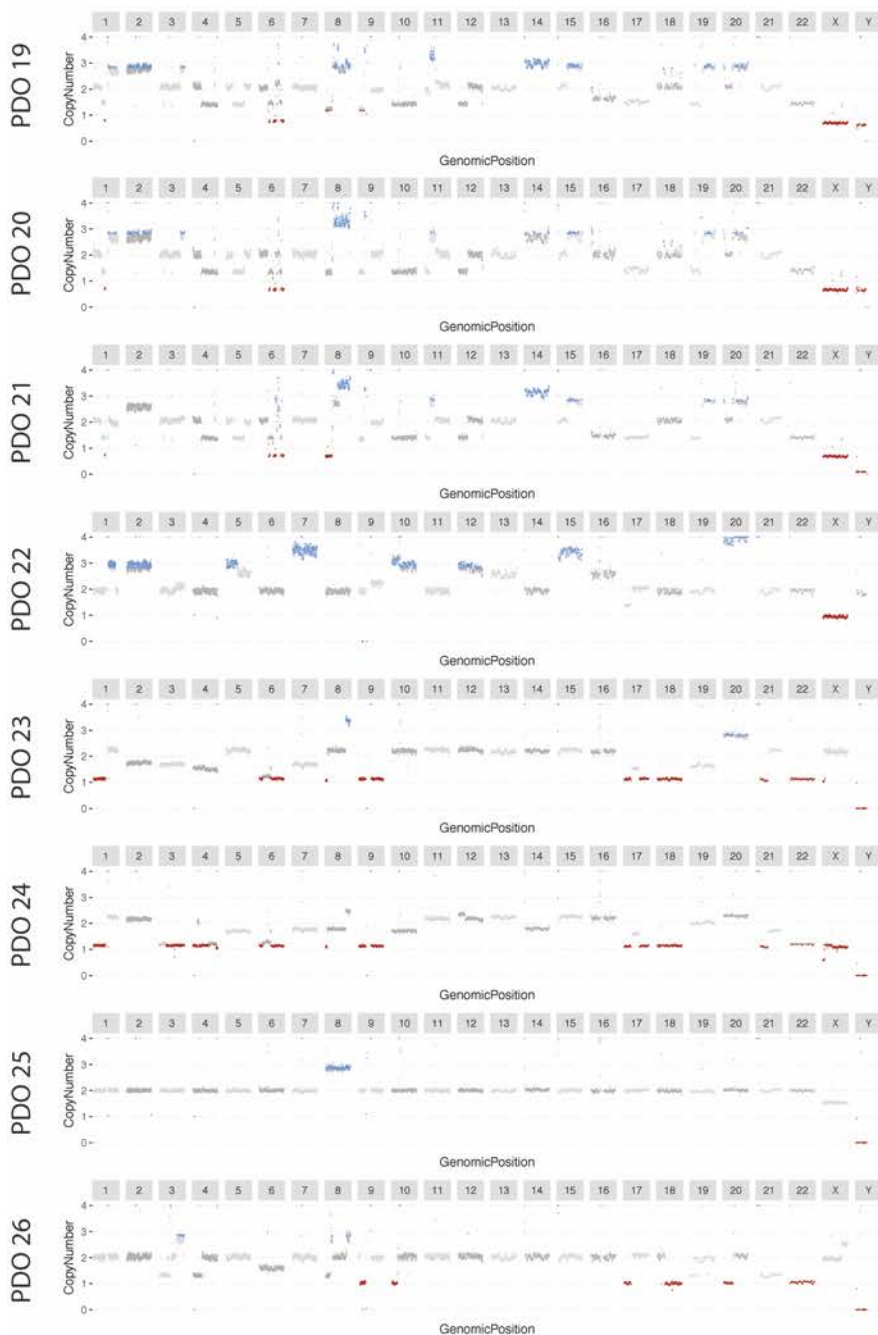


Figure S4. (continued)



Figure S4. (continued)

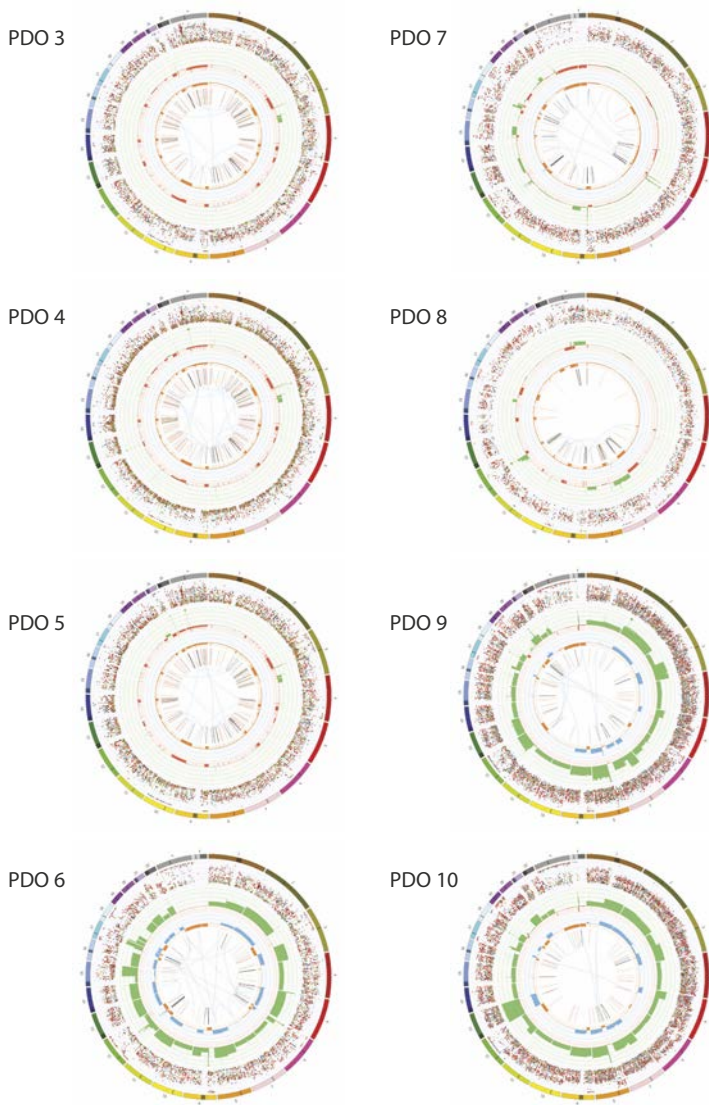
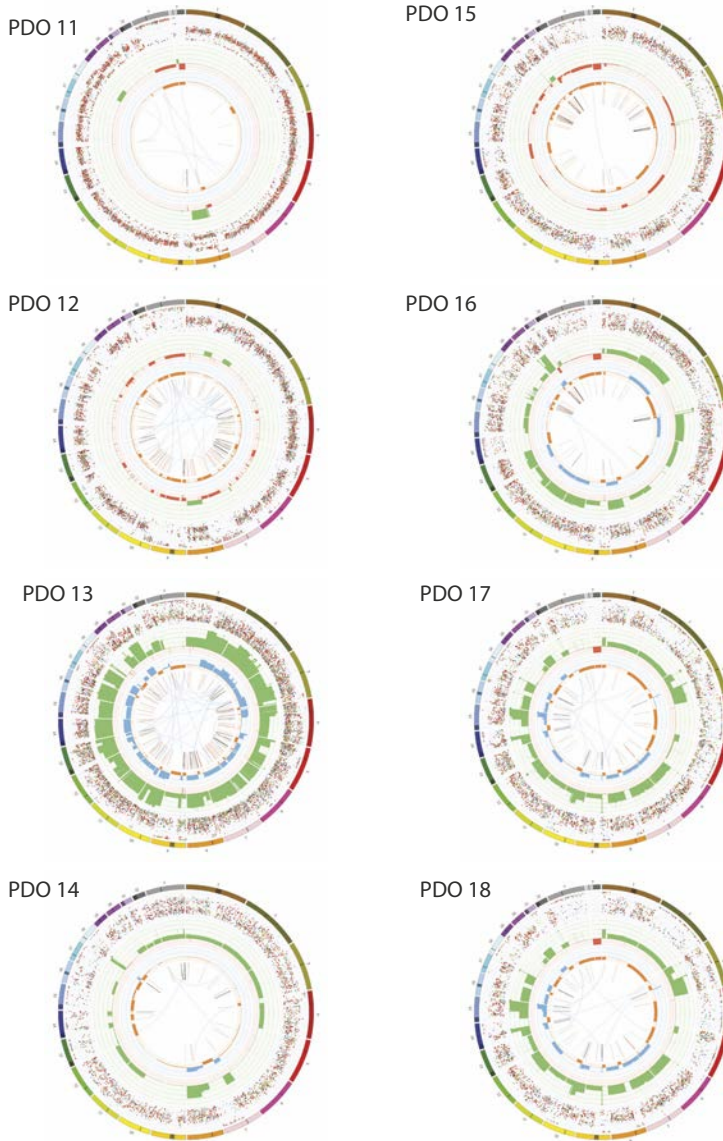


Figure S5. Circoplots of patient-derived organoids. For all PDOs for which germline DNA was available, circoplots were assembled based on WGS. The numbers in the outer circle represent the chromosomes. The second circle shows the somatic variants (incl. exon, intron and intergenic regions). Somatic variants are further divided into an outer ring of point mutations and an inner ring of INDELs. Each dot represents a single somatic variant scaled from 0 to 100% by its allele frequency score. Point mutations are colored according to the type of base change (e.g. C>T/G>A in red) and are in concordance with the coloring used in Alexandrov et al. that describes the use of mutational signatures (21). INDELs are colored yellow and red for insertions and deletions respectively. The third circle shows all observed tumor purity adjusted copy number changes. Copy number losses are indicated in red, green shows regions of copy number gain. The scale ranges from 0 (complete loss) to 6 (high level gains). If the absolute copy number is > 6 it is shown as 6 with a green dot on the diagram. The fourth circle represents the observed 'minor allele copy numbers' across the chromosome. The range of



► the chart is from 0 to 3. The expected normal minor allele copy number is 1, and anything below 1 is shown as a loss (orange) and represents a LOH event. Minor allele copy numbers above 1 (blue) indicate amplification events of both A and B alleles at the indicated locations. The innermost circle displays the observed structural variants within or between the chromosomes. Translocations are indicated in blue, deletions in red, insertions in yellow, tandem duplications in green and inversions in black. (B) Histogram showing the allele frequencies of all single base substitutions. Single base substitutions with a VAF score between 0.3 and 0.7 are considered as clonal which were used for *de novo* mutational pattern characterization. (C) Mutational spectra of all SBSs for each human intestinal organoid line used for *de novo* mutational pattern characterization. The six upper samples are non-exposed control organoid lines, while the two samples below are 5-FU exposed organoids. Different mutation types and the direct sequence context are indicated.

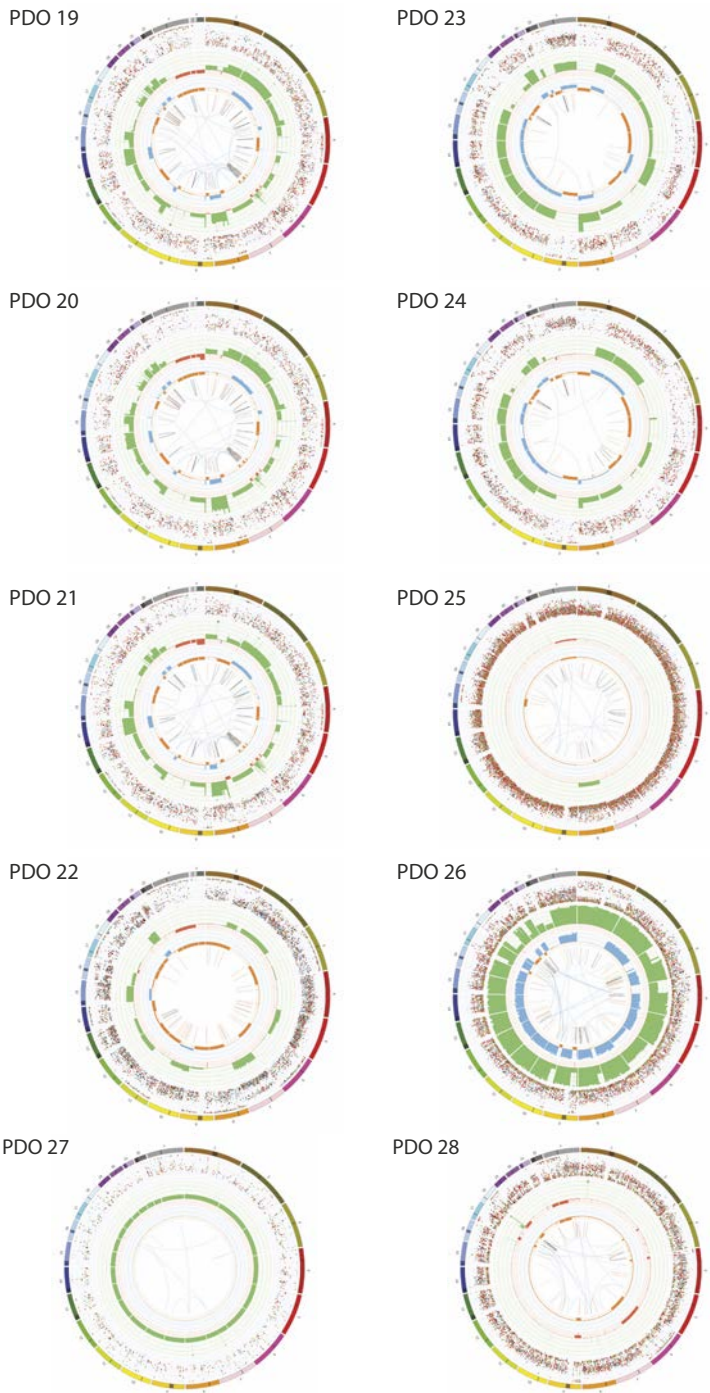
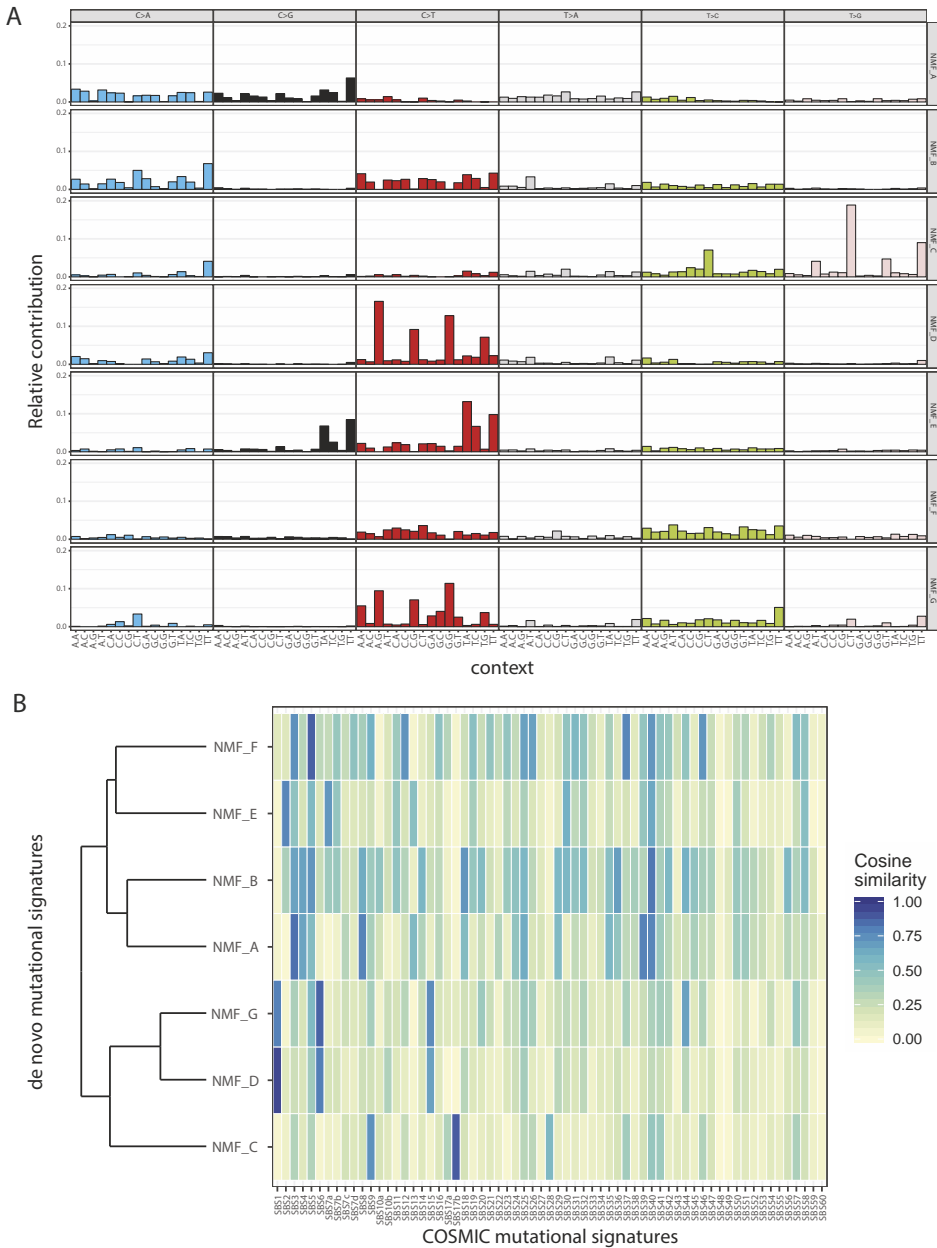


Figure S5. (continued)



5

Figure S6. Overview of the de novo mutational signatures detected in PDOs. A. Mutational spectra of the de novo mutational signatures. Different mutation types and the direct sequence context are indicated on the x-axis while the y-axis shows the mutation likelihood. B. Heatmap showing the cosine similarity scores, which is used as a measurement of closeness varying from 0 (distinct) to 1 (identical) for each indicated de novo mutational signature on the y-axis and all COSMIC signatures on the x-axis. NFM: Non-negative matrix factorization, SBS: single base substitution signatures.

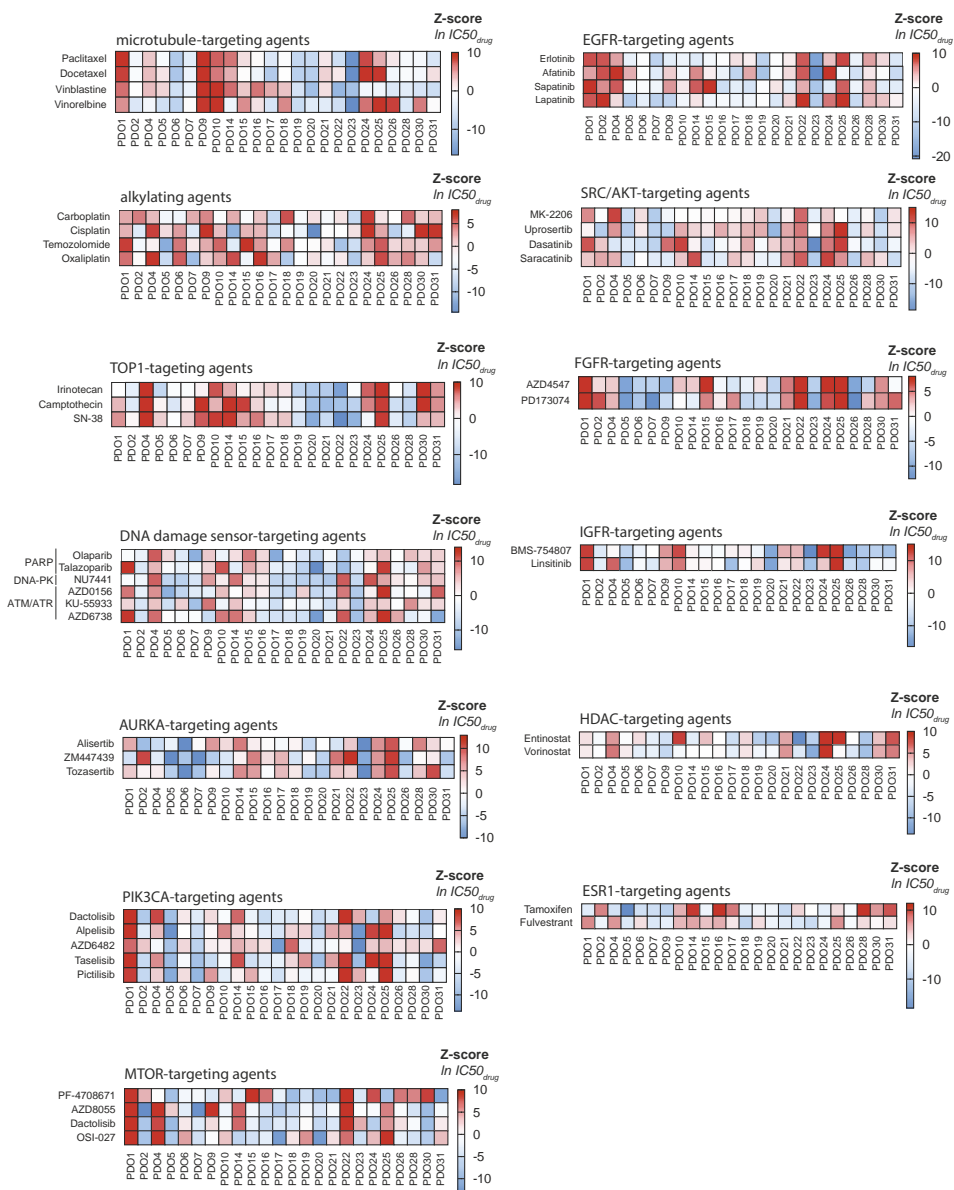
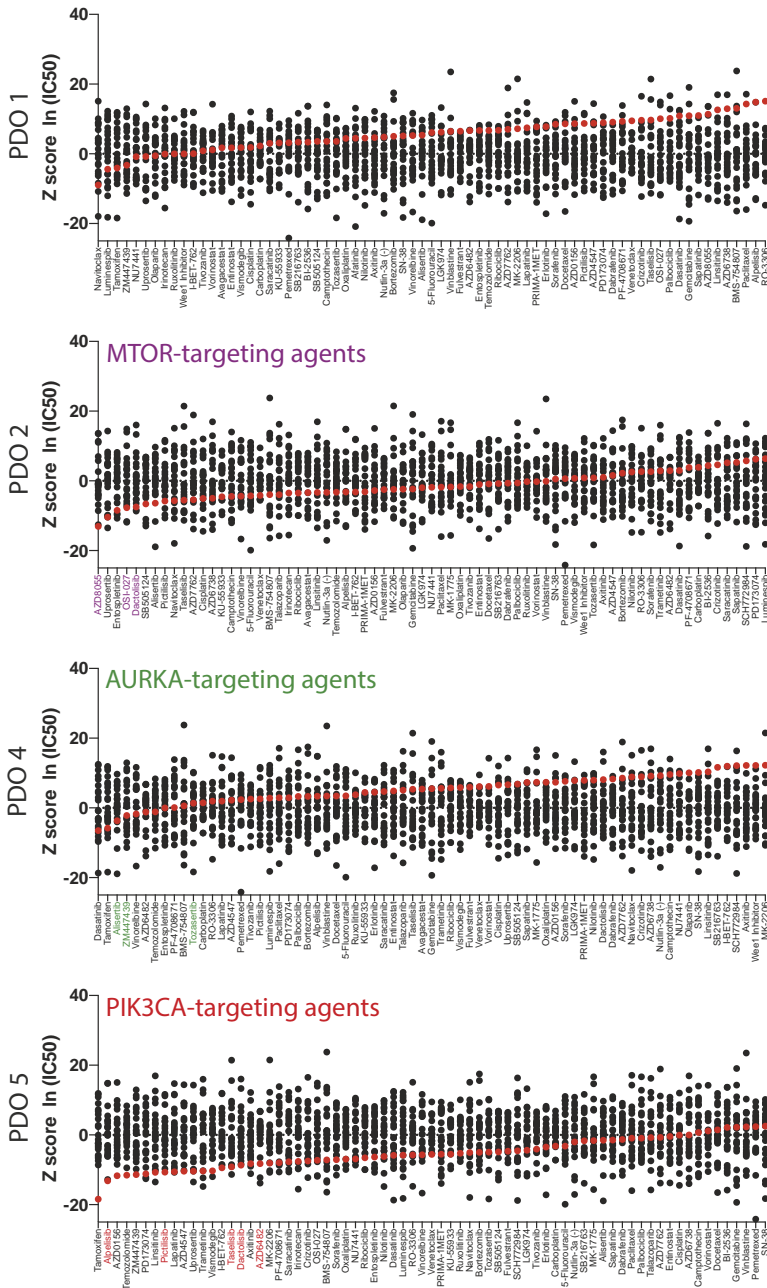


Figure S7. *In vitro* therapy response of PDOS. Here, the response of PDOs to therapeutic agents targeting the same biological process or molecular pathway is shown to highlight the similar response observed upon exposure to these agents. Depicted are Z-scores, calculated from the natural logarithm of obtained IC50 values. Here, response to microtubules-targeting agents, alkylating agents, TOP1-targeting agents, DNA damage sensor-targeting agents, AURKA-targeting agents, PIK3CA-targeting agents, EGFR-targeting agents, SRC/AKT-targeting agents, FGFR-targeting agents, IGFR-targeting agents, HDAC-targeting agents and ESR1-targeting agents is shown. High values (indicating resistance) are depicted in red, low values (indicating sensitivity) in blue.



5

Figure S8. Response of individual PDOs to a panel of 76 compounds. Here, compounds are arranged from most effective to least effective in each individual PDO line, similar to Figure 3C. Enrichment of compounds that target the same biological process or pathway is observed. Inhibitors targeting the same target are shown in identical colors.

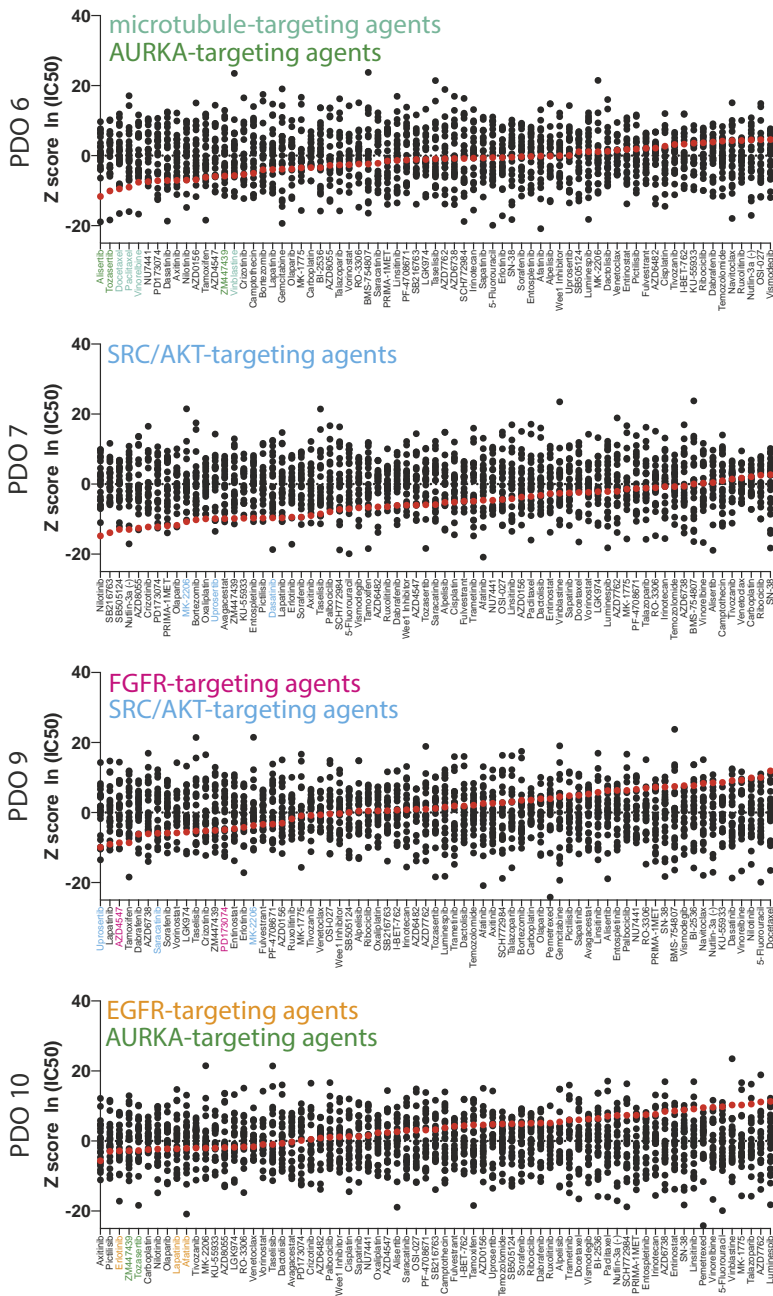
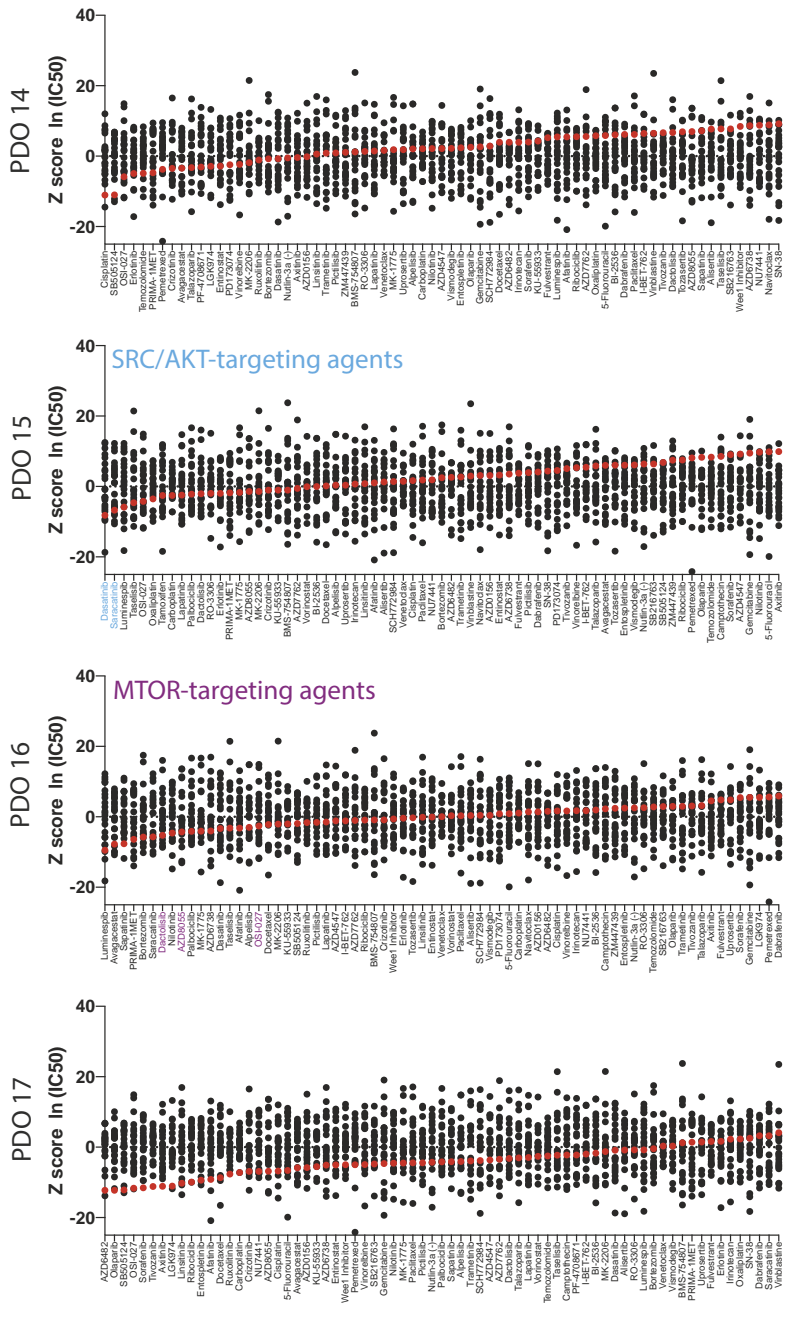


Figure S8. (continued)



5

Figure S8. (continued)

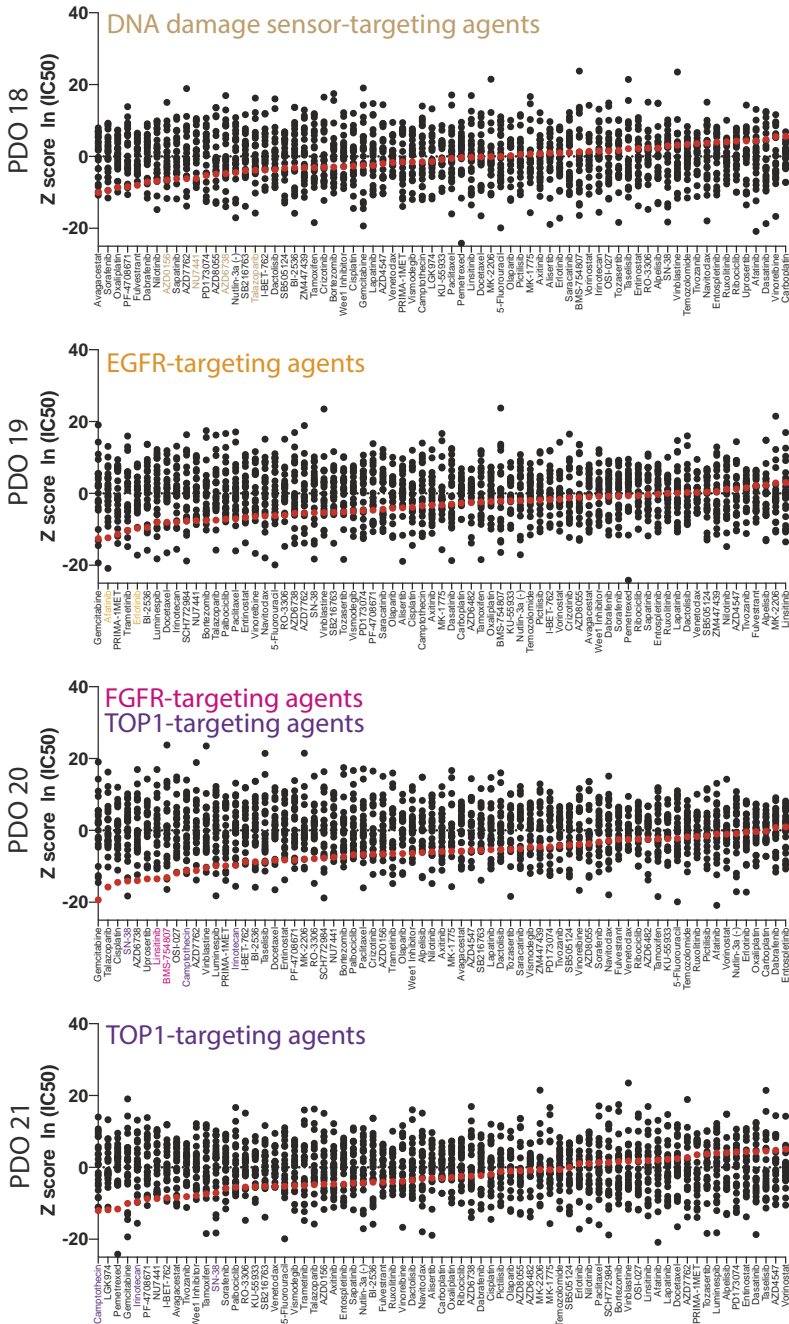


Figure S8. (continued)

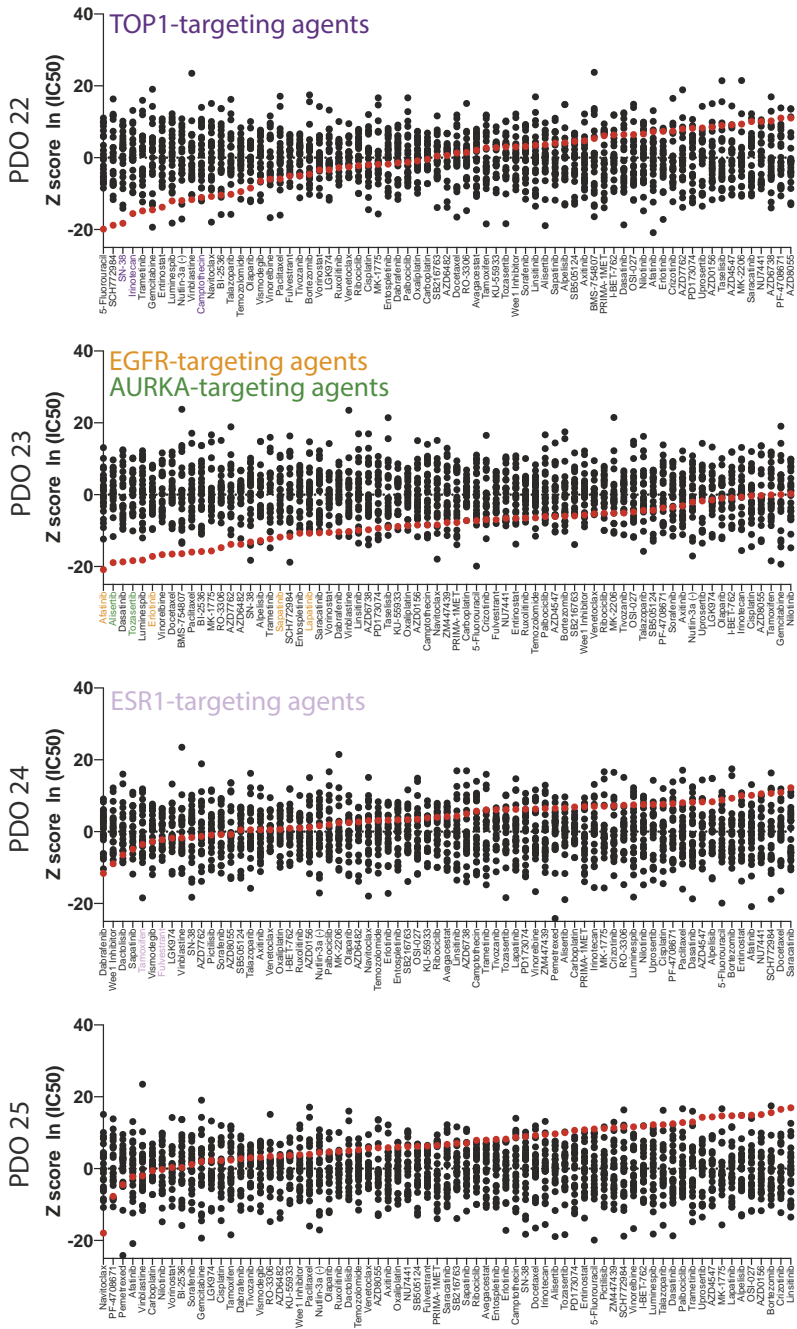


Figure S8. (continued)

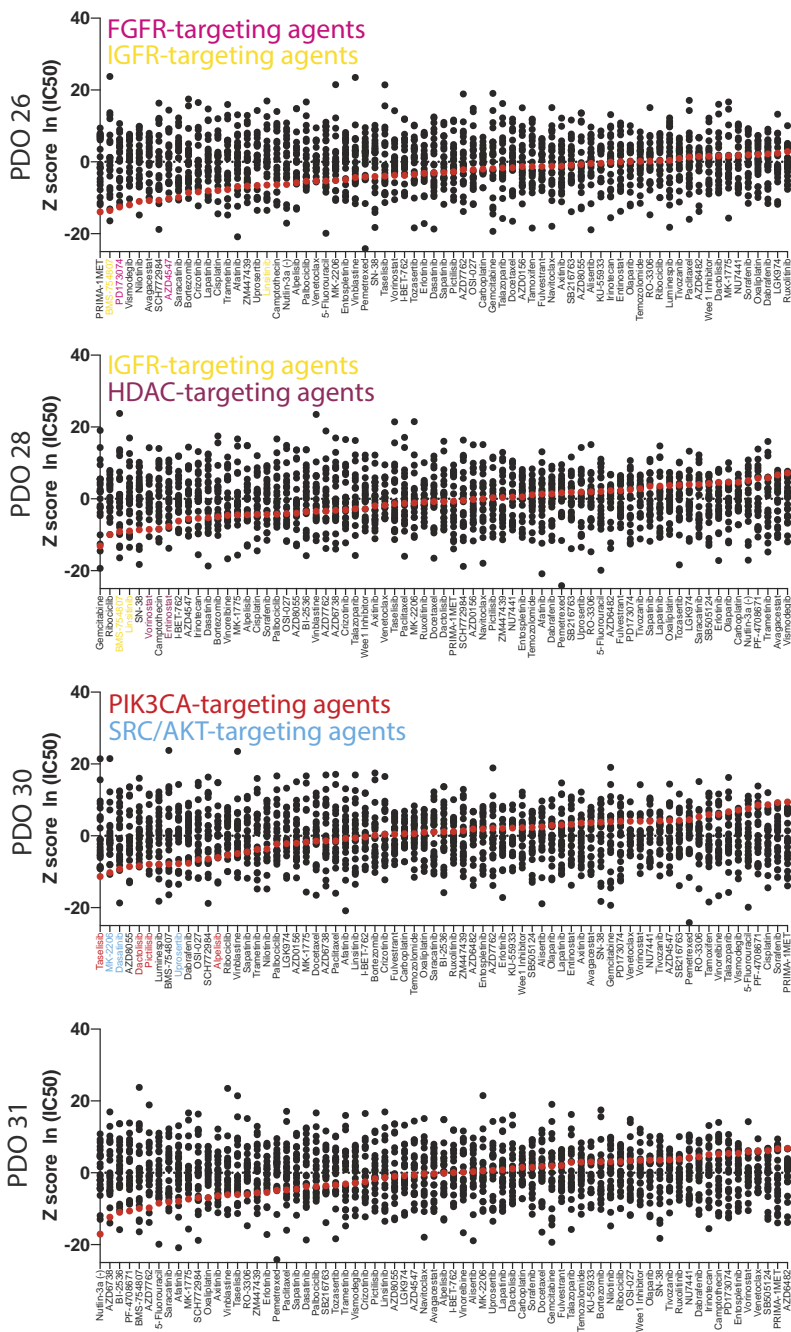


Figure S8. (continued)

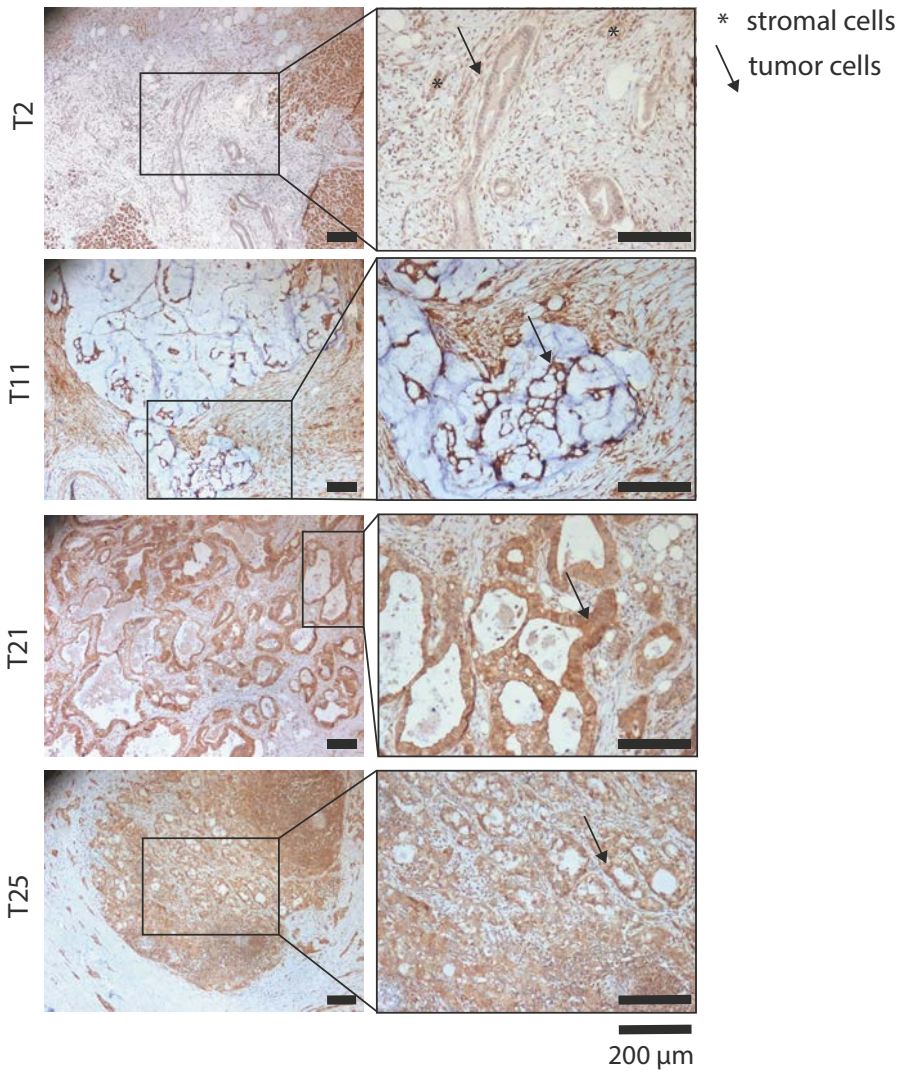


Figure S9. MTAP immunohistochemistry in patient tissue. For patient 2, 11, 21 and 25, MTAP IHC was performed on paraffin-embedded tissue. Indeed, MTAP staining was absent in tumor cells of sample T2, but present in all others, concordant with MTAP RNA status. Tumor cells are indicated by arrows, stromal (MTAP+) cells serve as internal control in the MTAP negative sample T2 and are indicated with an asterisk (*).

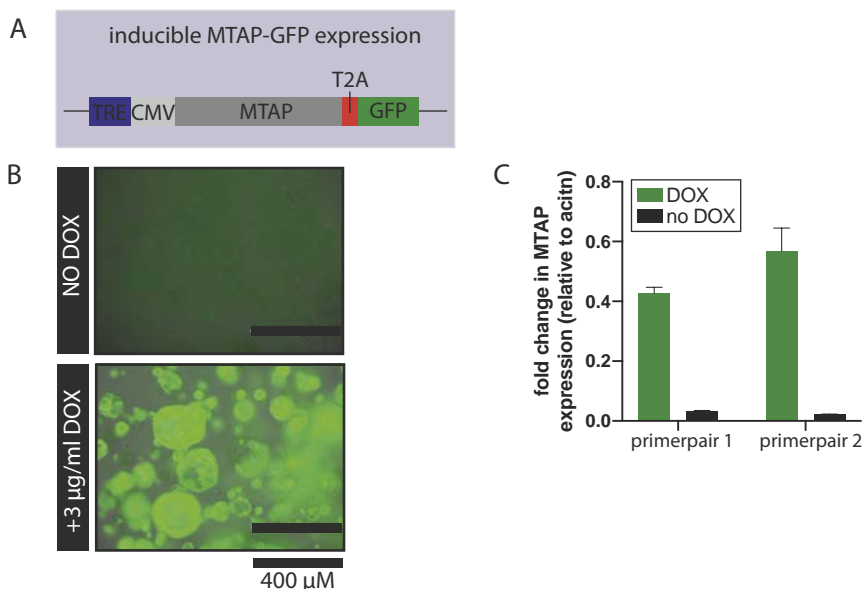


Figure S10. EZP01556 drug screens and induced MTAP expression in PDOs. A. Response of all tested PDOs to PRMT5 inhibitor EZP015556. MTAP⁻ lines are depicted in light blue, MTAP⁺ lines in dark blue. B. Schematic representation of the construct used to lentivirally overexpress MTAP in the PDOs. A cytomegalovirus promoter (CMV, grey) is preceded by a tetracyclin responsive element (TRE, blue) to allow inducible expression of the MTAP open reading frame (MTAP, dark grey). The MTAP encoding DNA is fused to the sequence encoding green fluorescent protein (GFP, green) by a T2A linker (T2A, red). This self-cleaving peptide results in cleavage of the MTAP coding peptide from GFP, once the mRNA is translated. C. Induction of GFP expression upon doxycycline administration. 24 hours after start of doxycycline administration, GFP expression is observed by fluorescence microscopy. No GFP signal is observed without doxycycline administration D. Quantitative RT-PCR confirming expression of MTAP upon doxycycline administration. Two primerpairs, amplifying different regions of the MTAP mRNA, were used to confirm the expression of MTAP in the doxycycline-induced cells (green bars), compared to non-induced controls (black bars). Experiment was performed in triplicate. Expression is shown relative to housekeeping gene actin. This experiment was performed with PDO 15. E. Quantification of the effect of induction of MTAP expression in a panel of two MTAP⁺ insensitive PDOs (dark blue), four MTAP⁻ PDOs (light blue) and three MTAP⁺ sensitive PDOs (red). Increase in AUC is compared to uninduced controls.

Table S1. Patient and PDO information. Relevant clinical information of patient participating in this study, and of the organoid lines generated from the patient-derived tissue.

Table S2. Mutations detected by WGS in PDOs in a panel of 202 genes commonly altered in pancreatic cancer. All mutations are shown that were detected in the panel of PDOs in the 202 selected genes.

Table S3. Comparison of the de novo mutational signatures with COSMIC signatures. De novo obtained mutational signatures (first column) are compared with the highest cosine similarity score (second column) to the COSMIC signatures (third column). The last column highlights the proposed etiology.

Table S4. Patient information related to treatment. For patient 1, 25, 28 and 31, relevant clinical information related to treatment is given such as date of surgery, pathology result, treatment given and details of measured treatment response.

All supplemental tables can be found at:

http://tiny.cc/Supp_ElseDriehuis

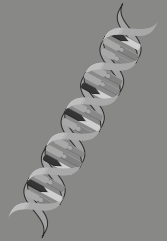
**ORGANOIDS AS
IN VITRO MODEL TO
STUDY TUMORIGENESIS**



CHAPTER

CRISPR/CAS 9 GENOME EDITING AND ITS APPLICATIONS IN ORGANOIDS

6



ABSTRACT

Organoids are three-dimensional structures derived from adult or embryonic stem cells that maintain many structural and functional features of their respective organ. Recently, genome editing based on the bacterial defense mechanism CRISPR/Cas9 has emerged as an easily applicable and reliable laboratory tool. Combining organoids and CRISPR/Cas9 creates exciting new opportunities to study organ development and human disease *in vitro*. The potential applications of CRISPR in organoids are only beginning to be explored. Here we summarize current status of application of CRISPR in organoids, and discuss both the advantages and potential pitfalls of using this technology in organoids.



Else Driehuis¹ and Hans Clevers^{1,2}

¹ Oncode Institute, Hubrecht Institute, Royal Netherlands Academy of Arts and Sciences (KNAW) and University Medical Center Utrecht, The Netherlands

² Princess Máxima Center for Pediatric Oncology, Utrecht, The Netherlands

INTRODUCTION

Since 2012, the technique of CRISPR/Cas9 genome engineering has rapidly developed. This technique, which exploits an innate bacterial defense mechanism against bacteriophages, is currently widely used in molecular biology. Applications and variations of this novel technique were published quickly after the first studies showed the potential of CRISPR-mediated genome engineering in mammalian cells. Discussions concerning the ethical questions raised barely can keep up with the speed at which this technique is developing.

The development of organoid culture from adult epithelial stem cells allows researchers to study the multicellular composition of tissue epithelia in a dish. In 2009, it was shown that organoids could be established from the epithelial lining of the intestine, and could be expanded indefinitely *in vitro* when provided with a basic matrix, necessary growth factors, and the stem cell-stimulating molecules Wnt and R-spondin (1). Since then, additional media requirements were established to allow the *in vitro* growth of many different epithelia, derived from both mouse and human tissue (1–20). Consequently, there has been a large increase in the number of research groups using organoids as a model system for a diverse range of applications. An organoid is best defined as a three-dimensional (3D) structure grown from stem cells and consisting of organ-specific cell types that self-organizes through cell sorting and spatially restricted lineage commitment (17,21,22).

CRISPR technology works well in adult stem cell-derived epithelial organoids. CRISPR technology was first applied in small intestinal and colon-organoids derived from cystic fibrosis patients, to demonstrate the feasibility of functional CFTR gene correction (23). Although the combination of both techniques generates a wide range of fascinating new opportunities, the number of published studies that combines the two is still limited since both techniques were relatively recently developed. In addition to giving an overview of this already published work, this review therefore highlights the recent advances made in the field of CRISPR/Cas genome engineering and organoid technology, and subsequently explores the potential of combining the two as a research tool.

CRISPR/CAS9

CRISPR (short for Clustered Regularly Interspaced Short Palindromic Repeats) is a defense mechanism of bacteria and archaea against viral infections. The presence of these tandem repeats in the *Escherichia coli* genome was first described in 1987, and was further characterized two years later (24,25). The biological function of these repeats was revealed 20 years later by researchers of a dairy company that were studying the bacteriophages infecting their dairy bacteria cultures. In the meantime, CRISPR loci and the genes associated with this genomic region (named Cas genes for CRISPR-associated genes) were found to be present in many bacterial species (26). It was proposed that the small unique sequences that are interspersed between the repeats were derived from bacteriophages, and that, somehow, the CRISPR/Cas system provided protection against these viruses

(27–29). Finally, in 2007, Barrangou and coworkers observed a direct relationship between integrated DNA sequences and resistance to phage infection (30). The researchers showed that, upon infection with phages, naive strains of *Streptococcus thermophilus* obtained new spacers that showed high sequence similarity to the infecting phages. After this integration, the bacteria became resistant to phage infection. Collectively, these data led the authors to propose a model of nucleic-acid based “immunity” that is heritable due to its stable integration into the bacterial genome.

Five types of CRISPR systems have been identified so far, of which type II is the most studied. All CRISPR systems function slightly differently and are summarized elsewhere (31). As the type II CRISPR system has been adapted as a genome-editing tool, we will only discuss this system in more detail here. The CRISPR system is characterized by a region in the bacterial genome where fragments of foreign DNA (protospacers) are integrated between repetitive DNA sequences (spacers) that are present in tandem in the host DNA. Transcription of this region results in formation of CRISPR RNA (crRNA), generating transcripts that contain both the spacer and protospacer sequence. The crRNA molecule subsequently hybridizes with the so-called transactivating CRISPR RNA (tracrRNA) to allow it to form a complex with the Cas9 nuclease, encoded by one of the Cas genes. After processing of the crRNA and tracrRNA by RNase III and Cas9, the spacer sequence guides Cas9 to its target: a complementary DNA sequence in the genome of the invading organism. Here, the nuclease introduces a double strand break (DSB) in the DNA. Protospacer-complementary DNA can only be cut by the nuclease if it is followed by a protospacer-adjacent motif (PAM), a consensus sequence that differs between Cas9-nucleases from different bacterial strains. So, as the nuclease cuts the phage DNA, the absence of the PAM in the host genome protects the bacterial DNA from self-destruction. In addition to recruiting Cas9 to potential target sites, the PAM sequence has been shown to trigger activation of Cas9 nuclease activity (32). A schematic overview of the mechanism of action of the CRISPR system is given in Figure 1.

Even before thorough mechanical understanding of this system, it was already suggested that CRISPR and its programmable nuclease could be exploited for genome editing in molecular biology (33). The CRISPR system is much more flexible than existing techniques that use proteins such as transcription activator-like effectors (TALEs) and zinc-finger proteins. Although effective for targeting DNA in a sequence-specific manner, these systems utilize proteins that contain a DNA-binding domain (rather than nucleic acids) for their target specificity. Consequently, this protein domain needs to be extensively reengineered for each new target sequence (34). Additionally, as the structure of the targeted protein needs to be maintained, these techniques are limited in the number of DNA sequences that can be targeted. As CRISPR is based on complementary strand hybridization of DNA, it might therefore not be surprising that the potential of CRISPR as a tool for genome editing was already noted early on. Since the CRISPR system consists of a universal endonuclease whose activity is targeted to any desired location by a small RNA molecule, this could potentially make genome editing much faster and easier.

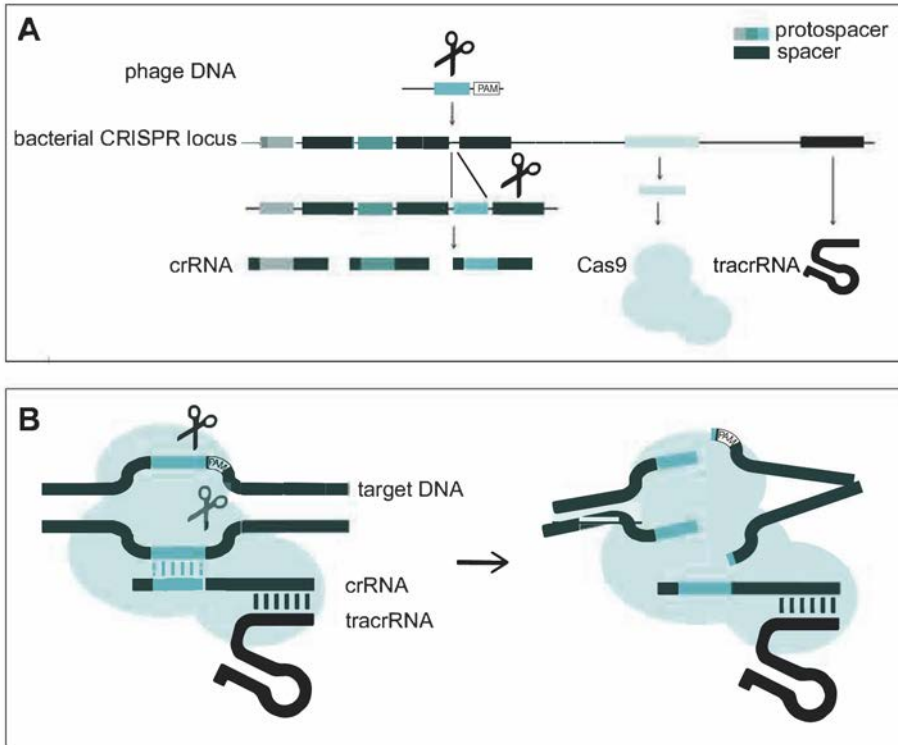


Figure 1. The mechanism of action of the type II CRISPR system of *Streptococcus pyogenes*.

A: a region of viral DNA is excised and integrated as protospacer between the repetitive elements (spacers) present in the bacterial CRISPR locus. Trimming of the resulting transcript generates crRNAs that encode both viral and bacterial DNA. In addition to crRNAs, the nuclease Cas9 and tracrRNA molecules are transcribed from nearby regions of the CRISPR locus. B: the complex formed by assembly of Cas9, crRNA, and tracrRNA can cut DNA regions that are complementary to the spacer sequence encoded by the crRNA. Importantly, the presence of the PAM is essential for the nuclease activity of the complex. When both spacer and PAM are detected in the phage DNA, Cas9 introduces a DSB into the virus genome. However, as the PAM is only present in the phage genome and absent in the bacterial genome, the nuclease activity is only guided toward the invaders DNA. In this way, the absence of the PAM prevents the host genome from self-destruction

After elucidating its different components and their function, the type II CRISPR system was quickly adapted as a tool for genome editing. The first reports using CRISPR-based editing systems *in vitro* were published in 2012 (30,35). As early as January 2013, CRISPR was adapted to function in mammalian cells (36,37), and soon the first applications of the technique were reported. One of these early studies showed effective genome editing of the zebrafish germline (38). Since then, new applications and improvements of the technique have appeared with ever-increasing frequency in many different fields. One of

the most profound consequences of the introduction of CRISPR as a genomic engineering tool is the potential to manipulate genes in the germline. Up to now, genetically modified fish, flies, mice, and primates have been created from CRISPR-edited zygotes (39).

CRISPR provides researchers with a tool to introduce a DSB at any desired location in the genome with high specificity. Under physiological condition, a DSB can be repaired via one of two repair pathways: nonhomologous end joining (NHEJ) or homology directed repair (HDR). NHEJ is the predominant repair pathway for DSBs in the DNA and is active throughout the cell cycle. As the name implies, this repair pathway does not require a homologous template to repair a DSB. Therefore, NHEJ-mediated repair is more error-prone than HDR and can result in small “scars” (small insertions or deletions) at the site of the repaired DSB. HDR has a lower capacity for repair than NHEJ and requires a template to repair the DSB. Therefore, HDR can only occur during S/G2-phase of the cell cycle, when a sister chromatid is present to serve as a template. Although more complex, HDR repairs DNA with more precision and has a much higher fidelity than NHEJ. Through homologous recombination of carefully designed DNA templates, virtually any change can be engineered near the DSB without leaving scars.

In the four years since the CRISPR genome editing has been introduced, adaptations of the system have expanded the “CRISPR toolbox” significantly. The technique can now, amongst others, be applied to either activate or repress gene expression, cause epigenetic modifications, and detect RNA abundance and localization. Furthermore, additional tools were developed, amongst which a mouse strain that constitutively expresses Cas9 (40). Organoids established from these mice have a higher efficiency of acquiring desired mutations upon introduction of sgRNAs into the cell.

Organoid culture

Although the term “organoid” has lingered around for much longer to describe aggregates of cells, the first studies describing self-organizing structures grown from stem cells appeared about a decade ago. Sasai and colleagues described the culture of pluripotent stem cells in “balls of neural cells that self-organize” (18). Our laboratory described that single adult stem cells isolated from mouse intestine could give rise to 3D structures that could be maintained indefinitely when given the correct growth factors and stimuli (1). In these “mini guts,” stem cells gave rise to progeny that represented all differentiated cell types of the gut.

Organoid cultures can be classified into two subtypes: organoids derived from tissue-restricted adult stem cells (ASC) and those that are derived from embryonic or induced pluripotent stem cells (ESC or iPSC), which are collectively named pluripotent stem cells (PSC). Organoids more closely resemble their tissue of origin than “classical” cell lines that are grown in 2D. While cell lines typically are homogenous and harbor oncogenic mutations to maintain proliferative capacity *in vitro*, organoids contain multiple cell types and, to a certain extent, recapitulate the 3D organization of the tissue. Importantly, organoids do not require immortalization before *in vitro* culture and thus allow the study

of primary cells over longer periods of time. In line with this rationale, organoid culture can be seen as a missing link between monolayer cultures and *in vivo* models (41).

Stem cells derived from mice and humans have been used to establish ASC-organoid lines of intestine, stomach, salivary gland, esophagus, pancreas, liver, breast, lung, prostate, fallopian tube, oral mucosa and taste bud (1,3,6,8,9,13–15,20,42–45). 3D reconstructions of organoids derived from intestinal and liver organoids are depicted in Figure 2. Organoids derived from ASC generally only contain epithelial cells. As an exception, organoids derived from neonatal intestinal material were reported to consist of both epithelial and mesenchymal cells (7). PSC-derived organoids can contain cells derived of all three germ layers, depending on the tissue attempted to mimic and the differentiation protocol applied. Among others, ESC-derived organoids have been described as a model for brain, optic cup, kidney, intestine, stomach, lung, thyroid gland, and liver (4,5,10–12,16,46). An overview of the different organoid types and how they are established is given in Figure 3.

Despite the advantages of organoid technology, there are some characteristics of this culture system that have to be kept in mind. For example, ASC-derived organoids only consist of epithelial cells, which makes this model unsuitable to study the interaction between epithelial cells and other cell types such as immune or mesenchymal cells. Nevertheless, adding such cells or their products of interest separately to the organoid cultures is feasible, allowing study of the relevant contribution or interactions of these cells with the epithelial cells present in the organoids (47,48). Alternatively, PSC-derived organoids can be used, as these have the potential to produce cell types derived from all three germ layers.

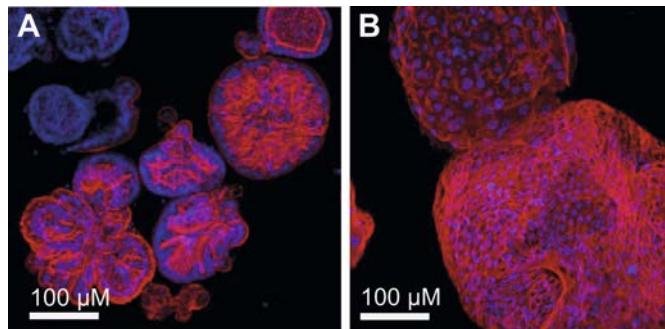


Figure 2. Morphology of ASC-derived organoids. Three-dimensional (3D) reconstruction of the midsection of ASC-derived colon and liver organoids, stained for the actin cytoskeleton (red) and nuclei (blue) and imaged by confocal microscopy. *A*: human intestinal organoids. *B*: human liver organoids. (Kretzschmar K, Gerhart H, Clevers H, unpublished data).

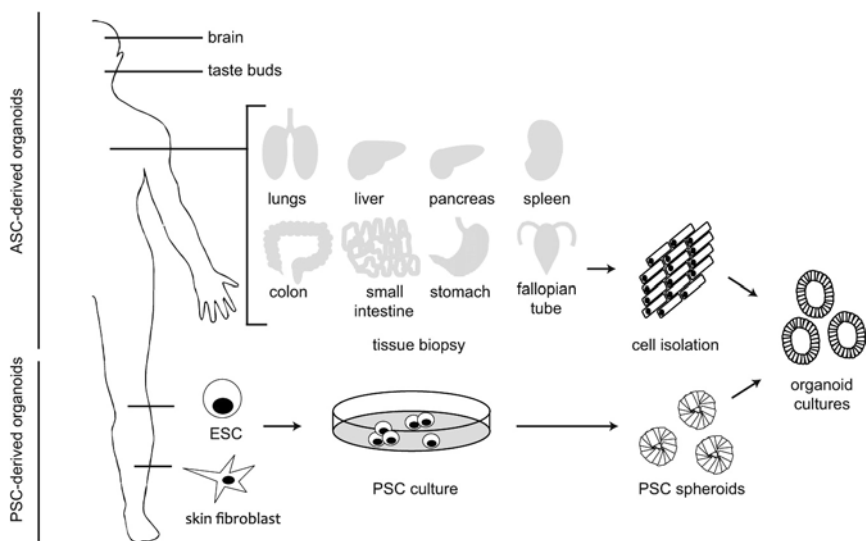


Figure 3. Establishment of ASC- and PSC-derived organoids. ASC-derived organoids can be established from either digested tissue pieces or specific cell populations (such as *Lgr5*⁺ stem cells). After isolation of the desired cell population, cells are suspended in Matrigel and kept in medium containing growth factors. The exact composition of the medium depends on the cultured tissue type. PSC-derived organoids can be obtained either from ESCs or iPSC, which are derived from, e.g., skin fibroblasts. Depending on the differentiation protocol applied, stem cells can be differentiated *in vitro* toward different organoid types. Redrawn from (21,72).

CRISPR and organoids

In 2013, it was shown that CRISPR could be applied in mouse and human intestinal organoids either to knock out a gene or to correct a disease-causing mutation (23). We first showed the feasibility of CRISPR targeting in wildtype mouse small intestinal organoids by causing frame shifts in the two *APC* alleles, *APC* being the most prominent tumor suppressor in intestinal cancer and a negative regulator of WNT signaling. The resulting organoids indeed grew in a WNT-independent fashion, while sequencing confirmed the presence of NHEJ-based “scars.” We then asked whether HDR could be utilized to repair gene mutations in the gene coding for the cystic fibrosis transmembrane conductor receptor (*CFTR*) in organoids derived from cystic fibrosis (CF). Mutations in the *CFTR* gene in CF patients result in an inactive chloride channel protein, causative of the disease. Organoid cultures derived from CF patients offer an ideal platform for *in vitro* research and diagnostics. Previously, it was shown that colon organoids established from CF patients show reduced or absent swelling upon exposure to forskolin, a cyclic AMP-inducing agent (49). When the *CFTR* mutation was restored using CRISPR, the organoids showed restored swelling in response to forskolin. Moreover, the detected level of swelling was comparable

to that of wildtype organoids, confirming that *CFTR* is the single impaired gene causing this effect. Although this use of CRISPR is not directly amenable for clinical applications, this study did reveal the potential of CRISPR for gene correction in monogenetic diseases. Moreover, it showed the potential of combining organoid and CRISPR techniques in research. Taken together, organoids can be modified by CRISPR/Cas9, both by utilizing “simple” NHEJ and by HDR, the latter allowing for more complex genetic modifications. An overview of the applications of CRISPR in organoids that are discussed in this review is given in Figure 4.

CRISPR in ASC-derived organoids

The introduced mutation of *APC* suggested that CRISPR could thus be used to modify the genome of organoids to model tumorigenesis. Tumorigenesis is characterized by multistep genetic changes that result in inactivation of tumor suppressor genes and activation of oncogenes, which collectively drive cancer growth. CRISPR enables the introduction of mutations at specific sites in the genome, which makes it possible to specifically modify

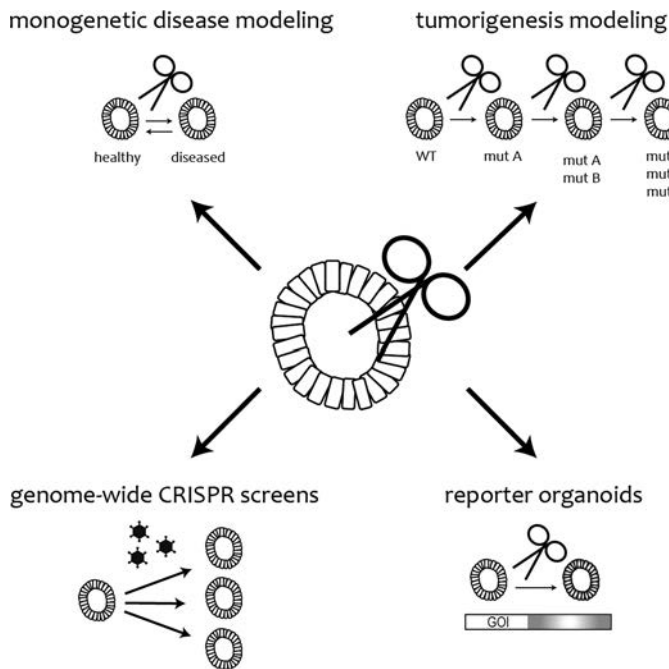


Figure 4. Applications of CRISPR-based gene editing in organoids that are discussed in this review. CRISPR can be applied to organoid cultures to model monogenetic diseases or tumorigenesis *in vitro*, to perform genome-wide CRISPR screens or to create reporter organoids. WT, wildtype; MutA; CRISPR-induced mutation in gene A; MutB, CRISPR-induced mutation in gene B.

commonly mutated genes in cancer to create a model for tumorigenesis. Inactivation of tumor suppressor genes such as *APC* usually only requires the induction of frameshifts by CRISPR-induced NHEJ. Activation of proto-oncogenes typically relies on HDR-mediated knock-in of the desired oncogenic mutation.

Following the “Vogelgram” (a sequence of mutations accompanying the adenoma to carcinoma transition in colon cancer as originally suggested by Fearon and Vogelstein (50)), two independent studies showed that CRISPR can be used to efficiently introduce mutations that are found in colon cancer in organoids (51,52). The genes targeted in these studies were *KRAS*, *APC* (see above), *TP53*, and *SMAD4*. *KRAS* is an oncogene that is commonly altered in colon cancer, resulting in a constitutively active protein. With the use of a DNA template carrying the *KRAS* G12D mutation that is commonly found in cancer, this specific genomic alteration was introduced in organoids by HDR-directed DNA repair. For the other three genes, that are all tumor suppressors, NHEJ-directed repair of the DSB introduced in the coding region of these tumor suppressors resulted in inactivation of these genes. Phenotypically, the genetically modified organoids showed characteristics observed cancer, including chromosomal instability. When transplanted into mice, mutant organoids grew out as tumors that, depending on the number of genes altered by CRISPR, could be characterized by varying levels of differentiation and invasive behavior.

In recent years, it has become clear that colorectal tumors are molecularly heterogeneous, and that this diversity is reflected in the premalignant precursor lesions (53). In a study published in 2015, *BRAF* V600E mutant organoids were used as a model for the precursor lesions of sessile serrated adenomas (SSA), a tumor type that is both histologically and molecularly distinct from the “classical” *APC* tumors and their precursor lesions (54). The researchers studied the effect of TGF- β on these two different tumor precursor lesions, to see whether there was a difference. As it showed impossible to culture SSAs or their corresponding precursor lesions, the researchers used CRISPR-modified organoids to model these tumor precursor lesions *in vitro*. SSAs are characterized by activating mutations in the proto-oncogene *BRAF*, and the commonly found V600E mutation was introduced in wildtype organoids using CRISPR technology. Interestingly, while exposure to TGF β induced apoptosis in *APC* organoids, the *BRAF* V600E organoids did not show this response. Moreover, in response to TGF β , the *BRAF* V600E organoids underwent epithelial-to-mesenchymal transition (EMT), a phenotype associated with poor prognosis. This shows that TGF- β can have opposing effects on different tumor precursors types, inducing cell death in one and invasive behavior in another.

An alternative way in which genetically modified organoids can contribute to research is illustrated by a recent study (55). In this study, EGFR and MEK inhibitors were tested on a panel of colorectal organoids lines. The goal was to determine the effect of *KRAS* mutation status on the sensitivity to these drugs. In this work, the authors showed that activation of the oncogene *KRAS* decreased sensitivity to combined EGFR/MEK inhibitory treatment. To confirm that this difference in sensitivity was a direct result of *KRAS* status, CRISPR was used. In a *KRAS* wildtype colon tumor line that was sensitive to the combinational therapy,

the introduction of a *KRAS* G12D mutation via CRISPR resulted in a loss of drug sensitivity. As the genetic makeup of these isogenic lines is otherwise identical, this finding proved that the loss in drug sensitivity was a direct consequence of the introduced activating *KRAS* mutation. In this way, CRISPR-guided genetic modification of organoids can serve to strengthen conclusions based on large drug screens. More specifically, if a correlation between gene status and drug response is detected in a large cohort of tumors or cell lines, CRISPR can be used to validate these results and show a direct relation between the genetic alterations of interest and the drug sensitivity.

Other epithelial organoid types have also been successfully targeted using CRISPR. Organoids derived mammary ducts of a inducible *PIK3CA* overexpression mouse model have been used to introduce inactivating mutation in *Mll3*, a histone methyltransferase commonly mutated in breast cancers (56). Hyperplasia could be observed upon transplantation of *Mll3* negative, but not *Mll3* wildtype organoids. Moreover, when tumor formation was induced by tamoxifen administration (resulting in *PIK3CA* overexpression), *Mll3* negative tumors developed much faster than their *Mll3* wildtype counterparts. Also, mouse tracheal cells have been successfully modified using CRISPR. To study the role of the transcription factor Grainyhead-like 2 (*Grhl2*) in airway epithelium, a knockout of this gene was created in organoids using CRISPR technology (57). The authors found that loss of this transcription factor prevents proper differentiation of stem cells into ciliated cells and resulted in decreased barrier function. In summary, these studies show how CRISPR/Cas provides researchers with the possibility to rapidly create combinations of multiple genetic changes in human cells in culture, something that was previously only feasible in animal models.

CRISPR IN PSC-DERIVED ORGANOIDS

CRISPR technology has also been applied in PSC-derived organoids. PSC-derived organoids were used to study the disease dyskeratosis congenita (DC). This disease, caused by a failure to maintain telomere length, is characterized by degeneration of highly proliferative tissues such as the hematopoietic system, epidermis, and gastrointestinal tract (58). One of the most commonly affected genes in DC is *DKC1*, the gene encoding Dyskerin. Dyskerin is a protein that is critical for telomere maintenance (59). In this particular study, the researchers created isogenic pairs of iPSCs. They did this either by establishing these cells from a healthy individual and subsequently introducing the disease-causing mutation, or, reversibly, by establishing iPSCs from an affected individual and restoring the mutation to wildtype. After introduction of the desired mutation, stem cells were differentiated toward an intestinal phenotype and cultured as human intestinal organoids. Indeed, in *DKC1* defective organoids, telomeres were shorter when compared with isogenic *DKC1* wildtype controls. Furthermore, while wildtype organoids matured into gut-like tubes containing budding crypts, the mutant organoids failed to form these cryptlike structures

in vitro. These results agree with clinical findings, where DC patients present with mucosal ulceration and malabsorption. Interestingly, the authors found that restoration of WNT-signaling in these diseased organoids could partially rescue the phenotype, a finding that might carry important implications for the clinic.

The other study that applies CRISPR in PSC-derived organoids was published in 2015. Here, Freedman et al. showed that CRISPR can be used to model disease phenotypes in hPSC-derived organoids (60). These researchers created an *in vitro* model for the monogenetic disease polycystic kidney disease (PKD). As the name implies, patients affected by PKD present with intrarenal cystic structures that eventually disrupt the architecture of the kidney. CRISPR was used to introduce bi-allelic truncating mutations in either *PKD1* or *PKD2*, the genes causative for PKD. The authors subsequently described a protocol to differentiate hPSCs into kidney organoids. Indeed, after differentiation, organoids derived from mutated hPSCs displayed a different phenotype compared with isogenic wildtype organoids. Although the initial stages of differentiation appeared identical between *PKD* mutant and control organoids, *PKD*-mutant organoids behaved differently when differentiated toward more mature kidney cells. In addition to the tubular structures that develop in wildtype hPSC-derived organoids, maturation of PKD organoids results in the formation of large cystic structures. These *in vitro* findings are in line with clinical observations, where PKD patients present with large renal cysts.

Two important conclusions can be drawn from these findings. First, in addition to ASC-derived organoids, PSC-derived organoids are amenable to genome editing by CRISPR. Second, PSC-based organoids create the unique opportunity to introduce pathogenic mutations in a precursor cell-state, where the mutation does not necessarily result in a phenotype. This allows us to study the molecular effects of mutations that would normally prevent the affected cell type from growing in culture. In theory, an *in vivo* cell type-specific phenotype will only appear *in vitro* when organoids are differentiated towards that specific cell type.

When kept in an undifferentiated state, mutant cells can be therefore expanded and studied using this approach.

LIMITATIONS OF THE USE OF CRISPR/CAS9 IN ORGANOIDS

Although effective, there are some limitations to using organoids in combination with CRISPR. Methods for the lentiviral transduction (61), liposomal transfection (23,51), and electroporation (52) of organoids have been described. A detailed protocol describing the method of electroporation for genetic engineering of human intestinal organoids was recently published (62). However, the efficiency of transfection using any of these approaches is relatively low compared with other culture systems. In addition, not all cells that are transfected with the required CRISPR components acquire the desired mutation.

Transfected stem cells must be expanded clonally and screened to confirm the clonal presence of mutations and their mono- or bi-allelic nature. When introducing a specific mutation using homology cassettes, validation of the resulting genetic alterations in one or both alleles is essential. Generally, when one allele is targeted via HDR, the other allele contains a frameshift introduced by NHEJ. Therefore, introduction of homozygous nonsynonymous mutations occurs with an even lower efficiency. In summary, the number of cells that are required to establish an organoid line with the desired genomic alteration is relatively high and dependent on the cell origin, cell type, and desired genetic alteration. As such, a method to select cells with the desired mutation is therefore essential when performing CRISPR experiments in organoids. Such selections can be based on growth factor withdrawals when the targeted gene is known to be directly involved in growth factor dependence (selection of *KRAS* mutant organoids by EGF withdrawal, and *APC* mutants by WNT withdrawal (51)). Other selection methods include the use of Cas9 or sgRNA constructs that additionally encode fluorescent proteins. After transfection, efficiently transfected cells can be enriched using FACS. A third approach involves the introduction of antibiotic resistance cassettes using HR-directed repair. As HDR-directed repair occurs with a lower frequency than NHEJ-directed repair, this approach does decrease efficiency.

Second, the number of cells that can be kept in culture as organoids is restricted by the cost of growth factors and Matrigel as well as by the growth rate of organoids, which, depending on tissue type, can be slow. It is not unlikely that some of these potential limitations might be overcome in the future, as new techniques that can be used to transfect, culture, and select organoids are still being developed. For example, a synthetic gel has now been described which can replace Matrigel (63).

FUTURE DIRECTIONS

Genome-wide CRISPR screens

After the initial reports on the use of this technique in 2013, CRISPR was quickly applied to genome-wide genetic screens. Before the introduction of CRISPR, reverse genetic screens were performed by using mutagens that damage the DNA in a random fashion. Therefore, subsequent identification of the causative mutations (that could be located anywhere in the genome) was required, which was a time-consuming and laborious process (64). Later on, this technique was largely replaced by RNA interference (RNAi) studies, where mRNA molecules are targeted for degradation when small complementary RNA oligos are introduced into the cell. Nevertheless, RNAi in general leads to incomplete gene silencing and only affects the transcriptome, not the genome. From this perspective, this technique is not a good model system for the genetic changes that underlie biological processes such as tumorigenesis. CRISPR allows direct modelling of genetic alterations underlying such processes. The first studies using CRISPR in genome-wide screens were already published early in 2014 (40,65–67). In these reports, sgRNA libraries were used

to find genes involved in resistance to drugs and bacterial toxins in an unbiased manner. For reasons that were already mentioned previously, organoids represent a more suitable model system for tissue composition and structure than the 2D cell lines that were used in the studies described above.

To our knowledge, genome-wide CRISPR screens in organoids have not yet been reported. However, in a recent study, organoid cultures were used to validate the results obtained by performing such a screen in cell lines (68). This particular study aimed to identify targets of *Clostridium difficile* toxins by using a genome-wide sgRNA library in HeLa cells that stably expressed Cas9. By using increasing concentrations of toxins, the authors could select for cells that lost sensitivity to these molecules. *FZD2*, the gene encoding the membranous WNT-receptor Frizzled2, was found to be one of the top hits of the screen. Cells with inactive *FZD2* (caused by infection with *FZD2* targeting sgRNAs from the library) were enriched in the toxin-resistant cell population. Because HeLa cells are not the optimal *in vitro* model to mimic the colonic infection that is observed in infected patients, the authors used human colon organoids to study the effect of *FZD2* knockout *in vitro*. They found that *FZD2* mutant organoids were not affected by the presence of *C. difficile* toxin B, whereas wildtype organoids showed decreased viability upon exposure to this compound. Furthermore, they found that the interaction between *FZD2* and the *C. difficile* toxin B prevented the binding to WNT. As WNT signaling is essential for stem cells to maintain their undifferentiated state it was expected that exposure to inactivated toxin B would still inhibit organoid growth, as long as the interaction between the toxin and *FZD2* was not disturbed. Indeed, this is what the authors observed. These findings suggest that, by disrupting WNT signaling, the binding of *C. difficile* toxin B may directly contribute to the disruption of the colon epithelium upon infection. Indeed, this detrimental effect could be rescued by the addition of with CHIR99021, a WNT pathway activator acting downstream of *FZD2*.

This work underscores the added value of organoid cultures over 2D cell lines. In this particular case, the biological effect of the toxin-FZD interaction could not have been understood by merely working with 2D cell lines, as these do not mimic the stem cell-based maintenance of the intestinal epithelial sheet. The authors of this work elegantly combined the use of 2D cell lines for high-throughput screening with organoid culture to validate their results, as this was the more suited *in vitro* model system to model intestinal epithelium. We expect that high-throughput screens such as CRISPR-based whole genome library screens become feasible to perform in organoids, both cost- and timewise. As DNA delivery approaches are improving and less expensive alternatives for Matrigel are being developed, these limitations might be overcome in the future.

Reporter organoids

Apart from modeling genetic alterations that occur during tumor formation, CRISPR can also be applied to introduce reporter sequences into organoid DNA. Prior to CRISPR

technology, introduction of a reporter gene often included the expression of a transgene under the regulation of the promoter from the gene of interest (GOI). Although valuable, there are obvious limitations to this technique. Most importantly, regulation of gene expression is highly dependent on the genomic context, and thus placing a reporter gene outside its genetic context will impair this regulation. With the aid of CRISPR, we can now introduce reporter proteins in the endogenous site of virtually any GOI, either by inserting the reporter sequence downstream of the gene product or by replacing it. For example, if a fluorescent reporter is introduced under the endogenous regulation of a cell type-specific marker, this will create the opportunity to set up a large-scale screen to test a wide range of differentiation conditions. In such a scenario, the readout will be fluorescence, making it much quicker and easier than other readouts such as gene expression analysis or immunohistochemistry. Such a tool will greatly aid the establishment of differentiation protocols that push organoids into a range of developmental fates.

CONCLUDING REMARKS

In this review, we discussed the combined use of CRISPR-based genome editing and organoid technology. Organoids derived from pluripotent stem cells are the model of choice to study developmental processes “in a dish” or to generate model tissues (such as the brain) that cannot be grown from ASCs. Organoids derived from ASCs can be used to directly model hereditary diseases such as CF or cancer. While we discuss only CRISPR-based gene editing, other interesting CRISPR tools have been developed, for instance to modify gene expression using CRISPRi or CRISPRa (69–71). The coming years should witness the generation of many more organoid- and CRISPR-based technologies. It will be exciting to watch progress in both research fields and the merging of the two.

AUTHOR CONTRIBUTIONS

E.D. prepared figures; E.D. drafted manuscript; H.C. edited and revised manuscript.

ACKNOWLEDGEMENTS

We thank Jasper Mullenders for critically reading the manuscript. We thank Kai Kretzschmar and Helmuth Gerhart for contributing images for this review.

REFERENCES

1. Sato T, Vries RG, Snippert HJ, van de Wetering M, Barker N, Stange DE, et al. Single Lgr5 stem cells build crypt-villus structures in vitro without a mesenchymal niche. *Nature*. Nature Publishing Group; 2009;459:262–5.
2. Boj SF, Hwang C-I II, Baker LA, Chio IIC, Engle DD, Corbo V, et al. Organoid models of human and mouse ductal pancreatic cancer. *Cell*. Elsevier; 2015;160:324–38.
3. Linnemann JR, Miura H, Meixner LK, Irmeler M, Kloos UJ, Hirschi B, et al. Quantification of regenerative potential in primary human mammary epithelial cells. *Development*. 2015;142:1–13.
4. Longmire TA, Ikonomou L, Hawkins F, Christodoulou C, Cao Y, Jean JC, et al. Efficient derivation of purified lung and thyroid progenitors from embryonic stem cells. *Cell Stem Cell*. 2012;10:398–411.
5. McCracken KW, Catá EM, Crawford CM, Sinagoga KL, Schumacher M, Rockich BE, et al. Modelling human development and disease in pluripotent stem-cell-derived gastric organoids. *Nature*. 2014;516:400–4.
6. Nanduri LSY, Baanstra M, Faber H, Rocchi C, Zwart E, De Haan G, et al. Purification and Ex vivo expansion of fully functional salivary gland stem cells. *Stem Cell Reports*. 2014;3:957–64.
7. Ootani A, Li X, Sangiorgi E, Ho QT, Ueno H, Toda S, et al. Sustained in vitro intestinal epithelial culture within a Wnt-dependent stem cell niche. *Nat Med*. 2009;15:701–6.
8. Ren W, Lewandowski BC, Watson J, Aihara E, Iwatsuki K, Bachmanov AA, et al. Single Lgr5- or Lgr6-expressing taste stem/progenitor cells generate taste bud cells ex vivo. *Proc Natl Acad Sci U S A*. 2014;111:16401–6.
9. Rock JR, Onaitis MW, Rawlins EL, Lu Y, Clark CP, Xue Y, et al. Basal cells as stem cells of the mouse trachea and human airway epithelium. *Proc Natl Acad Sci U S A*. 2009;106:12771–5.
10. Spence JR, Mayhew CN, Rankin SA, Kuhar MF, Vallance JE, Tolle K, et al. Directed differentiation of human pluripotent stem cells into intestinal tissue in vitro. *Nature*. 2011;470:105–9.
11. Takasato M, Er PX, Becroft M, Vanslambrouck JM, Stanley EG, Elefanty AG, et al. Directing human embryonic stem cell differentiation towards a renal lineage generates a self-organizing kidney. *Nat Cell Biol*. 2014;16:118–26.
12. Takebe T, Zhang R-R, Koike H, Kimura M, Yoshizawa E, Enomura M, et al. Generation of a vascularized and functional human liver from an iPSC-derived organ bud transplant. *Nat Protoc*. Nature Publishing Group; 2014;9:396–409.
13. Huch M, Dorrell C, Boj SF, Van Es JH, Li VSWW, Van De Wetering M, et al. In vitro expansion of single Lgr5+ liver stem cells induced by Wnt-driven regeneration. *Nature*. 2013;494:247–50.
14. Karthaus WR, Iaquinta PJ, Drost J, Gracanin A, Van Boxtel R, Wongvipat J, et al. Identification of multipotent luminal progenitor cells in human prostate organoid cultures. *Cell*. 2014;159:163–75.
15. Barker N, Huch M, Kujala P, van de Wetering M, Snippert HJ, van Es JH, et al. Lgr5+ve Stem Cells Drive Self-Renewal in the Stomach and Build Long-Lived Gastric Units In Vitro. *Cell Stem Cell*. 2010;6:25–36.
16. Dye BR, Hill DR, Ferguson MA, Tsai Y-H, Nagy MS, Dyal R, et al. In vitro generation of human pluripotent stem cell derived lung organoids. *Elife*. 2015;4:e05098.
17. Eiraku M, Sasai Y. Mouse embryonic stem cell culture for generation of three-dimensional retinal and cortical tissues. *Nat Protoc*. 2012;7:69–79.
18. Eiraku M, Watanabe K, Matsuo-Takasaki M, Kawada M, Yonemura S, Matsumura M, et



- al. Self-Organized Formation of Polarized Cortical Tissues from ESCs and Its Active Manipulation by Extrinsic??Signals. *Cell Stem Cell*. 2008;3:519–32.
19. Chua CW, Shibata M, Lei M, Toivanen R, Barlow LJ, Bergren SK, et al. Single luminal epithelial progenitors can generate prostate organoids in culture. *Nat Cell Biol*. 2014;
 20. Kessler M, Hoffmann K, Brinkmann V, Thieck O, Jackisch S, Toelle B, et al. The Notch and Wnt pathways regulate stemness and differentiation in human fallopian tube organoids. *Nat Commun*. 2015;6:8989.
 21. Kretzschmar K, Clevers H. Organoids: Modeling Development and the Stem Cell Niche in a Dish. *Dev Cell*. Elsevier Inc.; 2016;38:590–600.
 22. Lancaster M a., Knoblich J a. Organogenesis in a dish: modeling development and disease using organoid technologies. *Science*. 2014;345:1247125.
 23. Schwank G, Koo BK, Sasselli V, Dekkers JF, Heo I, Demircan T, et al. Functional repair of CFTR by CRISPR/Cas9 in intestinal stem cell organoids of cystic fibrosis patients. *Cell Stem Cell*. 2013;13:653–8.
 24. Ishino Y, Shinagawa H, Makino K, Amemura M, Nakata A. Nucleotide Sequence of the *iap* Gene , Responsible for Alkaline Phosphatase Isozyme Conversion in *Escherichia coli* , and Identification of the Gene Product. 1987;5429–33.
 25. Nakata A, Amemura M, Makino K. Unusual Nucleotide Arrangement with Repeated Sequences in the *Escherichia coli* K-12 Chromosome. 1989;171:3553–6.
 26. Jansen R, Embden JDA Van, Gastra W, Schouls LM. Identification of genes that are associated with DNA repeats in prokaryotes. 2002;43:1565–75.
 27. Bolotin A, Quinquis B, Sorokin A, Ehrlich SD. Clustered regularly interspaced short palindrome repeats (CRISPRs) have spacers of extrachromosomal origin. 2005;1066:2551–61.
 28. Mojica FJM. Intervening Sequences of Regularly Spaced Prokaryotic Repeats Derive from Foreign Genetic Elements Intervening Sequences of Regularly Spaced Prokaryotic Repeats Derive from. 2005;
 29. Pourcel C, Salvignol G, Vergnaud G. CRISPR elements in *Yersinia pestis* acquire new repeats by preferential uptake of bacteriophage DNA , and provide additional tools for evolutionary studies. 2005;653–63.
 30. Gasiunas G, Barrangou R, Horvath P, Siksnys V. Cas9 – crRNA ribonucleoprotein complex mediates specific DNA cleavage for adaptive immunity in bacteria. 2012;109:2579–86.
 31. Wiedenheft B, Sternberg SH, Doudna J a. RNA-guided genetic silencing systems in bacteria and archaea. *Nature*. 2012;482:331–8.
 32. Marraffini LA, Sontheimer EJ. Self versus non-self discrimination during CRISPR RNA-directed immunity. *Nature*. 2010;463:568–71.
 33. Marraffini LA, Sontheimer EJ. CRISPR Interference Limits Horizontal Gene Transfer in *Staphylococci* by Targeting DNA. 2009;322:1843–5.
 34. Gaj T, Gersbach CA, Barbas CF. ZFN, TALEN, and CRISPR/Cas-based methods for genome engineering. *Trends Biotechnol*. 2013. page 397–405.
 35. Jinek M, Chylinski K, Fonfara I, Hauer M, Doudna JA, Charpentier E. A Programmable Dual-RNA – Guided DNA Endonuclease in Adaptive Bacterial Immunity. 2012;337:816–22.
 36. Cong L, Ran FA, Cox D, Lin S, Barretto R, Hsu PD, et al. Multiplex Genome Engineering Using CRISPR/Cas Systems. 2013;339:819–23.
 37. Mali P, Yang L, Esvelt KM, Aach J, Guell M, Dicarlo JE, et al. RNA-Guided Human Genome engineering via Cas9. 2013;
 38. Hwang WY, Fu Y, Reyon D, Maeder ML, Tsai SQ, Sander JD, et al.

- Efficient genome editing in zebrafish using a CRISPR-Cas system. *Nat Biotechnol.* 2013;31:227–9.
39. Hockemeyer D, Jaenisch R. Induced pluripotent stem cells meet genome editing. *Cell Stem Cell.* 2016. page 573–86.
 40. Platt RJ, Chen S, Zhou Y, Yim MJ, Swiech L, Kempton HR, et al. CRISPR-Cas9 knockin mice for genome editing and cancer modeling. *Cell.* 2014;159:440–55.
 41. Fatehullah A, Tan SH, Barker N. Organoids as an *in vitro* model of human development and disease. *Nat Cell Biol.* 2016;18:246–54.
 42. Huch M, Bonfanti P, Boj SF, Sato T, Loomans CJM, van de Wetering M, et al. Unlimited *in vitro* expansion of adult bi-potent pancreas progenitors through the Lgr5/R-spondin axis. *EMBO J.* 2013;32:2708–21.
 43. Tadokoro T, Wang Y, Barak LS, Bai Y, Randell SH, Hogan BLM. IL-6/STAT3 promotes regeneration of airway ciliated cells from basal stem cells. *Proc Natl Acad Sci U S A.* 2014;1–9.
 44. Driehuis E, Kolders S, Spelier S, Lohmussaer K, Willems SM, Devriese LA, et al. Oral mucosal organoids as a potential platform for personalized cancer therapy. *Cancer Discov.* 2019;CD-18-1522.
 45. DeWard AD, Cramer J, Lagasse E. Cellular heterogeneity in the mouse esophagus implicates the presence of a nonquiescent epithelial stem cell population. *Cell Rep.* 2014;9:701–11.
 46. Lancaster MA, Renner M, Martin C-A, Wenzel D, Bicknell LS, Hurles ME, et al. Cerebral organoids model human brain development and microcephaly. *Nature.* 2013;501:373–9.
 47. Farin HF, Van Es JH, Clevers H. Redundant sources of Wnt regulate intestinal stem cells and promote formation of paneth cells. *Gastroenterology.* 2012;143.
 48. Farin HF, Karthaus WR, Kujala P, Rakhshandehroo M, Schwank G, Vries RGJ, et al. Paneth cell extrusion and release of antimicrobial products is directly controlled by immune cell-derived IFN- γ . *J Exp Med.* 2014;211:1393–405.
 49. Dekkers JF, Wiegerinck CL, de Jonge HR, de Jong NWM, Bijvelds MJC, Nieuwenhuis EES, et al. A functional CFTR assay using primary cystic fibrosis intestinal organoids. *J Cyst Fibros. Nature Publishing Group;* 2012;11:S32.
 50. Fearon ER, Vogelstein B. A genetic model for colorectal tumorigenesis. *Cell.* 1990. page 759–67.
 51. Drost J, van Jaarsveld RH, Ponsioen B, Zimmerlin C, van Boxtel R, Buijs A, et al. Sequential cancer mutations in cultured human intestinal stem cells. *Nature.* 2015;521:43–7.
 52. Matano M, Date S, Shimokawa M, Takano A, Fujii M, Ohta Y, et al. Modeling colorectal cancer using CRISPR-Cas9-mediated engineering of human intestinal organoids. *Nat Med.* 2015;21:256–62.
 53. Ijspeert JEG, Vermeulen L, Meijer GA, Dekker E. Serrated neoplasia-role in colorectal carcinogenesis and clinical implications. *Nat. Rev. Gastroenterol. Hepatol.* 2015. page 401–9.
 54. Fessler E, Drost J, van Hooff SR, Linnekamp JF, Wang X, Jansen M, et al. TGF β signaling directs serrated adenomas to the mesenchymal colorectal cancer subtype. *EMBO Mol Med.* 2016;8:e201606184.
 55. Verissimo CS, Overmeer RM, Ponsioen B, Drost J, Mertens S, Verlaan-Klink I, et al. Targeting mutant RAS in patient-derived colorectal cancer organoids by combinatorial drug screening. *Elife. England;* 2016;5.
 56. Zhang Z, Christin JR, Wang C, Ge K, Oktay MH, Guo W, et al. Mammary Stem Cell Based Somatic Mouse Models Reveal Breast Cancer Drivers Causing Cell Fate Dysregulation. *Cell Rep.* 2016;16:3146–56.
 57. Gao X, Bali AS, Randell SH, Hogan BLM. GRHL2 coordinates regeneration of a polarized mucociliary epithelium



- from basal stem cells. *J Cell Biol.* 2015;211:669–82.
58. Fernández García MS, Teruya-Feldstein J. The diagnosis and treatment of dyskeratosis congenita: a review. *J Blood Med.* 2014;5:157–67.
 59. Armanios M, Blackburn EH. The telomere syndromes. *Nat Rev Genet.* 2012;13:693–704.
 60. Freedman BS, Brooks CR, Lam AQ, Fu H, Morizane R, Agrawal V, et al. Modelling kidney disease with CRISPR-mutant kidney organoids derived from human pluripotent epiblast spheroids. *Nat Commun.* 2015;6:8715.
 61. Koo B-KK, Stange DE, Sato T, Karthaus W, Farin HF, Huch M, et al. Controlled gene expression in primary *Lgr5* organoid cultures. *Nat Methods.* 2012;9:81–3.
 62. Fujii M, Matano M, Nanki K, Sato T. Efficient genetic engineering of human intestinal organoids using electroporation. *Nat Protoc.* 2015;10:1474–85.
 63. Gjorevski N, Sachs N, Manfrin A, Giger S, Bragina ME, Ordonez-Moran P, et al. Designer matrices for intestinal stem cell and organoid culture. *Nature.* England; 2016;539:560–4.
 64. Agrotis A, Ketteler R. A new age in functional genomics using CRISPR/Cas9 in arrayed library screening. *Front. Genet.* 2015.
 65. Koike-Yusa H, Li Y, Tan E-P, Velasco-Herrera MDC, Yusa K. Genome-wide recessive genetic screening in mammalian cells with a lentiviral CRISPR-guide RNA library. *Nat Biotechnol.* 2014;32:267–73.
 66. Shalem O, Sanjana NE, Zhang F. High-throughput functional genomics using CRISPR-Cas9. *Nat Rev Genet.* 2015;16:299–311.
 67. Wang T, Wei JJ, Sabatini DM, Lander ES. Genetic screens in human cells using the CRISPR-Cas9 system. *Science.* 2014;343:80–4.
 68. Tao L, Zhang J, Meraner P, Tovaglieri A, Wu X, Gerhard R, et al. Frizzled proteins are colonic epithelial receptors for *C. difficile* toxin B. *Nature.* 2016;538:350–5.
 69. Cheng AW, Wang H, Yang H, Shi L, Katz Y, Theunissen TW, et al. Multiplexed activation of endogenous genes by CRISPR-on, an RNA-guided transcriptional activator system. *Cell Res.* 2013;23:1163–71.
 70. Larson MH, Gilbert L a, Wang X, Lim W a, Weissman JS, Qi LS. CRISPR interference (CRISPRi) for sequence-specific control of gene expression. *Nat Protoc.* 2013;8:2180–96.
 71. Qi LS, Larson MH, Gilbert LA, Doudna JA, Weissman JS, Arkin AP, et al. Repurposing CRISPR as an RNA-guided platform for sequence-specific control of gene expression. *Cell.* 2013;152:1173–83.
 72. Clevers H. Modeling Development and Disease with Organoids. *Cell.* Elsevier Inc.; 2016;165:1586–97.

CHAPTER

CRISPR-INDUCED *TMPRSS2-ERG* GENE FUSIONS IN MOUSE PROSTATE ORGANOIDS



ABSTRACT

TMPRSS2-ERG fusions are common genetic events in prostate cancer. Until now, this genetic alteration was modelled by *ERG* overexpression. Here, we report the creation of mouse prostate organoids that have undergone gene fusion through a CRISPR/Cas9-based strategy. The genetic fusion of *TMPRSS2* and *ERG* results in *ERG* overexpression. This effect is Androgen Receptor-mediated, as expression of the fusion transcript can be restored to wildtype *ERG* levels by treatment with the androgen receptor antagonist Nilutamide.



Else Driehuis^{1,2} and Hans Clevers^{1,3*}

¹Hubrecht Institute, Royal Netherlands Academy of Arts and Sciences (KNAW), The Netherlands

²University Medical Center Utrecht, The Netherlands

³Princess Maxima Center, The Netherlands

*corresponding author

INTRODUCTION

Gene fusions are genetic events occurring during tumorigenesis of both solid and blood-borne cancers (1). The best known fusion events are those occurring in leukemia, the first disease in which these genetic events were discovered (2). In prostate cancer (PC), 40–80% of tumors contain a gene fusion between the androgen receptor (*AR*) responsive gene Transmembrane protease serine 2 (*TMPRSS2*) and an ETS family transcription factor, which is most commonly the oncogene ETS-related gene (*ERG*) (3–5). A deletion of a region of approximately 3 million basepairs results in the fusion of these two genes, both located on chromosome 21, thereby driving *AR* induced overexpression of the *ERG* oncogene. A diverse range of *TMPRSS2-ERG* hybrids has been described (6,7). In all cases, the open reading frame of exon 1 of *TMPRSS2* is included, thereby retaining the androgen response element (*ARE*) that is present in the 5' UTR of this gene (8). For *ERG*, the fusion most often results in an N-terminal truncation of the transcript that retains its functional domains (7).

Since the first report of this genetic alteration in 2005 (4), research studying *TMPRSS2-ERG* has relied on mouse models, cell lines that overexpress *ERG* and human PC cell lines carrying this genetic alteration (9–11). Although mouse models mimic the *ERG* overexpression that is observed in *TMPRSS2-ERG* tumors, they lack the correct genomic context of *TMPRSS2*-driven expression, such as the heterozygous loss of genes encoded by the genomic region between *TMPRSS2* and *ERG* (12). Furthermore, these models do not retain the transcription control of the fusion gene as it occurs in PC, but are instead driven by artificial overexpression of the oncogene. PC cell lines that carry *TMPRSS2-ERG* fusions do recapitulate this genetic context, but contain additional genetic alterations, often of unknown relevance, that might obscure the molecular effects of the gene fusion.

In 2013, the technique of CRISPR/Cas9-mediated genome engineering became available as a versatile tool for genome editing (13,14). Shortly thereafter, we showed that organoids, which are 3D structures grown from stem cells that resemble their respective tissue of origin, could be established from both murine and human prostate epithelial cells (15). As it was previously shown that CRISPR/Cas9 can be applied in organoids (16–21), here we set out to create a *TMPRSS2-ERG* gene fusion in mouse prostate organoids.

TMPRSS2-ERG organoids were found to recapitulate the *ERG* overexpression observed in tumors carrying this genetic alteration. This *ERG* overexpression was driven by *AR* signaling, as previously described (4,22,23), as it could be inhibited by blocking androgen signaling. To our knowledge, we are the first to report the use of CRISPR/Cas9 to create gene fusions in organoids. The *TMPRSS2-ERG* organoids described here can serve as an *in vitro* model to study the short- and long-term molecular consequences of this gene fusion in an otherwise wildtype background.

RESULTS

Mouse prostate organoids can be genetically modified to carry *TMPRSS2-ERG* gene fusions

To create organoids carrying a *TMPRSS2-ERG* gene fusion at the endogenous genomic location, we used a targeting construct in which intron 2-3 of *TMPRSS2* was fused to intron 2-3 of *ERG* (Figure 1A). Transcription of this fusion would result in a transcript containing exon 1 and 2 of *TMPRSS2* and exons 3-11 of *ERG*, which is comparable to the human transcript hybrid that is most commonly observed in PC (4,24,25). In addition, the construct also contained an eGFP-puromycin puromycin selection cassette that could be used to select for transfected organoids. The cassette was flanked by homology arms assuring integration in the intron 3-4 of *ERG* (Figure 1A). As such, the puromycin cassette would be integrated in a non-coding region of the gene (see supplementary data for the complete sequence of the targeting construct). In addition, we developed constructs encoding Cas9 and individual sgRNAs targeting the region of both *TMPRSS2* and *ERG* in the vicinity of the fusion site (Figure 1B). These constructs were created as previously described (26). sgRNAs targeting intronic regions of *TMPRSS2* and *ERG* were designed using the online CRISPR design tool at <http://crispr.mit.edu> (for used sequences see Figure 1C). To prevent Cas9-mediated cleavage, sgRNA target region were synonymously mutated in our targeting construct.

Subsequently, mouse prostate organoids were transfected with the developed targeting construct, a *TMPRSS2*-targeting sgRNA, a *ERG*-targeting sgRNA and a construct encoding Cas9. After approximately one week on selection medium, single organoids could be observed growing in selection medium. We handpicked these organoids, dissociated them into single cells and expanded them as clonal lines. *TMPRSS2-ERG* organoids appeared folded, dense and morphologically different from their wildtype counterparts (Figure 2A). Ki67 staining on paraffin-embedded sections revealed increased proliferation rate when compared to their wildtype counterparts (Figure 2B).

Genomic DNA was isolated and PCR was performed to confirm gene editing (Table S1). In 85% of the clones, PCR using a forward primer for *TMPRSS2* and reverse primer for *ERG* resulted in the formation of a product (Figure 2C). Sanger sequencing confirmed the successful fusion of *TMPRSS2* and *ERG* (Figure 2D). We also sequenced the sgRNA-targeted regions of the remaining wildtype alleles of both *TMPRSS2* and *ERG*. We detected small insertions and deletions caused by incorrect repair of the sgRNA-induced cuts (Figure S1). As these indels are located in the intronic regions of the genes, they are not expected to affect transcription.

TMPRSS2-ERG fusion organoids are responsive to androgen inhibiting treatment

Next, we investigated if the created *TMPRSS2-ERG* organoids were functional. It was previously shown that tumor lines carrying this fusion, overexpress *ERG* in an androgen-

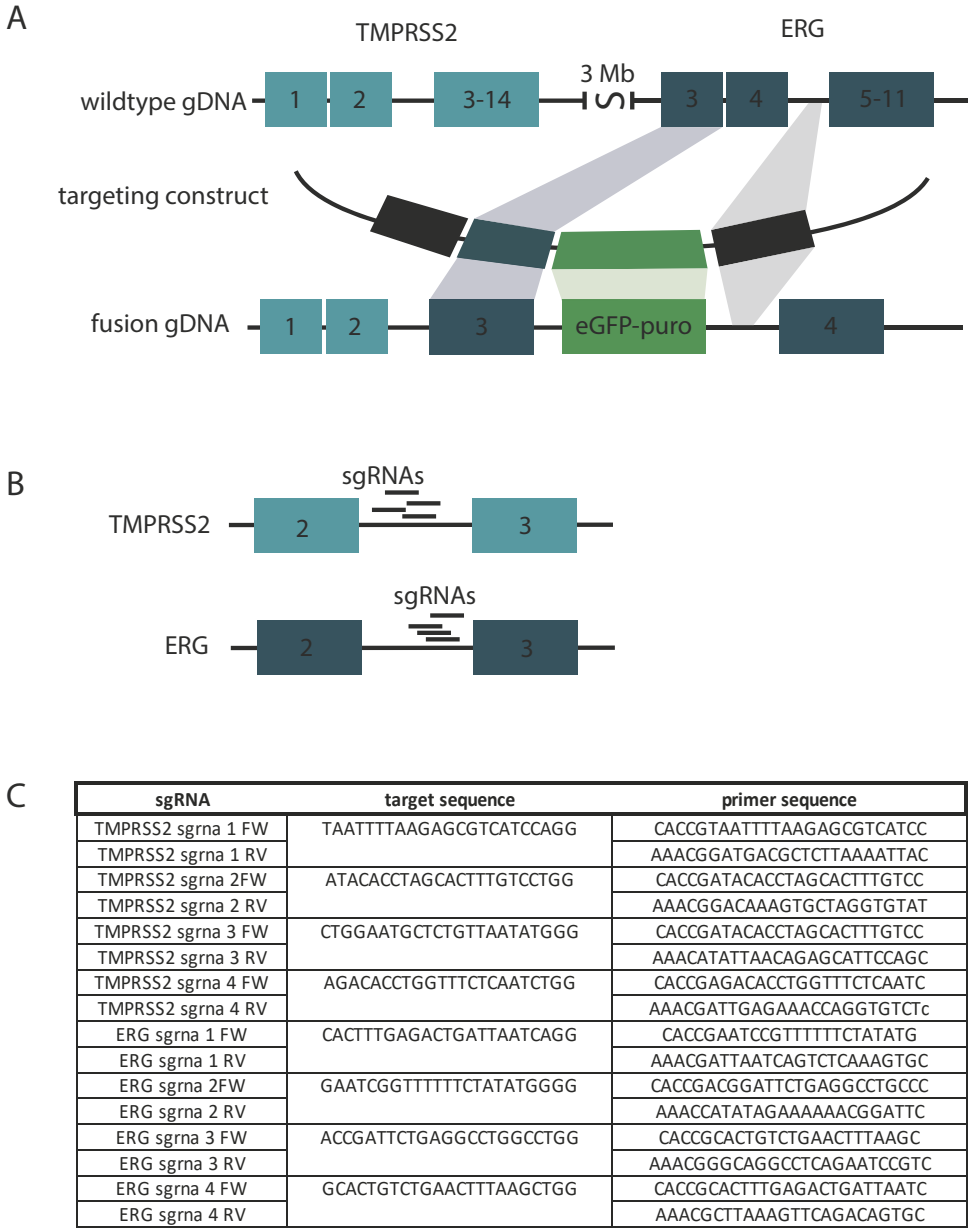


Figure 1. TMPRSS2-ERG fusion targeting construct. A. The developed targeting construct fuses intron 2-3 of *TMPRSS2* to intron 2-3 of *ERG*, which are approximately 3 Mb apart. In addition, a eGFP-puro cassette is integrated in intron 3-4 of *ERG*. B. Used sgRNAs target intronic regions of both *TMPRSS2* and *ERG*. C. Sequences targeted by used sgRNAs and the primers used to construct the sgRNA constructs following the protocol of Ran et al. (26)

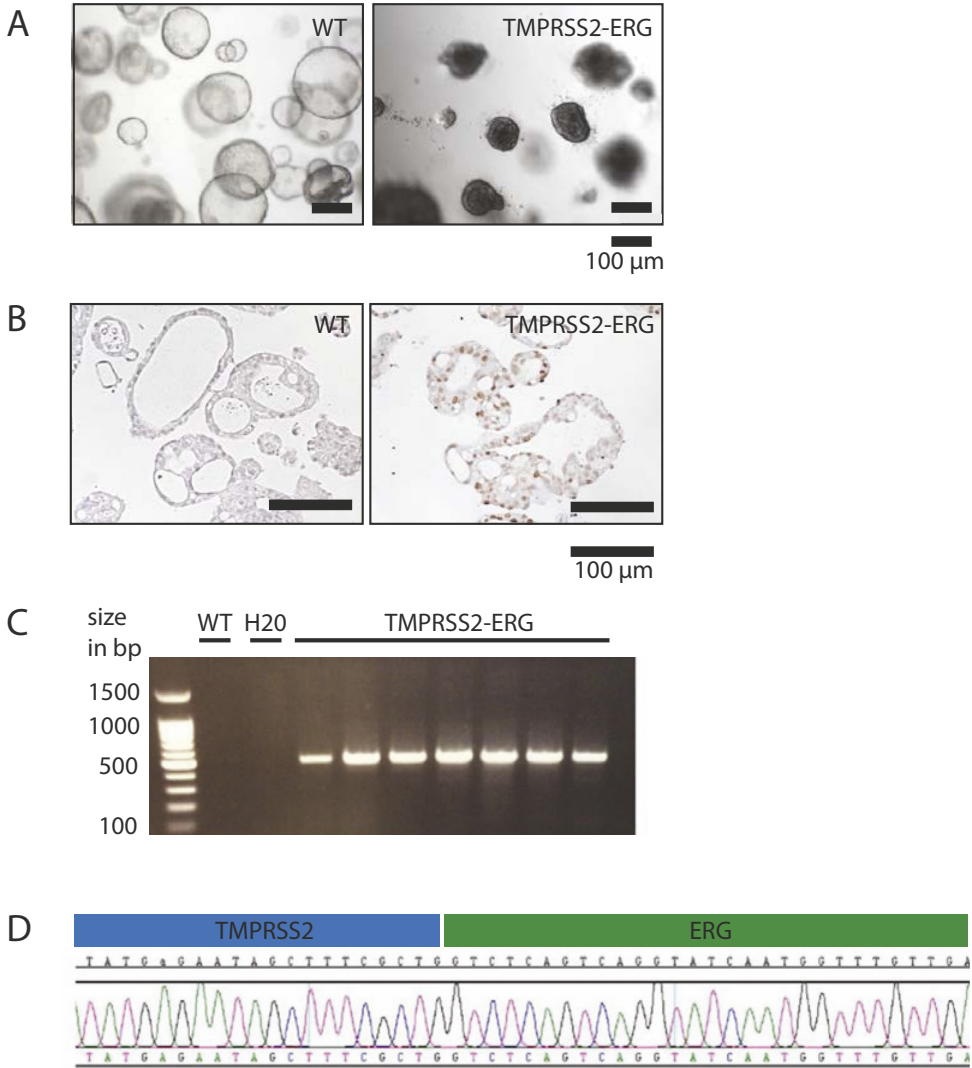


Figure 2. Transfection of mouse prostate organoids with the produced *TMPRSS2-ERG* targeting construct. A. Morphology of *TMPRSS2-ERG* organoids compared to WT organoids after clonal expansion of handpicked single organoids. B. Morphology of *TMPRSS2-ERG* organoid ten passages after transfection. C. Ki67-staining on paraffin embedded organoids reveals increased proliferation in the fusion organoids compared to their wildtype counterparts. D. Conformation of *TMPRSS2-ERG* gene fusion on the DNA level. E. Sanger sequencing of the fusion-specific PCR on gDNA shown in D, reveals ligation of *TMPRSS2* to *ERG*.

dependent manner (4). Therefore, we performed gene expression analysis of *TMRPSS2* and *ERG*, either in the presence or absence of AR blocking agents. Compared to wildtype organoids, we observed an increase in *ERG* expression in *TMRPSS2*-*ERG* organoids. Expression was not altered significantly (Figure 3A). Of note, the extent of increase in *ERG* expression varied between the different *TMPRSS2*-*ERG* organoid lines.

As our culture medium contains dihydrotestosterone (DHT), the active form of testosterone, we hypothesized that inhibition of AR signaling would result in decreased expression of *ERG* in the *TMPRSS2*-*ERG* organoid lines. To investigate this, we treated organoids for 24 hours with Nilutamide, a competitive antagonist of AR, and subsequently assessed *ERG* expression levels (Figure 3B). As expected, we observed a restoration of *ERG* expression levels in the presence of Nilutamide, which was consistent for all three

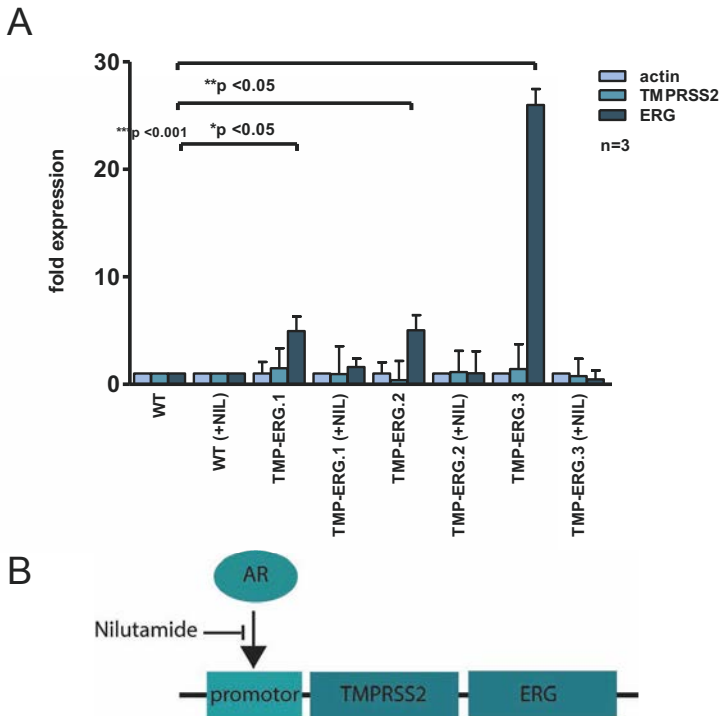


Figure 3. *ERG* expression in *TMPRSS2*-*ERG* organoids is driven by AR signaling. A. Expression analysis of wildtype and three clonal *TMPRSS2*-*ERG* organoid lines. Expression of *TMPRSS2* and *ERG* is calculated relative to β -actin. All expression values are calculated relative to wildtype organoids. B. Schematic overview of the effect of Nilutamide on *ERG* expression in *TMRPSS2*-*ERG* organoids. Due to the presence of an ARE in its protomer region, *TMRPSS2* gene expression is driven by AR. As such, in *TMPRSS2*-*ERG* organoids, AR drives *ERG* overexpression. However, when Nilutamide is added to the medium, *TMPRSS2* expression is prevented and *ERG* expression levels are restored to wildtype levels.

tested *TMPRSS2-ERG* organoid lines (Figure 3A). These data support the findings of others that ERG expression in *TMPRSS2-ERG* positive PC is AR-driven and can be inhibited by using AR-inhibiting agents. Our findings imply that AR-blocking treatments directly affect the molecular consequences of *TMPRSS2-ERG* gene fusion in PC.

DISCUSSION

By introduction of the *TMPRSS2-ERG* fusion at the endogenous location in the DNA, this approach more closely recapitulates the *in vivo* situation than artificial ERG overexpression models, where ERG overexpression is driven by for example the probasin promoter. In this system however, the genomic region between *TMPRSS2* and *ERG* is deleted on the allele carrying the *TMPRSS2-ERG* fusion, thereby resulting in heterozygous deletion of genes encoded by this region. This concomitant hemizyosity of a number of genes cannot be modeled by ERG overexpression. One of the genes encoded by this genomic area is *HMGN1*. Heterozygous loss of *HMGN1* was reported to increase N-cadherin expression (27) and alter the G2/M checkpoint (28). Indeed, increase of N-cadherin expression is observed in progressing PC (29).

In addition, this model can be used to better understand the molecular effects of *TMPRSS2-ERG* gene fusion without the confounding effect of other genetic alterations (which is an issue when using PC cell lines). This might aid the development of new therapies for tumors carrying this genetic alteration. In addition, *TMPRSS2-ERG* organoids might serve to aid the implementation of already existing targeted therapies for *TMPRSS2-ERG* tumors in the clinic. It was previously shown that patient-derived organoids can predict tumor response *in vivo* (30). Although the organoids described here are of murine origin, technically the described technique should be applicable to human prostate organoids. To our knowledge, this is the first study showing that CRISPR/Cas9 technology can be applied in organoids to create endogenous gene fusions.

CONCLUSION

Here we demonstrate that CRISPR/Cas9 can be applied in organoids to create endogenous gene fusion through the creation of a 3 million base pair long deletion. We generated mouse prostate organoids carrying a commonly found variant of *TMPRSS2-ERG* gene fusion. Our approach creates the unique opportunity to study the effect of this genetic alteration in an otherwise wildtype background.

METHODS

Targeting construct cloning

Homology arms containing synonymous mutations to prevent cleavage by Cas9 were ordered as g blocks from IDT. eGFP-puro sequence was amplified using from an in-house construct created in the lab. PCR from genomic DNA was used to create the second homology arm for ERG. Short overhangs complimentary to the homology arms were added to these fragments by integrating them into the used primers. Individual fragments plus backbone (created by restriction digestion of cloning vector) were ligated using HiFi DNA Assembly Cloning kit (NEB).

Organoid culture and transfection

Mouse prostate organoids were established and cultured as described previously (15,31). To obtain mutant organoids, we used the psCas9 vector described by Wright et al.(26), that encoded both our sgRNA and the Cas9 protein of *S. pyogenes*. Transfections were performed using Lipofectamin (Invitrogen). 500 ng DNA was used per construct and resuspended in 50 μ L Optimum prior to transfection. 50 μ L of a 8% Lipofectamine in optimum solution was mixed with the DNA and incubated at room temperature for 20 minutes. 450 μ L of cell suspension (in complete medium - antibiotics) was added to the DNA/Lipofectamine mix in a 48-well cell culture plate. Cells were centrifuged at 600x g for 1 hour to increase transfection efficiency. Subsequently, cells were incubated for 4–6 hours at 37°C 5% CO₂. After that, cells were washed, centrifuged, resuspended in BME and plated as normal. After three days of recovery, selection on 1 μ g/ml puromycin-containing medium was started and TMPRSS2-ERG organoids were maintained on this medium. Five days prior to RNA isolation for RT-qPCR experiments, puromycin was removed from the medium, and - if applicable - Nilutamide (10 μ M) was added.

RNA isolation and reverse transcription

RNA was extracted from the organoids using the QIAGEN RNA easy kit. Organoids were pelleted by centrifugation and dissolved in 300 μ L RLT, 300 μ L 70% ethanol was added. The mixture was put on the RNA columns, which were subsequently centrifuged. Columns were washed once with RW1 buffer and twice with RPE buffer. To assure removal of all buffer, columns were spin down once more. RNA was eluted using 30 μ L RNAase-free water. RNA was kept on ice at all times. 500 ng RNA was taken as starting material for the reverse transcription reaction. To 500 ng of RNA in 10 μ L water, 1,5 μ L of a oligo (dT)15 primer (0,5 μ g per reaction) was added on ice. The mixture was incubated for 5 min at 70°C and cooled on ice. 8,5 μ L of GoScript buffer with 0,5 mM dNTPs, 2,5 mM MgCL, 1 μ L of GoScript reverse transcriptase and 20 units of RNase-inhibitor (all Promega) was added and the mixture was incubated for 5 min at 25°C, 15 min at 42°C and 15 min at 70°C. cDNA was stored at -20°C until use.

Quantitative PCR

25 ng of cDNA was used per reaction. Used primers are depicted in supplementary (Table 1). 25 μ l of iQ SYBR Green supermix (Biorad) with a primer concentration of 500 nM was used for each reaction. Actin was used as housekeeping gene. PCR reaction was as follows: 2 minutes 95°C, followed by a repeat of the following incubations: 30 seconds at 95°C, 55°C, 72°C.

Statistical analysis

For expression levels, $\Delta\Delta$ CT values were calculated by making all data relative to actin, and subsequently to wildtype values. For statistical analysis of the RT-qPCR experiments, we used Graphpad software and performed a two-way ANOVA. Subsequent bonferetti posttests revealed a statistically significant deviation of ERG expression in all three TMPRSS2-ERG clones.

ACKNOWLEDGEMENTS

We thank Kai Kretzschmar for critically reading this manuscript.

REFERENCES

1. Mertens F, Johansson B, Fioretos T, Mitelman F. The emerging complexity of gene fusions in cancer. *Nat Rev Cancer*. Nature Publishing Group; 2015;15:371–81.
2. Nowell P, Hungerford D. A minute chromosome in human chronic 9 granulocytic leukemia. *Science* (80-). 1960;132:1488–501.
3. Demichelis F, Fall K, Perner S, Andren O, Schmidt F, Setlur SR, et al. TMPRSS2:ERG gene fusion associated with lethal prostate cancer in a watchful waiting cohort. *Oncogene*. England; 2007;26:4596–9.
4. Tomlins S a, Rhodes DR, Perner S, Dhanasekaran SM, Mehra R, Sun X-W, et al. Recurrent fusion of TMPRSS2 and ETS transcription factor genes in prostate cancer. *Science*. 2005;310:644–8.
5. Hermans KG, van Marion R, van Dekken H, Jenster G, van Weerden WM, Trapman J. TMPRSS2:ERG fusion by translocation or interstitial deletion is highly relevant in androgen-dependent prostate cancer, but is bypassed in late-stage androgen receptor-negative prostate cancer. *Cancer Res*. United States; 2006;66:10658–63.
6. Soller MJ, Isaksson M, Elfving P, Soller W, Lundgren R, Panagopoulos I. Confirmation of the high frequency of the TMPRSS2/ERG fusion gene in prostate cancer. *Genes*. Chromosomes Cancer. United States; 2006. page 717–9.
7. Clark J, Merson S, Jhavar S, Flohr P, Edwards S, Foster CS, et al. Diversity of TMPRSS2-ERG fusion transcripts in the human prostate. *Oncogene*. 2007;26:2667–73.
8. Wang Q, Li W, Liu XS, Carroll JS, Janne OA, Keeton EK, et al. A hierarchical network of transcription factors governs androgen receptor-dependent prostate cancer growth. *Mol Cell*. United States; 2007;27:380–92.
9. Tomlins S a, Laxman B, Varambally S, Cao X, Yu J, Helgeson BE, et al. Role of the TMPRSS2-ERG gene fusion in prostate cancer. *Neoplasia*. 2008;10:177–88.
10. Wang J, Cai Y, Yu W, Ren C, Spencer DM, Ittmann M. Pleiotropic biological activities of alternatively spliced TMPRSS2/ERG fusion gene transcripts. *Cancer Res*. 2008;68:8516–24.
11. Klezovitch O, Risk M, Coleman I, Lucas JM, Null M, True LD, et al. A causal role for ERG in neoplastic transformation of prostate epithelium. *Proc Natl Acad Sci U S A*. United States; 2008;105:2105–10.
12. Yoshimoto M, Joshua AM, Chilton-Macneill S, Bayani J, Selvarajah S, Evans AJ, et al. Three-color FISH analysis of TMPRSS2/ERG fusions in prostate cancer indicates that genomic microdeletion of chromosome 21 is associated with rearrangement. *Neoplasia*. 2006;8:465–9.
13. Cong L, Ran FA, Cox D, Lin S, Barretto R, Hsu PD, et al. Multiplex Genome Engineering Using CRISPR/Cas Systems. 2013;339:819–23.
14. Jinek M, East A, Cheng A, Lin S, Ma E, States U, et al. RNA-programmed genome editing in human cells. 2013;1–9.
15. Karthaus WR, Iaquinia PJ, Drost J, Gracanin A, Van Boxtel R, Wongvipat J, et al. Identification of multipotent luminal progenitor cells in human prostate organoid cultures. *Cell*. 2014;159:163–75.
16. Drost J, van Jaarsveld RH, Ponsioen B, Zimmerlin C, van Boxtel R, Buijs A, et al. Sequential cancer mutations in cultured human intestinal stem cells. *Nature*. 2015;521:43–7.
17. Schwank G, Koo BK, Sasselli V, Dekkers JF, Heo I, Demircan T, et al. Functional repair of CFTR by CRISPR/Cas9 in intestinal stem cell organoids of cystic fibrosis patients. *Cell Stem Cell*. 2013;13:653–8.
18. Freedman BS, Brooks CR, Lam AQ, Fu H, Morizane R, Agrawal V, et al. Modelling kidney disease with CRISPR-mutant kidney organoids derived from human pluripotent epiblast spheroids. *Nat Commun*. 2015;6:8715.

19. Fessler E, Drost J, van Hooff SR, Linnekamp JF, Wang X, Jansen M, et al. TGF β signaling directs serrated adenomas to the mesenchymal colorectal cancer subtype. *EMBO Mol Med.* 2016;8:e201606184.
20. Gao X, Bali AS, Randell SH, Hogan BLM. GRHL2 coordinates regeneration of a polarized mucociliary epithelium from basal stem cells. *J Cell Biol.* 2015;211:669–82.
21. Zhang Z, Christin JR, Wang C, Ge K, Oktay MH, Guo W, et al. Mammary Stem Cell Based Somatic Mouse Models Reveal Breast Cancer Drivers Causing Cell Fate Dysregulation. *Cell Rep.* 2016;16:3146–56.
22. Casey OM, Fang L, Hynes PG, Abou-Kheir WG, Martin PL, Tillman HS, et al. TMPRSS2- driven ERG expression in vivo increases self-renewal and maintains expression in a castration resistant subpopulation. *PLoS One.* 2012;7.
23. Robinson D, Van Allen EM, Wu YM, Schultz N, Lonigro RJ, Mosquera JM, et al. Integrative clinical genomics of advanced prostate cancer. *Cell.* 2015;161:1215–28.
24. Lapointe J, Kim YH, Miller MA, Li C, Kaygusuz G, van de Rijn M, et al. A variant TMPRSS2 isoform and ERG fusion product in prostate cancer with implications for molecular diagnosis. *Mod Pathol an Off J United States Can Acad Pathol Inc.* United States; 2007;20:467–73.
25. Wang J, Cai Y, Ren C, Ittmann M. Expression of variant TMPRSS2/ERG fusion messenger RNAs is associated with aggressive prostate cancer. *Cancer Res.* United States; 2006;66:8347–51.
26. Ran FA, Hsu PD, Wright J, Agarwala V, Scott DA, Zhang F. Genome engineering using the CRISPR-Cas9 system. *Nat Protoc.* 2013;8:2281–308.
27. Rubinstein YR, Furusawa T, Lim J-H, Postnikov Y V, West KL, Birger Y, et al. Chromosomal protein HMGN1 modulates the expression of N-cadherin. *FEBS J.* 2005;272:5853–63.
28. Birger Y, Catez F, Furusawa T, Lim JH, Prymakowska-Bosak M, West KL, et al. Increased tumorigenicity and sensitivity to ionizing radiation upon loss of chromosomal protein HMGN1. *Cancer Res.* 2005;65:6711–8.
29. Jaggi M, Nazemi T, Abrahams NA, Baker JJ, Galich A, Smith LM, et al. N-cadherin switching occurs in high Gleason grade prostate cancer. *Prostate.* 2006;66:193–9.
30. Van De Wetering M, Francies HE, Francis JM, Bounova G, Iorio F, Pronk A, et al. Prospective derivation of a living organoid biobank of colorectal cancer patients. *Cell.* Elsevier Inc.; 2015;161:933–45.
31. Drost J, Karthaus WR, Gao D, Driehuis E, Sawyers CL, Chen Y, et al. Organoid culture systems for prostate epithelial and cancer tissue. *Nat Protoc.* Nature Publishing Group; 2016;11:347–58.

SUPPLEMENTARY DATA

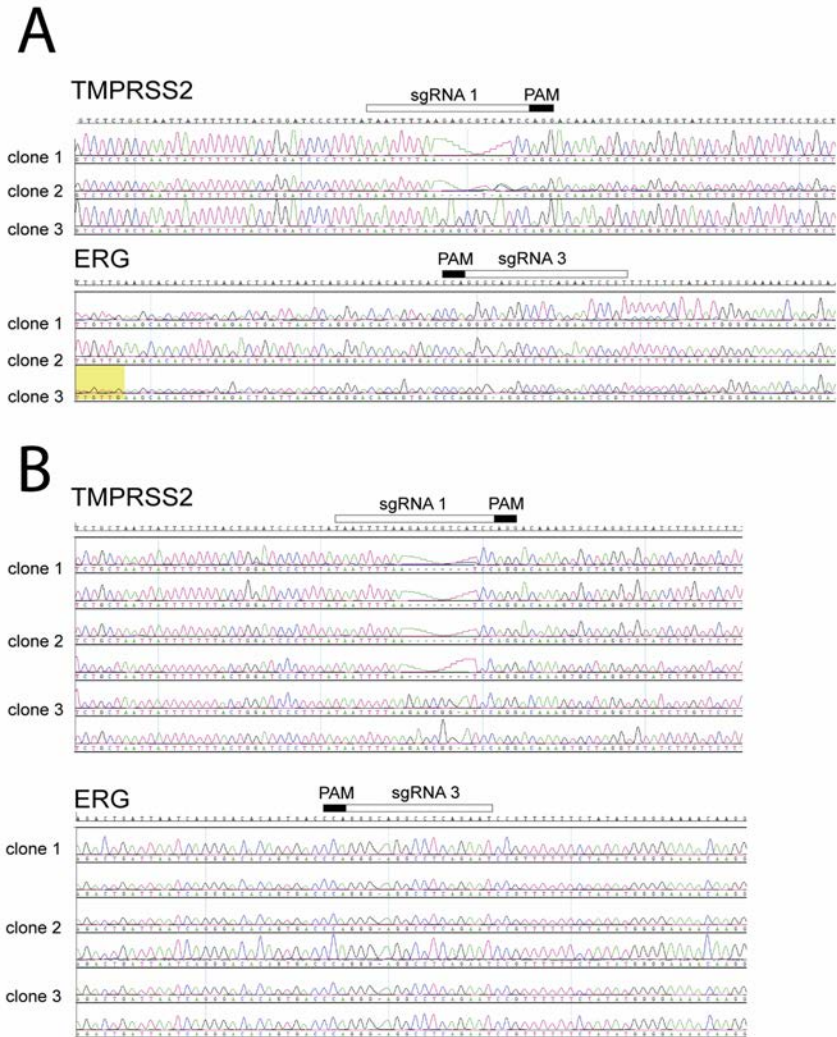
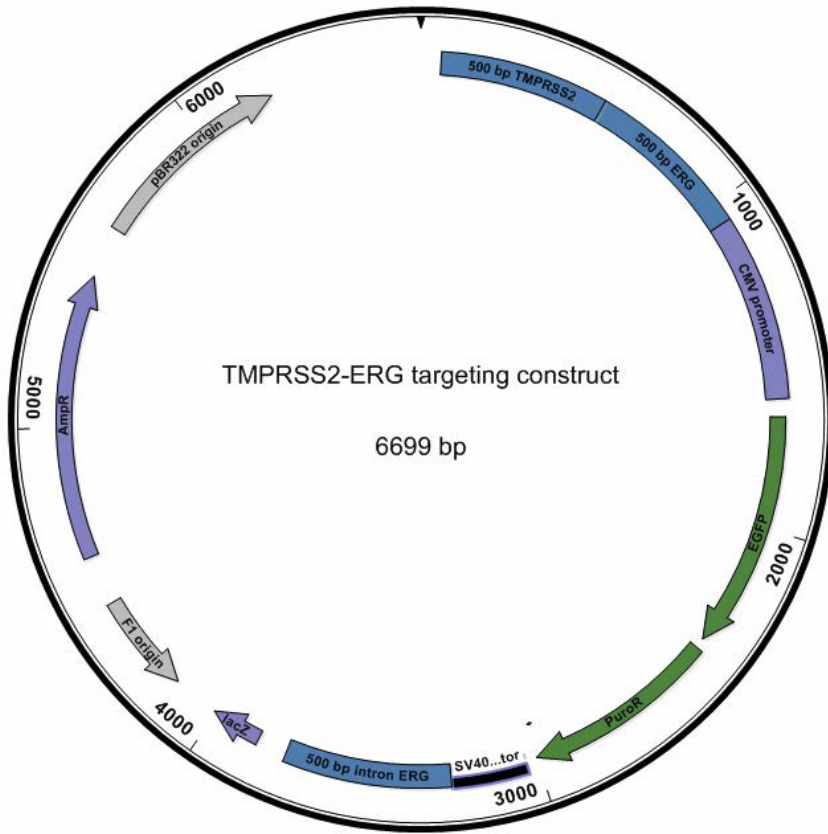


Figure S1. Sequencing results of *TMPRSS2* and *ERG* areas targeting by the sgRNAs used to create the *TMPRSS2*-*ERG* gene fusion.



Supplementary Figure 2. *TMPRSS2-ERG* targeting construct used in this work. the complete sequence of the used vector can be found in the supplemental data available at: http://tiny.cc/Supp_ElseDriehuis

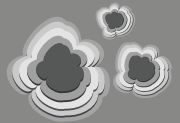
Table S1. DNA primers used for PCR

Primer	Sequence
TMPRSS2 FW gDNA	TATATGAGTCTATGGGGACA
TMPRSS2 RV gDNA	CTAGCACTCTCCTTCAAAGG
ERG FW gDNA	AGCTCGGCGTCTAACTTACT
ERG RV gDNA	CCAGACCCAGCCTACTAGCT
TMPRSS2-ERG FW	CCAGGACAAAGTGCTAGGTGT
TMPRSS2-ERG RV	TCATGCAGTACGGTGAGTGT
TMPRSS2 FW qPCR	CAGTCTGAGCACATCTGTCCT
TMPRSS2 RV qPCR	CTCGGAGCATACTGAGGCA
ERG FW qPCR	ACCTCACCCCTCAGTCCAAA
ERG RV qPCR	TGGTCGGTCCCAGGATCTG

CHAPTER

SUMMARIZING DISCUSSION

8



Else Driehuis¹

¹ Oncode Institute, Hubrecht Institute, Royal Netherlands Academy of Arts and Sciences (KNAW) and University Medical Center Utrecht, The Netherlands

INTRODUCTION

At the time the research that is presented in this thesis was commenced, organoid technology was increasingly applied in molecular laboratories around the world. This technique has multiple advantages over conventional 2D cell cultures. Most importantly, due to their 3D organization and the fact that they can consist of multiple cell types, organoids more closely resemble organs *in vivo* than cell lines do (1). Here, we used this culture technique mainly for two reasons. First, as a tool to efficiently grow and maintain patient-derived (tumor) cells in culture. Organoids derived from patient material were established from head and neck squamous cell carcinoma (HNSCC) (Chapters 2 and 4) and pancreatic cancer (Chapter 5). Second, organoid culture was used as a tool to grow wildtype, healthy cells without the need for immortalization. For example, wildtype cells were used to establish an *in vitro* model for methotrexate-induced oral mucosa cell death, a common side-effect of chemotherapy in pediatric cancer patients (Chapter 4) (2). Additionally, wildtype cells were genetically altered using CRISPR/Cas9 to build *in vitro* tumorigenesis models (Chapter 7). Here, we will summarize our findings, discuss the implications of these results, and highlight potential follow-up research.

8

TUMOR-DERIVED ORGANOIDS AS A PLATFORM FOR (PERSONALIZED) DRUG SCREENS

Two organoid biobanks were presented in this work, one derived from HNSCC and one from pancreatic tumors.

HNSCC-derived organoids

Long-term culture of organoids derived from HNSCC and corresponding normal tissue was not previously described, although others have reported on the short-term culture of HNSCC cells (3,4). The study described in this thesis was the first to show an in-depth analysis of HNSCC-derived organoids and corresponding organoids from normal tissue, that can be maintained in culture long-term. HNSCC-derived tumoroids were shown to recapitulate genetic, functional and histological characteristics of this tumor type, and resulted in tumor formation when transplanted into mice.

As such, this study has added a new tumor type to the large repertoire of patient-derived organoid biobanks (5). However, it is the current clinical situation of HNSCC that makes HNSCC-derived organoids, in our opinion, highly relevant. Currently, HNSCC treatment can consist of surgery and/or radiotherapy, either used as single agents or combined with chemotherapy. Most commonly used chemotherapeutics include the alkylating agents cisplatin and carboplatin. When a patient is found unfit for treatment with these strong chemotherapeutics, the recently approved anti EGFR-antibody Cetuximab can be used. Compared to radiotherapy alone, addition of these chemotherapeutics to treatment regimens has been shown to increase overall survival of HNSCC patients (6,7). However,

relapse rates remain high, varying between 30 and 40% (8). Currently, no biomarkers are available to identify these non-responders prior to undergoing this debilitating therapy. Even for targeted therapies such as Cetuximab, no biomarker is identified to robustly predict patient response (9). Therefore, if organoids can help identify which patients are going to respond to these treatments, this technology might be of great value to the clinical field. The predictive potential of organoids has been shown for cystic fibrosis (10). However, the predictive value of organoids seems not to be restricted to non-oncological disease, as a recent publication showed correlation between organoid and clinical response in colon cancer patients (11). Others have shown similar results for organoids derived from pancreatic and breast cancers, although, here, numbers are much smaller (12,13).

Taking this into account, we believe that the main value of the HNSCC organoids lies in the promise it holds to aid personalized therapy. In this thesis we present a high-throughput approach to test chemotherapeutic agents on HNSCC. We show that chemotherapy can be combined with radiotherapy to mimic the chemoradiation treatment as given to patients. Before embarking on a study to compare organoid and patient response, it is important to know that such drug screens are feasible, reproducible and can be performed high-throughput. Therefore, we believe that with this study, we have set the stage for the observational Oncode Proof of Principle trial (ONCODE-P2018-0003) that was introduced in Chapter 2 of this thesis.

In addition to the previously mentioned chemotherapeutics that are currently used in clinical practice, novel targeted therapies are currently explored to treat HNSCC in patients. Here, we believe organoids can be a powerful model to validate or follow-up on the results of such tests. As an example, two recent publications report on the outcome of Phase 1 clinical trials where Alpelisib (a PIK3CA inhibitor) was given to patients whose tumors were found to carry an activating mutation in this gene (14,15). One study reported that patients carrying mutations in the helicase domain (affecting amino acid 1047) responded better than patients carrying mutation in the kinase domain (affecting amino acid 545 or 542) (14). The other trial reported the opposite, with 542/545 mutants showing a better response to Alpelisib than amino acid 1047 changes (15). Such contradictory results can be due to small sample size and heterogeneity in patient populations (tumor type, previously received therapies, additional genetic alterations etcetera). Validation of such hypothesis requires large cohorts of homogeneous patient groups. These studies are however expensive and time consuming. In our dataset that is presented in Chapter 2, H1047R mutants were more responsive than the three organoid lines tested that carry mutations in amino acids 545 or 542. Organoids could be used to validate such observed correlations between responses and mutation types, or help to understand the role of additional mutations, thereby potentially decreasing time to clinical implementation of novel therapeutics such as Alpelisib. As an example, one of the studies found that a clinical benefit was only observed if tumors were *TP53* wildtype (14). Indeed, we find that the three *TP53* wildtype organoid lines tested in our panel are amongst the most sensitive to treatment with this agent. In addition to such validation

based on patient-derived cells, direct relations between mutations and therapy response can be studied. Organoids have been shown to be easily genetically manipulated (5), allowing the introduction of a mutation of interest to test its effect on therapy response. Taken together, organoid technology might complement currently performed clinical trials that test novel therapies. Their high take rate and easy genetic manipulation allows both personalized testing on patient-derived cells and validation of causality of genetic alterations and therapy response. To further elucidate underlying response mechanisms, additional analysis including RNA sequencing of organoids before and during treatment, or whole genome sequencing could be performed. Such analysis are quicker and easier to perform on organoids than on primary patient material. Taken together, we believe that organoids can validate or support the results of such clinical trials, by allowing a more in-depth analysis on underlying biology, something that is not feasible in patients.

HNSCC ORGANOID AS A MODEL FOR EGFR-TARGETED PHOTODYNAMIC THERAPY

8

In Chapter 3 of this thesis, HNSCC organoids are applied to test a novel therapeutic approach to treat this tumor type: EGFR-targeted photodynamic therapy (PDT). We describe how EGFR-targeting nanobodies can be used to specifically kill HNSCC tumor cells. No previous studies have investigated the effect of PDT in 3D structures derived from patient-material before. EGFR expression of organoids was assessed before performing PDT. Here, it was found that EGFR expression detected on organoids was lower than that of cell lines commonly used in PDT research and closely recapitulates EGFR levels detected on patient tissues. In contrast, cell lines commonly used in PDT research express much higher levels of EGFR, highlighting the need for models that more closely recapitulate the *in vivo* situation. As such, it was highly encouraging to see that EGFR-targeted PDT was effective in organoids that express physiological EGFR levels. Moreover, organoids allowed comparison of the response of both wildtype and tumor cells from the same patient. We found that tumor cells indeed overexpress EGFR and are therefore more efficiently killed by EGFR-targeting PDT than their wildtype counterparts. Taken together, the two main findings encourage clinical implementation of this novel therapy. First, EGFR-targeted PDT was found effective on cells expressing EGFR at levels comparable to those found *in vivo*. Secondly, wildtype cells were found to be less affected by EGFR-targeting PDT than their tumor counterparts. As such, we believe this study highlights the potential of organoids to bring novel therapeutic approaches a step closer to the clinic.

Pancreatic tumor organoids

In Chapter 5 of this thesis, we present a biobank consisting of 30 organoid lines derived from pancreatic and bile duct tumors. This chapter describes the potential advantages, but also potential pitfalls of organoid technology in a translational setting. Organoids were

characterized in more detail to assess to what extent organoids recapitulate characteristics of the patient material of which they are derived. We found that, for most of the tested markers, these organoids histologically recapitulated the characteristics of the respective primary tumor tissue. However, expression of certain markers was not retained in culture, and could only be detected upon functional selection or growth factor deprivation (such as removal of Noggin and TGF- β inhibitor to functionally identify *SMAD4* mutant tumor cells). These findings underline the importance of a careful comparison between *in vitro* organoids and *in vivo* tumor tissue before any claims can be made on, for example, the predictive potential of the respective organoids. On the other hand, this chapter also highlights how organoid culture might enrich diagnostics. For example, we show how organoid culture allows for in depth DNA analysis that would not be possible in primary tumor tissue, or can result in the identification and enrichment of rare pre-cancerous cells.

In Chapter 5 we show the genomic landscape of the organoid lines that recapitulates this disease *in vivo*. We describe the single nucleotide alterations, small and large insertions or deletions, and large chromosomal rearrangements detected in the organoids.

24 of the established organoid lines were subsequently exposed to a panel of 76 therapeutic agents, including both commonly used chemotherapeutics and novel targeted therapies. These high-throughput drug screens revealed targetable vulnerabilities of tumor organoids, that differed per patient-derived organoid line. These results underscore the importance of a personalized approach, where the right drug is selected for each individual patient. How this selection should be made remains to be resolved, although our results indicate that functional selection based on *in vitro* drug screening is feasible and technically possible. Regardless, before any claims can be made on the predictive potential of this system, it is important to validate that findings obtained *in vitro* correlate to patient responses. Future plans include the correlation of drug screen responses to genetic alterations. As the drug panel tested here includes targeted therapies that interfere with signaling pathways commonly found altered in pancreatic cancer, it would be interesting to see if a correlation between therapy response and common genetic alterations can be found. If so, this model can be used to identify potential biomarkers for therapy response.

Lastly, we explored the potential of PRMT5 inhibition in more detail. Although others have previously shown that selective inhibition of this specific methyltransferase resulted in selective killing of *MTAP* negative tumor cells, this is the first time this was confirmed in a large cohort of patient-derived cells. Loss of *MTAP* results in accumulation of MTA, which inhibits the enzyme PRMT5, thereby making *MTAP* negative cells sensitive to PRMT5 inhibitions. Interestingly, we found that in addition to *MTAP* negative organoid lines, a selection of *MTAP* positive tumor samples also responded to this therapy. Moreover, we found that these samples show levels of MTA that are comparable to those measured in *MTAP* negative samples, suggestive of defective *MTAP* function. In line with this, overexpression of wildtype *MTAP* reduced sensitivity to PRMT5 inhibition in these samples. This observation suggests that, at least in some cases, genetic testing is not

the best way to identify responders. However, in order to make this claim, it would be essential to see if response to PRMT5 inhibition *in vitro*, correlates to tumor response *in vivo*. Three clinical trials testing efficacy of PRMT5 inhibitors are ongoing, although only one of these currently recruits pancreatic cancer patients (NCT03614728, NCT02783300, NCT03573310). Organoids established from these patients that will receive PRMT5 inhibitors, could be used to address this question. Here, the fact that we and others have already shown a correlation between patient response and tumor organoid response *in vitro* is encouraging (although here, different therapies were tested) (11,13,16).

Taken together, we believe this chapter addresses both the limitations and potential of organoid technology for personalized treatment approaches. The work presented here describes and validates the used organoid model and the drug screens performed with it. The next step would be to validate this potential in an observational trial, to test the predictive value of organoid assays also in this clinical setting and see if the promise holds true.

WILDTYPE ORGANOIDS AS A MODEL FOR ORAL MUCOSITIS, A COMMON SIDE-EFFECT OF CHEMOTHERAPY

8

In the other chapters of this thesis we use organoids as a model to grow wildtype epithelial cells. In Chapter 4, we use organoids established from wildtype oral mucosa to model MTX-induced mucositis. One in five pediatric leukemia patients develops mucositis in response to MTX treatment (2). To decrease the incidence and severity of MTX side-effects, Leucovorin (LV) is administered to the patient 24 to 48 hours after MTX infusion. LV partly rescues the toxicity of MTX (17), and is expected to also exert this effect in oral mucosa cells. However, this direct effect has never been shown *in vitro*. As organoids provided us with the unique opportunity to culture wildtype oral mucosa cells, we set out to study if MTX-induced toxicity could indeed be (partly) rescued by LV in this cell type. We found that folic acid (that can be converted to LV) deprivation from the organoid culture medium was essential to observe MTX sensitivity *in vitro*. Administration of LV after the start of MTX exposure decreased MTX-induced cell death, and did so in a dosing- and timing-dependent manner.

Apart from providing an *in vitro* model to test the effect of LV administration of MTX-induced cell death in wildtype organoids, we also used this model to explore options to reduce MTX-induced cell death in oral mucosa. Prior to MTX treatment, cells were exposed to LV for one day. Upon start of MTX treatment, LV was removed. This 'LV pre-treatment' intervention, was inspired by the fact that MTX-induced oral mucositis most commonly presents after the first dose of MTX, and less common after the later ones (2). It is hypothesized that this is due to higher plasma levels of LV present from the LV rescue

of the first MTX cycle. Indeed, it was found that this pre-treatment resulted in a decrease of MTX-induced cell death.

To validate if pre-treatment will influence the effect of MTX on leukemia cells, we exposed leukemia-derived cell lines to MTX, both pre-treated and not pre-treated. We found that such a pre-treatment also affects MTX sensitivity of leukemia lines. As shown in Chapter 4, we believe these effects will be less pronounced in leukemia cells than in oral mucosa cells, as, in general, leukemia cells show a much higher sensitivity to MTX, and therefore will be killed by this compound regardless of whether a pre-treatment is given. Nevertheless, these results should be considered when thinking about potential implementation of such a pre-treatment. A local application of LV to the oral mucosa would allow the effect of this intervention on the oral mucosa cells, whilst preventing any effect on the systemic leukemia cells. Locally applicable formulas to apply LV on oral mucosa already exists. Such local application will result in negligible systemic concentrations of MTX, as described in the discussion of Chapter 4. We believe therefore that, based on this work, tests with local application could be performed to assess safety and efficacy to reduce oral mucositis in pediatric leukemia patients.

Taken together, we present an *in vitro* model for MTX-induced cell death in wildtype oral mucosa epithelial cells. As no such model existed yet, we believe this technique contributes to the field and allows for the testing of modifications of current clinical protocols in a preclinical setting prior to testing it in patients. However, there are limitations to this model, of which some might be overcome in the future. For example, this model currently does not contain any immune cells (or other cells from the usual microenvironment), although the immune system has been shown to be important in oral mucositis. This limitation might be overcome by the combination of immune cells and epithelial cells. Co-cultures of immune cells and organoids have been described by others (4,18). Therefore, an interesting follow-up on this work could be to extend this system by the addition of (ideally, patient-derived) immune cells (or other cells from the usual microenvironment) and investigate their contribution to pathology.

Ultimately, the use of these organoids in a personalized approach, where organoids would be established from the oral mucosa of pediatric leukemia patients that receive MTX treatment, would be most interesting. As such, we can test if organoids can be used to predict which patients will present with mucositis. However, to establish organoids, oral mucosa biopsies are required, and these are not taken during clinical course of pediatric leukemia patients. Even if patients present with mucositis after MTX treatment, no biopsy is obtained for diagnosis. Therefore, we have explored other possibilities to obtain patient material. We have tested if organoids can be established from buccal swaps of healthy donors. Although perhaps not surprising, in none of the cases organoids grew out from these swaps (n=3). However, we could successfully establish organoids from resection material obtained at a pediatric tonsillectomy (n=1). As the tonsils are lined with squamous epithelium, organoids can be obtained when this material is digested and put into culture. As tonsillectomies are routinely performed (frequency of 1.3% in the Netherlands), this

would result in easy access to large amounts of pediatric donor material. At the time of this pilot, informed consent for the long-term culture of these organoids was not possible. However, when these regulatory affairs are addressed, access to this material could result in the establishment of a pediatric biobank. It would be interesting to see if the behavior of pediatric cells is different than adult oral mucosa in response to MTX.

Based on the frequency of tonsillectomy (1.3%) in the Netherlands, it is expected that one to two patients presenting with leukemia (130 patients a year) will require a tonsillectomy in childhood. When this surgery is performed after the patient was cured from leukemia, this material could be put in culture to establish organoids. Although we understand that numbers are low, this could lead to the establishment of oral mucosa organoids that could be linked to a clinical response (mucositis yes/no). Following this route, no extra clinical intervention is required to obtain this material, and it would provide us with the unique opportunity to grow oral mucosa cells that are mucositis-prone or resistant in culture. Then, comparing MTX sensitivity, FGPS and MTX-PG levels and expression profiles between these two groups could help us understand if 1) this difference sensitivity is retained in culture and 2) what are the differences between these cells. Understanding this might lead to changes in treatment regimens or precautions that can be taken to prevent mucositis in the group of patients at risk.

GENETIC MODIFICATION OF WILDTYPE ORGANOID MODEL TUMORIGENESIS

Chapter 7 describes how wildtype mouse prostate organoids were genetically modified using CRISPR technology. Here, a DNA template carrying the first part of the androgen receptor-responsive gene *TMPRSS2* and the last part of oncogene *ERG* was used to create a gene fusion. Transfection of this template together with sgRNAs targeting corresponding areas of these genes in mouse prostate organoids, resulted in endogenous gene fusion between these genes, that are separated by approximately 3 million base pairs. Gene fusion involving *TMPRSS2* and an ETS family member such as *ERG* is found in over 40% of prostate cancers (19–21). Both tumor cell lines and tumor organoids carrying this genetic alteration exist (22,23), but these models carry additional genetic alterations that might complicate studies focusing on the effect of the *TMPRSS2-ERG* fusion alone. As these gene fusions are believed to be early events during tumorigenesis, this model creates the opportunity to study the consequences of this genetic alteration in a furthermore wildtype background. In addition to its biological relevance, the introduction of this *TMPRSS2-ERG* fusion was the first endogenous gene fusion created in organoids, thereby underscoring the value of this, at the time, novel genome editing tool.

CONCLUDING REMARKS

In conclusion, this thesis describes a range of organoid applications, including personalized drug testing and the development of novel *in vitro* models for currently applied therapeutic approaches. We developed culture conditions for a novel organoid subtype, derived from HNSCC and corresponding wildtype epithelium. We have optimized and standardized organoid drug screens, that allow the testing of sensitivity to a wide range of therapeutics. These developments will be further optimized and applied in the Onco clinical trial to test if clinical decision making can be improved using this technology. In our opinion, this work and the resulting clinical trial highlight the potential of organoid technology to bridge the gap between the laboratory and the clinic. Similar drug screens were performed on pancreatic tumor-derived organoids to test therapy sensitivity. Additionally, we have explored other applications of organoid technology to address relevant oncological questions. As such, we showed that HNSCC organoids are a suitable model to test EGFR-targeted PDT, and that wildtype oral mucosa can be used to study oral mucositis, a common side effect of the chemotherapeutic agent MTX, *in vitro*. In both of these examples, organoids provided a model that more closely resembles the *in vivo* situation than already existing models. As such, organoid technology brings the laboratory closer to the patient, by allowing follow-up research in models that better recapitulate human physiology.

PERSONAL VIEW ON THE WORK PRESENTED IN THIS THESIS

The work presented in this thesis can be seen as one of the first attempts to bring organoid technology toward the oncology clinic. I realize much work remains to be done before this will be possible. However, considering that the technology to grow ASC-derived organoids was only developed ten years ago, I believe the progress made since then is encouraging. I hope the work presented here will aid the future clinical implementation of organoids, either by guiding personalized therapy or improving currently applied clinical protocols. With this, I hope that organoid technology can aid clinicians in making more informed decisions and, ultimately, improve patient care.

REFERENCES

1. Kretzschmar K, Clevers H. Organoids: Modeling Development and the Stem Cell Niche in a Dish. *Dev Cell*. Elsevier Inc.; 2016;38:590–600.
2. Den Hoed MAH, Lopez-Lopez E, Te Winkel ML, Tissing W, De Rooij JDE, Gutierrez-Camino A, et al. Genetic and metabolic determinants of methotrexate-induced mucositis in pediatric acute lymphoblastic leukemia. *Pharmacogenomics J*. 2015;
3. Tanaka N, Osman AA, Takahashi Y, Lindemann A, Patel AA, Zhao M, et al. Head and neck cancer organoids established by modification of the CTOS method can be used to predict in vivo drug sensitivity. *Oral Oncol*. 2018;87:49–57.
4. Neal JT, Li X, Zhu J, Giangarra V, Grzeskowiak CL, Ju J, et al. Organoid Modeling of the Tumor Immune Microenvironment. *Cell*. United States; 2018;175:1972-1988.e16.
5. Drost J, Clevers H. Organoids in cancer research. *Nat Rev Cancer*. England; 2018;18:407–18.
6. Bonner J a, Harari PM, Giralt J, Azarnia N, Shin DM, Cohen RB, et al. Radiotherapy plus cetuximab for squamous-cell carcinoma of the head and neck. *N Engl J Med*. 2006;354:567–78.
7. Ho GY, Woodward N, Coward JIG. Cisplatin versus carboplatin: Comparative review of therapeutic management in solid malignancies. *Crit. Rev. Oncol. Hematol*. 2016. page 37–46.
8. Beijer YJ, Koopman M, Terhaard CHJ, Braunius WW, Van Es RJJ, De Graeff A. Outcome and toxicity of radiotherapy combined with chemotherapy or cetuximab for head and neck cancer: Our experience in one hundred and twenty-five patients. *Clin. Otolaryngol*. 2013. page 69–74.
9. Bossi P, Resteghini C, Paielli N, Licitra L, Pilotti S, Perrone F. Prognostic and predictive value of EGFR in head and neck squamous cell carcinoma. *Oncotarget*. 2016;7:74362–79.
10. Dekkers JF, Wiegerinck CL, de Jonge HR, de Jong NWM, Bijvelds MJC, Nieuwenhuis EES, et al. A functional CFTR assay using primary cystic fibrosis intestinal organoids. *J Cyst Fibros*. Nature Publishing Group; 2012;11:S32.
11. Vlachogiannis G, Hedayat S, Vatsiou A, Jamin Y, Fernández-mateos J, Khan K, et al. Patient-derived organoids model treatment response of metastatic gastrointestinal cancers. *Science* (80-). American Association for the Advancement of Science; 2018;926:920-6.
12. Tiriác H, Belleau P, Engle DD, Plenker D, Deschênes A, Somerville T, et al. Organoid profiling identifies common responders to chemotherapy in pancreatic cancer. *Cancer Discov*. 2018;
13. Sachs N, de Ligt J, Kopper O, Gogola E, Bounova G, Weeber F, et al. A Living Biobank of Breast Cancer Organoids Captures Disease Heterogeneity. *Cell*. United States; 2018;172:373-386.e10.
14. Mayer IA, Abramson VG, Formisano L, Balko JM, Estrada M V, Sanders ME, et al. A Phase Ib Study of Alpelisib (BYL719), a PI3K α -specific Inhibitor, with Letrozole in ER+/HER2-Negative Metastatic Breast Cancer. *Clin Cancer Res*. 2017;23:26–34.
15. Juric D, Rodon J, Tabernero J, Janku F, Burris HA, Schellens JHM, et al. Phosphatidylinositol 3-Kinase α -Selective Inhibition With Alpelisib (BYL719) in PIK3CA -Altered Solid Tumors: Results From the First-in-Human Study. *J Clin Oncol*. 2018;36:1291–9.
16. Driehuis E, Kolders S, Spelier S, Lohmussaar K, Willems SM, Devriese LA, et al. Oral mucosal organoids as a potential platform for personalized cancer therapy. *Cancer Discov*. 2019;CD-18-1522.
17. Zhao R, Goldman ID. Resistance to antifolates. *Oncogene*. 2003.

18. Dijkstra KK, Cattaneo CM, Weeber F, Chalabi M, van de Haar J, Fanchi LF, et al. Generation of Tumor-Reactive T Cells by Co-culture of Peripheral Blood Lymphocytes and Tumor Organoids. *Cell. Elsevier*; 2018;174:1586–98.
19. Demichelis F, Fall K, Perner S, Andren O, Schmidt F, Setlur SR, et al. TMPRSS2:ERG gene fusion associated with lethal prostate cancer in a watchful waiting cohort. *Oncogene. England*; 2007;26:4596–9.
20. Tomlins S a, Rhodes DR, Perner S, Dhanasekaran SM, Mehra R, Sun X-W, et al. Recurrent fusion of TMPRSS2 and ETS transcription factor genes in prostate cancer. *Science*. 2005;310:644–8.
21. Hermans KG, van Marion R, van Dekken H, Jenster G, van Weerden WM, Trapman J. TMPRSS2:ERG fusion by translocation or interstitial deletion is highly relevant in androgen-dependent prostate cancer, but is bypassed in late-stage androgen receptor-negative prostate cancer. *Cancer Res. United States*; 2006;66:10658–63.
22. Gao D, Vela I, Sboner A, Iaquinta PJ, Karthaus WR, Gopalan A, et al. Organoid cultures derived from patients with advanced prostate cancer. *Cell. Elsevier Inc.*; 2014;159:176–87.
23. Tomlins S a, Laxman B, Varambally S, Cao X, Yu J, Helgeson BE, et al. Role of the TMPRSS2-ERG gene fusion in prostate cancer. *Neoplasia*. 2008;10:177–88.



ADDENDUM

NEDERLANDSE SAMENVATTING

CURRICULUM VITAE AND
LIST OF PUBLICATIONS

DANKWOORD



NEDERLANDSE SAMENVATTING

Organoïden als model voor fundamenteel en translationeel oncologisch onderzoek

Organoïden, hier gedefinieerd als driedimensionale, zelf-organiserende structuren gegroeid vanuit stamcellen (1–3), stellen wetenschappers in staat orgaanstructuur en -functie te bestuderen in het laboratorium. Er bestaan twee soorten stamcellen: pluripotente stamcellen (PSCs) en adulte stamcellen (ASCs). PSCs kunnen alle celtypen die in het menselijk lichaam voorkomen maken, en komen alleen voor in het vroege embryo. Deze stamcellen kunnen (onder de juiste condities) voor lange tijd in het lab worden geëxpandeerd als embryonale stamcellen (ESCs) (4). Synthetische varianten van PSCs kunnen gemaakt worden door genetische manipulatie van volwassen cellen. Deze stamcellen worden ‘induced Pluripotent Stem Cells’ genoemd (iPSCs) (5). ASCs zijn beperkt in de celtypen die ze kunnen produceren, maar blijven een leven lang aanwezig in ons lichaam. ASCs produceren enkel de celtypen van het orgaan waarin ze resideren, wanneer deze bijvoorbeeld door slijtage, afsterven, of ziekte moeten worden vervangen. Op die manier zijn ze verantwoordelijk voor het in standhouden van ‘hun’ orgaan.

Dat stamcellen in het lab uitgegroeid konden worden tot organoïden, bleek zo’n tien jaar geleden. Sasai en collega’s stelden PSCs bloot aan een reeks van groeifactoren om hiermee de cellen te differentiëren. Het resultaat waren driedimensionale hersenstructuren (6). In dezelfde periode werden in het Hubrecht Instituut voor het eerst organoïden gegroeid vanuit ASCs. Organoïden gegroeid vanuit het darmepitheel van muizen bleken alle (gedifferentieerde) celtypen te bevatten die in dit epitheel voorkomen. Bovendien konden deze structuren ook in kweek geëxpandeerd worden, wat bewees dat stamcellen nog altijd aanwezig waren in deze structuren (7).

Na deze initiële studies raakte het organoïd-veld in een stroomversnelling en volgde er een reeks van ontwikkelingen die elkaar in hoog tempo opvolgden. Inmiddels zijn PSC organoïden onder andere beschreven voor de hersenen, retina, schildklier, nier, darm, maag, long en lever (8–14). Vandaag de dag kunnen ASC organoïden gegroeid worden uit gezond of tumorweefsel van onder andere de darm, maag, speekselklier, slokdarm, pancreas, lever, borst, long, prostaat, smaakpapil, ovarium, blaas en mondepitheel (7,15–29). PSC organoïden zijn uitermate geschikt zijn om embryonale ontwikkeling te bestuderen. Daarentegen zijn ASC organoïden een goed model voor weefsel homeostase. Bovendien maakt het feit dat ASC organoïden gegroeid kunnen worden uit patiëntmateriaal, dit model potentieel geschikt voor ‘personalized medicine’, waarbij het effect van vele verschillende medicijnen in het laboratorium getest kunnen worden op de cellen van de patiënt.

Niet alleen het aantal weefseltypen waaruit organoïden gegroeid konden worden nam toe, ook op andere gebieden heeft de techniek zich ontwikkeld. Zo zorgde de introductie van de genetische modificatie tool CRISPR/Cas9 er bijvoorbeeld voor dat organoïden gebruikt konden worden om het effect van specifieke mutaties te bestuderen in het

lab. De eerste toepassing van deze techniek in organoïden was de correctie van een ziekteverwekkende mutatie in een organoïden lijn gegroeid uit materiaal van een patiënt met Cystic Fibrosis (taaislijmziekte). Deze DNA reparatie resulteerde in functieherstel in het lab (30). Andere verbeteringen aan bestaande organoïd kweektechnieken werden gemaakt op het gebied van differentiatie, zodat specifieke celtypen verrijkt kunnen worden in kweek (31,32). Technische verbeteringen (betere kwaliteit groeifactoren gebruikt voor het kweken, verbeterde beeldvormende technieken, optimalisatie van de protocollen voor isolatie uit primair weefsel, efficiëntere transfectie etc.) zorgen ervoor dat de mogelijkheden van organoïd technologie steeds groter worden.

Het werk met ASC organoïden dat beschreven wordt in dit proefschrift werd uitgevoerd in de periode van 2015 tot 2019, een periode waarin organoïd technologie nog volop in ontwikkeling was. Het onderzoek beschreven in dit werk richt zich voornamelijk op de klinische toepassing van organoïden in een oncologische setting (beschreven in Hoofdstuk 1 tot en met Hoofdstuk 5). Het tweede deel van dit werk (bestaande uit Hoofdstuk 6 en 7) beschrijft het gebruik van CRISPR/Cas9 in organoïden om het proces van tumorigenese (het ontstaan van tumoren) te modelleren in het laboratorium.

Nadat **Hoofdstuk 1** een algemene samenvatting geeft van het werk dat tot nu toe is uitgevoerd om de potentie van organoïd technologie voor de oncologische kliniek te onderzoeken, beschrijft **Hoofdstuk 2** een nieuw model van organoïden, waarbij deze mini-orgaantjes worden gegroeid uit plaveiselcelcarcinomen uit het hoofdhal gebied (HHPCC). Deze organoïden kunnen gegroeid worden uit tumorweefsel, maar ook uit gezond weefsel van dezelfde patiënt. Nadat was vastgesteld dat deze cellen histologisch, functioneel en genetisch lijken op de tumorcellen *in vivo*, wordt dit model gebruikt om de gevoeligheid van tumoren voor diverse geneesmiddelen te bepalen. Hierbij wordt gekeken naar de respons op cisplatine, carboplatine en het anti-EGFR antilichaam cetuximab; allemaal geneesmiddelen die op dit moment in de kliniek worden gebruikt voor de behandeling van dit tumortype. Vervolgens wordt deze chemotherapie *in vitro* gecombineerd met radiotherapie, aangezien deze in de kliniek ook vaak gecombineerd wordt met bestraling. Bovendien wordt de gevoeligheid van de organoïden voor een panel van 'targeted therapies' bepaald, medicijnen die nu nog niet regulier worden gebruikt voor behandeling van deze patiëntengroep. Voor elk van deze medicijnen bleek in ieder geval één organoïd lijn te reageren op dergelijke medicatie. Uiteindelijk wordt onderzocht of – op individueel patiënten niveau – deze organoïden kunnen helpen bij het kiezen van de juiste therapie voor de juiste patiënt. Dit concept wordt verder uitgewerkt in het addendum van Hoofdstuk 2, waarbij dieper wordt ingegaan op de Oncode Proof of Principle Clinical Trial (ONCODE-P2018-0003), die voortvloeit uit het werk beschreven in dit hoofdstuk.

In **Hoofdstuk 3 en 4** wordt hetzelfde organoïd model gebruikt dat beschreven is in Hoofdstuk 2. Echter, hier wordt onderzocht of deze mini-orgaantjes een geschikt *in vitro* model zijn voor het testen van nieuwe anti-tumor therapieën (Hoofdstuk 3), ofwel voor het verminderen van de bijwerkingen van chemotherapie (Hoofdstuk 4).

Hoofdstuk 3 beschrijft het gebruik van HHPCC organoïden om het effect van Epidermale Groei Factor Receptor (EGFR) gerichte photodynamische therapie (PDT) te testen. Bij PDT wordt een photosensitizer (PS) gebruikt die, indien geactiveerd door licht met een specifieke golflengte, reageert met zuurstof om reactieve zuurstofverbindingen (reactive oxygen species, ROS) te creëren. ROS zorgt voor schade aan DNA, RNA en eiwitten en kan op die manier resulteren in celdood (33–35). In de kliniek wordt een PS aan de patiënt gegeven, en wordt, na een incubatieperiode, de tumor belicht om de PS specifiek op de tumorlocatie te activeren (bijvoorbeeld tijdens een operatie). Om eventuele bijwerkingen te verminderen kan een PS worden gekoppeld aan antilichamen die gericht zijn tegen tumormarkers. Aangezien EGFR vaak tot overexpressie komt in HHPCC (36), kan EGFR-gerichte PDT mogelijk een manier zijn om het effect van deze therapie te vergroten en bovendien bijwerkingen te verminderen. In de kliniek wordt op dit moment in studieverband de veiligheid en effectiviteit van Cetuximab-PS PDT getest in patiënten met HHPCC. Het gebruik van een PS gekoppeld aan een anti-EGFR antilichaam of nanobody (een antigeen bindend molecuul, kleiner dan een antilichaam) is bovendien *in vitro* effectief gebleken tegen cellen die EGFR tot overexpressie brengen (37,38). Hierbij werd echter gebruik gemaakt van cellen met EGFR-expressie levels die vele malen hoger zijn dan die in patiëntmateriaal. In Hoofdstuk 3 wordt het effect van EGFR-gerichte PDT daarom getest in organoïden afkomstig van patiënten met HHPCC. EGFR-expressie in HHPCC organoïden blijkt, in tegenstelling tot de expressie in veelgebruikte cellijnen, wel vergelijkbaar te zijn met de levels gemeten in primair weefsel. EGFR-expressie is bovendien hoger in tumor organoïden dan in wildtype organoïden, net zoals dat in primair patiëntmateriaal wordt gezien.

In de organoïden vinden we dat de respons op EGFR-gerichte PDT afhankelijk is van het molecuul dat gebruikt wordt om EGFR te herkennen; zo werkt PDT met nanobody-PS beter dan Cetuximab-PS. Bovendien verschilt de therapierespons per organoïd lijn. De respons op EGFR-gerichte PDT is direct gecorreleerd met de mate van EGFR overexpressie; hoe hoger EGFR expressie op de tumor organoïd, hoe groter het effect van deze therapie. Het effect van *in vitro* PDT is afwezig in gezonde cellen van een patiënt wiens tumorcellen wel worden aangevallen door deze therapie. Samenvattend introduceert Hoofdstuk 3 HHPCC organoïden als een nieuw model voor *in vitro* EGFR-gerichte PDT, waarbij cellen getest kunnen worden die 1) direct van de patiënt afkomstig zijn, 2) EGFR in fysiologische levels tot expressie brengen, en 3) gematchte wildtype cellen ook getest kunnen worden.

Hoofdstuk 4 beschrijft het gebruik van organoïden om celdood geïnduceerd door methotrexaat (MTX) te modelleren. MTX is een chemotherapeuticum dat gebruikt wordt bij (onder andere) de behandeling van kinderen met leukemie. Eén van meest voorkomende bijwerkingen van MTX is orale mucositis, een ontsteking van het slijmvlies in de mondholte (39,40). Mucositis treedt in 20% van de patiënten op tijdens behandeling, en zorgt hierdoor voor vertraging in de behandeling. Om de bijwerkingen van MTX te verminderen wordt in de kliniek tussen de 24 en 48 uur na MTX-infusie leucovorine (LV) toegediend. LV is een middel dat het effect van MTX tegengaat. Deze huidige protocollen zijn gebaseerd op

klinische ervaring, er bestaat namelijk geen *in vitro* model om MTX-geïnduceerde celdood te modelleren. Hierdoor kunnen eventuele wijzigingen van dit protocol ook niet *in vitro* getest worden, vóór de stap naar patiënten wordt gemaakt. Het expanderen van wildtype cellen was tot de introductie van organoïden onmogelijk. Dit model biedt ons daarom voor het eerst de mogelijkheid om het effect van MTX en LV op wildtype cellen te bestuderen in het laboratorium. In Hoofdstuk 4 laten we zien dat organoïden gevoelig zijn voor MTX, en dat deze gevoeligheid verminderd kan worden door toediening van LV. Wat de studie klinisch interessant maakt, is dat we laten zien dat het effect van LV inderdaad afhankelijk is van de timing van LV toediening (iets wat per ziekenhuis kan verschillen). Tot slot wordt dit nieuwe *in vitro* model gebruikt om een potentiële verbetering van het huidige protocol te onderzoeken: een voorbehandeling met LV voor de start van MTX. Een dergelijke voorbehandeling vermindert MTX-geïnduceerde celdood in epitheelcellen, maar heeft ook een effect op leukemie cellijnen. Verder onderzoek is daarom nodig om te kijken of bijvoorbeeld een lokale LV-voorbehandeling kan helpen om de incidentie van orale mucositis omlaag te brengen.

Hoofdstuk 5 beschrijft een collectie (ofwel biobank) van tumor organoïden gekweekt uit pancreas tumoren. In dit hoofdstuk wordt onderzocht of dit model gebruikt kan worden om nieuwe behandelingen te identificeren. Om het model te karakteriseren wordt eerst een vergelijking gemaakt tussen primair patiëntmateriaal en de desbetreffende organoïd lijn. De organoïden bevatten mutaties beschreven voor dit tumor type, en maken bovendien de detectie van specifieke DNA-veranderingen mogelijk die in primair weefsel (door laag tumorpercentage) niet mogelijk zijn. Aangezien organoïden van dit tumor type al eerder zijn beschreven (41,42), richten we ons hier op de potentie van dit model om potentieel effectieve therapieën te valideren. In dit hoofdstuk laten we zien hoe de respons van 24 organoïden op 76 verschillende medicijnen wordt getest. Uit dit werkt komt naar voren dat het per organoïd lijn verschilt welk medicijn het beste werkt. Deze resultaten pleiten daarom voor een gepersonaliseerde aanpak van kankerbehandeling, waarbij er voor iedere individuele patiënt wordt gekeken welk medicijn het beste werkt. Bovendien laten deze proeven zien dat dergelijke grootschalige testen mogelijk zijn met organoïden, en dat deze – indien bewezen wordt dat organoïd respons inderdaad predictief is voor de kliniek – geschikt zouden zijn om medicijnen op te testen.

Tot slot wordt de respons van organoïden op een specifiek medicijn, namelijk een Protein Arginine N-Methyltransferase-5 (PRMT5) remmer, in detail geanalyseerd. Voor aanvang van deze studie was al bekend dat deze medicijnen specifiek werken tegen tumoren met verlies van Methylthioadenosine Phosphorylase (*MTAP*), een gen dat naast het tumor suppressor gen *CDKN2A* ligt (43–45). Inderdaad blijkt ook in organoïden dat *MTAP* negatieve tumoren gevoeliger zijn voor deze therapie dan *MTAP* positieve tumoren. Echter, er lijkt een subset van *MTAP*⁺ tumoren te zijn die ook goed reageert op PRMT5 remmers, in ieder geval *in vitro*. Expressie van wildtype *MTAP* in deze lijnen zorgt voor een afname in gevoeligheid voor de PRMT5 remmer, wat impliceert dat *MTAP* in deze tumor lijnen niet of minder functioneel is. In een poging te begrijpen wat deze subset van *MTAP*⁺

tumoren onderscheidt van de ongevoelige *MTAP*⁺ tumoren, worden deze twee groepen vergeleken met behulp van differentiële genexpressie en DNA-analyse. Echter, deze analyses geven geen duidelijke verklaring voor het verschil in gevoeligheid tussen deze twee groepen van *MTAP*⁺ tumoren. Aanvullende experimenten zijn nog gaande om deze subset van tumoren te identificeren. Dit is relevant, aangezien deze resultaten impliceren dat PRMT5 remmers mogelijk geschikt zijn voor een bredere groep patiënten.

Tot slot richten **Hoofdstuk 6 en 7** zich op het gebruik van CRISPR/Cas9 in organoïden. Sinds de introductie van CRISPR/Cas9 als genetische modificatie tool, heeft deze technologie zich snel ontwikkeld. **Hoofdstuk 6** geeft daarom eerst een overzicht van het werk dat tot nu toe is uitgevoerd met CRISPR/Cas9 in organoïden. Hier worden de voor- en nadelen besproken van het combineren van deze twee technieken.

Hoofdstuk 7 beschrijft het gebruik van CRISPR/Cas9 in wildtype prostaat cellen. In dit hoofdstuk beschrijven we hoe, met behulp van deze techniek, een endogene fusie van *TMPRSS2* (een gen dat geactiveerd wordt door testosteron) en *ERG* (een oncogen) wordt gecreëerd in wildtype prostaat cellen. Deze genfusie, resulterend in overexpressie van het oncogen ERG, is een veel voorkomende genetische verandering in prostaatkanker (46–49). Er bestaan al organoïden en cellijnen die deze genetische verandering bevatten (50). Echter, deze zijn gegroeid uit tumormateriaal en bevatten daarom ook andere genetische veranderingen die het gedrag van de cel kunnen beïnvloeden. Aangezien wordt aangenomen dat de *TMPRSS2-ERG* fusie een van de initiërende gebeurtenissen is tijdens het ontstaan van prostaatkanker, is het relevant om het effect van deze DNA-verandering te bestuderen in genetisch wildtype achtergrond. De *TMPRSS2-ERG* organoïden, gemaakt door een stuk DNA van drie miljoen baseparen te verwijderen en daarmee coderende sequenties van de twee genen te fuseren, zijn daarom een interessant model om tumorigenese te bestuderen.

Tot slot worden in **Hoofdstuk 8** de implicaties van het werk beschreven in de de eerdere hoofdstukken bediscussieerd. Bovendien worden hier eventuele vervolgstappen voor onderzoek aangedragen en besproken, om de klinische implementatie van organoïd technologie te bevorderen.



REFERENTIES

1. Kretschmar K, Clevers H. Organoids: Modeling Development and the Stem Cell Niche in a Dish. *Dev Cell*. Elsevier Inc.; 2016;38:590–600.
2. Eiraku M, Sasai Y. Mouse embryonic stem cell culture for generation of three-dimensional retinal and cortical tissues. *Nat Protoc*. 2012;7:69–79.
3. Lancaster M a., Knoblich J a. Organogenesis in a dish: modeling development and disease using organoid technologies. *Science*. 2014;345:1247125.
4. Thomson JA. Embryonic Stem Cell Lines Derived from Human Blastocysts. *Science (80-)*. 1998;282:1145–7.
5. Takahashi K, Yamanaka S. Induction of Pluripotent Stem Cells from Mouse Embryonic and Adult Fibroblast Cultures by Defined Factors. *Cell*. 2006;126:663–76.
6. Eiraku M, Watanabe K, Matsuo-Takasaki M, Kawada M, Yonemura S, Matsumura M, et al. Self-Organized Formation of Polarized Cortical Tissues from ESCs and Its Active Manipulation by Extrinsic??Signals. *Cell Stem Cell*. 2008;3:519–32.
7. Sato T, Vries RG, Snippert HJ, van de Wetering M, Barker N, Stange DE, et al. Single Lgr5 stem cells build crypt-villus structures in vitro without a mesenchymal niche. *Nature*. Nature Publishing Group; 2009;459:262–5.
8. Dye BR, Hill DR, Ferguson MA, Tsai Y-H, Nagy MS, Dyal R, et al. In vitro generation of human pluripotent stem cell derived lung organoids. *Elife*. 2015;4:e05098.
9. Lancaster MA, Renner M, Martin C-A, Wenzel D, Bicknell LS, Hurler ME, et al. Cerebral organoids model human brain development and microcephaly. *Nature*. 2013;501:373–9.
10. Longmire TA, Ikonomou L, Hawkins F, Christodoulou C, Cao Y, Jean JC, et al. Efficient derivation of purified lung and thyroid progenitors from embryonic stem cells. *Cell Stem Cell*. 2012;10:398–411.
11. McCracken KW, Catá EM, Crawford CM, Sinagoga KL, Schumacher M, Rockich BE, et al. Modelling human development and disease in pluripotent stem-cell-derived gastric organoids. *Nature*. 2014;516:400–4.
12. Spence JR, Mayhew CN, Rankin SA, Kuhar MF, Vallance JE, Tolle K, et al. Directed differentiation of human pluripotent stem cells into intestinal tissue in vitro. *Nature*. 2011;470:105–9.
13. Takasato M, Er PX, Becroft M, Vanslambrouck JM, Stanley EG, Elefanti AG, et al. Directing human embryonic stem cell differentiation towards a renal lineage generates a self-organizing kidney. *Nat Cell Biol*. 2014;16:118–26.
14. Takebe T, Zhang R-R, Koike H, Kimura M, Yoshizawa E, Enomura M, et al. Generation of a vascularized and functional human liver from an iPSC-derived organ bud transplant. *Nat Protoc*. Nature Publishing Group; 2014;9:396–409.
15. Barker N, Huch M, Kujala P, van de Wetering M, Snippert HJ, van Es JH, et al. Lgr5+ve Stem Cells Drive Self-Renewal in the Stomach and Build Long-Lived Gastric Units In Vitro. *Cell Stem Cell*. 2010;6:25–36.
16. Rock JR, Onaitis MW, Rawlins EL, Lu Y, Clark CP, Xue Y, et al. Basal cells as stem cells of the mouse trachea and human airway epithelium. *Proc Natl Acad Sci U S A*. 2009;106:12771–5.
17. Tadokoro T, Wang Y, Barak LS, Bai Y, Randell SH, Hogan BLM. IL-6/STAT3 promotes regeneration of airway ciliated cells from basal stem cells. *Proc Natl Acad Sci U S A*. 2014;1–9.
18. Lee SH, Hu W, Matulay JT, Silva M V., Owczarek TB, Kim K, et al. Tumor Evolution and Drug Response in Patient-Derived Organoid Models of Bladder Cancer. *Cell*. 2018;173:515-528.e17.

19. Driehuis E, Kolders S, Spelier S, Lohmussaar K, Willems SM, Devriese LA, et al. Oral mucosal organoids as a potential platform for personalized cancer therapy. *Cancer Discov.* 2019;CD-18-1522.
20. Hu H, Gehart H, Artegiani B, Lopez-Iglesias C, Dekkers F, Basak O, et al. Long-Term Expansion of Functional Mouse and Human Hepatocytes as 3D Organoids. *Cell.* United States; 2018;175:1591-1606.e19.
21. Kopper O, de Witte CJ, Lohmussaar K, Valle-Inclan JE, Hani N, Kester L, et al. An organoid platform for ovarian cancer captures intra- and interpatient heterogeneity. *Nat Med.* United States; 2019;
22. DeWard AD, Cramer J, Lagasse E. Cellular heterogeneity in the mouse esophagus implicates the presence of a nonquiescent epithelial stem cell population. *Cell Rep.* 2014;9:701-11.
23. Huch M, Bonfanti P, Boj SF, Sato T, Loomans CJM, van de Wetering M, et al. Unlimited in vitro expansion of adult bi-potent pancreas progenitors through the Lgr5/R-spondin axis. *EMBO J.* 2013;32:2708-21.
24. Huch M, Dorrell C, Boj SF, van Es JH, Li VSW, van de Wetering M, et al. In vitro expansion of single Lgr5+ liver stem cells induced by Wnt-driven regeneration. *Nature.* 2013;494:247-50.
25. Karthaus WR, Iaquina PJ, Drost J, Gracanin A, Van Boxtel R, Wongvipat J, et al. Identification of multipotent luminal progenitor cells in human prostate organoid cultures. *Cell.* 2014;159:163-75.
26. Kessler M, Hoffmann K, Brinkmann V, Thieck O, Jackisch S, Toelle B, et al. The Notch and Wnt pathways regulate stemness and differentiation in human fallopian tube organoids. *Nat Commun.* 2015;6.
27. Linnemann JR, Miura H, Meixner LK, Irmeler M, Kloos UJ, Hirschi B, et al. Quantification of regenerative potential in primary human mammary epithelial cells. *Development.* 2015;142:1-13.
28. Nanduri LSY, Baanstra M, Faber H, Rocchi C, Zwart E, De Haan G, et al. Purification and Ex vivo expansion of fully functional salivary gland stem cells. *Stem Cell Reports.* 2014;3:957-64.
29. Ren W, Lewandowski BC, Watson J, Aihara E, Iwatsuki K, Bachmanov AA, et al. Single Lgr5- or Lgr6-expressing taste stem/progenitor cells generate taste bud cells ex vivo. *Proc Natl Acad Sci U S A.* 2014;111:16401-6.
30. Schwank G, Koo BK, Sasselli V, Dekkers JF, Heo I, Demircan T, et al. Functional repair of CFTR by CRISPR/Cas9 in intestinal stem cell organoids of cystic fibrosis patients. *Cell Stem Cell.* 2013;13:653-8.
31. Beumer J, Artegiani B, Post Y, Reimann F, Gribble F, Nguyen TN, et al. Enteroendocrine cells switch hormone expression along the crypt-to-villus BMP signalling gradient. *Nat Cell Biol.* England; 2018;20:909-16.
32. Basak O, Beumer J, Wiebrands K, Seno H, van Oudenaarden A, Clevers H. Induced Quiescence of Lgr5+ Stem Cells in Intestinal Organoids Enables Differentiation of Hormone-Producing Enteroendocrine Cells. *Cell Stem Cell.* United States; 2017;20:177-190.e4.
33. Plaetzer K, Krammer B, Berlanda J, Berr F, Kiesslich T. Photophysics and photochemistry of photodynamic therapy: fundamental aspects. *Lasers Med Sci.* Springer; 2009;24:259-68.
34. Trachootham D, Alexandre J, Huang P. Targeting cancer cells by ROS-mediated mechanisms: a radical therapeutic approach? *Nat Rev Drug Discov.* Nature Publishing Group; 2009;8:579.
35. Curtin JF, Donovan M, Cotter TG. Regulation and measurement of oxidative stress in apoptosis. *J Immunol Methods.* Elsevier; 2002;265:49-72.
36. Kalyankrishna S, Grandis JR. Epidermal growth factor receptor biology in head and neck cancer. *J Clin Oncol.* American Society of Clinical Oncology; 2006;24:2666-72.
37. Heukers R, van Bergen en Henegouwen P, Oliveira S. Nanobody-photosensitizer

- conjugates for targeted photodynamic therapy. *Nanomedicine Nanotechnology, Biol Med. Elsevier*; 2014;10:1441–51.
38. Van Driel PBAA, Boonstra MC, Slooter MD, Heukers R, Stammes MA, Snoeks TJA, et al. EGFR targeted nanobody–photosensitizer conjugates for photodynamic therapy in a pre-clinical model of head and neck cancer. *J Control Release. Elsevier*; 2016;229:93–105.
 39. Den Hoed MAH, Lopez-Lopez E, Te Winkel ML, Tissing W, De Rooij JDE, Gutierrez-Camino A, et al. Genetic and metabolic determinants of methotrexate-induced mucositis in pediatric acute lymphoblastic leukemia. *Pharmacogenomics J.* 2015;
 40. Villa A, Sonis ST. Mucositis: Pathobiology and management. *Curr. Opin. Oncol.* 2015.
 41. Seino T, Kawasaki S, Shimokawa M, Tamagawa H, Toshimitsu K, Fujii M, et al. Human Pancreatic Tumor Organoids Reveal Loss of Stem Cell Niche Factor Dependence during Disease Progression. *Cell Stem Cell. Elsevier*; 2018;22:454–467.e6.
 42. Tiriach H, Belleau P, Engle DD, Plenker D, Deschênes A, Somerville T, et al. Organoid profiling identifies common responders to chemotherapy in pancreatic cancer. *Cancer Discov.* 2018;
 43. Mavrakis KJ, McDonald ER 3rd, Schlabach MR, Billy E, Hoffman GR, deWeck A, et al. Disordered methionine metabolism in MTAP/CDKN2A-deleted cancers leads to dependence on PRMT5. *Science. United States*; 2016;351:1208–13.
 44. Kryukov G V, Wilson FH, Ruth JR, Paulk J, Tsherniak A, Marlow SE, et al. MTAP deletion confers enhanced dependency on the PRMT5 arginine methyltransferase in cancer cells. *Science. United States*; 2016;351:1214–8.
 45. Marjon K, Cameron MJ, Quang P, Clasquin MF, Mandley E, Kunii K, et al. MTAP Deletions in Cancer Create Vulnerability to Targeting of the MAT2A/PRMT5/RIOK1 Axis. *Cell Rep.* 2016;
 46. Demichelis F, Fall K, Perner S, Andren O, Schmidt F, Setlur SR, et al. TMPRSS2:ERG gene fusion associated with lethal prostate cancer in a watchful waiting cohort. *Oncogene. England*; 2007;26:4596–9.
 47. Hermans KG, van Marion R, van Dekken H, Jenster G, van Weerden WM, Trapman J. TMPRSS2:ERG fusion by translocation or interstitial deletion is highly relevant in androgen-dependent prostate cancer, but is bypassed in late-stage androgen receptor-negative prostate cancer. *Cancer Res. United States*; 2006;66:10658–63.
 48. Tomlins S a, Rhodes DR, Perner S, Dhanasekaran SM, Mehra R, Sun X-W, et al. Recurrent fusion of TMPRSS2 and ETS transcription factor genes in prostate cancer. *Science.* 2005;310:644–8.
 49. Klezovitch O, Risk M, Coleman I, Lucas JM, Null M, True LD, et al. A causal role for ERG in neoplastic transformation of prostate epithelium. *Proc Natl Acad Sci U S A. United States*; 2008;105:2105–10.
 50. Tomlins S a, Laxman B, Varambally S, Cao X, Yu J, Helgeson BE, et al. Role of the TMPRSS2-ERG gene fusion in prostate cancer. *Neoplasia.* 2008;10:177–88.

CURRICULUM VITAE AND LIST OF PUBLICATIONS

Curriculum vitae

Else Driehuis was born on the 22th of August 1991, in Deventer, The Netherlands. In 2009, she graduated from Almere College in Kampen (*cum laude*), majoring in Nature and Health and Nature and Technology tracks. She obtained a Bachelor Degree in Biomedical Sciences (*cum laude*) from the VU University in Amsterdam, additionally obtaining a grade two teaching degree in Biology during the minor of her Bachelor. In 2012, she enrolled in the Masters program in Oncology at the faculty of Medicine of VU University, where her first internship was performed at the department of Clinical Genetics in the group of Johan de Winter. Here she was inspired to pursue a PhD and got selected for the Huygens Honors program of the VU University, where a PhD proposal was written by the candidate. In parallel, she worked as a teaching assistant for medical, biomedical and health science students at the VU University for three years. Her Major internship was performed at the laboratory of KJ Patel at the MRC Laboratory of Molecular Biology in Cambridge, UK. She graduated the Masters program in Oncology in 2014 (*cum laude*) and started her PhD at the lab of Hans Clevers in Utrecht in 2015.

List of publications related to this thesis

Organoid culture systems for prostate epithelial and cancer tissue. J. Drost, W.R. Karthaus, D. Gao, E. Driehuis, C.L. Sawyers, Y. Chen, H. Clevers. *Nat Protoc.* 2016 Feb;11(2):347-58.

CRISPR-Induced TMPRSS2-ERG Gene Fusions in Mouse Prostate Organoids, E. Driehuis and H. Clevers. *JSM Biotechnol Biomed Eng.* 2017;4(1). pii: 1076.

CRISPR/Cas 9 genome editing and its applications in organoids. E. Driehuis and H. Clevers. *Am J Physiol Gastrointest Liver Physiol.* 2017 Mar 1;312(3):G257-G265.

WNT signalling events near the cell membrane and their pharmacological targeting for the treatment of cancer. E. Driehuis and H. Clevers. *Br J Pharmacol.* 2017 Dec;174(24):4547-4563.

Organoid profiling identifies common responders to chemotherapy in pancreatic cancer. H. Tiriac, P. Belleau, D.D. Engle, D. Plenker, A. Deschênes, T.D.D. Somerville, F.E.M. Froeling, R.A. Burkhart, R.E. Denroche, G.H. Jang, K. Miyabayashi, C.M. Young, H. Patel, M. Ma, J.F. LaComb, R.L.D. Palmaira, A.A Javed, J.C. Huynh, M. Johnson, K. Arora , N. Robine, M. Shah, R. Sanghvi, A.B. Goetz, C.Y. Lowder, L. Martello, E. Driehuis, N. LeComte, G. Askan, C.A. Iacobuzio-Donahue, H. Clevers, L.D. Wood, R. H. Hruban, E. Thompson , A.J. Aguirre, B.M. Wolpin, A. Sasson, J. Kim, M. Wu, J.C. Bucobo, P. Allen, D.V. Sejjal, W. Nealon, J.D. Sullivan, J.M. Winter, P.A. Gimotty, J.L. Grem, D.J. DiMaio,



J.M. Buscaglia, P.M. Grandgenett, J.R. Brody, M.A. Hollingsworth, G.M. O’Kane, F. Notta, E. Kim, J.M. Crawford, C. Devoe, A. Ocean, C.L. Wolfgang, K.H. Yu, E. Li, C.R. Vakoc, B. Hubert, S.E. Fischer, J.M. Wilson, R. Moffitt, J. Knox, A. Krasnitz, S. Gallinger, D.A. Tuveson. *Cancer Discovery*. 2018 Sep;8(9):1112-1129.

Organoïden als in vitro model: mini-organen in het laboratorium. Organoids as an in vitro model: mini-organs in the lab. E. Driehuis, H. Clevers. *Nederlands Tijdschrift voor Oncologie*. 2018; 15:244-51

Oral mucosal organoids as a potential platform for personalized cancer therapy. E. Driehuis, S. Kolders, S. Spelier, K. Löhmußaar, S.M. Willems, L.A. Devriese, R. de Bree, E.J. de Ruiter, J. Korving, H. Begthel, J.H. van Es, V. Geurts, G.W. He, R.H. van Jaarsveld, R. Oka, M.J. Muraro, J. Vivié, M.M.J.M. Zandvliet, A.P.A. Hendrickx, N. Iakobachvili, P. Sridevi, O. Kranenburg, R. van Boxtel, G.J.P.L. Kops, D.A. Tuveson, P.J. Peters, A. van Oudenaarden, H. Clevers. *Cancer Discovery*. 2019. Jul;9(7):852-871.

Under revision



Patient-derived oral mucosa organoids as an in vitro model for methotrexate induced toxicity. E. Driehuis, N. Oosterom, S. G. Heil, I.B. Muller, M. Lin, S. Kolders, G. Jansen, R. de Jonge, R. Pieters, H. Clevers, M. M. van den Heuvel-Eibrink.

Pancreatic cancer organoids recapitulate disease and allow personalized drug screening. E. Driehuis, A. Hoeck, S. Kolders, H.E. Francies, M.C. Gulersonmez, E.C.A. Stigter, B. Burgering, V. Geurts, A. Granacin, F.H. Morsink, R. Vries, S. Boj, J. van Es, G.J.A. Offerhaus, O. Kranenburg, M.J. Garnett, E. Cuppen, L.A.A. Brosens, H. Clevers.

Patient-derived head and neck cancer organoids recapitulate clinically relevant EGFR expression levels and are responsive to EGFR-targeted photodynamic therapy. E. Driehuis, S. Spelier, I. Beltrán Hernández, E.J. de Ruiter, R. de Bree, S.M. Willems, H. Clevers, S. Oliveira.

Fasting-mimicking diet and endocrine therapy induces EGR1 to promote breast cancer regression and prevent resistance. I. Caffa, V. Spagnolo, P. Becherini, F. Valdemarin, C. Zucal, M. Passalacqua, L. Mastracci, M. Wei, S. Brandhorst, E. Driehuis, R. Gradashi, C. Mantero, V. Vellone, S. Piazza, L. Ferrando, G. Zoppoli, A. Arrighi, F. Piacente, M. Cea, C. Gianotti, F. Monacelli, A. Ballestrero, P. Odetti, S. G. Sukkar, G. Salvadori, S. Cortellino, H. Clevers, A. Provenzani, V. D. Longo, and A. Nencioni.

DANKWOORD

Het werk beschreven in dit proefschrift werd uitgevoerd in de periode 2015 tot en met 2019. In 2015 was organoïden technologie nog volop in ontwikkeling. In de afgelopen jaren is er grote vooruitgang geboekt op dit gebied, en is het aantal “tools” in de “organoïde tool box” enorm toegenomen. Ik vond het een voorrecht om in deze periode te werken in een lab dat zo centraal geïmplementeerd is in dit onderzoeksgebied. Een lab bestaande uit een groep onderzoekers die in deze periode groeide van zo’n twintig naar vijftig man, met een interessegebied dat zich van ongeveer tien naar dertig verschillende celtypen uitbouwde. In mijn ogen een aanpak die een bepaalde kijk op wetenschap ademt. Ik vond het bijzonder dit te mogen ervaren en te mogen leren van alle gedreven, intelligente en leuke mensen die in die vijf jaar in de Clevers groep hebben gewerkt.

Het was lastiger dan ik had gedacht, dat promoveren. Doorzetten als dingen weer mislukken en weten wanneer je een hypothese moet laten varen, ook al heb je hier al veel tijd in gestopt. Leren hoe je een paper schrijft en een verhaal structureert. Beursaanvragen schrijven, soms papers reviewen, presentaties geven, studenten begeleiden en samenwerken met anderen. En, in ieder geval voor m’n gevoel, dat soms allemaal tegelijkertijd. Dat ging echt niet altijd goed, maar ik heb erg veel geleerd in de afgelopen jaren, op veel verschillende fronten. Ik ben trots dat ik mijn promotietraject op deze manier heb kunnen doorlopen en ben dankbaar voor iedereen die me hierbij heeft geholpen.

De jaren van mijn promotietraject zijn bijzonder geweest. Ze hebben zich tot de nok toe gevuld met nieuwe ervaringen. Lange dagen vol experimenten (want in een dag zitten sowieso te weinig uren: er is veel te veel te ontdekken), muziek (ik was nog zo gewaarschuwd: Dekoor wordt je leven), en nieuwe vrienden (zoveel uren op een lab met mensen met dezelfde interesses en ervaringen schept een band). Ik wil van de gelegenheid gebruik maken om een aantal mensen in het bijzonder te bedanken.

Allereerst, mijn promotor **Hans**. Ik wil je bedanken voor de gelegenheid om onderzoek te mogen doen in jouw onderzoeksgroep, tussen al deze gedreven en getalenteerde mensen. Ik blijf het bijzonder vinden hoe je -ondanks je drukke agenda- altijd goedghumeurd en ontspannen lijkt te zijn. Ik moest wennen aan de vrijheid in je lab, maar ik wil je bedanken voor de sfeer die je daarmee creëert, die mensen uitdaagt kritisch na te denken en zelfstandig tot oplossingen te komen. Ik denk dat er maar weinig andere plekken zijn waar ik dezelfde vaardigheden en ervaringen had mogen en kunnen ontwikkelen in deze fase van mijn carrière. Ik heb als onderzoeker van je geleerd om grote vragen te stellen, en heb ontdekt dat deze verassend vaak simpele antwoorden blijken te hebben. Bedankt voor de mogelijkheid die je me gaf om zelfstandig projecten op te zetten en het vertrouwen dat je daarbij in me had.

Mijn tweede promotor, **Paul**. Ondanks dat ik je niet op dagelijkse basis sprak, was je input tijdens mijn commissie meetings waardevol. Ik heb met veel plezier je enthousiasme voor onderzoek aanschouwd en genoten van je oneliners. De keren dat wij samen naar coupes van tumoren hebben gekeken vond ik waardevol en hebben mijn eerste interesse in de pathologie aangewakkerd. Bedankt voor je betrokkenheid en doelgerichtheid. In het bijzonder bedankt voor je motiverende woorden, die ik zowel digitaal als in real-life mocht ontvangen.

Mijn copromotor, **Stefan**. Stefan, in de eerste plaats bedankt voor je onvoorwaardelijke enthousiasme. Door een gesprek met jou (volgens mij over een thymoom) is het hele hoofd hals project van de grond gekomen. Ik heb je input en advies tijdens dit project als onmisbaar ervaren en wil je bedanken voor alle tijd die je hier, ondanks je volle agenda, in hebt geïnvesteerd. Je hebt een essentiële rol gehad in het hoofd hals project (het grootste project van dit proefschrift), wat zonder jouw inzet en bijdrage zeker weten niet was gelukt. Ik ben tijdens mijn PhD erg geïnteresseerd geraakt in de pathologie, wat zeker ook komt doordat een deel van jouw bevlogenheid op mij is overgewaaid. Ik vind het mooi om te zien dat je met zoveel enthousiasme bezig bent met je vak en hoop je in de toekomst tegen te blijven komen.

&

Mijn paranimfen, **Frans** en **Yorick**. Frans, voor mij ben je niet één, maar twee onmisbare personen geweest tijdens mijn promotietraject. Allereerst een fijn kamergenootje om op te bouwen in een groot lab vol indrukwekkende wetenschappers én bijzondere persoonlijkheden. Gaandeweg werd je een goede vriend (mien maat!) om mee te lachen, maar ook mee te sparren over proeven of situaties in het lab. Door samen te fietsen zorgde je er bovendien voor dat ik om zeven uur echt een keer naar huis ging, iets wat na jouw vertrek dan ook echt áltijd misging. Ten tweede ben je als mijn vriend (of partner, zoals dat volgens de VU pathologen heet) onmisbaar voor mij. Dankjewel voor de vanzelfsprekendheid in je vertrouwen. Daarnaast bedankt voor je optimisme en relativiseringsvermogen, die me vaak erg helpen. Het had niet anders gekund dan dat jij mijn paranimf bent.

Yorick, heel tof dat jij mijn paranimf wil zijn! Bedankt voor je goede raad omtrent experimenten en papers, maar nog meer voor onze gesprekken en de oneindige koppen koffie die we hebben gedronken samen. Jij was degene die relevante papers altijd direct aan me doorstuurde, waardoor ik er zeker van was dat ik niks belangrijks miste! Ik blijf onder de indruk van je discipline, vastberadenheid en de kwaliteit van je werk. Je lijkt niet snel onder de indruk en gaat recht op je doel af. Ik hoop dat je het naar je zin krijgt in Amerika, en weet zeker dat je daar succesvol zult zijn.

Lieve **papa, mama** en **Femke**. Bedankt voor de fijne basis van ons gezin, waar ik altijd op mag en kan terugvallen. Bedankt voor alle mogelijkheden die jullie mij hebben gegeven én voor het meegeven van het vertrouwen dat ik kan bereiken wat ik wil. Bedankt voor het aanhoren van alle verhalen over het lab, collega's, organoïden en tumoren, die jullie écht niet allemaal interessant gevonden kunnen hebben. Papa, bedankt voor je adviezen en het doorlezen van mijn reviews.

Lieve **opa** en **oma**, wat fijn dat jullie het eindproduct van mijn promotie kunnen zien. Het betekent veel voor me dat jullie hierbij kunnen zijn en ben blij dat ik jullie kan laten zien waar ik de afgelopen jaren zo druk mee bezig ben geweest.

Dekoor, lief Dekoor, wat fijn dat jij er bent. Repetities, theatertours door heel (en dan ook echt héél) Nederland, Ziggo Dome, AFAS Live, DWDD, Sziget, Luxemburg, Denemarken, Zuid-Afrika; niks was je te gek. Bevangen door een koortsachtige gedrevenheid denderde jij altijd maar door, ons naar muzikale hoogtes stuwend. Je was essentieel tijdens mijn promotie. Een bestuursjaar heeft me wijzer gemaakt, zowel op sociaal als (muzikaal) inhoudelijk vlak. Repetities op dinsdagavond zorgden voor een relativerende pauze in mijn werkweek, waardoor ik me weer besepte dat mijn werk, hoe leuk ook, niet alles in het leven is. Drie jaar zingen heeft me vrienden voor het leven opgeleverd. Elke week bezig zijn met Dekoor heeft me veel geleerd over zingen en muziek. Maar bovenal heb je me de volgende wijze les geleerd: door volledige inzet en focus, wordt het onmogelijke soms toch mogelijk. Het maakt niet uit hoe het met je gaat, bij Dekoor ben je welkom. Wie je bent en wat je doet is goed, en dat is altijd goed genoeg. Dekoor, en alle mensen uit wie je bestaat of hebt bestaan: ik vond het zo onwijs tof deel van je te hebben mogen uitgemaakt. Ik voel me nog altijd vereerd en mis je vaak. Dekoor, lief Dekoor, je hebt mijn leven verrijkt.

Mijn kamergenoten: **Janny, Wim, Karien, Stieneke, Frans, Fjodor** en **DJ**. Janny, bedankt voor je gezelligheid en goede zorgen tijdens de eerste paar jaar van mijn promotietraject. Als je bij jou op de kamer zit ben je altijd van alles op de hoogte, wat heel handig kan zijn! Wim, bedankt voor de fijne gesprekken, goede adviezen, maar maar ook de complimenten die ik soms zomaar van je kreeg, en die me zeker zijn bijgebleven. Bedankt voor je bemoedigende schouderklopjes ("dag meid" als je langs me liep als je naar huis ging of juist binnenkwam) en bovenal je gezelligheid. Ik vond het heel fijn deze jaren een kamer met je te delen en ik ga je missen. Karien, bedankt voor je goede zorgen, muziek- en theatertips en de waardevolle gesprekken die we hebben gevoerd. Ik vond het gezellig om naast je te mogen zitten. Stieneke, ik heb genoten van je no-nonsense aanpak van problemen op het lab, je rake opmerkingen omtrent persoonlijke issues en je doorzettersmentaliteit, die ik als inspirerend heb ervaren. Frans, als kamergenoot was je voor mij belangrijk: degene om een blik mee te delen als Janny op hol sloeg, om mee



te lachen samen met Wim, en om mee te sparren als ik vast zat met een project. Fjodor, ik vond het heel leuk om jou als kamergenoot te hebben. Ik heb genoten van je gezellige geklets, ongeëvenaarde enthousiasme rondom experimenten (een goede “reality check” voor mij), je attentheid (“jaaaaa meer chocola met groene thee-smaak”) en je motivatie om allerlei activiteiten met de PhD-studenten te ondernemen. Heel veel succes tijdens je promotie en de daaropvolgende opleiding tot arts, die jij toch echt wel in hart en nieren (snap je ‘m, snap je ‘m) bent. DJ, I enjoyed having you as a roommate, to share advice on which store has the nicest clothes on sale, what is the best coffee, but also discuss the best experimental approach. I hope we helped you settle back in in the lab after your return and wish you the best for your future.

Sigrid, bedankt voor je inzet tijdens de laatste twee jaar van mijn promotietraject. Fijn dat je daarnaast goed meedacht en zo mijn experimenten verbeterde. Ik hoop dat je het naar je zin hebt op je nieuwe werkplek!

Sacha, bedankt voor je gedrevenheid en het enthousiasme dat je met je meebracht tijdens je stage. Ik heb veel gehad aan onze discussies en veel geleerd van uitleg aan je geven. Ik hoop dat ik je alles heb kunnen leren wat je wilde, en wens je heel veel succes tijdens je -ongetwijfeld succesvolle- carrière. Hopelijk komen we elkaar nog eens tegen!



Jarno, bedankt voor het mij “inwerken” in het lab, je geduld bij het mij leren kweken van organoïden en je adviezen over vervolgstappen in het begin van mijn promotietraject.

Sylvia, thank you for making me familiar with the techniques and people in the lab during the first months of my PhD. Thank you for your patience and kindness. I admire your dedication to your work and the care and attention you have for people in that process, even when you must be very busy. I am looking forward to working with you again.

Joep, bedankt voor je humor, wijze raad en altijd enthousiaste ‘Elsieeee’ waarmee ik (echt waar!) elke dag door je begroet werd. Ik heb erg veel bewondering voor je oneindige gedrevenheid en onbezorgd enthousiasme voor de biologie. Vergeet niet af en toe een heel weekend vrij te nemen. In het bijzonder heb ik de gesprekken over ons persoonlijk leven als heel waardevol ervaren. Bedankt voor je adviezen omtrent proeven, lezen van mijn reviews en artikelen, en het trouwe delen van je vrijdag frietjes! Heel veel succes in de toekomst. En ook al weet ik dat je zenuwachtig wordt als mensen dat zeggen (“neeeee, niet zeggen, niet zeggen”), ik doe het hier lekker toch: ik weet zeker dat, wat je ook gaat doen, je het tot een groot succes zal maken. Ik ga jou, en je puppy-achtige enthousiasme, erg missen.

Maarten, ondanks een ingewikkelde situatie bij de start van jouw PhD waar ik je moest begeleiden bij je literatuurstudie, heb ik altijd goed met je kunnen kenen. Ik vond het gezellig dat je aansloot als vast lid van de koffieclub voor koffies met koekjessaus en heb dankbaar gebruik gemaakt van je adviezen over een toekomstige carrière. Bedankt voor je hulp in de laatste fase van mijn promotietraject, of dat nou was door me naar feestlocaties te rijden of door feedback te geven op figuren. Gelukkig is de lol die we samen konden hebben voor eeuwig vastgelegd als Whatsapp sticker. Succes met je promotieonderzoek!

Kim, bedankt voor je goede zorgen, gezelligheid en gesprekken. Ondanks dat het niet leuk is om ziek te zijn, vond ik het prettig hier met je over te praten en had ik het idee dat we elkaar hierin goed begrepen. Succes met je promotie en alles wat je in de toekomst gaat uitspoken!

Jens, ik heb genoten van je goede grappen en gezelligheid. Bedankt voor je waardevolle input omtrent figuren en analysis, en de tijd die je hierin hebt gestoken.

The other current PhD-students in the lab: **Kadi, Jelte, Cayetano, Marie** and **Carla**. Thank you for making the lab such a fun environment that was filled with valuable scientific discussions and lots of fun activities and trips. Thanks for collaborations, countless chats in tissue culture and numerous PhD-outings. I wish you all the best with your PhD projects. I hope we meet again!

Jasper, de leukste en meest op hol geslagen senior postdoc die ik ooit ga ontmoeten: bedankt voor je grappen, maar ook goede adviezen, meelevendheid, enthousiasme, reisadvies en eerlijkheid. Je hebt een belangrijke bijdrage gehad in mijn promotietraject. Ik vind het leuk om te zien dat je het naar je zin hebt bij de HUB en kijk er naar uit elke werkdag weer begroet te gaan worden door jouw geschreeuw.

Benedetta, thanks for your really valuable advice on research, career, and life in general ('lose that calendar Else, it will not make you happy' and 'mice should be immediately killed, how can you live like this'). I've really enjoyed going to the gym with you and Carmine, the excuses you made up for not having to go, and the 'why do you make me do this' faces you made during the gym classes. But I must give you credit, because you did keep showing up and thereby also helped me to keep going. On a more serious note, I have always been very impressed by the quality of the work you do, and the oversight you keep in your projects. I really want to thank you for your interest in my research and all your help and valuable advice on my projects, submissions and papers. I have enjoyed working in the lab with you.



Helmuth, thanks for all your input on my research projects, your valuable critical questions during labmeetings and your advice on experiments and publications. I wish you all the best.

Oded, I am very glad I have met you and hope you are doing well back in Israel. Thank you for your patience, kindness and valuable advice. Hope we meet again.

Kai, thanks for always saving me by booking a culture hood for me for the next day (which I really always forgot), for helping me out when I started my head and neck project, and for proofreading my manuscripts. Most of all, thank you for your humor and patience. Ik vond het gezellig Nederlands met je te praten in de celkweek. Good luck in Würzburg!

Shanna and **Roksan**, thanks for your motivation during your internships and helping me learn a lot from supervising you!

All the other (former) lab members: **Nobu, Norman, Inha, Stefan, Luc, Johan, Mascha, Laura, Robert, Yotam, Jochem, Lena, Angelos, Huili, Priyanca, Veerle, Anjali, Maaïke, Harry, Jeroen, Carola, Yoshi, Tomo, Dymph, Talya, Amanda, Delilah, Georg, Dominique, Marrit, Florijn, Lisanne, Marc, Onur, Ana, Paul, Sangho, Gui-Wei** and **Matteo**. Thanks for making the lab such an inspiring and fun environment, where everybody is always willing to help you and give advice.



Lot, wat fijn dat ik jou via Stefan heb leren kennen. Bedankt voor al je input rondom ons hoofd hals project en de moeite die je hebt gedaan om mij actief te betrekken bij de klinische kant van dit onderzoek. Ik heb het met je meelopen op de poli, het aansluiten bij congressen en onze gesprekken over het behandelen van patiënten als enorm waardevol ervaren. Ik heb veel bewondering voor hoe je omgaat met patiënten, in mijn ogen vol respect en betrokkenheid. Ik wil je bedanken dat je altijd tijd maakte voor mijn vragen. Je hebt me geholpen te realiseren dat ons onderzoek mogelijk écht iets kan betekenen voor (toekomstige) patiënten.

Remco, bedankt voor je bijdrage aan het hoofdhals project. Ik je bedanken voor de mogelijkheden die je me hebt gegeven om mijn onderzoek te presenteren aan klinici op vergaderingen en congressen en het aandragen van mij als auteur voor het NtvO. Ik vond het schrijven van deze review enorm leerzaam en waardevol.

Natanja, bedankt voor de fijne samenwerking tijdens onze promotietrajecten. Ik vond het leuk om met je samen te werken en zo een indruk te krijgen van de meer klinische kant van oncologisch onderzoek. Ik vond het tof dat we in dezelfde fase zaten in ons promotietraject en elkaar daarom goed begrepen. Het samen schrijven aan ons artikel was een van de hoogtepunten van mijn promotie. Ik vind dat we best wel trots mogen zijn

op onze doelgerichtheid in dit project, zeker gezien de soms ingewikkelde situaties die er omheen speelden. Succes in Amersfoort!

Lodewijk, allereerst dank voor je geduld en vertrouwen in me, maar ook je hulp bij het opzoeken van patiënten informatie, je waardevolle advies, en alle tijd die je hebt geïnvesteerd in onze samenwerking.

Willem, ik vind het leuk dat ik je heb leren kennen en heb je hopelijk een beetje bekend kunnen maken met het organoïden-werk. Ik heb genoten van je droge opmerkingen. Ik wens je veel succes met je promotie en specialisatie en kijk er naar uit om met je samen te blijven werken.

Litha, Annemiek en Annemieke, dank voor jullie hulp bij al het papierwerk dat kwam kijken bij het afronden van een promotietraject, waarmee jullie me erg geholpen hebben in deze (toch best wel stressvolle) periode.

Anneta, Anne en alle andere betrokkenen van de weefselfaciliteit. Bedankt voor jullie geduld en inzet, zonder jullie werk waren mijn projecten niet mogelijk geweest.

Tot slot wil ik graag mijn lieve en allerleukste vrienden bedanken, die altijd maar snappen dat ik aan het werk wil of het alweer wil hebben over die tumorcellen. Ik besepte me pas hoe bevoorrecht ik ben toen ik deze lange lijst met namen mocht opschrijven. Lieve **Dieke, Sofia, Lisa-Milou, Eva, Hélène, Elsemiek, Suzanne, Lindy, Eline, Joyce, Annemarie, Nynke, Marte, Julia, Nika, Lisa, Lonneke, Joost, Luuk, Jesse, Robin, Josje** en **Josine**. Jullie zijn me oneindig dierbaar, bedankt dat ik jullie vriend mag zijn. Dankjewel voor jullie gezelligheid en het delen van mooie ervaringen, muziek, festivals, reizen, sportsessies, goede gesprekken, oneindige kopjes koffie, etentjes en heel veel slappe lach sessies. Ik hoop dat dat nog lang zo blijft.



